



University
of Glasgow

Dozynkiewicz, Marta Anna (2011) *The role of the Chloride Intracellular Channel-3 (CLIC3) in integrin trafficking and tumour progression*.
PhD thesis.

<http://theses.gla.ac.uk/2310/>

Copyright and moral rights for this thesis are retained by the author

A copy can be downloaded for personal non-commercial research or study, without prior permission or charge

This thesis cannot be reproduced or quoted extensively from without first obtaining permission in writing from the Author

The content must not be changed in any way or sold commercially in any format or medium without the formal permission of the Author

When referring to this work, full bibliographic details including the author, title, awarding institution and date of the thesis must be given

The role of the Chloride Intracellular Channel-3 (CLIC3) in integrin trafficking and tumour progression

Marta Anna Dożynkiewicz (B.Sc, MRes)

Thesis submitted to the University of Glasgow for the degree of
Doctor of Philosophy

September 2010

Beatson Institute for Cancer Research
Garscube Estate
Switchback Road
Glasgow G61 1BD

Abstract

Rab25 is a small GTPase of the Rab11 family that is known to control endosomal trafficking and the return of internalised receptors to the plasma membrane. Recent reports that Rab25 can act as either a promoter or suppressor of tumourigenesis highlight the need for greater understanding of how it controls integrin trafficking. In this thesis I show data indicating that Rab25 permits the sorting of ligand-occupied, active conformation $\alpha 5\beta 1$ integrin to late endosomes/lysosomes. Novel photoactivation and biochemical approaches show that integrins thus sorted are not degraded, but rapidly recycled from late endosomes/lysosomes to the plasma membrane. This requires the Chloride Intracellular Channel 3 (CLIC3); a protein resident in late endosomes/lysosomes of previously unknown function, that is upregulated in Rab25-expressing cells. Here I show that CLIC3 exists in close proximity with active $\alpha 5\beta 1$ in late endosomes/lysosomes and is required for cancer cell invasion into fibronectin-containing three-dimensional matrices. Clinical data indicate that CLIC3 is expressed in ovarian cancers, pancreatic ductal adenocarcinoma (PDAC) and pancreatic intraepithelial neoplasia (PanIN), but is absent from normal pancreas and tumour-associated stroma. Moreover, Kaplan-Maier analyses demonstrate a strong correlation between high levels of CLIC3 (at both mRNA and protein levels) and poor prognosis in operable cases of PDAC.

Taken together, the findings presented in this thesis identify CLIC3 both as a regulator and component of a novel vesicular transport route that returns lysosomally-targetted integrins to the plasma membrane, and as an independent prognostic indicator in pancreatic cancer.

Table of Contents

1	Introduction	16
1.1	Cancer cell invasion and metastasis	16
1.1.1	Features of cancer	16
1.1.2	Cancer metastasis	18
1.1.3	Modes of tumour cell migration.....	21
1.1.3.1	Individual cell migration.....	21
1.1.3.2	Collective tumour cell migration and motility mode-switching	22
1.2	Integrin receptors.....	25
1.2.1	An overview of integrins	25
1.2.2	Extracellular domain of integrins.....	27
1.2.3	Integrin cytoplasmic domain	30
1.2.4	Integrin signalling	33
1.2.4.1	Importance of integrin activation	33
1.2.4.2	Insights into integrin activation mechanism.....	34
1.2.4.3	Integrin activation by talin and kindlin as an example of inside- out signalling	36
1.2.4.4	Outside-in signalling and regulation of the cytoskeleton	40
1.3	Integrin trafficking	42
1.3.1	Different routes to endocytosis	42
1.3.1.1	Clathrin-mediated and clathrin-independent B1 integrin internalisation.....	45
1.3.2	Integrin recycling.....	47
1.3.3	Signalling endosomes	51
1.3.4	Integrin trafficking in cell migration	53
1.3.5	Integrin recycling in cancer.....	57
1.4	Rab25 and its disputed role in cancer progression	61
1.4.1	Rab25 is a member of the RAS-superfamily.....	61
1.4.2	Rab25 as tumour promoter	62
1.4.3	Rab25 can function as tumour suppressor.....	63
2	Materials and Methods.....	65
2.1	Materials	65
2.1.1	Reagents and Solutions	65
2.1.2	Antibodies and dyes.....	67
2.1.3	Enzymes and kits	68
2.1.4	Tissue Culture plastic ware	69
2.2	Methods.....	70
2.2.1	Microarray screen and validation	70
2.2.1.1	Total RNA extraction and quality control.....	70
2.2.1.2	Microarray data analysis	70
2.2.1.3	cDNA synthesis	71
2.2.1.4	Primers for real time PCR	72
2.2.1.5	qPCR	72
2.2.2	Cloning and DNA manipulation	73
2.2.2.1	Bacterial strains.....	73
2.2.2.2	Bacterial transformation.....	73
2.2.2.3	Plasmid preparation	73
2.2.2.4	Polymerase chain reaction (PCR).....	74
2.2.2.5	Intermediate cloning into pGEM-T-Easy	75
2.2.2.6	Restriction enzyme digestion and ligation	75
2.2.2.7	Agarose gel electrophoresis	75

2.2.3	Recombinant protein production	76
2.2.3.1	Protein expression	76
2.2.3.2	Protein purification.....	76
2.2.4	Mammalian cell culture techniques	77
2.2.4.1	Cell origin	77
2.2.4.2	Cell maintenance	77
2.2.4.3	Nucleofection.....	78
2.2.4.4	Inverse invasion assay	78
2.2.4.5	Generation of cell derived matrix.....	79
2.2.4.6	Labelling of fibronectin	80
2.2.4.7	Live cell imaging, photoactivation and colocalisation quantification	80
2.2.4.8	Fixing and staining cells for microscopy	81
2.2.4.9	FLIM-FRET	82
2.2.4.10	Recycling assays.....	82
2.2.4.11	FACS.....	83
2.2.5	Protein extraction and analysis	83
2.2.5.1	Cell lysis for protein	83
2.2.5.2	Protein extraction from mouse tissue	84
2.2.5.3	Protein quantification.....	84
2.2.5.4	SDS-PAGE and Coomassie staining.....	84
2.2.5.5	Western Blotting	85
2.2.6	Protein expression analysis in tissue samples.....	85
2.2.6.1	Immunohistochemistry	85
2.2.6.2	Pancreatic tumour TMA cohort and analysis.....	86
2.2.6.3	Ovarian tumour TMA.....	87
2.2.7	Pull downs for mass spectrometry.....	87
3	Chloride intracellular channel 3 (CLIC3) is a component of Rab25 driven invasive phenotype	88
3.1	Introduction.....	88
3.2	Results	93
3.2.1	Microarray analyses identified constituents of Rab25-driven invasive phenotype	93
3.2.1.1	The quality and purity of RNA was sufficient to perform microarray hybridisation	93
3.2.1.2	GCRMA normalisation yields good clustering of experimental microarray replicas.....	96
3.2.1.3	Microarray analyses identify genes whose differential expression is driven by Rab25 in two dimensional and in three dimensional-like environments.....	98
3.2.1.4	Eighteen genes (three of which are ion carriers) are upregulated by Rab25 in a matrix specific fashion.....	101
3.2.2	Use of qPCR to validate CLIC3, SLCA16A6 and KCNJ2 upregulation.....	105
3.2.2.1	qPCR primer pairs amplify a single product and they do so in a linear manner over a range of cDNA concentrations	105
3.2.2.2	CLIC3, SLC16A6 and KCNJ2 mRNA levels increase when A2780- Rab25 cells are seeded onto CDM.....	110
3.2.3	The role of Rab25 in upregulation of CLIC3 expression	113
3.2.3.1	Upregulation of CLIC3 mRNA but not SLC16A6 or KCNJ2 is opposed by RNAi of Rab25	113

3.2.3.2	CLIC3 protein levels increase following Rab25 expression and even more so with Rab25 expression and exposure to a three-dimensional matrix	116
3.2.3.3	Expression of CLIC family members other than CLIC3 is not affected by Rab25 or CDM.....	118
3.2.3.4	Suppressing the function of β 1 integrin with blocking antibodies increases CLIC3 mRNA level	120
3.3	Discussion	122
3.3.1	Summary	122
3.3.2	How could upregulation of CLIC3 mRNA occur?	122
3.3.3	What is the source of discrepancy between CLIC3 mRNA and protein level?	125
3.3.4	Other potentially interesting hits.....	125
4	CLIC3 is a late endosomal/lysosomal protein and controls the return of lysosomally-targeted active-conformation integrins to the plasma membrane	128
4.1	Introduction.....	128
4.1.1	Phylogeny and structural conservation of CLICs.....	128
4.1.2	CLICs as membrane-inserted proteins	132
4.1.3	Biochemical diversity	133
4.1.3.1	Ion conductance.....	133
4.1.3.2	CLICs as glutathione transferases?	136
4.1.4	Functional diversity	136
4.1.4.1	CLICs in membrane remodelling and tubulogenesis.....	136
4.1.4.2	Cell growth and survival	138
4.1.4.3	Other functions.....	139
4.1.5	CLIC3	142
4.2	Results	144
4.2.1	CLIC3 is necessary for Rab25-driven invasion into fibronectin-supplemented matrigel.....	144
4.2.2	CLIC3 is localised to vesicular-like structures but not to early or recycling endosomes.....	150
4.2.3	CLIC3 is localised to late endosomes/lysosomes	154
4.2.4	Active α 5 integrin is routed to CLIC3-positive late endosomes/lysosomes in a Rab25-dependent manner	161
4.2.5	α 5 β 1 integrin is trafficked from CLIC3-positive late endosomes/lysosomes to the plasma membrane	169
4.2.6	CLIC3 facilitates the recycling of active α 5 β 1 integrin back to the plasma membrane.....	173
4.3	Discussion	177
4.3.1	Summary and general points	177
4.3.2	Fibronectin uptake and sorting of α 5 β 1 integrin to late endosomes/lysosomes	180
4.3.3	Return of α 5 β 1 to the plasma membrane	182
5	CLIC3 drives tumour progression <i>in vivo</i> and is an independent prognostic factor in PDAC.....	187
5.1	Introduction.....	187
5.1.1	CLICs in cancer	187
5.1.2	Ovarian and pancreatic cancer.....	188
5.1.3	Tissue microarrays	194
5.2	Results	198
5.2.1	Generation of a CLIC3 specific antibody	198
5.2.2	CLIC3 antibody specifically recognises CLIC3, but not other members of the CLIC family	201

5.2.3	Optimisation of the antibody for immunohistochemistry	205
5.2.4	CLIC3 expression in ovarian carcinomas	212
5.2.5	CLIC3 is expressed in Pancreatic Intraepithelial Neoplasia (PanIN) and invasive pancreatic ductal adenocarcinomas (PDAC) but not in normal pancreatic ducts.....	216
5.2.6	CLIC3 predicts poor PDAC patient survival	218
5.2.7	CLIC3 expression correlates with enhanced Src signalling in pancreatic tumour tissue	225
5.3	Discussion	227
5.3.1	Summary	227
5.3.2	How does CLIC3 contribute to tumour progression in vivo?	227
5.3.3	Could CLIC3 explain conflicting roles of Rab25 in cancer?	228
6	Discussion.....	231
6.1	Summary	231
6.2	Future directions and preliminary observations	233
6.2.1	CLIC3 in tumour invasion and progression.....	233
6.2.2	CLIC3 interactome	234
6.3	Final discussion and conclusions.....	238
6.3.1	Signalling from late endosomes/lysosomes	238
6.3.2	Exosomes and cancer	241
6.3.3	Integrins in cancer progression and in the clinic.....	243
7	Appendices	246
8	Bibliography	254

List of Figures

Figure 1-1 The six acquired capabilities of cancer.	17
Figure 1-2 Cancer metastasis.	20
Figure 1-3 Depiction of different migration modes.	24
Figure 1-4 The integrin adhesion receptor family.	26
Figure 1-5 Schematic structure of an integrin heterodimer.	29
Figure 1-6 Mechanism of integrin activation.	39
Figure 1-7 Main endocytosis routes.	44
Figure 1-8 Schematic summary of integrin trafficking pathways.	50
Figure 1-9 Integrin trafficking in cell migration.	56
Figure 3-1 Cell derived matrices (CDM) are three-dimensional and fibronectin rich substrates.	91
Figure 3-2 Experimental paradigm.	92
Figure 3-3 Confirmation of the purity and integrity of the RNA samples used for microarray analysis.	95
Figure 3-4 GCRMA normalisation results in good clustering of experimental replicas.	97
Figure 3-5 Genes differentially expressed in Rab25-expressing cells when plated onto CDM.	99
Figure 3-6 Genes differentially expressed in Rab25-expressing cells when plated onto plastic surfaces.	100
Figure 3-7 Eighteen genes are differentially expressed in a Rab25 and CDM-dependent fashion.	103
Figure 3-8 Of the 18 genes that are upregulated in a Rab25 and CDM-dependent manner, three are transporters.	104
Figure 3-9 Primers for quantitative PCR (qPCR) amplify a single product.	108
Figure 3-10 Q-PCR primer pairs amplify a product in a linear manner over a range of cDNA concentrations.	109
Figure 3-11 Validation of three microarray hits by q-PCR when cells are grown on HDF-derived CDM.	111
Figure 3-12 Validation of three microarray hits by q-PCR when cells are grown on Tif-derived CDM.	112
Figure 3-13 CLIC3, SLC16A6 and KCNJ2 expression following transient overexpression of Rab25.	114
Figure 3-14 CLIC3, SLC16A6 and KCNJ2 expression following Rab25 suppression.	115
Figure 3-15 CLIC3 protein is upregulated in a Rab25 and CDM-dependent manner.	117
Figure 3-16 Expression of the other CLIC family members in A2780 cells.	119
Figure 3-17 Suppressing B1 integrin function increases CLIC3 mRNA levels.	121
Figure 4-1 The human CLICs share a high level of sequence conservation.	130
Figure 4-2 X-ray crystal structures of human CLICs: CLIC1, CLIC2, CLIC3 and CLIC4.	131
Figure 4-3 X-ray crystal structure of CLIC3.	143
Figure 4-4 Suppression of CLIC3 with siRNA smart pool and individual oligonucleotides.	146
Figure 4-5 Suppression of CLIC3 levels reduces invasiveness of A2780-Rab25 cells.	147
Figure 4-6 CLIC3 drives invasion of A2780-DNA3 cells into fibronectin-rich matrigel.	149
Figure 4-7 Cherry-CLIC3 expression and localisation in A2780-Rab25 cells.	151

Figure 4-8 CLIC3 does not colocalise with early endosomal markers: EEA1 or Rab4.....	152
Figure 4-9 CLIC3 does not colocalise with recycling endosomal markers: Rab11 or Rab25.	153
Figure 4-10 CLIC3 colocalises with a late endosomal/lysosomal marker, Rab7.	155
Figure 4-11 CLIC3 colocalises with a lysosomal marker, LAMP1.....	156
Figure 4-12 CLIC3 colocalises with a lysosomal protein, sialin.	157
Figure 4-13 CLIC3 colocalises with internalised fibronectin and lysotracker. ..	158
Figure 4-14 Late endosomal/lysosomal localisation of CLIC3 is independent of Rab25 expression.	160
Figure 4-15 Addition of soluble fibronectin and expression of a constitutively active mutant of $\alpha 5$ integrin enhances colocalisation between CLIC3 and $\alpha 5$ integrin vesicles.	163
Figure 4-16 Fibronectin-induced enhancement of colocalisation between CLIC3 and $\alpha 5$ integrin vesicles requires Rab25.	164
Figure 4-17 FLIM-FRET analysis of the proximity of $\alpha 5$ integrin and CLIC3 in Rab25 expressing cells.	167
Figure 4-18 FLIM-FRET analysis of the relationship between $\alpha 5$ integrin and CLIC3 in A2780-DNA3 cells.	168
Figure 4-19 Photoactivation shows that $\alpha 5$ integrin returns to the plasma membrane from CLIC3 vesicles.	171
Figure 4-20 Inhibition of CLIC3 suppresses recycling of lysosomally-targetted $\alpha 5\beta 1$	174
Figure 4-21 Inhibition of CLIC3 or addition of bafilomycin A1 suppress recycling of lysosomally-targetted $\alpha 5\beta 1$	175
Figure 4-22 Inhibition of CLIC3 suppresses recycling of constitutively active $\alpha 5\beta 1$	176
Figure 4-23 Working paradigm.	178
Figure 4-24 CLIC3 does not affect lysosomal pH.	185
Figure 5-1 Incidence and mortality rates for pancreatic cancer.	191
Figure 5-2 Multistep progression from PanINs to invasive pancreatic ductal carcinoma.	193
Figure 5-3 Construction of tissue microarrays (TMAs).	197
Figure 5-4 Bacterial expression and affinity purification of GST-CLIC3.....	200
Figure 5-5 Bacterial expression of GST-CLIC3, GST-CLIC1 and CLIC4 for antibody purification and validation.	202
Figure 5-6 Validation of the antibody from 1543 serum.	203
Figure 5-7 Antibody from 1544 serum specifically recognises CLIC.....	204
Figure 5-8 Trial CLIC3 immunohistochemistry (IHC) on mouse tissue.	207
Figure 5-9 CLIC3 IHC with no antigen retrieval and with Proteinase K retrieval on mouse tissue.	208
Figure 5-10 CLIC3 IHC on mouse tissue using EDTA buffer (pH8).	209
Figure 5-11 CLIC3 IHC on human placenta.	210
Figure 5-12 CLIC3 mRNA and protein in matching pancreatic tumour samples.	211
Figure 5-13 CLIC3 IHC on a practice TMA.	213
Figure 5-14 CLIC3 expression in ovarian tumours.....	215
Figure 5-15 CLIC3 IHC of normal pancreatic ducts, Pancreatic Intraepithelial Neoplasia (PanIN) and high grade and invasive pancreatic ductal adenocarcinomas (PDAC).	217
Figure 5-16 Scoring guide for the pancreatic ductal adenocarcinoma (PDAC) tissue microarray (TMA).	219
Figure 5-17 High CLIC3 protein expression renders poor survival in patients with operable pancreatic ductal adenocarcinoma (PDAC).	220

Figure 5-18 Predictors of survival in 118 patients with pancreatic ductal adenocarcinoma following pancreaticoduodenectomy according to multivariate Cox regression analysis.	221
Figure 5-19 High CLIC3 mRNA expression renders poor survival in patients with operable pancreatic ductal adenocarcinoma (PDAC).	223
Figure 5-20 Predictors of survival in 48 patients with pancreatic ductal adenocarcinoma following pancreaticoduodenectomy according to multivariate Cox regression analysis.	224
Figure 5-21 CLIC3 expression correlates with that of Phospho ⁴¹⁶ -Src, Phospho ⁷²⁷ -STAT3, cyclin D1 and p21 in pancreatic adenocarcinomas.	226
Figure 5-22 CLIC3 and Rab25 expression in PDAC and ovarian carcinoma.	230
Figure 6-1 CLIC3 interactome.	236
Figure 6-2 Preliminary data on PTPN14.	237

List of Tables

Table 2-1 Reagents and solutions	66
Table 2-2 Antibodies and dyes.....	67
Table 2-3 Enzymes and Kits	68
Table 4-1 Biophysical properties of CLICs based on the available literature. ..	135
Table 4-2 Diversity in the cellular functions fulfilled by CLIC family members.	141

List of accompanying material

Supplementary movies 1-4

Abbreviations

CA	Constitutively active
CDM	Cell-derived matrix
CLIC3	Chloride intracellular channel 3
CME	Clathrin-mediated endocytosis
DMSO	Dimethyl sulphoxide
DNA	Deoxyribonucleic acid
dNTPs	Deoxy nucleotide-5'-triphosphate
<i>E. coli</i>	<i>Escherichia coli</i>
ECM	Extracellular matrix
EDTA	Ethylene diamine triacetic acid
EEA	Early endosomal antigen
EGF	Epidermal growth factor
EGFP	Enhanced green fluorescence protein
EGFR	Epidermal growth factor receptor
EMT	Epithelial-mesenchymal transition
ERK	Extracellular signal-regulated kinase
EtBr	Ethidium bromide
FAK	Focal adhesion kinase
FCS	Foetal calf serum
FN	Fibronectin
GAP	GTPase activating proteins
GAPDH	Glyceraldehyde-3-phosphate dehydrogenase
GEFs	Guanine nucleotide exchange factors
GST	Glutathione S-transferase
HRP	Horseradish peroxidase
IHC	Immunohistochemistry
KDa	Kilodalton
LB	Leuria-Bertani medium
MMPs	Matrix metalloproteinases
mRNA	Messenger ribonucleic acid
NT	Non-targetting
OD	Optical density
PAGE	Polyacrylamide gel electrophoresis
PBS	Phosphate buffered saline
PBS-T	Phosphate buffered saline - Tween20
PCR	Polymerase chain reaction
PI-3 kinase	Phosphatidylinositol 3-kinases
PNRC	Perinuclear recycling compartment
PTB	Phosphotyrosine-binding
RCP	Rab-coupling protein
RNA	Ribonucleic acid
RNAi	Ribonucleid acid interference
ROCK	Rho-associated coiled-coil containing protein kinase
Rpm	Rotations per minute
RT-PCR	Reverse transcription polymerase chain reaction
SDS	Sodium dodecyl sulphate
Sec	Seconds
Ser	Serine
shRNA	Short hairpin RNA
siRNA	Short interfering RNA

TBS	Tris buffered saline
TBS-T	Tris buffered saline - Tween20
Tif	Telomerase immortalised fibroblast
Tween20	Polyoxyethylene sorbitan monolaurate
U	Units
V	Volts
VEGF	Vascular endothelial growth factor
Wt	Wild type

Acknowledgements

I would like to express my gratitude to Jim Norman for his supervision, guidance and help throughout my PhD. I would like to thank my advisor Brad Ozanne for his continuous enthusiasm and discussions. Many thanks to Nigel and Charlie, who made it possible to put my research into context of human cancer and to bring clinical significance to it. A special thanks to Pat, Kim and Marc for their guidance, assistance and optimism, especially during my first few months in the lab, but also thereafter. I am also indebted to Keith Vass, Jo Thurlow and Gabriela Kalna for their invaluable help with microarray analysis. A big thank you to all members of R20, past and present, and to the lovely friends I made, especially Alicia and Claire, for making the Beatson such an enjoyable place to work in. Also, I would like to express my thanks to the support staff throughout the Beatson Institute for their invaluable help.

Last but not least, many thanks to my family at home, my friends here in Glasgow and in Poland, for their constant and loving support throughout the PhD. Finally, I would like to dedicate this thesis in the memory of my dad.

I am grateful to Cancer Research UK for their generous funding.

Author's declaration

I am the sole author of this thesis. The work presented here is entirely my own, unless otherwise stated.

1 Introduction

1.1 Cancer cell invasion and metastasis

1.1.1 Features of cancer

Cancer is a multi-faceted disease represented by more than a 100 distinct types and subtypes originating from various organs in the body. It is believed that cancer development and progression mimics the process of evolution, in that successive genetic aberrations accumulate overtime and gradually lead to transformation of normal cells into tumour cells. Tumorigenesis requires the acquisition of six hallmarks, which allow the progressive transformation of normal tissue into malignancy (Fig. 1.1). Firstly, cells have to display growth signal autonomy, which removes their dependence on exogenous signals transmitted into the cell by transmembrane receptors, and that in turn allows them to progress from a quiescent into a proliferative state. Secondly, tumour cells acquire insensitivity to antiproliferative signals, which are also received by cell surface receptors and are utilised to maintain cellular quiescence and hence need to be circumvented in order for tumour cells to thrive. Thirdly, cancer cells have to acquire resistance towards programmed cell death - apoptosis - a process during which cellular components are being disrupted and cell remnants are being engrossed by the surrounding cells. Apoptosis allows for the elimination of cells harbouring activating oncogenic mutations, which if not eradicated, can proliferate to form a tumour mass. An additional prerequisite for the transformation of a normal cell to its cancerous counterpart is immortalisation, which is defined as the ability to replicate indefinitely, a feature, which normal cell populations lack since they enter the state of senescence after a certain number of doublings. Moreover, aberrant cells forming the initial neoplasia have to induce and sustain angiogenesis if they are to expand to bigger tumours. The proximity of vasculature is necessary to maintain oxygen and nutrient supply, which is indispensable for cell function and survival. Lastly, most tumours will acquire the ability to invade and spread to distant sites of the body, in a process called metastasis, which accounts for 90% of cancer-related deaths (Hanahan and Weinberg 2000).

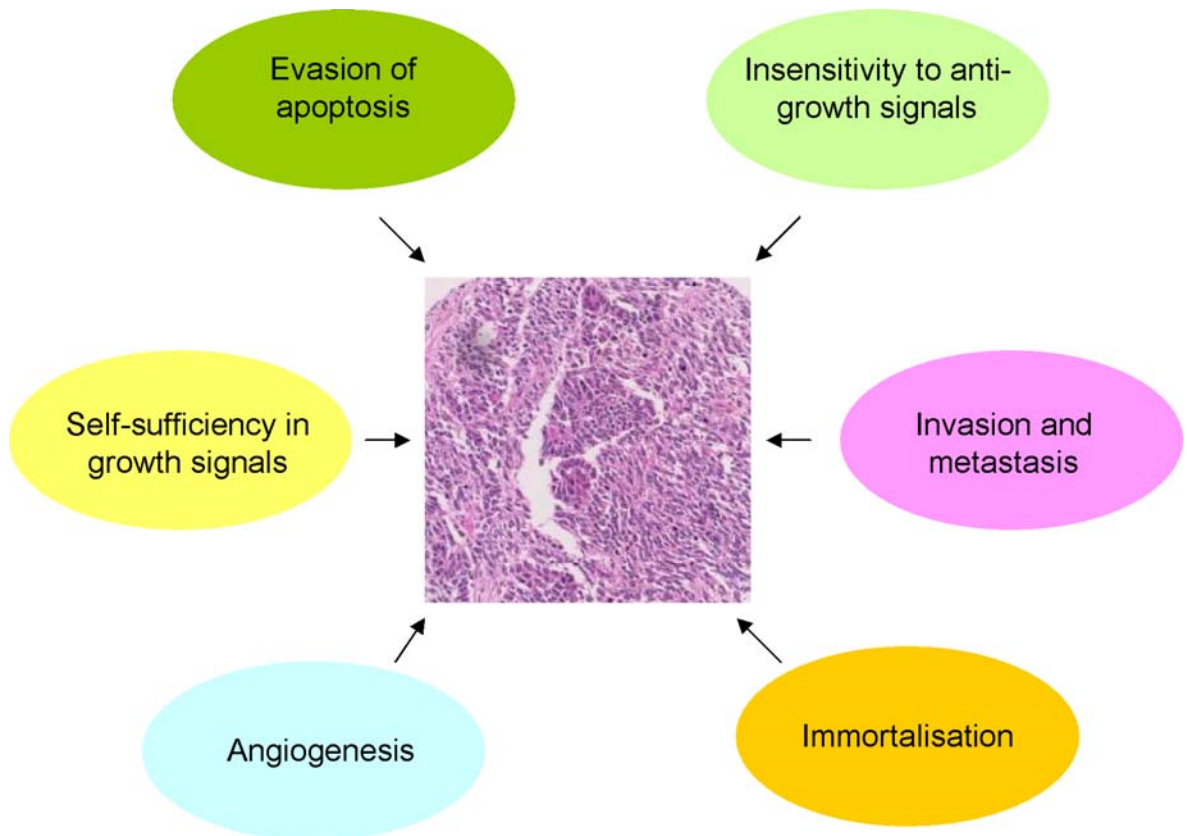


Figure 1-1 The six acquired capabilities of cancer.
Adapted from (Hanahan and Weinberg 2000).

1.1.2 Cancer metastasis

Metastatic spread is a multi-step process and involves a number of stages, such as alterations in cell adhesion, acquisition of invasive capabilities, entry into the circulation and transit to distant tissues, followed by exit into new sites and ultimately colonisation of new niches (Fig. 1.2). A primary step in the metastatic cascade is the detachment of cancer cells from a solid tumour mass, which is mediated by their decreased adhesive potential. Changes in the expression of a number of different protein classes can contribute to the loss of cellular adherence to both the surroundings and also to one another. These proteins include cell-cell adhesion molecules (CAMs) that mediate cell-cell interactions, and integrins, which provide a link between the extracellular matrix and the cell interior (Hanahan and Weinberg 2000). One of the most prominent changes occurring upon malignant epithelial transformation is the mutational inactivation of E-cadherin, which under normal circumstances provides a bridge between adjacent epithelial cells and also serves as a scaffold for anti-growth signalling to its downstream effectors such as β -catenin and Tcf transcription factor (Christofori and Semb 1999). Upon E-cadherin loss and detachment from the primary tumour mass, invasive cells need to breach the basement membrane, which underlies epithelial cell layers. The basement membrane is a well-organised, dense meshwork of glycoproteins and proteoglycans (such as type IV collagen and laminins), which maintains epithelial structure and provides a physical boundary for epithelial tumour invasion into the surrounding stroma. To disrupt the structure of this barrier, cancer cells employ matrix-degrading proteases. Under normal circumstances, the activity of extracellular matrix proteases is subject to tight regulation through both autoinhibition and secreted inhibitors. However, in tumours that exhibit metastatic capabilities, protease expression is elevated and accompanied by a decrease in the abundance of protease inhibitors, thus facilitating the invasion of cancer cells through the basement membrane and the adjacent extracellular matrix. Having invaded through the basement membrane and the surrounding matrix, tumour cells must penetrate the tumour-associated vasculature in a process referred to as intravasation. This is usually preceded by the activation of angiogenic processes, which result in the establishment of neo-vasculature, and which allow the tumour to grow beyond what would be possible if tumour cells relied only on

nutrient and oxygen supply from pre-existing blood vessels. The exact mechanism by which intravasating cells breach the boundaries of tumour-associated vessels is unclear, but it is believed to result from enhanced mesenchymal motility of invasive cell sub-populations and their responsiveness to chemoattractive gradients originating from the vasculature. When in circulation, disseminated cells must be able to avoid anoikis, oppose shear forces that could lead to physical damage and they also need to evade being targeted and killed by immune cells (Gupta and Massague 2006). Having intravasated and survived in the circulation, invasive cells must mechanically lodge themselves in the walls of capillaries and escape the vasculature to enter secondary sites: a process referred to as extravasation. Vascular endothelial growth factor (VEGF) released by metastatic cells is thought to yield vascular permeability by activating Src family kinases in the endothelial cells and thus disrupting endothelial cell junctions. This in turn can facilitate extravasation of circulating tumour cells and metastatic spread (Criscuoli, Nguyen et al. 2005). When out of the blood vessels and at a secondary site, cancer cells face yet another rate-limiting step, the hostility of the new environment. It is interesting to note that disseminated tumour cells will likely only colonise niches that are compatible with their growth requirements, and most cancer types have their preferred recurrence sites. Indeed, breast cancer will metastasise to the bones, lungs, liver and brain, even though no direct vasculatory connection exists between these sites and breast tissue. Prostate cancer on the other hand, will predominantly show metastatic outgrowth in the bones, whilst sarcomas tend to target the lungs (Gupta and Massague 2006). One mechanism, which is postulated to aid in the metastatic colonisation of target niches, is preconditioning of these sites by VEGFR1-positive bone marrow cells, which are recruited to these sites in response to factors released by the primary tumours and create a permissive environment for the incoming disseminated tumour cells (Kaplan, Riba et al. 2005). Once metastatic cells have adapted to the new site by overcoming possible quiescence, by establishing interactions with the microenvironment and by initiating angiogenic cues, the colonisation of the secondary organ can proceed through the formation of micrometastases and be successfully completed by their outgrowth into macrometastatic lesions.

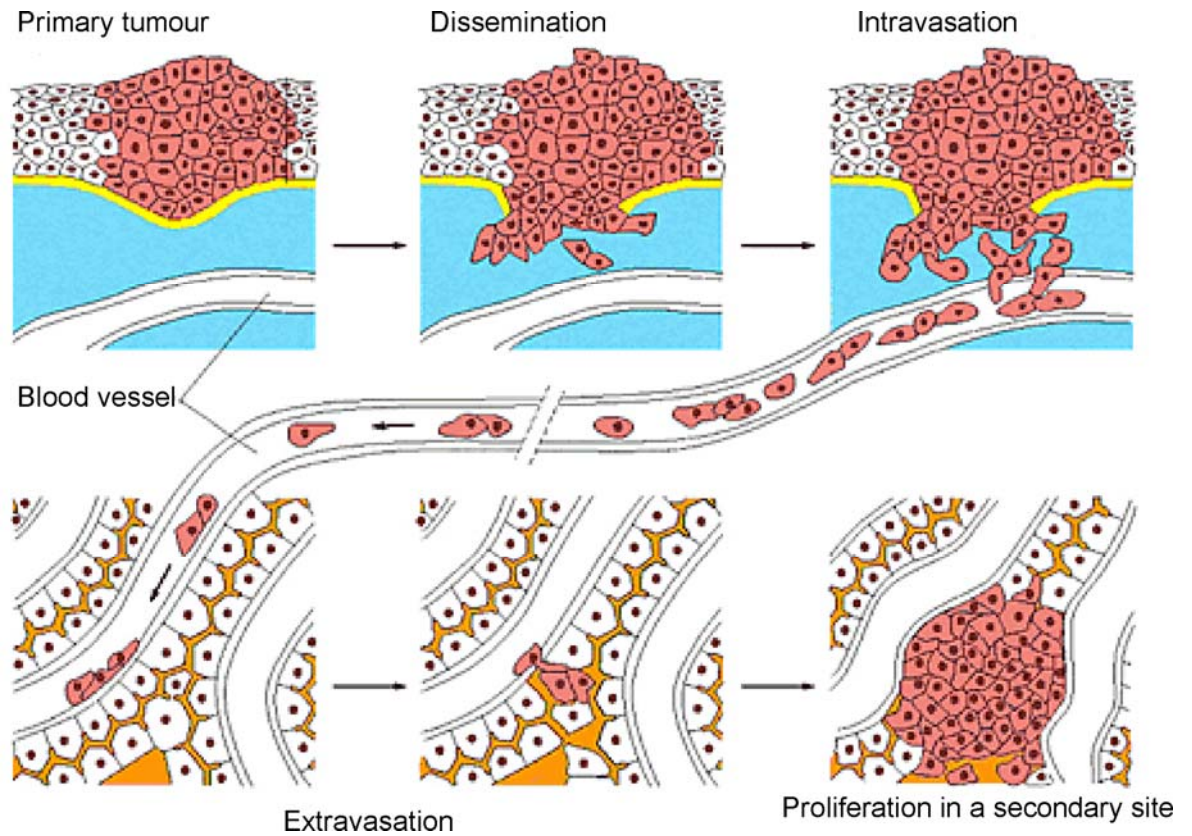


Figure 1-2 Cancer metastasis.

Formation of metastases is a multistep process, during which cancer cells disseminate from the primary tumour, enter the circulation with which they travel to distant sites of the body, where they extravasate to then populate new niches and form secondary lesions. Figure adapted from <http://cancer.scripps.edu/research.aspx>.

1.1.3 Modes of tumour cell migration

The process of metastasis, as it was described in the previous section, requires cancer cells to be motile. The acquisition of a motile phenotype by epithelial cells often requires a myriad of transcriptional alterations, which lead to epithelial-mesenchymal transition (EMT), a process mainly driven by the activation of AP1 and SMAD2 transcription factors and Snail/slugg transcription repressors (Thiery 2002). When invading through three dimensional environments, tumour cells can exhibit two major and mutually interchangeable modes of migration: mesenchymal and amoeboid, and migration can occur individually or collectively (Fig. 1.3) (Pankova, Rosel et al.).

1.1.3.1 Individual cell migration

The mesenchymal mode of migration is characterised by an elongated morphology with well-established front-to-back cellular polarity (represented by the presence of a leading and trailing edge), and it relies on proteolytic degradation of the extracellular matrix (ECM) by proteases such as MMPs. Cells utilising this mechanism of movement extend actin rich protrusions, in the form of a flat lamellipod, a cylindrical or rounded pseudopod or spiky filopodia. These protrusions form integrin-mediated focal contacts with the ECM, and these attachment sites can progress to form larger focal adhesions, which are capable of transmitting actomyosin contractile force to the ECM. This in turn facilitates the forward movement of the cell body, which follows the leading edges and allows for the retraction of the trailing edge. Velocities achieved by cells adopting this migratory behaviour are relatively low and in the range of 0.1-1 μ m/min. This migratory behaviour is frequently triggered by the activation of receptor tyrosine kinases, such as EGFR1 or c-Met, which is followed by the generation of phosphatidylinositol-3,4,5-triphosphate (PtdIns(3,4,5)P₃) at the cell front, where a GTPase Rac undergoes activation and recruits other components of mesenchymal migratory machinery, such as Scar/WAVE proteins and the Arp2/3 complex. Arp2/3 then nucleates monomeric G-actin into F-actin filaments. Alternatively, this cascade can be initiated either by the activation of Cdc42 or by oncogenic Ras proteins, which contribute to the augmentation in PtdIns(3,4,5)P₃ by activating PI-3 kinase. Conversely, tumour suppressor PTEN can, by dephosphorylating PtdIns(3,4,5)P₃, antagonise this process (Sahai 2005).

The mesenchymal mode of migration requires downregulation of the activity of RhoA and its effectors (Rho-associated coiled-coil containing protein kinases, ROCK1 and ROCK2), which in turn can activate Rac to drive polarised F-actin-rich protrusion formation (Vial, Sahai et al. 2003).

Another mode of migration, which is thought to resemble the crawling movement of leukocytes and the lower eukaryote *Dictyostelium discoideum*, can occur with speeds up to 4µm/min and is referred to as amoeboid motility. In contrast to mesenchymal motility, this mode of migration relies on the activity of the RhoA-ROCK pathway and does not require ECM proteolysis, but rather forces cells to squeeze through existing gaps in the matrix. Moreover, amoeboid motility is not characterised by the presence of large cell-ECM contacts, instead receptors mediating adhesion formation are diffusely distributed on the cell surface (Sahai 2005). This type of movement is thought to occur due to actin polymerisation around the cell cortex. This is driven by active RhoA, which recruits ROCK family of kinases to phosphorylate a number of cytoskeletal substrate proteins thus leading to stress fibre formation and generation of contractile force that drives amoeboid, bleb-like movement (Sahai and Marshall 2003)

1.1.3.2 Collective tumour cell migration and motility mode-switching

In contrast to individual cell motility modes described in the previous paragraph, collective cell movement involves migration of whole clusters, sheets or strings of invasive cells and is frequently employed by cancer lesions for tissue invasion *in vivo*. This requires the maintenance of adhesion contacts between migrating cells and relies on the cells that lead the invading sheet to release matrix-degrading enzymes, and thus create a migratory path for the remaining cells. During invasive migration, cells employ a number of different matrix remodelling proteases, which are capable of cleaving numerous ECM substrates, such as collagen, laminins, fibronectin or vitronectin. These ECM-degrading enzymes include matrix metalloproteinases (MMPs), serine proteases as well as cathepsins, and can be released by both tumour cells and tumour associated fibroblast at the leading edge of the migrating sheet. Microtracks, resulting from ECM-degradative activity of individual cells are formed and subsequently filled by adjacent cells from the migrating sheet thus leading to track widening, local

matrix regression and tissue macropatterning, which allows for collective gliding of the entire sheet. Although synergistic action of a number of proteolytic enzymes capable of breaking down collagen type I and type III fibres, such as MMP-1, MMP-2, MMP-13, MMP-14 and cathepsin B, K and L, is necessary for effective disruption of tissue integrity, it is MMP-14 that could potentially be targeted by anti-invasive therapy. This is due to the loss of function of MMP-14 not being easily compensated for by the activity of other proteases (Friedl and Wolf 2008).

An interesting feature of some disseminating tumour cells is their ability to switch between different modes of migration. Unlike EMT, mesenchymal-amoeboid transition (MAT), amoeboid-mesenchymal transition (AMT) and collective-to-amoeboid transition (CAT), can be triggered in response to changing tumour microenvironments during different stages of the metastatic cascade, and can occur as a consequence of differential control of specific signalling pathways (Pankova, Rosel et al.). This plasticity of motile tumour cells can allow evasion of anti-metastatic treatments that are targeted at one molecular pathway only. A successful anti-spread regimen in vivo is therefore likely to require a simultaneous anti-protease and anti-Rho/ROCK therapy, that would inhibit both types of motility and would prevent switching between the varying migratory modes (Sahai and Marshall 2003).

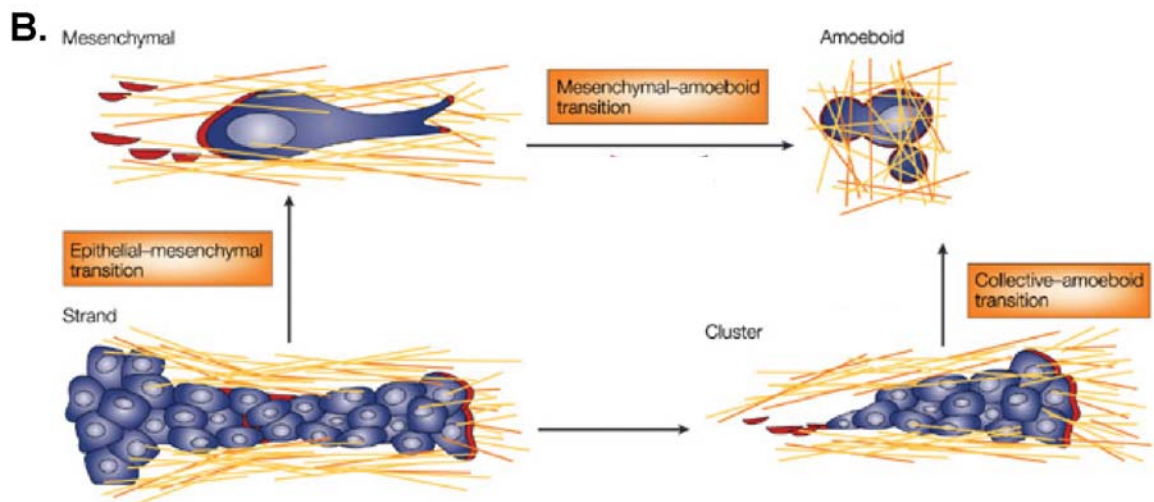
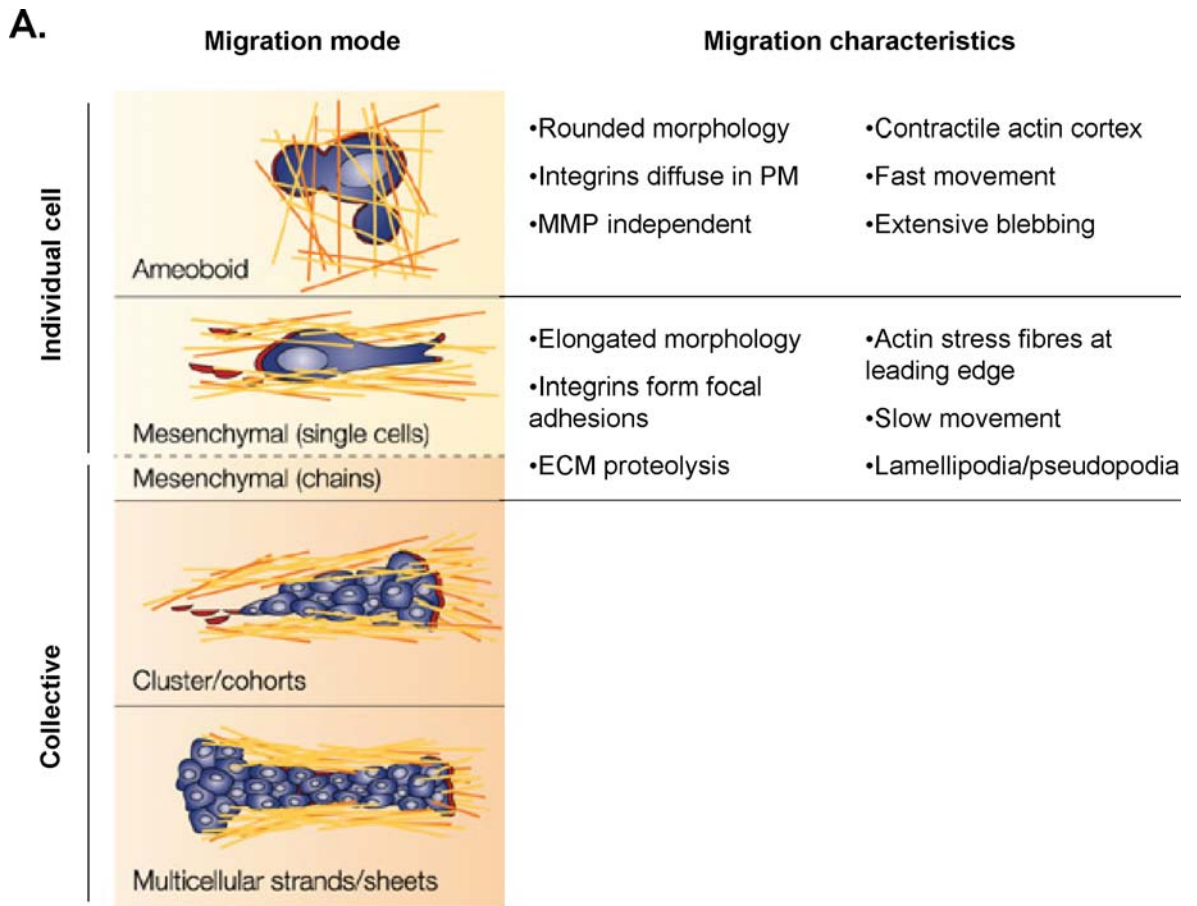


Figure 1-3 Depiction of different migration modes.

A. Individual cell migration can occur through the adaptation of two main phenotypes. Amoeboid cells are rounded and migrate through the ECM in a proteolysis-independent manner, whilst mesenchymal cells are elongated and require matrix degradation for their migration. Cell migration can also be collective and takes form of either strands or clusters. B. Tumour cells can switch between varying modes of migration in response to changing environment. Adapted from (Friedl and Wolf 2003).

1.2 Integrin receptors

1.2.1 An overview of integrins

The ability of cells to detect their environment is crucial for the development of multicellular organism and for maintaining its homeostasis. Cells can sense their surroundings by establishing interactions with neighbouring cells or with the extracellular matrix (ECM). These interactions are required for a range of processes such as cell growth, proliferation, differentiation and migration. The communication between the extracellular matrix and the cellular interior is primarily mediated by the integrin family of adhesion receptors.

Integrin receptors are transmembrane and heterodimeric glycoproteins, each composed of an α and a β subunit. Integrin expression is restricted to metazoan organisms and no homologues are detected in prokaryotes, plants or fungi. In mammals, 18 α ($\alpha 1$ - $\alpha 11$, D, E, L, M, V, X, IIb) and 8 β ($\beta 1$ - $\beta 8$) subunits are known, and they can assort to form 24 distinct heterodimers (Hynes 2002). Some integrins are specific to certain tissue or cell types, like $\alpha 11\beta 3$ to platelets or $\alpha 6\beta 4$ to keratinocytes, while others, such as $\alpha v\beta 3$ or $\alpha 5\beta 1$ are more widely expressed. α subunits share approximately 30%, and β subunits approximately 45% sequence identity, thus indicating that they could have arisen from gene duplication events. With respect to ligand specificity, integrins can be divided into laminin- or collagen-binding, those that recognise RGD sequences and leukocyte-specific integrins (Fig. 1.4). Most integrins recognise a short peptide sequence within their ligands, and the recognition and binding requires both subunits of the heterodimer (Hynes 2002; Takada, Ye et al. 2007). Each integrin subunit spans the plasma membrane once, and contains a short cytoplasmic domain (20-50 amino acids), with the majority of the polypeptide residing in the extracellular portion. The cytoplasmic tail of most integrins connects via a number of adaptor molecules, to the actin cytoskeleton, which these receptors can modulate (Hynes 2002). With regard to the connection to actin filaments and the size of cytoplasmic domain, integrin $\alpha 6\beta 4$ is an exception. It is unique in that its cytoplasmic domain is much larger and extends over 1000 amino acids (Tamura, Rozzo et al. 1990), whilst making connections not to the actin cytoskeleton but to intermediate filaments (Homan, Martinez et al. 2002).

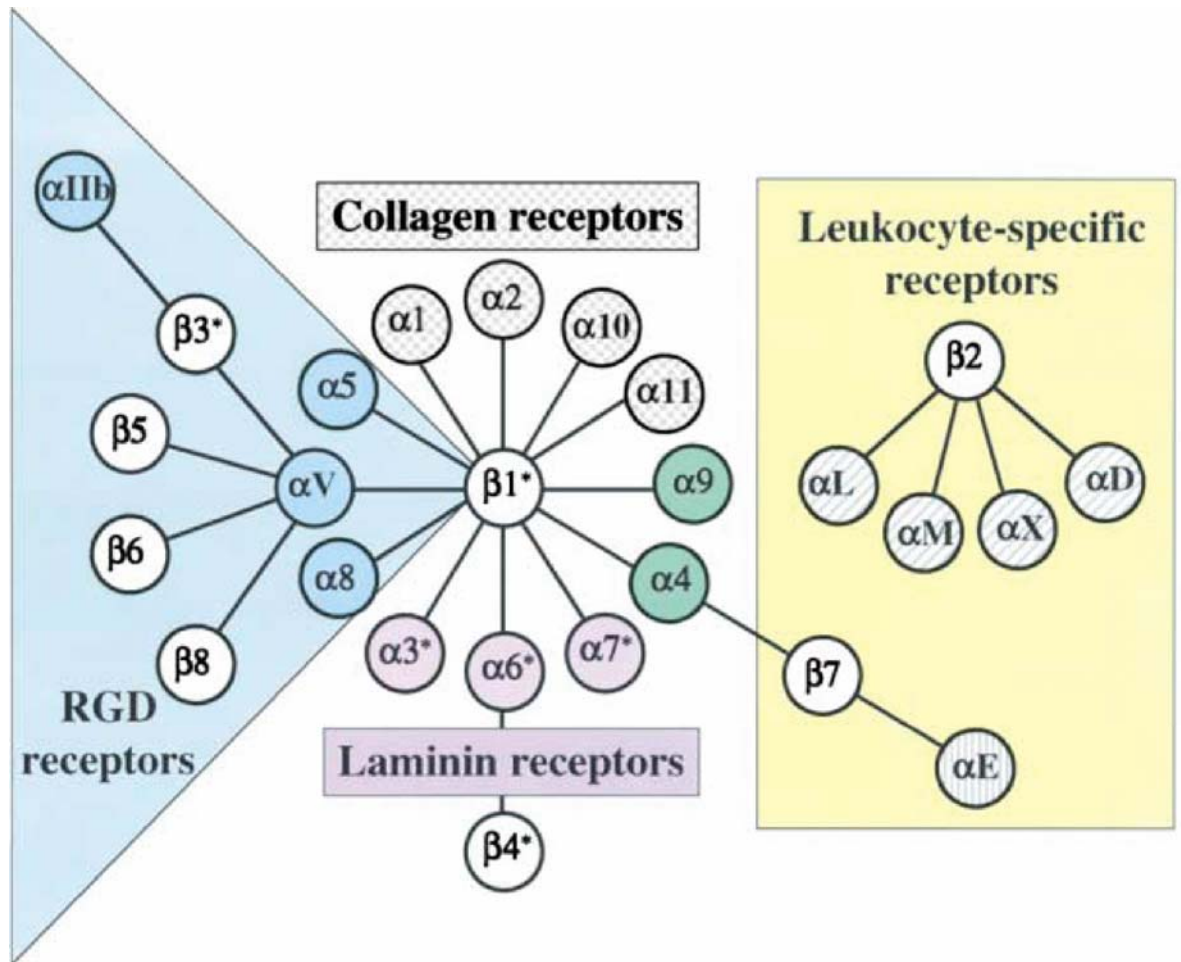


Figure 1-4 The integrin adhesion receptor family.

Integrins are composed of α and β subunits. There are 18 mammalian α and 8 β isoforms and they assemble to form 24 distinct heterodimers with defined ligand specificities. Asterix indicates subunits with alternative splice variants. Figure taken from (Hynes 2002).

1.2.2 Extracellular domain of integrins

In their extracellular portion, almost half of the mammalian α subunits ($\alpha 1$, 2, 10, 11, M, L, D, X) contain the I/A domain, which forms a Rossmann fold composed of parallel β -sheets within the core of this motif, and α -helices on its periphery. The I/A fold in the α subunit associates with the corresponding I/A domain in the β subunit (Lee, Bankston et al. 1995). This fold belongs to the group of von Willebrand factor A domains (VWA), which are approximately 180 amino acids long and mediate protein-protein interactions, and in the case of integrins, are responsible for ligand binding (Tuckwell 1999). The upper surface of the I/A motif contains a metal ion coordination site, which is formed by amino acids from three separate loops within that domain. The placement of the metal ion within the metal ion-dependent adhesion site (MIDAS) is thought to determine the conformation of the I/A domain, which can be either open or closed. The other half of mammalian α subunits, which lack the inserted I/A domain, contains seven sequence repeats that span over 440 amino acids and fold into a 7-bladed β -propeller, and this motif forms complexes with the I/A domain in the β subunit of the heterodimer (Springer 1997). More detailed insights into integrin structures were gained in 2001, when Xiong and colleagues solved the crystal structure of $\alpha v\beta 3$ integrin. These studies confirmed that the propeller contained within the α subunit complexes with the I/A domain in the β subunit to form the ligand binding pocket (Fig. 1.5). This N-terminal, extracellular tail of the integrin heterodimer has been shown to rest on two legs, each belonging to one of the subunits. Within the leg of the α subunit reside three domains termed: thigh, calf1 and calf2, each formed by β -sandwich motifs. Between the thigh and the first calf domain lies a high flexibility region, which is thought to allow for bending of the integrin head, and to take part in integrin activation and conformational change. The organisation of the β subunit is a little more complex, in that the most membrane distal extracellular part of the molecule, which forms the ligand-binding head, does not constitute its most N-terminal primary sequence. It is instead inserted into a β -sandwich loop and forms a so called hybrid-I/A domain, which in its primary sequence is preceded by a 54-amino acid stretch that forms the PSI domain. This domain, in the three-dimensional structure, lies beneath the head domain and is linked to the distal terminus of the β -subunit leg by a disulphide bond. The leg is composed of four

cystine-rich repeats, which form EGF-like folds. At the C-terminus of the EGF-like folds resides the β -sheet-rich motif, termed the β -tail domain (Xiong, Stehle et al. 2001).

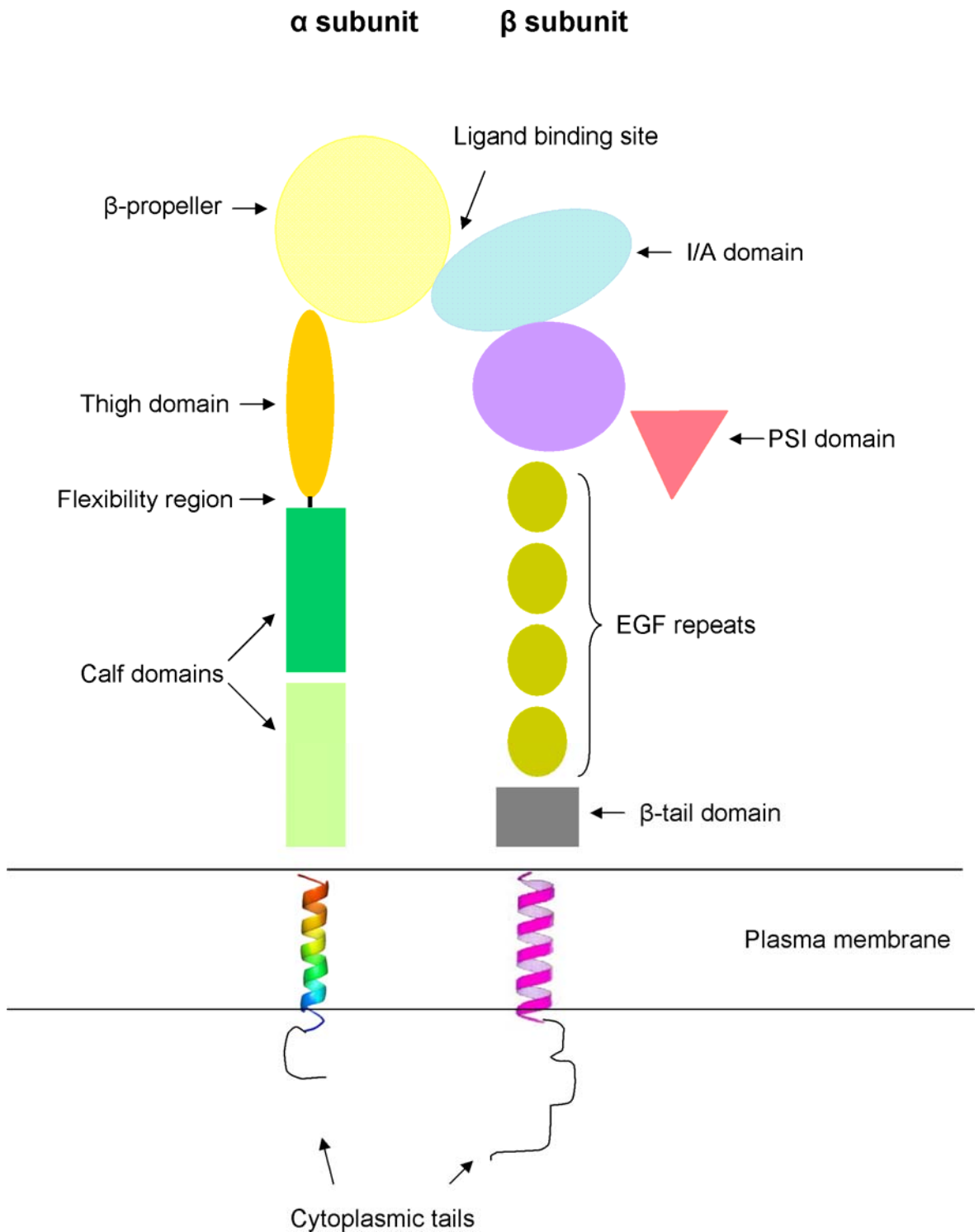


Figure 1-5 Schematic structure of an integrin heterodimer.

The α subunit contains in its extracellular part: two calf domains and a thigh domain, which form its leg. Positioned on the leg is β -propeller domain, which interacts with I/A domain of the β subunit. β -propeller and I/A domain form the head of the heterodimer, which contains the ligand binding site. The leg of the β subunit is composed of the PSI domain and four EGF repeats. Each subunit contains one transmembrane domain and a cytoplasmic tail.

1.2.3 Integrin cytoplasmic domain

The cytoplasmic domains of integrin receptors are much shorter than their extracellular portions and they only comprise approximately 50 amino acids. Even though they reside approximately 180Å away from the ligand binding site (Weisel, Nagaswami et al. 1992), truncations in the cytoplasmic domains of some integrins, for example $\alpha 2$ (Kawaguchi and Hemler 1993) or $\beta 2$ (Hibbs, Xu et al. 1991) have been shown to modulate their ligand binding affinity. This suggested that the integrin cytoplasmic tail is not only key for transducing ligand occupation and conformational changes to the cell interior, but it also controls the conformation of the extracellular domain and activity status of the receptor from within the cell.

The β integrin cytoplasmic tails have been described to exist in alternatively spliced forms and this contributes to the variety of biological functions played by these receptors. $\beta 1$ integrin, for example, is thought to have 4 distinct cytoplasmic splice variants: $\beta 1A$, $\beta 1B$ (Balzac, Belkin et al. 1993), $\beta 1C$ (Languino and Ruoslahti 1992) and $\beta 1D$ (Zhidkova, Belkin et al. 1995), and these are expressed in different tissues or cell types. The $\beta 1A$ integrin is the most ubiquitously expressed isoform and is involved in a wide range of biological processes (Almeida, Huovila et al. 1995; Fassler, Rohwedel et al. 1996), is capable of clustering, forming cell-matrix adhesions and mediating signalling. The $\beta 1B$ and $\beta 1C$ isoforms are minor variants and are expressed in some human cells and tissues, such as hematopoietic cell lines, platelets and osteosarcoma cells (Languino and Ruoslahti 1992), and differentiated epithelium (Fornaro, Tallini et al. 1996), respectively. The $\beta 1D$ isoform is specifically expressed in heart and skeletal muscle and is the most prominent $\beta 1$ integrin in these tissues (van der Flier, Kuikman et al. 1995). The functional differences between the different isoforms are exemplified by their varying affinity for binding of cytoskeletal proteins such as talin and filamin. Indeed, talin binding is inhibited in splice variants $\beta 1B$ and $\beta 1C$, whilst the $\beta 1D$ isoform binds talin more tightly than does $\beta 1A$ (Pfaff, Liu et al. 1998). In agreement with this, is the inability of the $\beta 1B$ variant to bind fibronectin, form cell-matrix adhesions and induce downstream signalling (de Melker and Sonnenberg 1999).

The highly conserved $\beta 1$ integrin cytoplasmic tail contains three amino acid sequences, which have been found to be necessary for integrin targeting to focal adhesions, heterodimer formation and binding of cytoplasmic partners. These conserved clusters include: cyto-1 (AA 764-774), cyto-2 (AA 785-788) and cyto-3 (AA 797-800), and they are conserved amongst β subunits, with the exception of $\beta 4$. Cyto-1 region is thought to mediate adhesion and to affect integrin affinity and specificity. Cyto-2 and cyto-3 contain NPXY and NXXY motifs (X represents a non-conserved amino acid), respectively, which function to recruit integrins to focal contacts and allow their binding to cytoskeletal proteins. Additionally, phosphorylation at conserved serine⁷⁹⁰ or tyrosine⁷⁸⁸ is thought to affect integrin function (Reszka, Hayashi et al. 1992). The $\beta 1A$ and $\beta 1D$ variants are very similar and only differ by 13 amino acid residues, half of which reside in the region that links cyto-2 and cyto-3 domains (Hannigan, Leung-Hagesteijn et al. 1996).

Surface plasmon resonance (Vallar, Melchior et al. 1999) and NMR spectrometry (Vinogradova, Velyvis et al. 2002) of $\alpha 11b\beta 3$ cytoplasmic tails have revealed an interaction between the α and β subunits within their membrane proximal regions. This association has been shown to require the presence of the conserved GFFKR sequence in the α subunit (Loh, Qi et al. 1996), and the cyto-1 domain of the $\beta 1$ integrin (which contains KLLMIHDDR sequence) has been proposed to be involved in this interaction (Briesewitz, Kern et al. 1995). Mutations in the above mentioned region of $\beta 1$ have been shown to ablate this association (Hayashi, Haimovich et al. 1990; Marcantonio, Guan et al. 1990). Additionally, heterodimerisation of the cytoplasmic tails has been proposed to occur via the hydrophobic stretches within the cyto-1 and GFFKR regions of β and α subunits, respectively (Williams, Hughes et al. 1994).

The cytoplasmic tails of integrins mediate their cell biological functions by binding to cytoplasmic proteins and this is thought to occur through a structurally conserved mechanism. Most β integrins contain one or two NPXY or NPXY-like motifs. The NPXY sequence has a propensity to form a β -turn (Ulmer, Yaspan et al. 2001), and such reverse-turn-forming modules often serve as a recognition site for phosphotyrosine-binding (PTB) domains that constitute most signaling and cytoskeletal molecules (Trub, Choi et al. 1995). Indeed, most integrin interactions with cytoplasmic proteins have been proposed to be

mediated by the NPXY-PTB affinity. For example, NPXY motif of the $\beta 1$ integrin is critical for PTB-mediated binding to integrin cytoplasmic domain-associated protein (ICAP)1- α (Chang, Hoang et al. 2002). Also $\beta 3$ integrin binding to the PTB domain of talin requires the presence of the NPXY fold in the cytoplasmic tail of the integrin (Calderwood, Yan et al. 2002). Furthermore, a number of other PTB domain-containing proteins, such as Numb, Dok-1, Dab1, EPS8, and tensin, have been shown to interact with β integrin cytoplasmic tails via this mechanism, which supports the generality of this type of association (Calderwood, Fujioka et al. 2003).

Phosphorylation of the tyrosine (Y) within the NPXY module of the β integrin cytoplasmic tail, which is mediated by Src family kinases, is thought to be key to processes such as cell adhesion and migration (Sakai, Jove et al. 2001). The addition of phosphate group is thought to modulate the binding of integrin to distinct PTB-containing effectors. Indeed, whilst the binding of ICAP1- α is phosphorylation independent (Chang, Hoang et al. 2002), the association with Shc is facilitated by this event (Cowan, Law et al. 2000). On the other hand, phosphorylation of the NPXY motif decreases the affinity of talin binding (Oxley, Anthis et al. 2008).

The cytoplasmic portions of α integrins are also capable of forming associations with cytoplasmic proteins, and although these interactions are more elusive than those formed by β subunits, they also seem to modulate integrin affinity and function. Mammary-derived growth inhibitor (MDGI) has been recently shown to bind to the tail of several α integrin cytodomains, such as $\alpha 1$, $\alpha 2$, $\alpha 10$ and $\alpha 11$, and this is thought to suppress integrin function (Nevo, Mai et al.). $\alpha 5$ integrin cytoplasmic tail has been shown to form complexes with zonula occludens-1 (ZO-1) at the leading edge of migrating cells, in a process that requires PKC ϵ activation (Tuomi, Mai et al. 2009). Also, Rab21 has been demonstrated to associate with the cytoplasmic tails of α integrin subunits through their membrane proximal conserved segment GFFKR, in which residue R1161 appears to be particularly important (Pellinen, Arjonen et al. 2006). Integrin $\alpha 1$ cytodomain can interact with T-cell protein tyrosine phosphatase (TCPTP) and this interaction activates the phosphatase, which in turn exerts negative regulation on EGFR phosphorylation (Mattila, Pellinen et al. 2005). Paxillin, a signalling adaptor protein, has been shown to bind to a 9 amino acid region (983-

991) in the $\alpha 4$ integrin cytodomain and this interaction is implicated in $\alpha 4$ integrin signalling (Liu and Ginsberg 2000). Interactions between the $\alpha 2$ as well as α_{IIb} cytotail and cytoplasmic molecules have also been described. CIB associates with a hydrophobic 15 amino acid membrane-proximal region of α_{IIb} cytotail (Barry, Boudignon-Proudhon et al. 2002), whilst $\alpha 2$ cytodomain directly associates with F actin (Kieffer, Plopper et al. 1995).

1.2.4 Integrin signalling

Integrin adhesion to their extracellular substrates exerts effects on a number of signal transduction pathways, which modulate a variety of cellular processes and behaviours, such as gene expression, proliferation, growth, apoptosis, cell shape, polarity and motility. Signalling downstream of integrins is similar to and intimately linked with signal transduction events originating from receptors for soluble ligands, such as G protein-coupled receptors (GPCRs) or receptor kinases. Importantly, activation of signalling pathways originating from ligation of soluble molecules; such as EGF, PDGF or thrombin; to their corresponding receptors, frequently requires adhesion of cells to the matrix via integrin receptors, in a way that determines anchorage dependence of cell survival and proliferation (Assoian 1997). An interesting feature of integrins, is their ability to signal bidirectionally. In other words, they can not only transduce information from extracellular stimuli (outside-in), but intracellular cues can also be translated into changes in the extracellular portions of the receptor (inside-out).

1.2.4.1 Importance of integrin activation

The majority of integrins can exist both in an inactive state, when they are not ligand-bound and do not transduce signals, or in an active form, that allows them to bind to extracellular ligands and signal to pathways within the cell. The ability to switch between these two activation states is crucial to their function.

A prime example of the importance of integrin activation is the regulation of the platelet integrin $\alpha IIb\beta 3$, which on circulating platelets exists in an inactive form. On platelet activation, a process triggered by thrombin, ADP, epinephrine (acting through appropriate GPCRs), von Willebrand factor (acting via GPIb/V/IX) or by collagen signalling through $\alpha 2\beta 1$ integrin, $\alpha IIb\beta 3$ is activated from within

the cell and can bind to fibrinogen, fibronectin and von Willebrand factor. This then allows their adhesion to blood vessel walls and aggregation with other platelets, leading to clot formation. Tight regulation of activation and inactivation prevents inactive platelet binding to fibrinogen, which could result in thrombosis, whilst allowing activated platelets to drive blood clotting, thus preventing hemorrhages (Kato 1997). Similarly, rapid activation of $\beta 2$ integrins on white blood cells allows their recruitment to infection sites and their immune function (Hogg, Henderson et al. 2002). The importance of integrin activation in human physiology and disease is further evidenced by two genetic disorders: Glanzmann thrombasthenia and leukocyte adhesion deficiency-3 (LAD-III). Glanzmann thrombasthenia is an inherited bleeding disorder, which can be caused by either deficiency or defects in the $\alpha \text{IIb}\beta 3$ integrin. Isolation of mutagen-induced thrombasthenia variants incapable of ligand binding, has identified mutations in the extracellular sites responsible for ligand binding, as well as in the sites of the cytoplasmic domain that mediate activation of the integrin. Interestingly, variants that have displayed defective integrin activation, but have shown no alterations in integrin sequence were also detected and this has indicated that mutated molecules responsible for integrin activation could be implicated in the generation of this thrombasthenia variant (Baker, Tozer et al. 1997). LAD-III is a condition manifested by immune defects and bleeding disorders, and is caused by mutations in *KINDLIN-3* gene, which result in the loss of kindlin-3 protein expression, and this in turn negatively affects integrin activation (Svensson, Howarth et al. 2009). Finally, even though rapid changes in the activation state have not been demonstrated for all integrins, it is believed that these processes are utilised by most, if not all, heterodimers to regulate cell adhesion in a spatio-temporal manner during dynamic processes such as cell invasion and metastasis (Hynes 2002).

1.2.4.2 Insights into integrin activation mechanism

Integrin activation is a shift from a low to a high affinity conformation for ligand binding and can be triggered from two directions. Firstly, the reorganisation of the extracellular domain of the receptor can be triggered by extracellular stimuli and ligand binding (outside-in). Secondly, high affinity cues can originate from within the cell, a process referred to as inside-out signalling.

It is believed that integrins are in the low affinity conformation for ligand binding when their extracellular domains are bent, and are in the high affinity state when these extend (Fig. 1.6A). Two models for integrin activation have been proposed, and they suggest different sequences of ligand binding and extension events. The switchblade model argues that only integrins with extended extracellular domains will bind the ligand (Luo, Carman et al. 2007), whereas the deadbolt model proposes that the extension can only occur following ligand binding (Xiong, Stehle et al. 2003). Both these models agree that ligand binding is facilitated by conformational changes within the extracellular head domain of the integrin. Indeed, the I/A domain of a collagen binding $\alpha 2\text{B1}$ integrin, has been shown to cooperate with the metal ion and the glutamate residue within the collagen recognition site, in the reorganisation and opening of the upper surface of the I/A domain, thus making it available for collagen binding. The conformational changes in the upper surface of the domain are then propagated to the lower part of the motif and could also extend to the rest of the molecule thus allowing the initiation of signalling cascades (Emsley, Knight et al. 2000). Subsequent studies have confirmed that the open conformation of the I/A domain is active and shows affinity for ligand binding, whilst the closed form is inactive and ligand-unbound. The transition from an inactive to active state occurs due to activating stimuli such as ligand binding or metal ion (such as Mn^{2+}) occupancy (Xiong, Li et al. 2000). Furthermore, a disulphide bond engineered in the C-terminus of the I/A domain, locks the integrin in an inactive conformation, whilst its disruption opens it and makes it available for ligand binding (Lu, Takagi et al. 2001; Shimaoka, Lu et al. 2001).

The transmembrane domains of both subunits of the heterodimer are also crucial for integrin activation, and in an inactive state are thought to associate with one another through GxxxG dimerisation motifs to form a coiled-coil association. Separation of the transmembrane domains is required for the transition from low affinity to high affinity mode (Gottschalk 2005).

The cytoplasmic tails of α and β integrins can interact with one another and this association is key to modulating integrin affinity and activation from within the cell. It has been shown for the platelet $\alpha \text{IIb}\beta 3$ integrin, that deletion of the entire cytoplasmic domain of the α subunit, or disruption of the conserved GFFKR sequence, generates a constitutively active integrin, thus suggesting that

this region acts as a negative regulator of activation and maintains low affinity state of the integrin (O'Toole, Mandelman et al. 1991; O'Toole, Katagiri et al. 1994). Similarly, 7 amino acids within the conserved membrane proximal region of the $\beta 3$ subunit control the ligand binding activity of the extracellular domain and have been demonstrated to maintain a low affinity state of the receptor (Hughes, O'Toole et al. 1995). It has subsequently been proposed, that these cytoplasmic regions of both α and β subunits, can maintain the low affinity states through the formation of a salt bridge between R995 in $\alpha 1b$ and D723 in $\beta 3$, which stabilises the association of α and β transmembrane domains and this locks the integrin in a closed, inactive conformation (Hughes, Diaz-Gonzalez et al. 1996). Indeed, an NMR study confirmed that this salt bridge maintains a low affinity constraint and forms a part of an interface between membrane proximal regions of α and β cytoplasmic tail (Vinogradova, Velyvis et al. 2002). Vinogradova also observed that talin binding to the cytoplasmic portion of integrin displaces cytoplasmic tail association. It has therefore been proposed that integrin activation necessitates separation of the α and β transmembrane and cytoplasmic domains. Indeed, FRET studies performed on cytoplasmic tails of $\alpha L\beta 2$ integrin confirmed the requirement for unclasping of cytoplasmic domains in integrin activation and bidirectional signalling (Kim, Carman et al. 2003). Also, the separation of transmembrane domains has been demonstrated to be necessary for integrin activation (Partridge, Liu et al. 2005). By contrast, introduction of disulfide bridges that oppose α and β tail dissociation locks the receptor in an inactive state (Luo, Springer et al. 2004), thus further substantiating the need for cytoplasmic domain unclasping in integrin activation.

1.2.4.3 Integrin activation by talin and kindlin as an example of inside-out signalling

As mentioned in the previous section, the affinity of an integrin for its ligand is tightly regulated by the structure of the receptor, and can be controlled from within the cell through the binding of activation mediators, such as talins and kindlins to the cytoplasmic portion of the integrin.

Talins are represented in mammals by two isoforms, talin1 and talin2 (Monkley, Pritchard et al. 2001) and both of these comprise an N-terminal head domain and a C-terminal actin-binding domain connected by a flexible rod region. The

head domain consists of FERM (4.1, ezrin, radixin, moesin) domain, with 3 main subdomains (F1, F2 and F3) and the F3 motif resembles a PTB domain and binds the NPXY motif on the integrin cytoplasmic tail (Garcia-Alvarez, de Pereda et al. 2003). The helical rod contains numerous vinculin binding sites as well as an additional integrin recognition site. Furthermore, it is believed that talin owes its ability to increase integrin affinity to the presence of an additional integrin binding site within the head domain. Upon PTB domain binding to the membrane distal NPXY motif within the β -cytotail, an additional loop contained within the F3 domain binds to the membrane proximal region of the cytoplasmic β -tail, which mediates the interaction between the two subunits of the heterodimer. This in turn displaces the α tail, thus opening up their extracellular domain and yielding a high affinity conformation of the receptor (Fig. 1.6B) (Wegener, Partridge et al. 2007). Interestingly, the capacity for integrin-binding is tightly controlled by conformational constraints within the talin molecule, which are imposed by the binding of the C-terminus of the rod domain to the PTB fold within the head domain. It is not entirely clear how this control is achieved and how the intramolecular autoinhibitory interaction is abrogated to facilitate integrin binding. It is thought that binding of phosphatidylinositol-4,5-bisphosphate (PtdIns(4,5)P₂) to talin, promotes its activation by liberating the integrin recognition sites and thus increases its association with the heterodimeric receptor (Martel, Rocaud-Sultan et al. 2001). There is also evidence for GTPase-mediated talin activation routes in hematopoietic cells, where the activity of a GTPase, Rap1, is required for talin-driven integrin β 1 and β 3 integrin activation (Sebzda, Bracke et al. 2002). This is thought to depend on formation of a talin/Rap1/RIAM (Rap1 interacting molecule) complex on the β -integrin tail (Watanabe, Bodin et al. 2008). Furthermore, phosphorylation of the tyrosine residue contained within the NPXY motif of the β -integrin cytoplasmic tail adds an extra level of complexity to the tight regulation of talin/integrin association. Indeed, addition of a phosphate group to the NPXY motif, has been shown to decrease the affinity with which it can bind the F3 domain on talin (Oxley, Anthis et al. 2008).

Talin is not the only regulator of integrin inside-out activation. A family of FERM-domain containing proteins called kindlins, has recently emerged as capable of binding to a region in β 1, β 2 and β 3 integrin tails, which is located C-terminally

with respect to the talin-binding motif. Mammals express three distinct kindlin isoforms: kindlin1, kindlin2 and kindlin3, and all three localise to integrin-dependent adhesion sites. Kindlins are thought to be necessary modulators of integrin function and to be required for integrin to switch from a low affinity to a high affinity state, and ultimately for integrin activation (Montanez, Ussar et al. 2008). Kindlin-driven integrin activation depends on a direct interaction between kindlin and the β -integrin cytoplasmic tail. The kindlin FERM domain resembles that of talin, but is distinct in that it is split into two halves by a pleckstrin homology (PH) domain inserted into the F2 fold. It is believed that the F3 subdomain, which is similar to a PTB fold, mediates direct interaction with β -integrin tails and drives the integrin affinity switch (Kloeker, Major et al. 2004). In contrast to talin, which binds to the membrane proximal NPXY motif in the β -integrin cytoplasmic tail, kindlin has affinity primarily for the distal NXXY domain in the β 1, β 2 and β 3 cytoplasmic tails. In light of the fact that talin and kindlin bind to two distinct regions of the cytoplasmic domain of β integrins, and given the requirement for kindlin in talin-mediated integrin affinity modulation and the insufficiency of kindlins for integrin activation, it is highly probable that they cooperate to promote integrin activation. As a consequence, two different mechanisms have been suggested to explain the sequence of events during integrin inside-out activation. According to the sequential model of binding, kindlin association with the membrane distal NXXY motif facilitates talin binding to the membrane proximal NPXY motif, which in turn displaces kindlin from the β -integrin tail and leads to integrin activation. However, due to distinct binding sites for both activators in the cytoplasmic tail of the integrin, simultaneous and cooperative interaction is also possible, but the order of events is thus far unclear (Fig. 1.6C) (Moser, Legate et al. 2009).

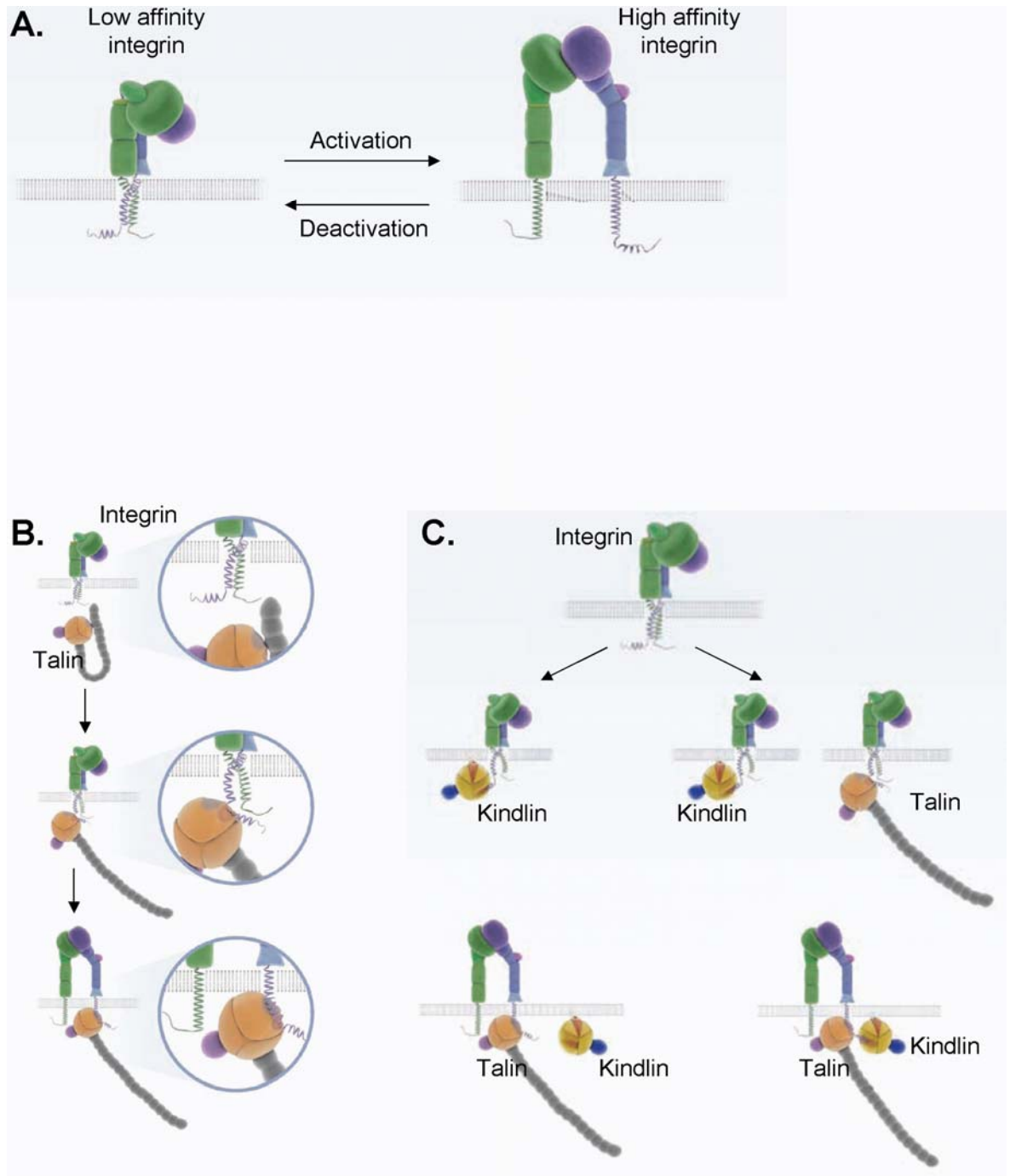


Figure 1-6 Mechanism of integrin activation.

A. Integrin heterodimers can switch from a bent inactive conformation to an active extended state. B. Integrin activation is mediated by talin binding to the NPXY motif in the β tail. Pulling forces on the β tail reorient the transmembrane domains of the heterodimer thus enabling transduction of conformational changes across the receptor. C. Proposed mechanisms for kindlin- and talin-driven activation of integrins. Kindlin binding to the β tail facilitates subsequent talin binding, which in turn displaces kindlin. Alternative model suggests simultaneous binding of kindlin and talin. Adapted from (Moser, Legate et al. 2009).

1.2.4.4 Outside-in signalling and regulation of the cytoskeleton

Upon ligand binding, conformational changes occur in the head and leg domains of the heterodimer, which result in the separation of the cytoplasmic tails thus making them available for interactions with cytoplasmic effector molecules. This in turn leads to the assembly of multimolecular complexes centred around the heterodimer, which organise the actin cytoskeleton and activate signalling pathways that lead to alterations in gene expression. Integrin receptors are devoid of catalytic activity and instead serve as scaffolds for the assembly of enzymatic and cytoskeleton-remodelling platforms. Over 150 adaptor, structural and signalling molecules have to date been associated with integrin-mediated adhesions (Zaidel-Bar, Itzkovitz et al. 2007).

Integrins are known to control the activity of cyclin D1, both at the level of transcription and protein accumulation, and this is thought to be the major hub through which integrins affect cell cycle progression and proliferation (Walker and Assoian 2005). This has been proposed to be mediated by extracellular signal-regulated kinase (ERK), whose activity can be promoted by integrin-driven adhesion in a number of ways. Firstly, as a result of integrin activation, focal adhesion kinase (FAK)/Src signalling complexes are formed. This is initiated by autophosphorylation of FAK at tyrosine 397, which in turn creates a binding site for the Src homology 2 (SH2) domain of Src (Schaller, Hildebrand et al. 1994). Upon association of Src with FAK, Src can catalyse phosphorylation of other tyrosine residues on FAK, which in turn opens new binding sites for downstream effectors, such as growth factor receptor binding protein-2 (Grb-2) or Shc, and stimulates Ras-Raf-MEK-ERK pathway (Schlaepfer, Hanks et al. 1994). Src can also phosphorylate a FAK-associated protein, Crk associated substrate (p130Cas), and therefore form a binding pocket for the adaptor protein Crk (Cary, Han et al. 1998; Klemke, Leng et al. 1998), which in turn can activate ERKs. Additionally, active FAK can associate with phosphatidylinositol-3-kinase (PI3K), which leads to the activation of the latter (Chen and Guan 1994), and this in turn can potentiate ERK signalling. Secondly, selected α -integrin subunits can associate with the Src family kinase Fyn, through an adaptor protein caveolin-1. Activation of Fyn drives the recruitment and activation of Shc, which switches on the Ras-Raf-MEK-ERK signalling pathway (Wary, Mariotti et al. 1998). Finally,

active integrins can activate Raf by recruiting protein kinase C (PKC) (Miranti, Ohno et al. 1999).

Integrin-mediated adhesion also affects cell survival and this occurs through the PI3K-driven stimulation of protein kinase B (PKB/Akt) activity and Bcl-2 expression. Additionally, integrin binding to its ligand, activates c-Jun N-terminal kinase (JNK) (Almeida, Ilic et al. 2000) and nuclear factor κ B (NF κ B) (Weaver, Lelievre et al. 2002), thus also enhancing survival signals.

Not only do integrins affect signalling pathways that modulate survival, growth and proliferation, they also link physically to the actin cytoskeleton, thus controlling cell shape and motility. Proteins such as talin, filamin and α -actinin can directly connect integrins to F-actin. Kindlin, FAK, paxillin and integrin-linked kinase (ILK) directly associate with integrins, but indirectly regulate the actin cytoskeleton. Vinculin, on the other hand, does not directly interact with integrins but does so with actin (Legate, Wickstrom et al. 2009). Upon integrin-mediated adhesion, the primary link between the ligand-bound integrin and the cytoskeleton is established through direct talin binding to the integrin and talin's actin-binding capacity (Zhang, Jiang et al. 2008), which is immediately followed by the recruitment of vinculin. Vinculin can associate with both talin and actin, thus acting as a crosslinker and stabilising the interaction (Humphries, Wang et al. 2007). α -actinin, is then also recruited to strengthen the adhesion that is further regulated by ILK, which forms a link between integrin and paxillin, which then binds to parvin and vinculin (Legate, Montanez et al. 2006). The affinity of α -actinin to actin can be modulated by its phosphorylation by FAK (Izaguirre, Aguirre et al. 2001). The above-described attachment of integrins to F-actin is necessary for cell protrusion and retraction during cell migration. This is achieved by tightly regulated F-actin polymerisation at the edge of the lamellipodium and requires the actin nucleation function of Arp2/3 complex, which mediates the assembly of branched actin filaments (Serrels, Serrels et al. 2007). Arp2/3 is recruited to the adhesion sites through its interactions with FAK and vinculin (DeMali, Barlow et al. 2002). The activity of Arp2/3 requires the binding of Wiskott-Aldrich Syndrome protein (WASP), which induces conformational changes in Arp2/3 thus allowing it to serve as actin filament elongation template (Pollard 2007). Subsequently, actin polymerisation

generates protrusive force at the leading edge of the lamellipodium, hence driving forward cell movement.

1.3 Integrin trafficking

It is now well-established that integrin receptors undergo endocytic-exocytic transport, a process that encompasses continual receptor internalisation from the plasma membrane into internal membraneous compartments, and subsequent sorting to different cellular locations followed by return of the internalised receptors to the plasma membrane (Bretscher 1989; Pellinen and Ivaska 2006; Caswell, Vadrevu et al. 2009). This cascade of events is frequently referred to as receptor trafficking and is recognised to affect their function. Integrin trafficking events are thought to facilitate the establishment and maintenance of cell polarity, to contribute to cell migration and to modulate Rho GTPase-mediated signalling (Pellinen and Ivaska 2006; Caswell, Vadrevu et al. 2009).

1.3.1 *Different routes to endocytosis*

The first stage in the trafficking of integrins is their internalisation from the plasma membrane, and this can occur through two main endocytic routes: clathrin-mediated endocytosis (CME) and clathrin-independent endocytosis (Fig. 1.7). During CME, cytoplasmic clathrin molecules assemble at the receptor-containing sites of the plasma membrane and form clathrin-coated invaginations, which then detach from the membrane, in a process that requires dynamin GTPase, to form clathrin-coated vesicles (Conner and Schmid 2003). The formation of clathrin-coated pits and vesicles is orchestrated by endocytic adaptor proteins, such as adaptor protein-2 (AP-2) or epsin, which can selectively package specific receptors, into clathrin-vesicles (Hirst and Robinson 1998). Following internalisation, clathrin-coated vesicles are deprived of their coating and fuse with early/sorting endosomes, where the fate of their cargo is decided. Clathrin-independent endocytosis (CIE) is thought to proceed via three distinct routes: dynamin-dependent caveolar endocytosis, frequently referred to as raft/caveolar endocytosis (RCE), dynamin-independent macropinocytosis (Nichols and Lippincott-Schwartz 2001), as well as through non-caveolar CIE

routes. RCE requires cholesterol-rich membrane rafts, which provide sites of enrichment for proteins that require endocytosis, and caveolae - minute uncoated plasma membrane pits that are frequently enriched in caveolin-1 (Nichols 2003). This endocytosis route delivers plasma membrane receptors to endosomal-like structures called caveosomes, which are distinct from early or recycling endosomes - structures that originate from the CME pathway. On the other hand, non-caveolar CIE internalisation proceeds via a mechanism that is regulated by RhoA (Lamaze, Dujancourt et al. 2001), ADP-ribosylation factor 6 (Arf6) (Radhakrishna and Donaldson 1997) or Cdc42 (Sabharanjak, Sharma et al. 2002). This pathway employs clathrin-independent carriers (CLICs), which are thought to be uncoated tubular or ring-shaped structures (Kirkham, Fujita et al. 2005), contain glycosylphosphatidylinositol-anchored proteins (GPI-APs) and have recently been shown to be implicated in endocytic sorting at the leading edge of migrating cells (Howes, Kirkham et al.). CLICs originate directly from the plasma membrane, and whilst they acquire early endosomal antigen (EEA)-1 and Rab5, they mature into the GPI-enriched early endosomal compartment (GEEC). The GEEC then fuses with the early endosomal compartment (Kalia, Kumari et al. 2006). Despite the different origin of the CME and CIE pathways, they do seem to intersect as receptors internalised through the CIE route appear to be sorted from caveosomes into early and recycling endosomes (Pelkmans, Burli et al. 2004).

Some receptors can only enter the cell through one internalisation route, for example the transferrin receptor is obliged to use clathrin-mediated endocytosis, while others, such as EGFR1 are more promiscuous with regard to their route into the cell (Sigismund, Argenzio et al. 2008). Similarly, particular integrin heterodimers can also enter the cell via more than one endocytosis pathway, as it is exemplified by the internalisation of $\alpha 5\beta 1$ and $\alpha v\beta 3$ integrins (Caswell, Vadrevu et al. 2009). In the next section, I will focus on the internalisation routes of the $\beta 1$ integrins and particularly on what is known about the endocytosis of the major fibronectin-binding receptor, $\alpha 5\beta 1$ integrin.

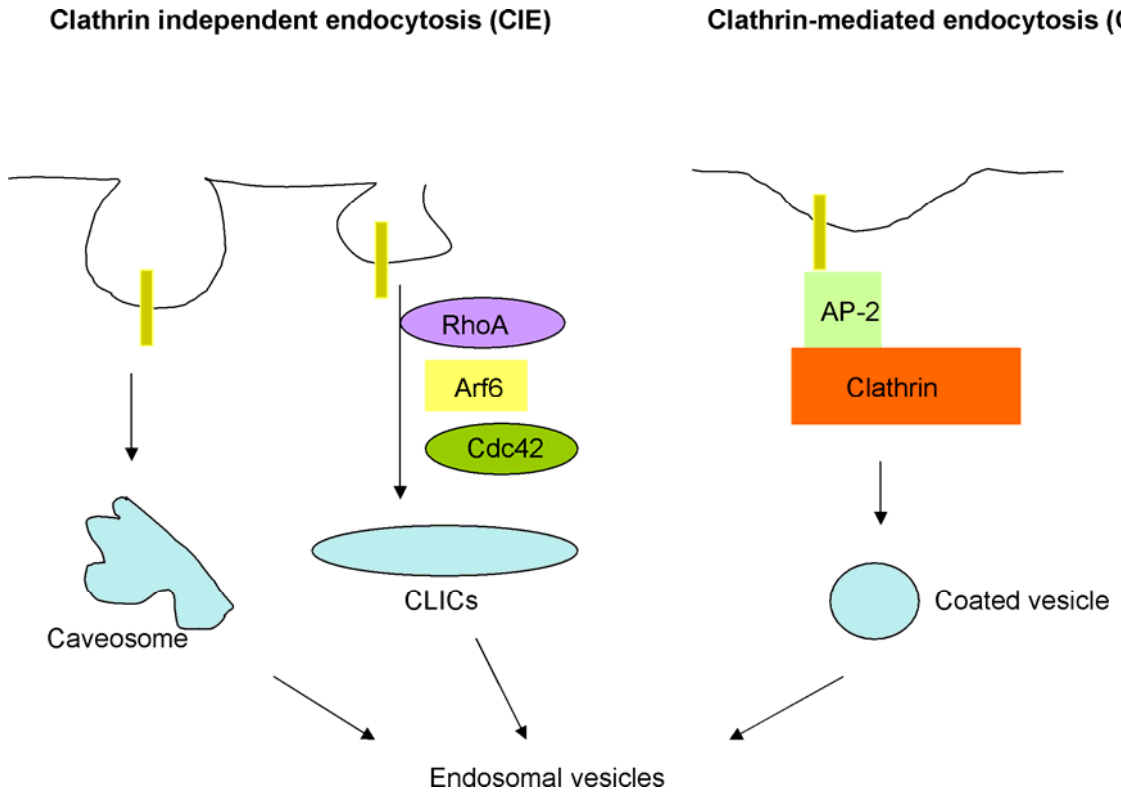


Figure 1-7 Main endocytosis routes.

Transmembrane receptors can be internalized via two main routes: clathrin dependent and clathrin independent endocytosis. Clathrin-mediated internalization requires a coat protein - clathrin - and a number of adaptor proteins such as AP-2 or Numb. Caveolar endocytosis does not depend on coat proteins but also requires dynamin-1. Non-caveolar clathrin-independent endocytosis requires regulation from RhoA, Arf6 and Cdc42. Receptors internalized through either of the pathways proceed to early endosomes for sorting.

1.3.1.1 Clathrin-mediated and clathrin-independent β 1 integrin internalisation

α 5 β 1 integrin is constitutively internalised, and can undergo both clathrin-mediated and caveolar endocytosis. As mentioned previously, the cytoplasmic portions of β subunits contain membrane proximal and membrane distal NXXY motifs, and these conserved sequences are known to recruit surface receptors, such as low density lipoprotein (LDL) (Chen, Goldstein et al. 1990) or insulin receptors (Rajagopalan, Neidigh et al. 1991), to clathrin coated structures, by allowing their interaction with adaptor proteins such as AP-2. Even though the initial studies, which utilised mutants either lacking the NXXY motifs or ones that contained mutated tyrosine residues, indicated no requirement for the conserved NXXY sequence in the internalisation of α 5 β 1 integrin (Vignoud, Usson et al. 1994), more recent approaches contradict this observation. Indeed, expression of β 1 integrin mutant β 1YYFF - in which tyrosine residues of the NXXY motif were substituted with phenylalanines - in β 1-null mouse embryonic fibroblasts (MEFs), clearly showed an endocytosis defect. Furthermore, integrin endocytosis was reduced in β 1YYFF MEFs isolated from mice that harboured this mutation in the germline in comparison to wild type MEFs, and the endocytosis of the wild type β 1 integrin was inhibited by a clathrin antagonist, thus further supporting the requirement for the conserved NXXY motif in clathrin mediated endocytosis of α 5 β 1 integrin (Pellinen, Tuomi et al. 2008).

Clathrin adaptors, other than the previously mentioned AP-2, have also been shown to recruit β 1 integrin cargos to clathrin-coated pits. Both disabled-2 (DAB2) and Numb, contain PTB domains, which can interact with NPXY motifs in the cytoplasmic tails of integrins, thus contributing to clathrin-mediated endocytosis of these receptors. Indeed, suppression of Numb by RNAi or interfering with its recruitment to clathrin coated structures (CCS) through its phosphorylation by atypical protein kinase C (aPKC), inhibits α 5 β 1 internalisation (Nishimura and Kaibuchi 2007). Although DAB2 has been shown to mediate clathrin-dependent endocytosis of β 1 integrins, binding of DAB2 to the NPXY motif of the β integrin tail is controversial. Even though DAB2 and β 1 integrin are known to bind to each other *in vitro* (Calderwood, Fujioka et al. 2003) and have been shown to coimmunoprecipitate from murine mammary epithelial cells (Prunier and Howe 2005), two research groups have been unable to reproduce

this interaction in HeLa cells (Chetrit, Ziv et al. 2009; Teckchandani, Toida et al. 2009), which argues against their direct association.

Not only is it still a subject of debate whether DAB2 can recruit integrins to clathrin-coated pits by a direct association with their $\beta 1$ cytotails, a consensus view on the location of this process and the activation status of the integrin that follows this route into the cell is still missing. One study has shown that DAB2 can recruit $\beta 1$ integrins to clathrin coated pits, when the integrins are dispersed along the cell surface, suggesting that it can control the bulk endocytosis of inactive integrins (Teckchandani, Toida et al. 2009). In contrast, another report implicates DAB-2 in the endocytosis of only active conformation integrins during focal adhesion turnover (Chao and Kunz 2009). In line with the view that certain endocytic machineries can select for integrin receptors in particular conformations is a study by Valdembri and colleagues, which identifies neuropilin 1 (NRP1) as a component of the integrin endocytic route in endothelial cells. This transmembrane glycoprotein supports the efficient endocytosis of active $\alpha 5\beta 1$ integrin at adhesion sites, whilst being dispensable for internalisation of inactive $\alpha 5\beta 1$ heterodimers. NRP1 supports $\alpha 5\beta 1$ internalisation by providing a physical link between the integrin and the endocytic adaptor GAIIP interacting protein C1 (GIPC1) (Valdembri, Caswell et al. 2009), thus linking the heterodimer to motor myosin VI (Myo6) which has also been proposed to be implicated in vesicular transport of protein cargos (Frank, Noguchi et al. 2004).

Whilst there is a growing body of evidence supporting clathrin-mediated endocytosis of $\beta 1$ integrins and explaining its molecular basis, reports on clathrin-independent internalisation of this receptor are still scarce. Nonetheless, as it was mentioned briefly above, there is clear evidence that in the context of mutant $\beta 1$ integrin ($\beta 1^{YYFF}$), which lacks the NXXY motif, expression of Rab21 can induce clathrin-independent endocytosis of this receptor (Pellinen, Tuomi et al. 2008). Also, in myofibroblasts endocytosis of $\alpha 5\beta 1$ integrin and its ligand fibronectin have been shown to depend on the expression of caveolin-1 (Shi and Sottile 2008). The modes of $\beta 1$ integrin recruitment to caveosomes and their entry into the cell via this route remain mostly unresolved and need further investigation. One possible molecular mechanism of clathrin-independent internalisation of integrins is provided by a

study, which identified protein kinase C alpha (PKC α), as necessary for caveolae-mediated internalisation of α 2B1 (Upla, Marjomaki et al. 2004). It is therefore possible that binding of PKC α to cytoplasmic domains of B1 integrin (Ng, Shima et al. 1999) can drive integrin endocytosis via this route.

1.3.2 Integrin recycling

Integrin recycling is defined as the return of these heterodimeric receptors to the plasma membrane, where they can re-engage with the extracellular matrix components or with counter-receptors on neighbouring cells, and most reports indicate that after internalisation the majority of the integrin is indeed returned to the cell surface, rather than undergoing lysosomal degradation (Bretscher 1989; Roberts, Barry et al. 2001). After internalisation by one of the above discussed routes, integrins reach early endosomes, where sorting events occur (in a Rab5 family protein dependent manner), which destine these receptors either for travel to late endosomes and lysosomes or for recycling to the plasma membrane. Cargo progression from early endosomes to late endosomes is thought to occur through the replacement of early endosomal Rab5 with late endosomal Rab7, and this is mediated by a Rab7 GEF - the class C VPS/HOPS complex - that interacts with Rab5 thus mediating this conversion (Rink, Ghigo et al. 2005).

Receptor return to the plasma membrane can occur through two distinct routes, in a direct and Rab4-dependent manner (short loop) or through a Rab11- and/or Arf6-dependent pathway (long loop) (Fig. 1.8). The latter requires the delivery of the recycling cargo from sorting endosomes to the perinuclear recycling compartment (PNRC) - which is located near to the microtubule organising centre and is often enriched in the Rab11 family GTPases - prior to its trafficking to the plasma membrane (Caswell, Vadrevu et al. 2009). These two recycling pathways differ with respect to the integrins, whose trafficking they supervise, and the signalling cascades that modulate them, but are similar in that both are tightly controlled. Indeed, PDGF-driven recycling of α v β 3 integrin through the short-loop endocytic pathway (Roberts, Barry et al. 2001) relies on a direct interaction between the C-terminal domain of the β 3 cytoplasmic tail and protein kinase D1 (PKD1) (Woods, White et al. 2004).

On the other hand, recycling of $\beta 1$ heterodimers proceeds through the PNRC and is controlled by Rab11, in a way that is promoted by kinases such as protein kinase B (PKB/Akt) (Roberts, Woods et al. 2004) or protein kinase C epsilon (PKC ϵ) (Ivaska, Whelan et al. 2002). Roberts and colleagues have shown that whilst $\alpha 5\beta 1$ integrin internalisation and delivery to the recycling compartment was independent of PKB/Akt, its return to the plasma membrane was regulated by the activity of PIP-3 kinase and PKB/Akt. Furthermore blockade of integrin recycling, which was implemented by inhibition of PKB/Akt, can be reversed by expression of inactive mutant of glycogen synthase kinase 3 (GSK-3), thus suggesting that PKB/Akt acts via GSK-3 inactivation to promote integrin recycling. This was further substantiated when integrin recycling was suppressed by the expression of active GSK-3 mutant, which is insensitive to phosphorylation-mediated inactivation by PKB/Akt. PKB is also thought to mediate the recycling of integrins by phosphorylating ACAP1 (Arf6 GTPase activating protein with coiled-coil, ANK repeat and PH domain protein 1), which when phosphorylated binds directly to internalised $\beta 1$ integrin and promotes its recycling (Li, Ballif et al. 2005). By contrast, PKC ϵ is thought to contribute to the recycling of internalised $\beta 1$ integrins by phosphorylating an intermediate filament protein, vimentin, which may facilitate integrin recycling by releasing mechanical constraints on integrin recycling vesicles. Indeed, upon inhibition of PKC ϵ and vimentin phosphorylation integrins become trapped in intracellular vesicles and fail to return to the plasma membrane (Ivaska, Vuoriluoto et al. 2005).

It is not only Rab11, but also Arf6, that contributes to the recycling of $\beta 1$ integrin from the PNRC to the plasma membrane upon serum stimulation and this process requires the actin cytoskeleton in an Arf6-dependent manner (Powelka, Sun et al. 2004). Furthermore, a key contribution to the recycling of $\beta 1$ integrin heterodimers is made by GTPases of the Rab5 family, as shown by studies focused on Rab21 and Rab5. Rab21 has been demonstrated to associate with several integrin α subunit cytoplasmic tails to facilitate the trafficking of these receptors, and this is dependent on Rab21 being in its active conformation. Indeed, expression of a Rab21-GDP-locked mutant leads to the accumulation of active integrin in large focal adhesion sites, whilst nucleotide

exchange and the presence of Rab21-GTP allows for the initiation of the β 1-endocytic pathway (Pellinen, Arjonen et al. 2006).

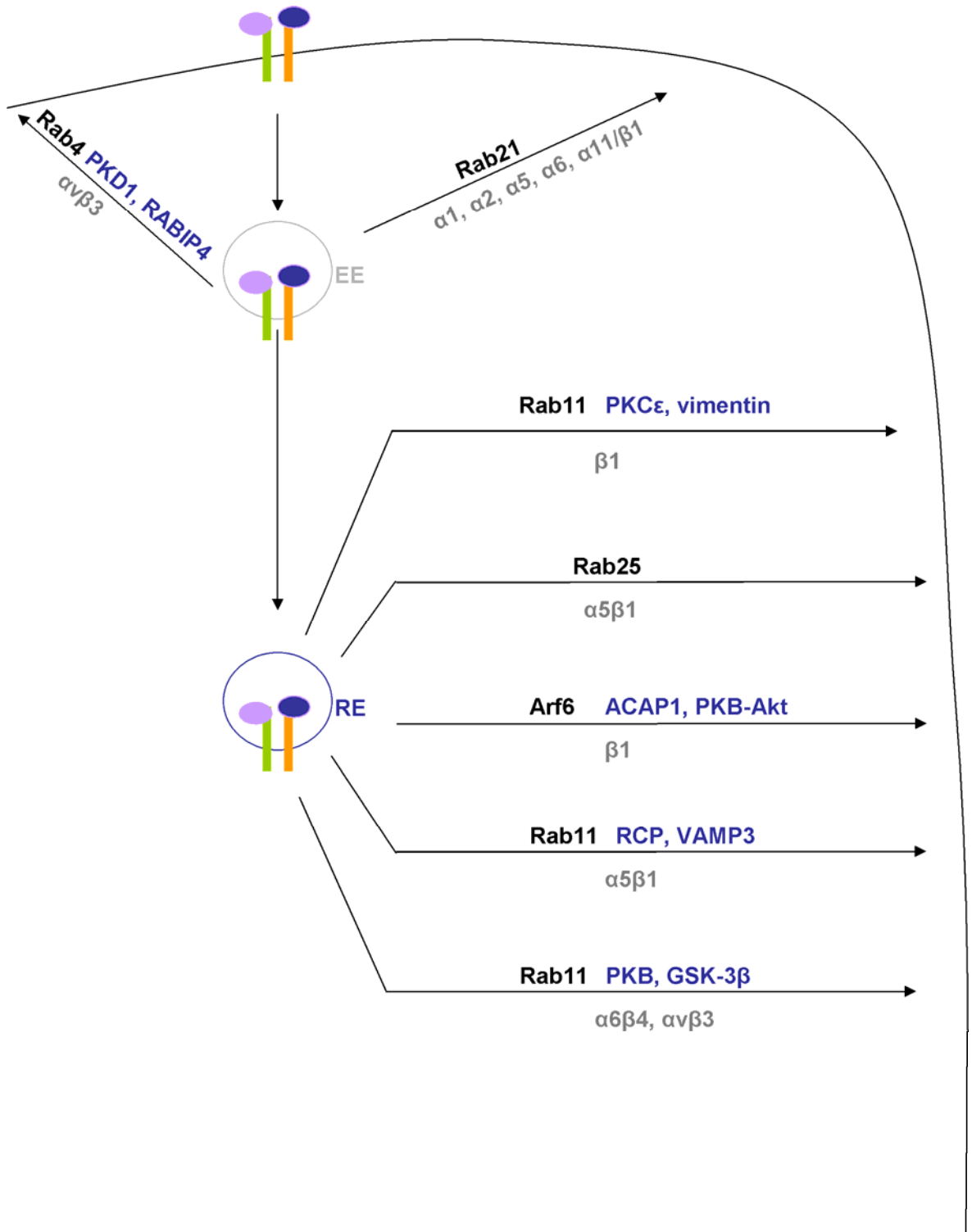


Figure 1-8 Schematic summary of integrin trafficking pathways.

Internalised heterodimers are trafficked to early endosomes from which they can directly and rapidly recycle back to the plasma membrane in a Rab4-dependent manner (short loop). Alternatively they can be transported to the perinuclear recycling compartment, from which they return to the cell surface in a Arf6/Rab11-dependent pathway (long loop).

1.3.3 Signalling endosomes

It is well established that endosomes can function to terminate signalling processes through receptor internalisation and degradation, but they are also recognised to act as platforms for the assembly of signalosomes downstream of signalling receptors (Miaczynska, Pelkmans et al. 2004; Gould and Lippincott-Schwartz 2009). It is also known that internalisation and recycling of receptors influence which of the downstream effectors are activated and also determine whether the nature of this activation is transient or sustained. Signalling downstream of Epidermal growth factor receptor (EGFR) is a good example of endocytosis-mediated modulation of receptor-activated pathways. Upon EGFR internalisation, Grb2 (growth factor receptor-bound protein 2), Shc (Src-homology containing protein) and SOS (son of sevenless) remain in association with EGFRs and this allows persistent signalling through the Ras-MAPK pathway on the endosomes (Di Guglielmo, Baass et al. 1994). In contrast, endocytosis of EGF receptors diminishes their signalling to PI3-kinase, due to the limited access of the receptor to PtdIns(3,4)P₂ in the vesicles (Haugh and Meyer 2002). Furthermore, distinct EGFR internalisation modes exert different effects on the longevity of signalling downstream of this receptor. EGFR can be endocytosed via clathrin-independent pathways, but it is CME that is mostly employed for the delivery of that receptor to intracellular vesicles. CME of EGFR has been shown to favour the recycling of the internalised receptor to the plasma membrane, thus prolonging the duration of EGFR-activated signalling (Sigismund, Argenzio et al. 2008). By contrast, clathrin-independent and lipid raft-dependent internalisation of EGFR predominates when this receptor becomes ubiquitinated following activation with high doses of EGF (Sigismund, Woelk et al. 2005), and this endocytosis route attenuates EGFR-signalling by targetting it for degradation (Sigismund, Argenzio et al. 2008).

Also other receptor tyrosine kinases have been shown to be capable of signalling from endosomes. The endosomal fraction of the platelet-derived growth factor receptor (PDGFR) has been shown to be specifically activated without the activation of the plasma-membrane pool of PDGFR. This in turn recruited signalling molecules such as Grb2, Shc, phospholipase C-gamma1 (PLC-γ1) and p85alpha subunit of PI3-K to PDGFR-positive endosomes and led to the activation

of signaling pathways involved in cell proliferation and survival (Wang, Pennock et al. 2004). Moreover, the nerve growth factor (NGF) has been proposed to induce the formation of signalling endosomes following the observation that it was bound to its activated receptor TrkA on endosomal structures. Under these conditions, TrkA was tyrosine-phosphorylated and bound to PLC- γ 1, which points to its competency for the initiation of signal transduction from endosome (Grimes, Zhou et al. 1996). Furthermore, internalization of β_2 -adrenergic receptor (β_2 -AR) into endosomal compartments is crucial for the full activation of MAPK pathway, as evidenced by the attenuation of Raf-mediated activation of MEK following endocytosis inhibition. This suggests that signalling cascades downstream of some GPCRs are preferentially activated after receptor internalisation into the endocytic pathway (Daaka, Luttrell et al. 1998).

Signalling endosomes have been implicated in regulation of signal transduction events within the osteoblastic niche and this occurs through intercellular transfer to signalling endosomes. Haematopoietic stem-progenitor cells (HSPCs) have been shown to make contacts with osteoblasts through membrane domains containing prominin 1, CD63 and rhodamine-phosphatidylethanolamine. At the contact sites, portions of these membrane domains were taken up by osteoblasts and internalised into SARA (SMAD anchor for receptor activation)-positive signalling endosomes. This in turn led to attenuated Smad signalling and increased synthesis of Stromal-Derived Factor-1 (SDF-1, also known as CXCL12), which mediates homing of HSPC to bone marrow (Gillette, Larochelle et al. 2009). Another physiologically relevant example of the importance of endosomal signalling is the diversification of signalling pathways downstream of tumour-necrosis factor receptor-1 (TNFR1). CME of TNFR1 and CD95 is necessary for the recruitment of DISC proteins and the initiation of apoptotic cascade from the endosomal signalling complex. On the other hand, anti-apoptotic signals are generated independently of receptor endocytosis and this occurs through the binding of TNFR1 to RIP and TRAF2, which then activates NF- κ B and MAPK (Schutze, Tchikov et al. 2008).

1.3.4 Integrin trafficking in cell migration

The initial demonstrations of integrin internalisation and recycling have encouraged a proposal that these processes contribute to focal adhesion turnover and cell migration on 2D substrates. For a number of years, this contribution has been thought to be driven by integrin internalisation at the rear of a migrating cell, a process which enables detachment of the trailing edge. Upon integrin endocytosis, heterodimer-containing vesicles would be transported to the leading edge of the cell, where they could be returned to the cell surface to further facilitate attachment and forward cell movement (Fig. 1.9A) (Bretscher 1996). This concept of long-range transport of endosomal integrins during cell migration has thus far not been substantiated. Nonetheless, there is experimental data demonstrates specific trafficking of internalised integrins from one end of the cell to the other during processes other than cell migration, i.e. to and from the cleavage furrow, during and after cytokinesis (Pellinen, Tuomi et al. 2008). In contrast to the above proposed long-range movement of integrins during cell migration, the more generally accepted view is that integrin heterodimers are both endocytosed and returned to the plasma membrane toward the cell front (Fig. 1.9B) (Caswell, Vadrevu et al. 2009). Consistent with this are observations that clathrin dependent endocytosis is largely polarised to the front proportion of the cell (Rappoport and Simon 2003) and the recycling compartment is normally also positioned near to the leading edge of migrating cells (Pierini, Lawson et al. 2000). Further support to this view, is lent by the recent investigations, which have indicated that integrin trafficking is spatially restricted to the leading edge during migration of cancer cells on a 3D matrix. Indeed, this study reported that both integrin internalisation and recycling takes place at the cell front, thus retaining a cycling pool of integrin at the leading edge of migrating cells (Caswell, Spence et al. 2007). These workers have proposed that such spatially-restricted cycling of adhesion receptors may act to localise downstream signalling and also promote focal adhesion turnover and actin dynamics at the cell front so as to drive membrane protrusion and cell movement.

It is thought that integrin trafficking exerts effects on cell migration by regulating recycling of other cell surface receptors, such as EGFR (Caswell, Chan

et al. 2008) and by controlling the balance of downstream signalling to different Rho GTPases, such as Rac1 and RhoA. Epithelial cells move on 2D substrates with high persistence whilst maintaining a fan-like morphology. This is supported by the activity of Rac1, which encourages the formation of a flat lamellipodium at the front of the migrating cell and RhoA which limits the lamellipodial activity to the leading edge thus aiding in lagging end retraction. When the balance between the activities of these two GTPases is disturbed, the persistence of migration changes. Increased Rac1 activity leads to the extension of multiple processes at the cell front and results in directionality loss. The same phenotype occurs when signalling to RhoA is enhanced, as this weakens adhesion sites not only at the rear, but also at the front of the cell, thus collapsing lamellipodial extensions (Pankov, Endo et al. 2005). The disturbance in the Rac1/RhoA balance and switch from persistent to random migration can occur following a change in the expression levels of $\alpha\text{v}\beta\text{3}$ with respect to $\alpha\text{5}\beta\text{1}$ integrin (Danen, van Rheenen et al. 2005), but can also be affected by the trafficking of these two heterodimers (Caswell, Chan et al. 2008). When $\alpha\text{v}\beta\text{3}$ integrin is expressed, Rac1 signalling is promoted, whilst $\alpha\text{5}\beta\text{1}$ expression drives RhoA activation (Danen, van Rheenen et al. 2005). Furthermore, when $\alpha\text{v}\beta\text{3}$ integrin is competent to bind to its ECM ligands, it is actively recycled through the Rab4 route in a PKD1 dependent manner (Woods, White et al. 2004) and this renders $\alpha\text{5}\beta\text{1}$ recycling slow. Under these circumstances Rho activity is low and cells migrate persistently. Upon blockade of $\alpha\text{v}\beta\text{3}$ integrin with ligand mimetics, such as Cilengitide, the recycling of $\alpha\text{5}\beta\text{1}$ through a Rab11- and RCP-dependent pathway is favoured. This mediates the activity of Rho, which in turn signals to ROCK and results in directionality loss and drives random and fast cell migration on 2D. Additionally, increased $\alpha\text{5}\beta\text{1}$ cycling enhances the recycling of EGFR1 in a way that potentiates its autophosphorylation and activates pro-invasive PKB/Akt signalling (Caswell, Chan et al. 2008).

The PKC ϵ -dependent recycling of β1 integrin has also been shown to promote directional cell movement towards β1 integrin substrates and this requires the catalytic activity of this kinase. When the activity of PKC ϵ is inhibited, it becomes trapped together with β1 integrin in a CD81-positive compartment and this results in decreased directional motility (Ivaska, Whelan et al. 2002). This is thought to occur through PKC ϵ -driven phosphorylation of an intermediate

filament protein, vimentin, which has been proposed to facilitate integrin recycling possibly through a release of a mechanical constraint. On inhibition of PKC ϵ and vimentin phosphorylation, integrins become trapped in intracellular vesicles, fail to return to plasma membrane and haptotaxis is severely attenuated. On the other hand, ectopic expression of vimentin promotes cell motility in a way that requires PKC ϵ , as evidenced by mutagenesis of PKC sites on vimentin (Ivaska, Vuoriluoto et al. 2005). Also, Rab21-mediated trafficking of integrin heterodimers has been shown to affect breast and prostate cancer cell adhesion and motility. This GTPase associates with α subunit cytoplasmic domains of integrin heterodimers following integrin internalisation and it facilitates integrin endo/exocytic cycling. Suppression of Rab21 results in the inhibition integrin-mediated cell adhesion and migration, whilst its overexpression promotes cell adhesion and motility (Pellinen, Arjonen et al. 2006)

An interesting insight into the contribution of integrin trafficking and degradation to cell migration has been provided by recent findings, which demonstrate that in migrating fibroblasts a proportion of internalised $\alpha 5 \beta 1$ integrin is sorted to multivesicular endosomes (MVEs) together with its ligand, fibronectin. These can be then routed from MVEs to lysosomes for degradation. This process requires fibronectin-mediated ubiquitination of the $\alpha 5$ subunit as well as the interaction of $\alpha 5 \beta 1$ with endosomal sorting complex required for transport (ESCRT) and is thought to control cell migration by preventing the accumulation of ligand-bound integrin on the endosomal pathway (Lobert, Brech et al.).

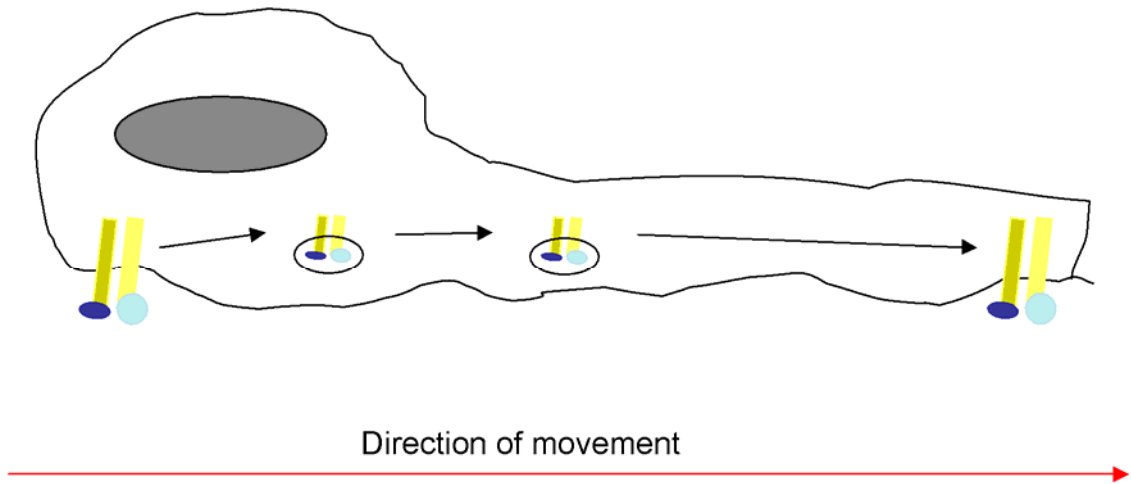
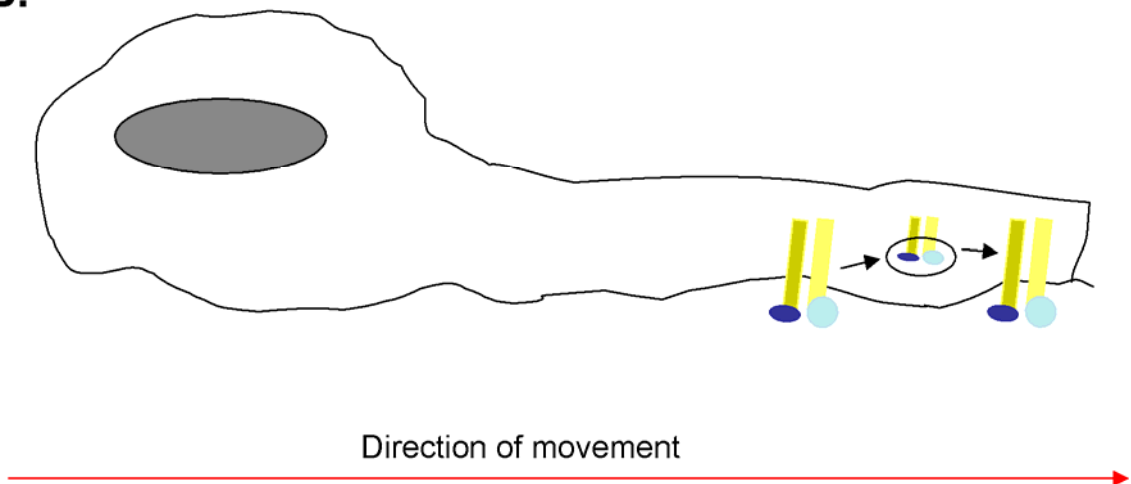
A.**B.**

Figure 1-9 Integrin trafficking in cell migration.

A. According to the initial model of integrin trafficking in cell migration, heterodimers are endocytosed at the rear of the cell and transported to the cell front for reinsertion into the membrane. B. Another model suggests that in invasive cells, both integrin internalization and recycling occur at the cell front.

1.3.5 Integrin recycling in cancer

It has in recent years become apparent that the trafficking of integrins can affect their function, and that dysfunctional integrin signalling caused by altered integrin internalisation and recycling can mediate tumour cell dissemination and cancer metastasis. Most of the investigations aimed at understanding the molecular machineries underpinning integrin internalisation and recycling and their contribution to cell adhesion and migration have been carried out in two-dimensional environments, with cells seeded onto inflexible plastic or glass substrates. When cells migrate *in vivo* during tumour invasion and metastasis, they have to migrate through a meshwork of extracellular matrix components, rather than simply moving on a flat substratum. Integrin trafficking should therefore be studied in a more physiologically-relevant environment if its contribution to cancer progression *in vivo* is to be understood. One of the first direct links between integrin trafficking and invasive migration of tumour cells within a physiologically relevant environment was provided in a study on $\alpha\beta6$ integrin trafficking performed by Ramsay and colleagues (Ramsay, Keppler et al. 2007). $\alpha\beta6$ integrin is not constitutively expressed in normal epithelia and its expression has long been associated with poorer clinical outcome in a range of cancer types. Expression of this heterodimer has also been linked to enhanced tumour cell invasion (Thomas, Nystrom et al. 2006). A HS-1 associated protein X1 (HAX-1) has been shown to bind directly to the cytoplasmic tail of $\beta6$ integrin. This association drives invasive migration of oral squamous carcinoma cells through matrigel and in organotypic invasion assays, by facilitating clathrin-mediated endocytosis of $\alpha\beta6$ integrin. These observations thus form a link between integrin trafficking and tumour cell invasion (Ramsay, Keppler et al. 2007). Also, Rab11-dependent endocytic pathways have been implicated in hypoxia-induced breast carcinoma cell invasion through matrigel plugs in a process that requires efficient trafficking of $\alpha\beta6$ integrin (Yoon, Shin et al. 2005). Furthermore, a member of the Rab11 family, Rab25 has been shown to mediate the trafficking of $\alpha5\beta1$ integrin and this contributes to invasive migration of ovarian carcinoma cells through three-dimensional matrices. Interestingly, Rab25 exerts no effects on directional migration of cancer cells across two dimensional surfaces, but it promotes tumour cell invasion into fibronectin-containing matrigel in a way that requires direct association of this

GTPase with the cytodomain of the β integrin subunit. Moreover, when cells are plated onto cell-derived matrices, Rab25 drives the extension of long pseudopods, at the tips of which this GTPase and its integrin cargo colocalise. This study also indicates that spatial restriction of the cycling integrin to the tip of a pseudopod may contribute to invasive migration of cancer cells (Caswell, Spence et al. 2007).

In addition to allowing membrane protrusion and focal adhesion turnover, integrin signalling and recycling can affect cancer progression *in vivo* and invasive tumour cell migration into three dimensional environments, by modulating the recycling of receptor tyrosine kinases (RTKs). Indeed, as mentioned previously, blocking $\alpha\beta3$ integrin function allows the binding of RCP to $\beta1$ integrin tail, but also recruits EGFR1 to RCP-containing vesicles and promotes the coordinate recycling of $\alpha5\beta1$ integrin and EGFR1. This in turn potentiates EGFR1 autophosphorylation and affects its signalling, in a way that favours PKB/Akt activation (Caswell, Chan et al. 2008). Given that PKB/Akt has been shown to promote tumour cell migration, it is possible that in the above context, decreased recycling of $\alpha\beta3$ contributes to increased tumour cell invasion by potentiating PKB/Akt signalling (Caswell, Vadrevu et al. 2009). In line with the loss of $\alpha\beta3$ integrin function and recycling acting to promote invasion, is a recent report of Kaur and colleagues. $\alpha\beta3$ integrin expression has been shown to decrease invasion of ovarian cancer cells, attenuate metastatic spread in xenograft models and to slow down tumour progression and therefore increase disease-free and overall survival in ovarian cancer. Importantly, this correlation between high $\alpha\beta3$ expression and favourable prognosis in ovarian cancer patients could explain why this integrin might not be a good therapeutic target in that type of tumours (Kaur, Kenny et al. 2009). Interestingly, mutant p53 expression - which is known to be involved in malignant transformation and metastasis (Petitjean, Achatz et al. 2007) - has been recently shown to promote loss of migrational directionality and to drive $\beta1$ -integrin-dependent tumour invasion by enhancing recycling of $\alpha5\beta1$ integrin and EGFR1. This occurs in a way that requires Rab-coupling protein (RCP) function and p63 inhibition, and results in constitutive activation of EGFR and integrin signalling (Muller, Caswell et al. 2009).

Integrin recycling is also thought to exert effects on tumour development and progression by altering the recycling of vascular endothelial growth factor receptors (VEGFRs) to affect angiogenesis. Tumour angiogenesis is a process that involves generation of new vasculature, which penetrates the cancerous growth and allows for the delivery of nutrients and oxygen to cancer cells. It is thought to be initiated through hypoxia-induced secretion of VEGF by tumour cells, which then binds to VEGFR2 on adjacent epithelial cells to activate signalling cascades leading to endothelial cell proliferation, tubulation and generation of new vessels (Olsson, Dimberg et al. 2006). Angiogenesis is also thought to be regulated by $\alpha\beta3$ integrin (Brooks, Clark et al. 1994). Indeed, it has been recently found that in the absence of agents that block $\alpha\beta3$ function (such as Cilengitide) VEGFR2 recycling is slow and its stimulation with VEGF drives internalisation and degradation of this receptor. However, low concentrations of Cilengitide activate the Rab4 recycling pathway and promote $\alpha\beta3$ and VEGFR2 trafficking, which protects VEGFR2 from degradation. This in turn increases surface levels of VEGFR2 and prolongs VEGFR2-mediated signalling, thus promoting endothelial cell migration and tubulation, which drive angiogenesis (Reynolds, Hart et al. 2009). This is consistent with observations that $\beta3$ -null mice display enhanced tumour angiogenesis (Reynolds, Reynolds et al. 2004) and could explain why $\alpha\beta3$ inhibitors that have entered clinical trials have had limited success as anti-angiogenic agents.

Recently, a link between integrin trafficking, cell division and human cancer has been established through the demonstration that Rab21-mediated integrin trafficking from the cell surface to the cytosolic compartment is required during cytokinesis. Successful cell division has been shown to require Rab21 activity, its association with α integrin subunits and efficient integrin-mediated cell/matrix adhesion at the cleavage furrow. More importantly, loss of Rab21 has been detected in ovarian human cancer cells and this is correlated with genetic instability and accumulation of multinucleate cells, and this phenotype can be rescued by introduction of Rab21. This suggests that dysregulation of integrin trafficking through Rab21 loss or inactivation can drive genetic instability and tumour progression (Pellinen, Tuomi et al. 2008).

Even though in the recent years multiple indications of the importance of integrin trafficking in tumour progression have emerged, some of the above

observations indicate that simply blocking integrin engagement with the matrix or its trafficking, might not be an efficacious way of designing anti-cancer therapies. This is mainly due to the implications of crosstalk between the pathways that traffic different integrin heterodimers and RTKs on the effectiveness, or rather ineffectiveness of integrin blocking-therapies, particularly in the context of $\alpha\beta3$ integrin blockade and EGFR1/VEGFR2 recycling. Taken together these descriptions highlight the need for more detailed understanding of integrin trafficking events occurring during tumour progression, as well as of the background in which they happen, if effective therapies that interfere with pro-invasive integrin function are to reach the clinic.

1.4 Rab25 and its disputed role in cancer progression

1.4.1 Rab25 is a member of the RAS-superfamily

Rab25 belongs to the superfamily of RAS-related proteins, of which the oncoproteins H-RAS, K-RAS and N-RAS, are prominent members. There are over 170 members of the RAS-superfamily of GTPases, and they all share a common ability to bind and hydrolyse GTP (guanosine triphosphate) to GDP (guanosine diphosphate) (Colicelli 2004). The binding of GTP to the GTPase induces conformational changes in the latter, which in turn affects its affinity for binding effector molecules. These small GTPases continuously cycle between active and inactive forms, and their activity depends on the ratio of active (GTP-bound) versus inactive (GDP-bound) complexes. The GDP/GTP exchange rate and thus the activity of the GTPase are controlled by guanine nucleotide exchange factors (GEFs), which allow disassociation of GDP and promote the formation of an active complex (Rossman, Der et al. 2005), and by GTPase activating proteins (GAPs), which enhance the GTPase activity of the enzyme thus accelerating the formation of inactive forms (Bernards and Settleman 2004).

RAS-superfamily of proteins can be divided into five main families: RAS, RHO, RAB, ARF and G α -family (Colicelli 2004). Rab proteins were first identified as Ras-related genes in a rat brain cDNA library, and were denoted as Rab1, Rab2, Rab3 and Rab4 (Touchot, Chardin et al. 1987). The human Rab family of small GTPases encompasses 70 members, whose roles in multiple stages of vesiculo-tubular transport have been studied in detail (Zerial and McBride 2001). Rab11A and Rab11B are the closest homologues of Rab25 and together they form the Rab11 subfamily. The crystal structure of Rab25 has been solved at 2.3Å (PDB: 2OIL) and it is largely similar to that of other Rabs with only subtle variations. Its core is formed by a six-stranded β -sheet, which is surrounded by five α -helices. The 72% sequence identity between Rab25 and Rab11 is reflected in the similarity between GDP-bound structure of Rab25 and that of Rab11 (PDB: 1OIX), with the exception of two loop regions spanning the residues 39-47 and 67-77. Also, some of the exposed surfaces are divergent due to the varying orientations of side chains, and these may also be responsible for distinct roles of Rab11 family members (www.thesgc.org/structures/structure_description/2OIL/).

Rab25 was first identified in rabbit gastric tissue and its expression shown to be restricted to gastrointestinal mucosa, lung and kidney, thus suggesting its epithelial distribution (Goldenring, Shen et al. 1993). It was then detected on immunisolated tubulovesicles from gastric parietal cells, along with secretory carrier membrane proteins (SCAMPs), and this suggested a role for Rab25 in gastric cell secretion, which requires fusion of intracellular tubulovesicles with the apical plasma membrane (Calhoun and Goldenring 1997). Rab25, together with Rab11A, has been shown to associate with the apical pericentriolar endosomal compartment of epithelial Madin-Darby Canine Kidney (MDCK) cells. The apical pericentriolar endosomal compartment, also known as the apical recycling compartment, is a site where apical and basolateral endocytic pathways in epithelia converge, and where sorting of apically and basolaterally internalised cargo occurs before its return to the site of origin or for transcytosis to the opposite pole of the membrane. Rab25 expression has been shown to decrease the rate of transcytosis and apical (but not basolateral) recycling of internalised ligand, whilst expression of its dominant-negative mutant did not alter either of these processes, thus suggesting that Rab25 may selectively modulate apical recycling and transcytosis (Casanova, Wang et al. 1999).

1.4.2 Rab25 as tumour promoter

There have recently been a number of reports implicating Rab25 in different facets of tumorigenesis. Rab25 was first implicated in tumour progression and invasion in a study performed by Wang and colleagues, where it was shown to be upregulated in tumours established from highly metastatic rat mammary carcinoma cells (MTLn3), by comparison to those generated using their non-metastatic counterparts (MTC tumour cell line) (Wang, Wyckoff et al. 2002). Rab25 was subsequently identified as a prominent component of the gene signature, which was associated with a subpopulation of mammary tumour cells that invaded from the primary subcutaneous tumour, into a matrigel-containing microneedle (Wang, Goswami et al. 2004). Not only has Rab25 been implicated in the invasiveness of breast tumours, it has also been reported to drive the progression of ovarian carcinomas. Cheng and colleagues reported this GTPase to be the driver of the 1q22 amplification in breast and serous ovarian cancers and demonstrated a correlation between enhanced Rab25 gene copy number (as well

as RNA levels) and poor prognosis, thus implicating it in progression and aggressiveness of these tumour types (Cheng, Lahad et al. 2004). Rab25 can also promote ovarian cancer cell proliferation, survival and colony formation *in vitro*, as well as subcutaneous and intraperitoneal growth of xenografts in nude mice (Cheng, Lahad et al. 2004; Fan, Xin et al. 2006). Other workers have shown that Rab25 is associated with a subpopulation of highly aggressive serous ovarian cancers (Davidson, Zhang et al. 2006) and the aforementioned work from our laboratory is consistent with a role for Rab25 in enhancing the invasive potential of human ovarian cancer cells (Caswell, Spence et al. 2007).

1.4.3 Rab25 can function as tumour suppressor

By contrast with its role as a tumour promoter, recent results indicate that Rab25 can suppress colorectal cancer initiation and progression. Loss of Rab25 has been associated with poor patient survival in human colorectal adenocarcinomas, and has been suggested to promote the development of this type of neoplasia. Similar results supporting the function of Rab25 as tumour suppressor in the intestinal epithelium were obtained from mouse models. Colorectal adenocarcinoma is thought to progress through a series of genetic aberrations and patients with hereditary colon cancer predisposition, such as those suffering from familial adenomatous polyposis (FAP), have been shown to develop a multitude of benign polyps due to mutations in the adenomatous polyposis coli (APC) gene. The mouse homologue of APC, which harbours a mutation designated multiple intestinal neoplasia (Min) contains a stop mutation codon at residue 850, which results in these mice (APC/Min⁺) presenting with adenomatous polyps in the small intestine and colon, but these lesions rarely develop into adenocarcinomas. Crossing *Apc/Min⁺* mice onto Rab25-deficient mice has resulted in a four fold increase in the number of intestinal polyps and a two fold increase in intestinal tumours when compared to *Apc/Min⁺* mice on a Rab25 wild type background, indicating that Rab25 loss can drive tumour progression (Nam, Lee et al.). In a report that focuses on breast cancer, Cheng and colleagues report loss of Rab25 expression in 33% of breast cancers when compared to matched normal breast tissue. Additionally, these authors found that overexpression of Rab25 in breast cancer cells impaired proliferation and anchorage-independent growth (Cheng, Ding et al. 2006). Interestingly, in a

subsequent study, they detected Rab25 loss in 75% of hormone receptor (HR)-negative breast cancer patients, whilst this GTPase was highly expressed in most (78.6%) HR-positive tumours and normal breast tissue, when measured by RT-PCR. Furthermore, immunohistochemical analysis of 32 samples revealed that the average Rab25 protein expression in ER-negative tumours was significantly lower when compared to ER-positive cancers, further indicating that Rab25's role in tumorigenesis is likely to be very context dependent (Cheng, Volk et al.). Indeed, in our laboratory we have seen a significant correlation between reduced levels of Rab25 and poor patient survival in ER-negative breast cancer patients (Claire Kelly, unpublished data).

Taken together, the above reports implicate Rab25 in various facets of tumour aggressiveness and progression, but the exact role played by Rab25 in these processes appears to be context specific. It is therefore imperative to determine the potential roles that Rab25 effector and interacting proteins can play in switching its function from tumour promoter to tumour suppressor, to resolve the conundrum surrounding Rab25's role in tumour progression.

2 Materials and Methods

2.1 Materials

2.1.1 Reagents and Solutions

Solution	Details	Source
2% gelatine		Sigma
Ampicillin		Sigma
Ascorbic acid		Sigma
DNA ladders	100bp and 1kb	Invitrogen
DNA loading dye	30% (w/v) sucrose, 0.35% Orange G (Sigma)	
DNaseI (10µg/ml)		Roche
Dulbecco's Modified Eagle Medium (DMEM)		Gibco
EGF		Peprotech
Ethidium bromide		Invitrogen
Foetal Bovine Serum (FBS)		Autogen Bioclear
Hybond-P PVDF membrane		GE Healthcare
IPTG	Isopropyl β-D-1-thiogalactopyranoside	Roche
Kanamycin		Sigma
LB Agar	LB + 1.5% agar	
L-Broth (LB)	1% w/v bacto-tryptone, 86mM NaCl, 0.5% yeast extract	Beatson Institute Central Services
L-Glutamine (200mM)		Gibco
Lyophilised fibronectin	1mg	Tebu-Bio
Matrigel		BD Biosciences
NDLB cell lysis buffer	150mM NaCl, 50mM Tris, 10mM NaF, 1mM Na ₃ VO ₃ , 5mM EDTA, 5mM EGTA, 1% Triton X-100, 0.5% Igepal CA-630	
NuPAGE MES SDS Running Buffer (20X)		Invitrogen
NuPAGE pre-cast gels		Invitrogen
NuPAGE Sample Buffer (4X)		Invitrogen
NuPAGE Sample Reducing Agent (10X)		Invitrogen
PBS/EDTA (PE)	PBS + 1mM EDTA	Beatson Institute Central Services
PBS-T	PBS + 0.1% Triton X-100	
Penicillin-Streptomycin		Gibco

Phosphate Buffered Saline (PBS)	170mM NaCl, 3.3mM KCl, 1.8mM Na ₂ HPO ₄ , 10.6mM H ₂ PO ₄	Beatson Institute Central Services
RNA loading buffer	6µl dye, 10.5µl formaldehyde, 30µl formamide, 3µl 10xMOPS, 3µl H ₂ O	
RPMI-1640 Medium		Gibco
Soluble fibronectin	1mg/ml	Sigma
TBS Tween (TBST)	TBS + 0.1% Tween-20	
Transfer Buffer	50mM Tris, 40mM glycine, 0.04% SDS, 20% methanol	Beatson Institute Central Services
Tris Buffered Saline (TBS)	10mM Tris-HCl, pH 7.4, 150mM NaCl	Beatson Institute Central Services
Tris-acetate-EDTA (TAE)	40mM Tris, 0.1% glacial acetic acid, 1mM EDTA	Beatson Institute Central Services
Tris-EDTA (TE)	10mM Tris-HCl, pH 8.0, 1mM EDTA	
Trypsin		Gibco
X-gal	5'-bromo-4-chloro-3-indolyl-D-galactopyranoside	Roche

Table 2-1 Reagents and solutions

2.1.2 Antibodies and dyes

Antigen	Details	Dilution for WB	Source
Active $\alpha 5$ integrin 9EG7			BD-Pharmingen (553715)
Alexa-647 succinimidyl ester			Molecular Probes
Calcein AM			Molecular Probes
CLIC3	Chicken	1:1000	Abcam (ab16050)
CLIC3	Rabbit	1:5000 (1:500 IHC)	In-house
dsRed	Rabbit	1:1000	Clontech (632496)
Flag	Mouse	1:1000	Sigma (F-3165)
GFP	Mouse	1:5000	Abcam (AB1218)
GST	Rabbit	1:5000	Santa Cruz (sc-459)
Phalloidin	TRITC/FITC-conjugated	1:500	Sigma
Rab11	Mouse	1:1000	Transduction Labs (r56320)
Rab25	Rabbit	1:5000 (1:1000 IHC)	In-house
Vinculin	Mouse	1:5000	In-house
$\alpha 5$ integrin	Mouse		BD-Pharmingen (555651)
β -actin	Mouse	1:5000	Sigma (A-1978)

Table 2-2 Antibodies and dyes

2.1.3 Enzymes and kits

Kit	Supplier
Amaxa Nucleofection Kit	Lonza
Coomassie Plus (Bradford) Protein Assay	Thermo Scientific
DNA Polymerase	Promega
Glutathione sepharose beads	GE Healthcare
HyperFect	Qiagen
Improm II Reverse Transcription Kit	Promega
pGEM-T-Easy Cloning Kit	Promega
PreScission Protease	GE Healthcare
Qiaprep Spin Miniprep Kit	Qiagen
QIAquick Gel Extraction Kit	Qiagen
QuantiTect Primer Assay	Qiagen
QuantiTect SYBR Green Master Mix	Qiagen
Rapid DNA Ligation kit	Roche
Restriction enzymes and reaction buffers	New England Biolabs
RNeasy Kit	Qiagen
SimplyBlue SafeStain	Invitrogen
siRNA oligonucleotides	Dharmacon
Slide-A-Lyser Dialysis Cassettes	Thermo Scientific
SuperSignal West Pico Chemiluminescent Substrate	Thermo Scientific
T-PER Tissue Protein Extraction Reagent	Thermo Fisher

Table 2-3 Enzymes and Kits

2.1.4 Tissue Culture plastic ware

Supplier: BD Biosciences

- Falcon tissue culture dishes (60mm and 90mm)
- Falcon multi-well plates

Supplier: TCS Biologicals

- Nunc tissue culture flasks and dishes
- Nunc cryotubes

Supplier: Corning Incorporated

- Transwell inserts (8 μ m pores)

Supplier: Appleton Woods

- IWAKI-3 cm glass bottom dishes

2.2 Methods

2.2.1 *Microarray screen and validation*

2.2.1.1 Total RNA extraction and quality control

Total cellular RNA was isolated from A2780-DNA3 and A2780-Rab25 cells grown for 16 hours on either plastic or CDM using the RNeasy kit, according to the manufacturer's instructions. Briefly, cells were grown to approximately 80% confluency in 10cm dishes, washed twice in ice-cold PBS (pH 7.4), residual PBS was allowed to drain and was aspirated. Cells were then lysed on ice, in 350µl of RLT buffer supplemented with β-mercaptoethanol (10µl per 1ml of the buffer). Cell lysates were homogenised by repeated suction through a sterile 25G needle. Samples were further homogenised using QIAshredder columns and RNA was extracted and purified as it is described in the handbook. Residual genomic DNA was removed by an on-column DNaseI digestion. RNA was eluted from the column in two sequential steps, each in 30µl of sterile water. RNA was then snap-frozen and stored at -80°C.

The integrity of the harvested RNA was verified on a 2% agarose gel. 1g of agarose was dissolved in 50ml of TAE buffer by heating in a microwave, cooling to approximately 50°C and adding ethidium bromide at a final concentration of 0.5µg/ml. The gel was then cast, allowed to set and 5µl of the RNA sample, previously boiled at 70°C for 5 minutes with 10µl of RNA loading buffer, was loaded into the pockets of the gel. Electrophoresis was performed in TAE buffer at 100V for one hour and the RNA was visualised by UV illumination. The concentration and purity of RNA samples was inspected using a NanoDrop spectrophotometer. Samples whose concentration was lower than 0.6µg/µl were concentrated by centrifugation in SpeedVac concentrator for approximately 1.5 hours, whilst the ones whose $A_{260/280}$ amounted to less than 1.9 were subjected to an additional clean-up step using the Qiagen RNeasy kit.

2.2.1.2 Microarray data analysis

Total RNA samples were generated in triplicate as described above. Biotinylated cRNA was hybridised to GeneChip® human genome U133 Plus 2.0 chip by Cancer

Research UK Paterson Institute Microarray Service. The cel files were normalized and analyzed in Partek[®] Genomics Suite Software, version 6.5beta Copyright © 2009. Default GCRMA normalization and log₂ transformation of the data was followed by the removal of technical batch effects. Multiway ANOVA was used to identify significantly regulated genes from one of experimental groups and linear contrasts performed between all pairs of experimental conditions. Multiple test corrections were performed for all calculated p-values. The fold change values were used for selection and ordering of differentially expressed genes. Finally, unadjusted p-value was used for further reduction of the gene lists. Initial analyses were performed by Keith Vass, then under the guidance of Jo Thurlow and eventually by Gabriela Kalna.

2.2.1.3 cDNA synthesis

cDNA was synthesised from total RNA using ImpromII kit according to the manufacturers instructions and in the final reaction volume of 20µl. The template/oligo-dT primer thermal denaturation was performed in the first instance and the reaction was set up as follows:

1µg RNA	x µl (as determined by RNA concentration)
Oligo-dT primer (0.5 µg/µl)	1 µl
H ₂ O	make up to 10 µl.

The mixture was heated to 70°C for 5 minutes in the Biorad DNA Engine Peltier Thermal Cycler and then chilled on ice for two minutes. The following reverse transcription reaction mix was then assembled:

H ₂ O	0.5 µl
5x Reaction buffer	4 µl
MgCl ₂ (25mM)	3 µl
dNTPs (10mM)	1 µl
RNasin (40U/µl)	0.5 µl

and added to the RNA containing tube. Subsequently, 1µl of Improm Reverse Transcriptase was added, the sample was then incubated at 25°C for 5 minutes to allow for the initial annealing and the elongation then proceeded for one hour at 42°C. Upon completion of the first strand synthesis, the reaction was terminated by incubation at 70°C for 15 minutes and the sample was then cooled at 4°C.

2.2.1.4 Primers for real time PCR

All primers utilised for real time PCR were purchased from Qiagen as QuantiTect Primer Assay kits and had been verified by the supplier to be suitable for use in RT-PCR. Their sequences are not disclosed, therefore corresponding catalogue numbers are listed below:

CLIC3	Hs_CLIC3_1_SG QuantiTect Primer Assay (200) (QT00011781)
SLC16A6	Hs_SLC16A6_1_SG QuantiTect Primer Assay (200) (QT00009338)
KCNJ2	Hs_KCNJ2_1_SG QuantiTect Primer Assay (200) (QT00001022)
B-actin	Hs_ACTB_2_SG QuantiTect Primer Assay (200) (QT00095431)
GAPDH	Hs_GAPDH_2_SG QuantiTect Primer Assay (200) (QT01192646).

2.2.1.5 qPCR

QuantiTect SYBR Green PCR kit was utilised to perform quantitative PCR on a BioRAD DNA Engine thermal cycler fitted with a Chromo4 Engine (Bio-Rad) and coupled to Opticon Monitor 3 software. Prior to the assembly of qPCR reactions the cDNA template was diluted 1:8 in sterile water. The qPCR reactions were then assembled on a cooling block as follows:

2x SYBR Green Mix	10 µl
10x Primer Assay	2 µl
cDNA template (1:8 diluted)	8 µl.

The PCR reaction was performed according to the protocol outlined below:

Initial Denaturation	95°C	15 min
40 cycles:		
Denaturation	95°C	30 sec
Annealing	60°C	30 sec
Elongation	72°C	30 sec
Plate Read		
Final Elongation	72°C	5 min
Dissociation Curve	70°C - 90°C in 0.3°C steps.	

Data was extracted from the Opticon Monitor 3 software and the $\Delta\Delta C(t)$ method (Livak and Schmittgen 2001) or one that also incorporates amplification efficiencies (Pfaffl 2001) was used to calculate changes in gene expression with β -actin and GAPDH serving as reference genes. Each experiment was performed in triplicate and each of the replicas incorporated three technical repeats.

2.2.2 Cloning and DNA manipulation

2.2.2.1 Bacterial strains

All cloning procedures utilised competent *E.coli* DH5 α , whilst recombinant protein production was performed in BL21(DE3)pLysS *E.coli* strain. Both were generated and supplied by the Central Services at the Beatson Institute.

2.2.2.2 Bacterial transformation

50 μ l of *E.coli* DH5 α cells was thawed on ice and gently mixed with 10-20ng of plasmid DNA or ligation reaction mix and incubated on ice for 10 minutes. The cells were then subjected to heat shock at 42°C for 45sec in a water bath, and then chilled on ice for further 2 minutes. 450 μ L of SOC medium was then added and the cells were allowed to recover at 37°C with shaking for approximately one hour. 200 μ L of the transformation mix was spread onto pre-warmed LB agar plates containing either 50 μ g/ml ampicillin or kanamycin and incubated at 37°C overnight. Individual colonies were then used to inoculate 5 ml of LB medium containing the appropriate antibiotic and the culture was grown overnight at 37°C with shaking. For long term storage 500 μ l of the bacterial culture was mixed with equal volume of sterile glycerol and stored at -80°C.

2.2.2.3 Plasmid preparation

Overnight bacterial culture was pelleted by centrifugation at 3000rpm for 10 minutes in a Beckman Coulter centrifuge. The pellet was processed using the QIAprep Spin Mini-Prep Kit by the Beatson Institute Central Services. If sequence verification was required, the samples were further processed by the Beatson Molecular Technology Services on an Applied Biosystems 3130xl sequencer and the sequences were mostly analysed using Vector NTI package (Invitrogen). For

large scale plasmid preparation bacterial transformants were cultivated overnight in 100ml of LB media containing the appropriate antibiotic, pelleted by centrifugation as described above but for 20 minutes. The pellets were processed by Central Services. Double stranded DNA was quantified using an Eppendorf Biophotometer and 260nm absorbance.

2.2.2.4 Polymerase chain reaction (PCR)

PCR was performed using GoTaq DNA Polymerase kit and the manufacturer's specifications were followed. Approximately 100ng of plasmid DNA template, 0.8mM of both forward and reverse primers, 0.2mM of each dNTP with 1.25 units of the polymerase were assembled in the provided reaction buffer and in the total volume of 50µl. Temperature cycling was performed in a DNA Engine Thermal Cycler (Biorad) under the following conditions:

Initial Denaturation	95°C	10 min
25 cycles:		
Denaturation	95°C	30 s
Annealing	55-60°C	30 s
Extension	68°C	1 min/1kb
Final Extension	68° C	10 min.

PCR products were then subjected to agarose gel electrophoresis and purification, before being later utilised in subsequent cloning procedures.

Primers used in this project were synthesised by Invitrogen and are listed below:

CLIC3 pGEX-6P-Fw BamHI	5' ACTGGGATCCATGGCGGAGACCAAGCTC 3'
CLIC3 pGEX-6P-Rev NotI	5' CAGTGCGGCCGCCTAGCGGGGGTGCACGG 3'
FLAG-CLIC3 pcDNA3-Fw BamHI	5' GATCGGATCCATGGACTACAAAGACGATGACGACAAGGCGGAGACCAAGCTCCAG 3'
FLAG-CLIC3 pcDNA3-Rev NotI	5' GATCGCGGCCGCCTAGCGGGGGTGCACGG 3'

2.2.2.5 Intermediate cloning into pGEM-T-Easy

Purified PCR-generated DNA fragments were ligated into pGEM-T-Easy vector, which utilises the adenosines added to the 3'-ends of the PCR products. Ligation reactions were carried out using T4 DNA ligase in the provided ligation buffer and in the total volume of 10 μ l. 50ng of pGEM-T-Easy vector and a vector to insert ratio of 1:3 were used. Ligations were performed at 4°C overnight. DH5 α cells transformed with pGEM-T-Easy ligation mix were spread onto LB plates containing 40 μ g/ml X-gal and 0.1mM IPTG in addition to 100 μ g/mL ampicillin. Following overnight incubation at 37°C, individual white colonies were used to inoculate 5ml of antibiotic supplemented LB media for further screening. Blue colonies were ignored and considered not to be bearing an insert.

2.2.2.6 Restriction enzyme digestion and ligation

Double DNA restriction digests were performed using the appropriate restriction enzymes and their corresponding reaction buffers. Typically, 1 μ g of plasmid was incubated with 1 unit of two restriction enzymes in the total volume of 20 μ l, at the appropriate temperature (mostly 37°C), usually for 2 hours. DNA from restriction digests was subjected to agarose gel electrophoresis to confirm the efficiency of the digest and to allow the subsequent DNA purification from the gel slice. The resultant fragment was then cloned into the recipient plasmid backbone using the same ligation conditions as those described in the previous section.

2.2.2.7 Agarose gel electrophoresis

DNA electrophoresis was carried out in 1% (w/v) electrophoresis grade agarose dissolved in 1xTAE buffer. Prior to gel solidification ethidium bromide was added at the final concentration of 0.5 μ g/ml. DNA samples were diluted in 6x DNA loading dye before electrophoresis and loaded on to the gel alongside suitable DNA ladder (mostly 1kb ladder). Electrophoresis was conducted in 1xTAE buffer at 100 V for approximately one hour. DNA samples were visualized using UV transillumination. Following electrophoresis, agarose slices containing DNA were excised and DNA purified using QIAquick Gel Extraction Kit according to manufacturer's instructions.

2.2.3 Recombinant protein production

2.2.3.1 Protein expression

500ml of sterile LB media, supplemented with 100ug/ml ampicillin, was inoculated with 10ml of an appropriate overnight culture and grown in an orbital shaker at 37°C for a couple of hours. After that time 1ml samples of culture were removed at half an hour intervals and the optical density was measured at 600nm (OD₆₀₀) against an LB media control. When OD₆₀₀ reached 0.6-0.8, ensuring logarithmic growth phase of bacteria, expression of the recombinant protein was induced with 0.25mM IPTG. Expression of the target protein was undertaken for 3 hours in an orbital shaker, at 37°C. 1ml of the culture was sampled prior to induction as well as one, two and three hours after induction and bacterial cells were pelleted at 3000rpm for 10 minutes. The whole culture was then harvested by centrifugation at 3000rpm for 25 minutes. The cell pellet was then frozen overnight and defrosted the following day. It was subsequently re-suspended in 10ml of PBS containing 0.1% TX-100 and additional 10ml of the same solution was then introduced. Following the addition of Roche Diagnostic's protease inhibitor cocktail tablet, lysosyme was added at a final concentration of 1mg/ml and the cell suspension subjected to 8-seconds-long sonication cycles until sufficient cell lysis was achieved. The cell debris was removed by centrifugation at 11000rpm for 45 min at 4°C. The pellet was resuspended in 20ml of PBS and 50µl were used to analyse the insoluble protein fraction. The cleared lysate was used to recover soluble recombinant protein in subsequent purification steps.

2.2.3.2 Protein purification

Glutathione sepharose beads were prepared as per the manufacturer's instruction. Approximately 20ml of the cell supernatant was recovered and applied to 0.5ml of pre-swollen 4% beads and incubated with gentle agitation for 3 hours at 4°C to allow the binding of the expressed fusion protein to the resin. The beads were then collected by centrifugation at 1000rpm for 10 minutes at 4°C and washed four times with 1ml PBS with 0.1% TX-100, followed by four washes in 1ml PBS. The protein was eluted from the glutathione beads with 1ml of 100mM NaCl, 50mM Tris-HCl, and 3mg/ml glutathione (pH 8.0) by incubating

for 10min at 4°C with repeated inversion. The beads were then collected by centrifugation at 7000rpm for 5 minutes at 4°C and the eluate was collected in a separate tube. This was repeated three times and resulted in the generation of three elution fractions. The eluted fractions were pooled and protein concentration was measured. Where necessary, PreScission cleavage was performed, which removed the GST tag from the recombinant protein. Typically, 1 unit of the enzyme was used for every 100µg of recombinant protein in 1mM DTT and 1mM EDTA and the digestion was carried out for 4 hours at 4°C. Following the removal of the GST-tag glutathione sepharose beads were applied and the sample was gently agitated for 2 hours at 4°C to capture cleaved GST and GST-tagged PreScission protease. The beads were then collected by centrifugation at 7000rpm for 5 minutes and the supernatant containing pure recombinant protein was collected. Where necessary, the above process was repeated. The expression time-course, soluble and insoluble fractions, as well as protease cleavage and purification efficiency were analysed by SDS-PAGE and Coomassie staining. The purified protein was dialysed overnight using Slide-A-Lyser dialysis cassette (10kDa MWCO) against 2L of PBS (pH 7.4), at 4°C. The purified protein was frozen on dry ice, and stored in aliquots, at -80°C.

2.2.4 Mammalian cell culture techniques

2.2.4.1 Cell origin

Stable clones of A2780-DNA3 and A2780-Rab25 cells were a kind gift from Gordon Mills and were generated as described previously (Cheng, Lahad et al. 2004). A number of cell lines were obtained from other groups within the Beatson Institute for Cancer Research, including Telomerase-immortalised human foreskin fibroblasts (Tifs) from Brad Ozanne. Primary cultured Human dermal fibroblasts (HDFs) were purchased from the American Type Culture Collection cell bank.

2.2.4.2 Cell maintenance

A2780 adenocarcinoma cells were cultivated in RPMI-1640 supplemented with 10% (v/v) serum, 2mM L-glutamine plus 10Units/ml penicillin and 10µg/ml streptomycin, at 37°C, in a humidified atmosphere containing 10% CO₂. HDF and

Tif fibroblasts were grown in DMEM media supplemented as it is described above. For sub-culturing, medium was removed by aspiration, the monolayer rinsed with PBS, then with 10% trypsin/PE solution. Following detachment the cells were re-suspended in culture media and subsequently transferred into appropriate tissue culture flasks.

For long term storage, cells were trypsinised and pelleted by centrifugation. They were then re-suspended in 10% DMSO in FCS, placed in cryotubes and frozen at -80°C over night to then be transferred to liquid nitrogen vapour tanks where they were stored.

2.2.4.3 Nucleofection

Nucleofection provides a more efficient alternative to DNA transfection and was used for the introduction of DNA plasmids and siRNA into A2780 cells. The cells were passaged the day before nucleofection and were 75-80% confluent when nucleofected. Cells were trypsinised, re-suspended in growth media and centrifuged for 5 minutes at 1000rpm. The media was then aspirated and cells washed in PBS. Following centrifugation, the cell pellet was suspended in 100 μl of pre-warmed Nucleofector Solution T, which was then mixed with the appropriate DNA or siRNA. Typically 3 μg of plasmid DNA or 5 μl of 20 μM siRNA (1 μM final siRNA concentration) were used for each transfection, with the exception of co-transfecting GFP- $\alpha 5$ and Cherry-CLIC3, when 4.8 μg of the integrin and 1.2 μg of the CLIC3 construct were used. The resultant suspension was then transferred to a nucleofection cuvette and inserted into the Amaxa Nucleofector. Nucleofection carried out using A-23 programme and the nucleofection mix was suspended in 500 μl of warm media and added to pre-prepared tissue culture dishes. Cells were allowed to recover and settle for at least 18 hours prior to live cell imaging, 4 or 12 hours prior to setting up invasion assays when siRNA or overexpression constructs were used, respectively.

2.2.4.4 Inverse invasion assay

Inverse invasion assays were performed as described previously (Hennigan, Hawker et al. 1994). An aliquot of complete matrigel was thawed slowly on ice and diluted in an equal volume of ice-cold PBS supplemented with 25 $\mu\text{g}/\text{ml}$

soluble fibronectin. 100µl of the diluted matrigel mix was pipetted into each Transwell (8µm diameter pores), which had previously been inserted into a well of a 24-well tissue culture plate, and left to set at 37°C. The transwells were then inverted and 4×10^4 cells, previously trypsinised and washed in PBS, were placed on the underside of the filter. The transwells were then covered with the base of the 24-well tissue culture plate so that they made contact with cell suspension droplets. Cell attachment was allowed to proceed for four hours, before the plate was inverted back and the non-adherent cells were washed off by three sequential washes in 1ml of serum-free medium. The transwells were left in the last 1ml of serum-free medium, which constituted the lower chamber of the assay, and 100µl of 10% FCS-RPMI supplemented with 25ng/ml EGF was pipetted on top of the transwell. The cells were then allowed to invade into the matrigel and towards the gradient of serum and EGF for 48 or 72 hours at 37°C in the atmosphere of 5% CO₂. To visualise cells that migrated into the matrigel plug, 4µM Calcein AM (acetoxymethyl ester of calcein) was used. This was done by placing the transwells in a new 24-well dish and pipetting 1ml of calcein solution in RPMI over the top of the transwell. After one hour at 37°C the cells were imaged by confocal microscopy using a Leica SP2 confocal microscope and a 20x objective at an excitation wavelength of 488 nm and emission wavelength of 515nm. Optical sections were captured at 15µm intervals, starting from the underside of the transwell filter and moving upwards in the direction of cell invasion. The resulting images were quantified using Image J software. The threshold fluorescence intensity of the images was set to only register cells that lay within each individual optical slice, and the sum of the fluorescence in the sections from 45µm and above was divided by the total fluorescence of all the sections, thus giving an invasion index 'beyond 45µm'. Data were generated from at least 3 individual experiments, in which each condition was represented by at least two transwells and optical sections were taken from at least 3 areas of each transwell.

2.2.4.5 Generation of cell derived matrix

Cell-derived matrix was generated as described previously (Cukierman, Pankov et al. 2001; Bass, Roach et al. 2007). Briefly, tissue culture plates were coated with 0.2% sterile gelatin for one hour at 37°C. Tissue culture dishes were then washed twice in PBS and cross-linked with 1% sterile glutaraldehyde for 30

minutes at 37°C. Following two washes with PBS, the cross-linker was quenched with 1M sterile glycine in PBS (pH~7) for 20 minutes at room temperature. Upon two further PBS washes the dishes were equilibrated in DMEM containing 10% FCS for half an hour at 37°C. Primary cultured human dermal fibroblasts (HDFs) or telomerase immortalised fibroblasts (Tifs) were then seeded at near confluence ($\sim 2 \times 10^4$ cells/cm²) and grown for 10-14 days in DMEM containing 10% FCS and 50µg/ml ascorbic acid. The media with ascorbic acid was changed every other day to ensure sufficient collagen production and the sticking of the matrix to the tissue culture plate. Matrices were denuded of living cells by incubation with PBS containing 20mM NH₄OH and 0.5% TritonX-100 for approximately two minutes or until no intact cells were present, as examined by phase light microscopy. Extraction buffer was gently aspirated and the matrix washed twice with PBS containing calcium and magnesium. DNA residues were removed by incubation with 10ug/ml DNaseI in PBS containing calcium and magnesium at 37°C for 30 minutes. The matrices were then washed twice with PBS containing calcium and magnesium and stored at 4°C in PBS with calcium and magnesium supplemented with pen/strep. The matrix was confirmed to be intact by phase microscopy prior to use. Matrices were blocked with 0.1% heat-denatured BSA prior to seeding of tumour cells.

2.2.4.6 Labelling of fibronectin

One mg of human lyophilised fibronectin (FN) was dissolved in one ml of filtered water and was allowed to stand at 4°C for one hour. It was then dialysed into ice-cold PBS using a Slide-A-Lyser dialysis cassette with a 3.5KDa molecular weight cut off. After an overnight dialysis, the fibronectin solution was recovered and 1 volume of filtered 1M NaHCO₃ (prepared directly prior to use) was added to 9 volumes of FN. 20µl of 10mg/ml Alexa-647 succinimidyl ester in DMSO was added to 1ml of FN and agitated for one hour at 37°C. The Alexa-FN preparation was then dialysed into ice-cold PBS overnight.

2.2.4.7 Live cell imaging, photoactivation and colocalisation quantification

A2780 cells were seeded onto glass-bottomed 3-cm plates and imaged with a 64x objective of an inverted confocal microscope (Fluoview FV1000, Olympus) in an

atmosphere of 5% CO₂ at 37°C. Different fluorescent channels within one sample were recorded sequentially to prevent bleed-through.

Photoactivation was performed with a 405nm laser of the above mentioned microscope and Olympus SIM scanner. Images were then captured every 2 seconds over a period of 120 seconds. Movies were generated from these time-lapse images and stills corresponding to individual frames from the movies were analysed. The integrated fluorescence intensity of the photoactivated region and adjacent plasma membrane region were determined for each frame using the Fluoview FV1000 software. The loss of fluorescence in the activated region (vesicle) and its gain in the proximal plasma membrane region (membrane) was calculated relative to the fluorescence of the photoactivated region in the frame immediately after photoactivation. The obtained relative fluorescence values were then plotted against time.

Colocalisation quantification was performed using Image J software, where the confocal images underwent two rounds of local contrast enhancement (image blurring, subtraction of the blurred image and subsequent contrast enhancement) and threshold adjustment. The number of pixels in the red channel was then expressed as a percentage of yellow pixels in the merged image. This was performed with the assistance from David Strachan.

2.2.4.8 Fixing and staining cells for microscopy

Cells were cultured on square cover slips placed in 8-well tissue culture dishes. Medium was aspirated and cells were washed in PBS and fixed in 4% formaldehyde for 15 minutes. Three PBS washes were performed and cells were then permeabilised with 0.2% Triton X-100 in PBS for 5 minutes. Following three more washes in PBS, non-specific binding sites were blocked with 1% BSA/PBS for 1 hour. Subsequently primary antibodies diluted in the block solution were applied for 45 minutes. The actin cytoskeleton was counterstained with fluorophore-conjugated-phalloidin in PBS for 10 minutes. Coverslips were washed twice before being mounted onto glass slides using DAPI Vectashield anti-fade reagent. All the above steps were performed at room temperature. Glass slides were stored at 4°C until viewed by confocal microscopy.

2.2.4.9 FLIM-FRET

A2780 cells transiently expressing the appropriate fusion proteins were plated onto 3cm glass bottom dishes. Fluorescence resonance energy transfer was detected using a Lambert Instruments Fluorescence Attachment (LIFA) on a Nikon Eclipse TE 2000-U microscope equipped with a 100x oil immersion objective and a filter block consisting of a 470/40 excitation filter, a T495LP dichroic mirror, and a 525/50M emission filter. A modulated 490 nm LED was used as light source, which in combination with the modulated intensifier from the LIFA system, allowed measurement of fluorescence lifetimes using frequency domain. Donor (D) lifetime, τ , was analyzed using the FLIM software (version 1.2.7; Lambert Instruments, The Netherlands). FRET efficiency was calculated from Donor lifetime with and without the presence of Acceptor using the given formula; $N_{fret} = 1 - (\tau_{fret} / \tau_d)$, where τ_{fret} is the lifetime of donor in the presence of acceptor and τ_d is the life time of donor in the absence of acceptor. Experiments performed under the guidance of Kiran Vadrevu.

2.2.4.10 Recycling assays

Cells were serum-starved for 30-45 minutes, washed twice in ice-cold PBS and then surface labelled with 0.2mg/ml NHS-SS-biotin for 30 minutes at 4°C. Labelled cells were washed twice in ice-cold PBS and transferred to media containing 10% FCS, which had previously been heated to approximately 15°C. Cells were then transferred to an incubator and internalisation was allowed to proceed for 30 minutes in the presence or absence of 2.5µg/ml fibronectin at 37°C. Cells were then transferred to ice, washed twice with ice-cold PBS and biotin removed from proteins remaining at the cell surface by a 20 minute reduction with MesNa in PBS (pH 8.6). The internalised proteins were then chased from the cells by returning them to 37°C in media containing 10%FCS. At the indicated times cells were returned to ice and biotin removed from the recycled proteins in a second reduction step. Residual MesNa (sodium 2-mercaptoethanesulphonate) was quenched with 20mM IAA (iodoacetamide) for 10 minutes and cells lysed. Levels of integrin recycled were determined by capture ELISA on 96-well plates pre-coated with 5µg/ml antibodies recognising either GFP, total $\alpha 5B1$ or active $\alpha 5B1$ integrin (9EG7 epitope) in 0.05M Na_2CO_3 (pH9.6) at 4°C. Non-specific binding sites were blocked with 5%BSA in PBS-T for

one hour at room temperature. 50µl of cell lysate was added to appropriate wells of the multitrete plate and gently agitated overnight at 4°C. Unbound proteins were removed by PBS-T washes and streptavidin-conjugated horseradish peroxidase in 1% BSA/PBS-T was then added for 1 hour. Following washes in PBS-T and then PBS, biotinylated integrins were detected by chromogenic reaction with 0.56mg/ml ortho-phenylenediamine in a buffer containing 25.4mM Na₂HPO₄, 12.3mM citric acid (pH 5.4) with 0.003% H₂O₂, at room temperature for 10 minutes. The reaction was terminated with 8M H₂SO₄ and absorbance was read at 490nm. The percentage of integrins recycled was inversely proportional to the proportion of biotinylated integrin remaining in the samples that recycled, versus the biotinylated integrin pool, which was not allowed to recycle. Assays performed with the assistance from Jim Norman.

2.2.4.11 FACS

Cells were stained with 1µM LysoTracker Red for 20 minutes at 37°C and subsequently washed once with PBS. 0.5ml trypsin was used to detach cells from the culture dish and they were then re-suspended in 2ml of ice-cold media and immediately sorted using a Becton Dickinson Cellquest FACScan on basis of fluorescence resulting from excitation of cells with a 568 nm laser. The FacsScan was operated by, and data analysed with the help of Simon Wilkinson, Beatson Institute.

2.2.5 Protein extraction and analysis

2.2.5.1 Cell lysis for protein

Protein extracts were prepared from cells when approximately 80% confluent. Cells were washed twice with ice cold PBS (pH 7.4) and lysed with 1.5x NDLB buffer containing protease inhibitors: 50µg/ml Aprotinin, 1mM AEBSF (4-[2-Aminoethyl]benzynesulphonyl fluoride), and 50µg/ml Leupeptin. Cell lysates were scraped with a cell scraper, transferred to a 1.5 ml tube and centrifuged at 13000rpm at 4°C for 10 minutes and cleared lysates were collected in new tubes. Samples were either processed immediately or stored at -20°C.

2.2.5.2 Protein extraction from mouse tissue

Protein extracts were prepared immediately after tissue harvesting using T-PER Tissue Protein Extraction Reagent. 10ml of T-PER buffer was supplemented with protease inhibitors: 125 μ l of 100mM PMSF (phenylmethylsulfonyl fluoride), 20 μ l of 0.5M NaF, 20 μ l of 100mM Na₃VO₄, 30 μ l AEBSF, 30 μ l Aprotinin and 30 μ l Leupeptin. Tissue was then placed together with 500 μ l of the lysis buffer in homogenisation tubes containing ceramic beads (Precellys 24 Lysis and Homogenisation) and three cycles of homogenisation were performed at 5000rpm, each consisting of two 20 seconds long steps with 10 second intervals. Following homogenisation lysates were clarified by centrifugation at 13000 rpm for 15 minutes at 4°C.

2.2.5.3 Protein quantification

The protein concentration in cell lysates was determined using the Coomassie Plus (Bradford) Protein Assay and a 2mg/ml stock of BSA. 10 μ l 1.5x NDLB buffer blanks, 10 μ l of protein standards (0.2, 0.4, 0.6, 0.8 and 1mg/ml BSA) were added to the wells of a flat-bottomed 96-well plate, as were 10 μ l of lysates (all in triplicate). 200 μ l of the protein assay reagent was then added to each well and the absorbance was measured on a Dynatech MR7000 plate reader at 595 nm. The absorbance values for the protein standards were used to generate a standard curve and the protein concentrations in the cell lysates were determined from the curve.

2.2.5.4 SDS-PAGE and Coomassie staining

SDS-poly-acrylamide gels were used to resolve protein samples. The required amount of lysate containing typically 40 μ g protein was mixed with 4x reducing sample buffer. Samples were then heated at 95°C for 10 minutes, briefly centrifuged to collect the whole sample, and resolved on gradient (4-12%), denaturing, pre-cast polyacrylamide gels. Electrophoresis was performed in gel tanks containing 1x MES running buffer, at 120V and for approximately 2 hours. Molecular weight markers were loaded on the gel adjacent to the lysate samples. After resolution by SDS-PAGE, the gel was either stained with

SimplyBlue SafeStain Coomassie reagent to visualise all proteins that were resolved, or Western Blotting was performed.

2.2.5.5 Western Blotting

Proteins previously separated by SDS-PAGE were transferred from the gel to PVDF membrane in blotting buffer for 75 minutes at 10V, using BioRad semi-dry transfer apparatus. Excess protein sites were blocked using 5% BSA in TBS-T at room temperature. The membranes were then incubated with primary antibodies at the appropriate dilutions, overnight at 4°C. Membranes were then washed 3 times with TBS-T for 10-30 minutes and incubated with appropriate HRP-conjugated secondary antibodies at 1:3500 dilutions, followed by 3 additional TBS-T washes. All incubation and wash steps were performed with gentle agitation. Proteins on the membranes were visualised by chemiluminescence using Pierce ECL Western Blotting Substrate. This was followed by autoradiography using Fuji Super RX medical X-ray film and a Kodak X-Omat 480 RA X-Ray processor.

2.2.6 Protein expression analysis in tissue samples

2.2.6.1 Immunohistochemistry

Immunohistochemical staining was performed by Colin Nixon at the Histology Service (Beatson Institute). Briefly, formalin-fixed and paraffin embedded tissue sections were dewaxed in Xylene and passed through Ethanol (2x 100%, 1x 70%) for rehydration. Heat-induced epitope retrieval was carried out in either TRIS-EDTA buffer (pH8) or citrate buffer (pH6). Enzymatic retrieval was attempted using proteinase K. Endogenous peroxidase was then blocked using 3% H₂O₂/methanol for 5 minutes before CLIC3 or Rab25-specific antibody was applied at 1:500 and 1:1000 dilution, respectively, for 45 minutes at room temperature. Tissue sections were then incubated in secondary antibody (Dako Envision rabbit kit, K4003) for 40 minutes and the staining was visualised with DAB and counterstained with Gills Heamatoxylin. Resulting whole sections were analyzed and images were captured digitally using a Zeiss Axioskop 50 microscope and Axiovision software version 3.1. TMA slides were scanned at 20x magnification using NanoZoomer NDP scanner (Hamamatsu) and were then

stored on a dedicated server and were available for viewing using Slidepath Digital Image Hub.

2.2.6.2 Pancreatic tumour TMA cohort and analysis

The human pancreatobiliary tissue microarray (TMA) was produced in the West of Scotland Pancreatic Unit, University Department of Surgery, Glasgow Royal Infirmary, and provided by Nigel Jamieson. The local Research ethics Committee approved tissue sample collection. All patients underwent pancreaticoduodenectomy and gave written and informed consent for sample collection. A total of 1500 cores from 224 patients with pancreatobiliary cancer (including 118 cases with pancreatic ductal adenocarcinoma; PDAC) were arrayed on the TMA. Clinicopathological parameters and complete follow up data were available. From each patient at least 6 tumour cores (0.6mm diameter) and 2 cores of adjacent normal tissue were sampled. CLIC3 expression levels were assessed by two independent scorers and according to the intensity of immunohistochemical staining, as well as to the area of tumour cells that were CLIC3-positive. This was done using a histoscore, which serves as a semi-quantitative assessment of staining intensity and is calculated from the formula: $\text{histoscore} = (1 \times \% \text{ cells with weak staining}) + (2 \times \% \text{ cells with moderate staining}) + (3 \times \% \text{ cells with strong staining})$. Statistical analysis was performed by Nigel Jamieson with the SPSS version 15.0 package (SPSS Inc., Chicago, IL, USA). A histoscore of 100 was used as a cut off for low and high CLIC3 expression. Kaplan-Meier survival analysis was used to assess the overall survival after surgery and patients alive at the time of follow up were censored. To compare the length of survival between the two expressor groups, a Log Rank analysis was performed. To adjust for competing risk factors, a Cox proportional hazards model and univariate analysis were used and hazard ratios (HR) with 95% confidence interval (CI) were reported as an estimate of the risk of disease specific death. Clinicopathological parameters that were identified as significant ($p < 0.10$) in univariate analysis were incorporated into the Multivariate Cox Regression Analysis in a backwards stepwise fashion. Statistical significance for independent outcome predictors was set at $p \leq 0.05$.

2.2.6.3 Ovarian tumour TMA

The ovarian tumour TMA containing 472 serous, mucinous, endometrioid and mesonephroid (clear cell) cancers was obtained from Charlie Gourley (Edinburgh Cancer Research UK). Ethical approval for the project was provided by the Lothian Research Ethics Committee. CLIC3 expression levels were assessed by two independent scorers and scoring system described earlier for the pancreatic TMA was followed. Statistical analysis of CLIC3 expression against the follow up data was performed by Charlie Gourley.

2.2.7 Pull downs for mass spectrometry

400µg of recombinant protein was mixed with 25µl of 50% slurry of glutathione sepharose beads and agitated for 1 hour at 4°C. The beads were washed twice in 0.1% BSA in PBS and were equilibrated in cell lysis buffer. Pre-cleared cell lysate was added to the beads coupled to recombinant protein and tumbled for 2 hours at 4°C. Following the binding of cellular proteins to the GST-fusion protein, the unbound material was removed by 3 washes in lysis buffer, followed by 3min centrifugation at 6000rpm, at 4°C. The protein complexes were eluted from the beads with 50µl of 1% SDS in lysis buffer. This was aided by inverting the tubes every couple of minutes for the total of approximately 10 minutes. The beads were collected by centrifugation for 8 minutes at 6000rpm at 4°C and 16µl of 4x reducing sample buffer was added to the eluate. Beads were also resuspended in 50µl of 1x sample buffer and samples were prepared for SDS-PAGE on a 10% pre-cast polyacrylamide gel and Coomassie stained, as described earlier. Following protein visualisation, the gel was transferred to Dr Willy Bienvenut of the Beatson Institute Proteomics facility for in-gel trypsin digestion and mass spectrometry analysis.

3 Chloride intracellular channel 3 (CLIC3) is a component of Rab25 driven invasive phenotype

3.1 Introduction

The mechanistic and cell biological detail of cell migration on two dimensional surfaces (2D) has been extensively studied in the past. However, it has only in recent years become apparent that clear discrepancies exist between migration in 2D and *in vivo*.

The forward movement of the cell is driven by the polymerisation of actin monomers into filamentous actin (F-actin), which generates contractile force capable of driving morphological rearrangements resulting in membrane protrusion that facilitates cell movement. Actin polymerisation occurs in a plasma membrane proximal region and is controlled by forming homology (FH) proteins, Ena/VASP, Arp2/3 in association with WAVE and WASP as well as by cofilin (Krause, Dent et al. 2003; Pollard 2007). The complexity of the actin polymerisation mechanism allows the generation of a number of different F-actin containing structures. On rigid 2D substrates, linear F-actin aggregates can laterally extend from the cell body to form filopodia or dorsally to establish microvilli, whereas arc-shaped F-actin sheets form lamellipodia. The formation of lamellipodia and filopodia depends on the Rac1- and Cdc42-driven organisation of cytoskeletal and adhesive structures (Ridley 2006). Small focal contacts are formed at the leading edge of these protrusions, which leads to integrin-mediated activation of RhoA and the recruitment of Rho activated kinase (ROCK) that facilitates the formation of actin-myosin bundles (Torka, Thuma et al. 2006). When cells move on thicker substrates, such as those composed of extracellular matrix proteins, they form ventral actin-rich protrusions called invadopodia, which mediate ECM proteolysis. On the other hand, cancer cells that disseminate and migrate away from the primary lesion to form metastases at distal sites of the body have to migrate through the extracellular matrix (ECM). The ECM is a three dimensional (3D) meshwork of extracellular proteins such as laminin, collagen and fibronectin and exists in three major forms; dense connective tissue, loose connective tissue and

basement membrane (Even-Ram and Yamada 2005). Cells migrating in 3D environments adopt different morphologies and modes of migration to those that move on 2D substrates, and this is particularly apparent both in that they can acquire epithelial polarity and in the type of contacts that they establish with the matrix components (Roskelley and Bissell 1995). When cells move in a truly 3D matrix, the ventral and dorsal organisation present in 2D environments is lost and the existence of structures such as lamellopodia, stress fibres and invadopodia *in vivo* is debatable. Instead cancer cells moving in a 3D environment have been observed to acquire either an amoeboid morphology, which is characterised by high Rho/ROCK signalling pathway activity and the formation of bleb-like protrusions, or to migrate in an elongated fashion, which does not require Rho/ROCK-mediated actino-myosin contractility, but relies on matrix proteolysis. When migrating in a mesenchymal fashion an actin-rich protrusion at the front of the cell called pseudopod is observed. It is also worth noting, that invading cells can switch from amoeboid to mesenchymal mode of migration and vice versa (Olson and Sahai 2009).

The differences in the nature of focal contracts established in 2D and 3D environments are worth noting. The ECM adhesion structures found in cells cultured on 2D surfaces are termed focal adhesions/contacts (which are rich in $\alpha_v\beta_3$ integrin, paxillin, vinculin and FAK) and fibrillar adhesions (that are composed mainly of $\alpha_5\beta_1$ integrin and tensin (Zamir, Katz et al. 1999)), are replaced by their 3D counterparts; termed 3D matrix adhesions which are characterised by both paxillin and $\alpha_5\beta_1$ integrin positivity (Cukierman, Pankov et al. 2001).

On account of these shortcomings in studying cell adhesion and migration on 2D surfaces, it is necessary to use models that more closely mimic 3D ECM microenvironments in order to study tumour cell migration in the appropriate context. One way to achieve this is to use mono-component self-polymerising ECM constituents to coat 2D substrates. This approach however, oversimplifies the 3D model and doesn't account for its structural complexity and varied composition. A better and more physiologically relevant model that offers many similarities to the ECM *in vivo* is cell derived matrix (CDM) (Cukierman, Pankov et al. 2001). CDMs are generated by growing confluent monolayers of fibroblasts over 10-14 days, during which period they assemble extracellular matrix-like

fibrils around themselves. Following this, the pliable fibrillar, collagen- and fibronectin-rich matrix is denuded of cellular components using a non-ionic detergent and the remaining fibrillar ECM may then be used as a substrate on which to plate cancer cells to study their migratory and cytoskeletal characteristics (Fig. 3.1A&B). Indeed we have recently found that Rab25, which had previously been implicated in the aggressiveness of ovarian and breast tumours (Cheng, Lahad et al. 2004) and shown to be a component of an invasive gene signature of breast cancer cells (Wang, Goswami et al. 2004), alters the way in which A2780 ovarian adenocarcinoma cells migrate on CDMs but not on 2D plastic surfaces (Caswell, Spence et al. 2007). When plated on 2D surfaces, A2780 migrate with the same speed, persistence and directionality regardless of the expression of Rab25. Conversely, when A2780 cells are plated onto CDMs Rab25 expression alters the way that they move, such that they migrate more persistently and do so by extending long pseudopods in the direction of migration (Fig. 3.2A), (Caswell, Spence et al. 2007). Furthermore, Rab25 increases the ability of A2780 cells to invade *bona fide* 3D matrices (such as matrigel or collagen plugs), and its ability to do so is potentiated when these plugs are supplemented with fibronectin, which is a ligand for $\alpha 5\beta 1$ integrin. Further studies performed with integrin blocking antibodies and Rab25/Rab11 mutants revealed that Rab25's invasive capacity requires the binding of $\alpha 5\beta 1$ integrin to the RGD sites in fibronectin and that Rab25's interaction with $\beta 1$ integrin cytoplasmic tail is indispensable for invasive tumour cell migration.

It is also apparent from the studies of Rab25 function in A2780 cells that the ability of Rab25 to drive invasive migration is greater following stable expression of the GTPase than after its transient expression. This suggested that expression of Rab25 could in the longer-term be influencing the expression of other genes, which could collaborate with the GTPase to further promote tumour cell invasion. I therefore decided to determine whether Rab25 expression was able to alter the gene expression profile of A2780 cells in a way that was dependent on the cells being plated onto a 3D matrix, and whether any of these changes may collaborate with Rab25 to drive cancer cell invasion and tumour progression. To this end, I performed a mRNA microarray screen and searched for genes that were differentially expressed in a Rab25 and CDM-dependent manner (Fig. 3.2B).

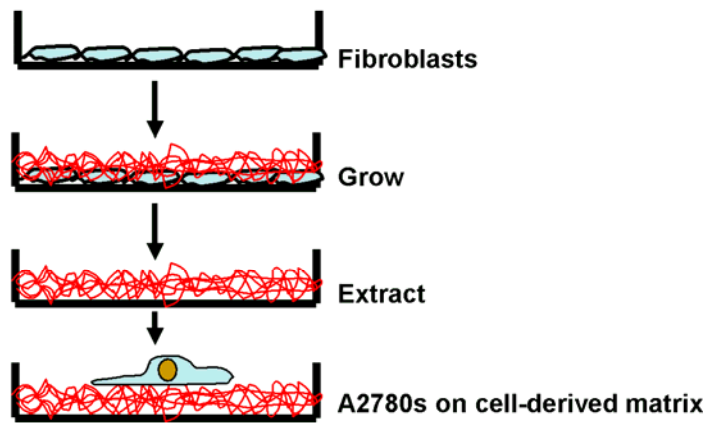
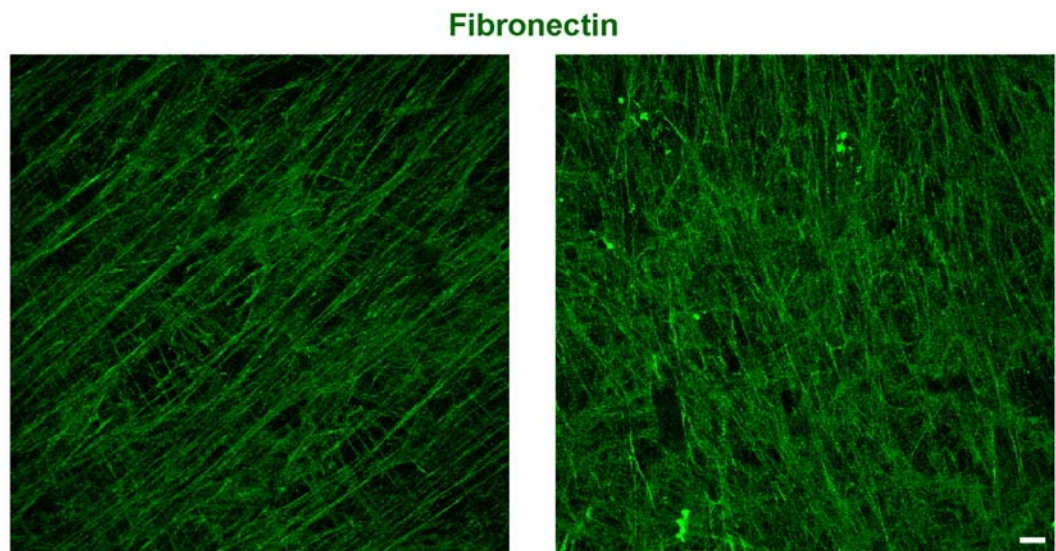
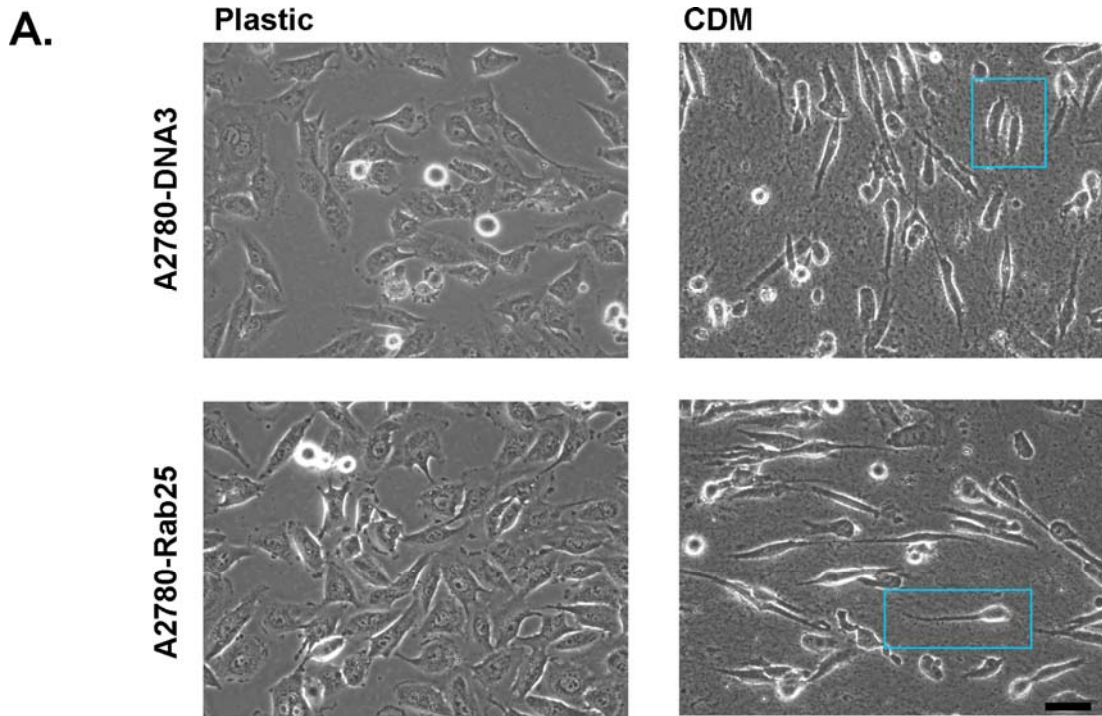
A.**B.**

Figure 3-1 Cell derived matrices (CDM) are three-dimensional and fibronectin rich substrates.

Schematic diagram illustrating the protocol for generation of CDM (A). Confocal sections of CDM displaying either parallel (left) or intersecting (right) fibronectin fibres. Fibronectin was visualised by indirect immunofluorescence using a Cy2-conjugated secondary antibody (green). Scale bar, 10 μ m (B).



B.

A2780-ovarian adenocarcinoma cell line	-Rab25	+ Rab25
plastic		
CDM		

‘✓’ defines situation in which cells exhibit pseudopodial, invasive mode of migration

Figure 3-2 Experimental paradigm.

A2780 cells lacking Rab25 expression (A2780-DNA3) and A2780 cells stably expressing Rab25 (A2780-Rab25) were seeded onto plastic and CDM coated dishes for 16 hours and visualised using a bright field microscope. Blue boxes highlight the phenotypes exhibited by both cell lines on CDM. Scale bar, 50µm (A). Diagram illustrating the experimental approach for the identification of genes upregulated by Rab25 in a matrix dependent fashion. The green tick indicates an invasive phenotype, whose gene signature I set out to analyse (B).

3.2 Results

3.2.1 Microarray analyses identified constituents of Rab25-driven invasive phenotype

3.2.1.1 The quality and purity of RNA was sufficient to perform microarray hybridisation

To identify alterations in gene expression profile that may be elicited by Rab25 expression and/or the presence of a 3D matrix, I plated A2780 cells stably expressing Rab25 (A2780-Rab25) or an empty vector (A2780-DNA3) onto two dimensional (2D) plastic surfaces as well as onto CDMs. 16 hours following plating, RNA was harvested from the cells and traces of genomic DNA were removed by the application of mechanical shear and the addition of DNase.

mRNA constitutes a very small proportion of total cellular RNA thus making its levels difficult to evaluate. Therefore it is the integrity of ribosomal RNA (rRNA), which is the most abundant cellular RNA component, that is commonly used to obtain an index of the condition of mRNA within the preparation of interest. Total RNA was resolved on a 2% agarose gel, which was then stained with ethidium bromide to visualise nucleic acids. This approach revealed the presence of intact 28S and 18S ribosomal RNAs (Fig. 3.3A) and showed no sign of RNA smear, indicating that RNAs had not been noticeably degraded during sample preparation.

The concentration and purity of nucleic acids within the sample were verified spectrophotometrically and corrected so that the RNA concentration for each sample was greater than 0.6 µg/µl and the $A_{260\text{nm}}/A_{280\text{nm}}$ absorbance ratio was at least 1.75 which gives an indication of RNA purity with respect to contamination with proteins (in accordance with the Paterson Cancer Research UK Microarray Facility guidelines). Having achieved these criteria for purity and content within our laboratory, the triplicate total RNA samples from A2780-DNA3 and A2780-Rab25 cells plated onto both plastic and CDMs were sent to the Microarray Facility whereupon they were reassessed by gel electrophoresis (Fig. 3.3B) and an Agilent Bioanalyzer (Fig. 3.3C). These approaches employ capillary

electrophoresis and fluorescence to provide a more accurate determination of RNA purity, concentration and 28S/18S ribosomal RNA ratio. These samples were then further processed by the Microarray Facility in preparation for microarray hybridisation on the GeneChip Human genome U133 Plus2 Array, which provides expression analysis of over 47000 transcripts.

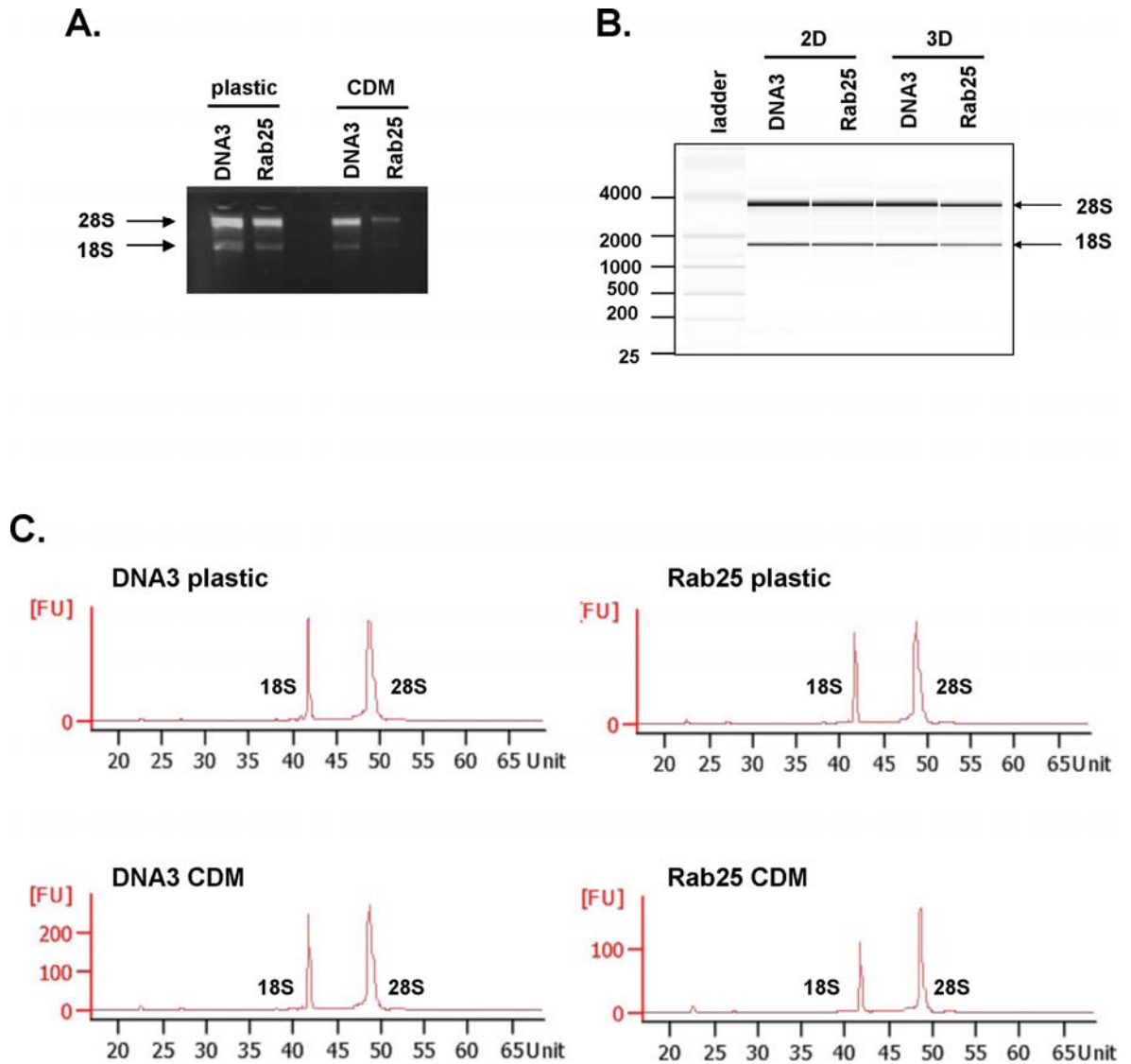


Figure 3-3 Confirmation of the purity and integrity of the RNA samples used for microarray analysis.

A2780-DNA3 and A2780-Rab25 cells were seeded onto either plastic or cell derived matrices (CDM) for 16 hours, RNA was then harvested and purified using QIAGEN RNeasy kit. Its concentration and purity was verified spectrometrically, whilst the integrity was analysed by examination of 28S and 18S ribosomal RNA (rRNA) by electrophoresis on a 2% agarose gel (A). The same procedure was repeated using an Agilent Bioanalyser (B). In (C) shown are electropherogram scans from Agilent Bioanalyser. Peaks corresponding to high and low molecular weight rRNA are indicated.

3.2.1.2 GCRMA normalisation yields good clustering of experimental microarray replicas

When analysing microarray data from multiple high density oligonucleotide chips it is imperative to remove non-biological variation between the arrays (such as differences in experimental procedures and differences in sample labelling intensities or technical divergences between replica arrays) as this may obscure any physiologically relevant alterations in gene expression. (Bolstad, Irizarry et al. 2003). Following hybridisation data acquisition, an automated normalisation step is performed on expression summary values, which relies on the proposal that intensities from each chip should be adjusted so that they have the same average value. This approach however isn't sufficient for all experimental set ups and requires a supplementation with another normalisation method. The Robust Multiarray Average (RMA) is a method that encompasses three steps: background adjustment, quantile normalisation and summarisation of log transformed values (Irizarry, Hobbs et al. 2003).

However, when applied to triplicate sets of four experimental samples (A2780-DNA3 cells and A2780-Rab25 cells both plated onto plastic and CDM) RMA normalisation did not yield a good clustering of the samples as shown by the gene expression histogram and by the Principal Component Analysis (PCA) scatter plot, which visualises experimental replica clustering (Fig. 3.4A). Since the triplicate experimental samples were prepared in separate batches and the samples clustered according to the date when they were hybridised rather than according to their biological characteristics, the batch effect removal filter was applied. This approach uses mixed-model ANOVA to assess batch effects and it adjusts the data in such a way that the batches are equivalent to one another (Kozulin and Provis 2009). Nonetheless, this did not improve sample clustering (Fig. 3.4B). Therefore an improved form of RMA, GeneChip RMA (GCRMA) was used for normalisation and resulted in an enhanced gene expression clustering, but still failed to provide experimental replica clustering as depicted on the PCA scatter plot (Fig. 3.4C). This discrepancy was removed by the application of batch removal filter which led to near perfect clustering of experimental replicas as shown on the PCA plot (Fig. 3.4D).

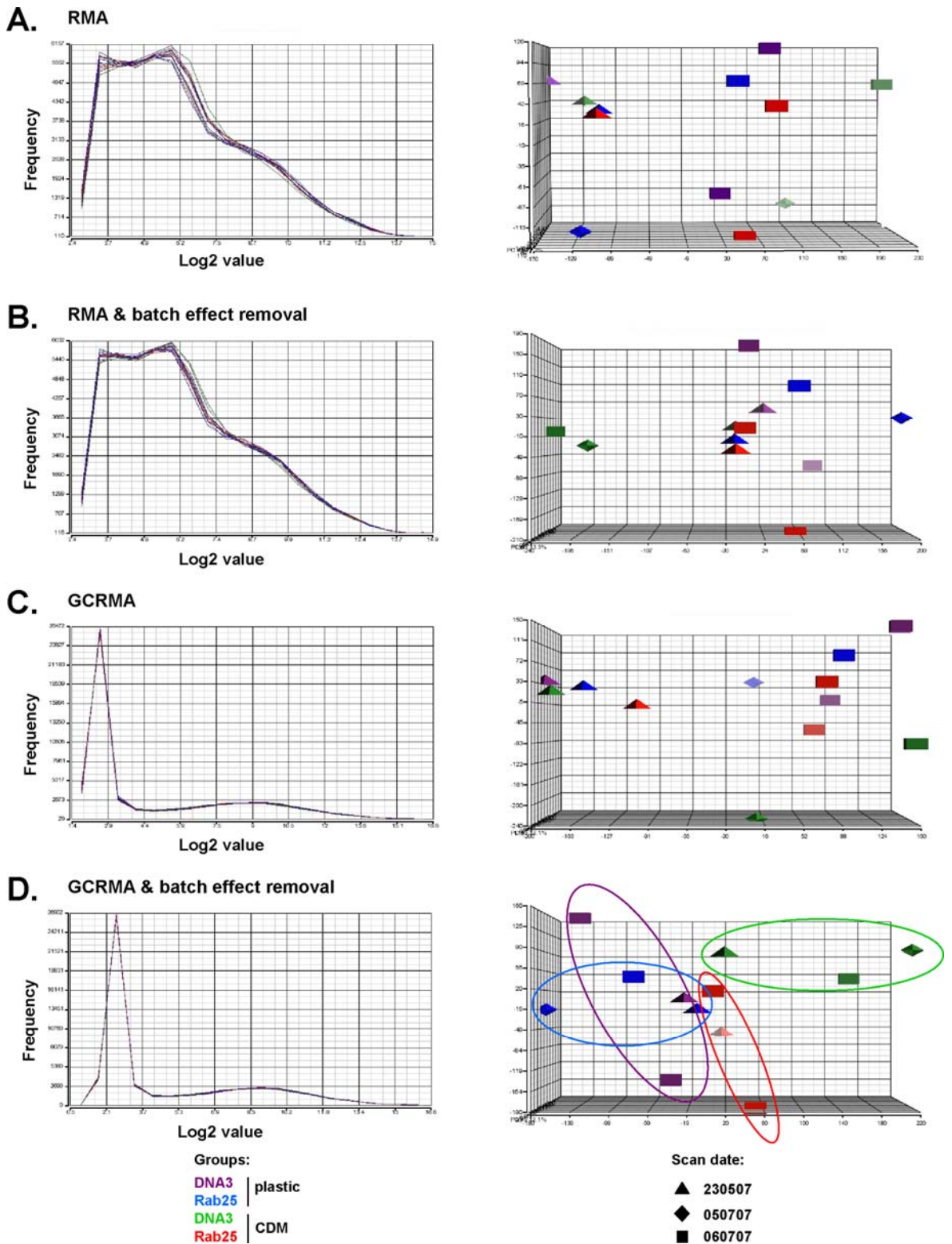


Figure 3-4 GCRMA normalisation results in good clustering of experimental replicates.

The Cel files were normalised and analysed in PARTEK® Genomics Suite Software. Indicted are the clustering patterns obtained after RMA normalisation (A), RMA followed by batch effect removal (B), GCRMA normalisation (C) and GCRMA followed by batch effect removal (D). The panel on the left depicts histograms of gene expression, while the panel on the right represents Principal Component Analysis (PCA) scatter plots. Triangles, diamonds and rectangles correspond to different sample processing times. A2780-DNA3 cells on plastic (DNA3 plastic) in purple, A2780-Rab25 on plastic (Rab25 plastic) in blue, A2780-DNA3 cells on CDM (DNA3 CDM) in green, A2780-Rab25 on CDM (Rab25 CDM) in red.

3.2.1.3 Microarray analyses identify genes whose differential expression is driven by Rab25 in two dimensional and in three dimensional-like environments

Following normalisation, batch effect removal and log transformation, Multiway ANOVA was used to identify genes that were differentially expressed in A2780-Rab25 *versus* A2780-DNA3 cells both plated onto CDM. Genes were primarily ranked according to fold change values (fold change ≥ 3) and subsequently p-value was used for final filtering (p-value ≥ 0.01). These analyses returned 78 and 22 genes that were up- and down-regulated, respectively, by Rab25 expression when A2780 cells were grown on CDMs (Fig. 3.5, Appendix 3.1&3.2). The same method was used to identify 28 and 36 genes that were respectively up- and down-regulated by Rab25 expression, when A2780 cells were cultured on plastic surfaces (Fig. 3.6, Appendix 3.3&3.4).

CDM Rab25 vs DNA3				CDM Rab25 vs DNA3			
Gene Symbol	Probe set ID	p-value	Fold-Change	Gene Symbol	Probe set ID	p-value	Fold-Change
GDA	224209_s_at	5.67E-08	100.14	F8	205756_s_at	5.71E-05	3.49
FKBP1B	206857_s_at	1.20E-08	24.32	FGFBP1	205014_at	4.55E-04	3.48
SULF2	224724_at	5.58E-05	10.77	CDH5	204677_at	1.82E-04	3.43
FN1	214702_at	9.97E-04	8.43	PRDX2	39729_at	3.59E-06	3.43
NMNAT2	209755_at	6.21E-08	8.24	DCLK1	229800_at	8.62E-04	3.42
KCNK3	205952_at	7.76E-06	8.00	PLXNA2	227032_at	1.62E-03	3.39
ODZ2	231867_at	2.81E-06	7.62	C10orf58	224435_at	4.82E-08	3.34
EDNRA	204463_s_at	3.54E-03	7.32	ACSS3	229222_at	2.51E-04	3.25
AJAP1	215789_s_at	9.31E-03	6.89	ADAMTS5	235368_at	3.71E-03	3.24
PTGS2	204748_at	3.60E-07	6.77	GPNMB	201141_at	3.10E-03	3.23
UCA1	227919_at	1.43E-06	6.33	EDIL3	225275_at	1.52E-03	3.20
NMNAT2	1552712_a_at	1.13E-05	6.21	PQLC3	225579_at	1.35E-04	3.20
CARD16	1552701_a_at	1.00E-05	6.08	SYTL1	227134_at	4.53E-03	3.16
GSTT1	203815_at	2.46E-05	5.98	F2RL1	213506_at	8.44E-04	3.12
SSPN	226932_at	1.54E-04	5.93	ZFP90	235698_at	3.27E-05	3.11
CPS1	217564_s_at	9.97E-04	5.75	FAM129A	217966_s_at	8.83E-04	3.11
AJAP1	206460_at	2.69E-03	5.73	KIAA1324	226248_s_at	1.72E-03	3.10
MT1M	217546_at	2.21E-04	5.73	ZFP90	226124_at	2.98E-05	3.09
HTRA1	201185_at	3.81E-03	5.47	KCNJ2	206765_at	1.00E-02	3.08
BEX5	229963_at	8.84E-04	5.43	C10orf58	228155_at	1.28E-06	3.06
MSLN	204885_s_at	2.40E-03	5.37	TP53INP1	225912_at	3.78E-04	3.06
DNAJC10	229588_at	4.25E-05	5.34	PPAPDC2	227385_at	4.62E-05	3.02
SULF2	233555_s_at	9.00E-03	5.27	EFEMP2	209356_x_at	3.96E-04	3.02
THSD4	226506_at	4.45E-04	5.20	FAM49A	209683_at	8.42E-04	3.00
NLRC3	236295_s_at	6.25E-04	5.16	IL12A	207160_at	1.03E-03	-3.03
ADAMTS5	219935_at	4.27E-03	5.10	BIRC3	210538_s_at	4.99E-06	-3.03
DCDC2	222925_at	2.59E-04	5.00	TIMP3	201148_s_at	2.47E-03	-3.06
SLC16A6	230748_at	1.07E-03	4.75	IGDCC4	227870_at	1.89E-03	-3.07
CLIC3	219529_at	2.25E-08	4.73	RAGE	205130_at	5.19E-06	-3.09
AHNAK2	212992_at	1.34E-04	4.48	IL13RA2	206172_at	1.09E-05	-3.14
NMNAT2	1556029_s_at	1.55E-06	4.47	BMPRI1B	229975_at	1.60E-03	-3.15
CHCHD5	223479_s_at	4.68E-07	4.42	PTPRR	206084_at	1.06E-03	-3.24
PLA2G4A	210145_at	6.95E-05	4.32	SLIT2	209897_s_at	5.40E-04	-3.36
PRKCQ	210038_at	1.87E-05	4.28	ITPR1	211323_s_at	1.48E-04	-3.50
CDC42EP5	227850_x_at	5.72E-04	4.11	PTPRR	210675_s_at	7.45E-04	-3.64
MYO5C	218966_at	2.53E-06	4.04	GDF15	221577_x_at	7.10E-04	-4.01
ALDH6A1	221589_s_at	1.60E-03	4.02	TGFB2	228121_at	1.40E-03	-4.04
LPAR5	230252_at	3.26E-08	3.89	PAG1	225626_at	2.04E-03	-4.28
ADAMTS5	229357_at	2.36E-05	3.85	DENND2D	221081_s_at	2.69E-05	-4.40
GLT8D2	227070_at	6.54E-04	3.80	TIMP3	201149_s_at	1.39E-03	-4.96
AHSA2	226665_at	5.06E-03	3.75	LXN	218729_at	1.70E-04	-6.94
KCNK3	228127_at	3.43E-06	3.69	AFF3	227198_at	4.68E-05	-10.23
DSP	200606_at	6.76E-04	3.66	S1PR3	228176_at	2.68E-05	-10.62
GPRASP2	228027_at	9.76E-07	3.65	TIMP3	201147_s_at	3.82E-07	-13.72
ZNF395	218149_s_at	1.00E-04	3.65	CDCP1	218451_at	2.24E-06	-18.56
TRIM2	202342_s_at	9.49E-04	3.62	TIMP3	201150_s_at	2.59E-08	-23.03
C1orf25	233750_s_at	6.74E-03	3.58				
GRK5	204396_s_at	6.71E-03	3.54				
F11R	221664_s_at	1.19E-03	3.53				
DNAJC10	221781_s_at	2.49E-05	3.52				
EDNRA	204464_s_at	2.49E-04	3.52				
CCND2	200953_s_at	2.29E-04	3.52				
LOC100132815	227234_at	5.82E-04	3.50				
FBLN7	229247_at	3.03E-03	3.49				

Figure 3-5 Genes differentially expressed in Rab25-expressing cells when plated onto CDM. In the columns from left to right listed are: gene symbols, corresponding microarray probe numbers, p-values and fold changes. When identifying differentially regulated genes a fold change threshold of 3 was applied and maximum p-value was 1.00E-02 (Multiway ANOVA). Genes are ordered by decreasing fold change. The orange line separates the upregulated from the downregulated genes.

<i>Plastic Rab25 vs DNA3</i>				<i>Plastic Rab25 vs DNA3</i>			
Gene Symbol	Probe set ID	p-value	Fold-Change	Gene Symbol	Probe set ID	p-value	Fold-Change
GDA	224209_s_at	7.03E-08	88.46	LPXN	216250_s_at	6.93E-05	-3.01
RAB25	218186_at	5.09E-03	24.95	RGS4	204337_at	4.56E-04	-3.06
FKBP1B	206857_s_at	2.95E-08	17.24	IFI44	214453_s_at	2.53E-05	-3.06
FGFBP1	205014_at	3.04E-06	12.27	TGFB2	220407_s_at	1.66E-03	-3.08
ODZ2	231867_at	8.57E-07	10.71	ITPR1	211323_s_at	2.82E-04	-3.13
UCA1	227919_at	1.70E-06	6.07	TIMP3	201149_s_at	7.78E-03	-3.26
NFATC2	226991_at	2.31E-03	5.77	FBXO32	225803_at	1.30E-03	-3.28
ST6GALNAC5	220979_s_at	3.95E-03	5.15	ARRDC3	224797_at	1.60E-03	-3.28
CHCHD5	223479_s_at	2.77E-07	4.90	COL6A3	201438_at	2.23E-03	-3.34
KCNK3	205952_at	5.60E-05	4.89	LRIG1	211596_s_at	1.81E-06	-3.39
CCND2	200953_s_at	4.56E-05	4.87	CXCL1	204470_at	3.22E-09	-3.42
NMNAT2	1552712_a_at	5.84E-05	4.29	STC1	204597_x_at	5.63E-05	-3.44
CRIP1	205081_at	2.05E-04	4.17	RGS4	204338_s_at	7.46E-03	-3.47
CDC42EP5	227850_x_at	5.37E-04	4.16	HIP1	226364_at	5.74E-04	-3.57
DSP	200606_at	4.47E-04	3.98	NF-E4	1560527_at	9.09E-05	-3.58
BEX5	229963_at	3.02E-03	3.97	PNMA2	209598_at	4.20E-04	-3.74
DCDC2	222925_at	9.47E-04	3.74	CD163L1	223655_at	3.94E-04	-3.79
SULF2	224724_at	2.81E-03	3.69	DENND2D	221081_s_at	4.66E-05	-3.95
MYO5C	218966_at	4.25E-06	3.68	IGDCC4	227870_at	4.70E-04	-4.06
NMNAT2	209755_at	2.58E-06	3.68	CYP2J2	205073_at	1.43E-04	-4.09
AHSA2	226665_at	6.98E-03	3.47	COL5A1	203325_s_at	1.37E-04	-4.11
LOC100132815	227234_at	6.11E-04	3.46	STC1	204595_s_at	1.72E-04	-4.31
DNAJC10	229588_at	3.92E-04	3.37	RNF182	230720_at	1.59E-04	-4.48
PRDX2	39729_at	7.22E-06	3.08	IL13RA2	206172_at	1.30E-06	-4.54
PLA2G4A	210145_at	4.31E-04	3.07	PAG1	225626_at	1.49E-03	-4.63
FAM129A	217966_s_at	9.66E-04	3.06	LOC100288985	230746_s_at	1.89E-04	-4.66
NMNAT2	1556029_s_at	1.43E-05	3.05	CXCL3	207850_at	3.35E-04	-4.69
CARD16	1552701_a_at	3.36E-04	3.01	TGFB2	228121_at	2.41E-04	-6.25
				TGFB2	209909_s_at	2.69E-07	-6.61
				LXN	218729_at	1.59E-04	-7.08
				GDF15	221577_x_at	5.89E-05	-7.40
				S1PR3	228176_at	5.24E-05	-8.61
				TIMP3	201147_s_at	8.15E-07	-10.74
				AFF3	227198_at	1.26E-05	-16.19
				TIMP3	201150_s_at	5.44E-08	-17.34
				CDCP1	218451_at	6.89E-07	-30.18

Figure 3-6 Genes differentially expressed in Rab25-expressing cells when plated onto plastic surfaces.

The hits are ranked and ordered as for the previous figure. The panel on the left lists the genes upregulated by Rab25, whilst the one on the right the downregulated transcripts.

3.2.1.4 Eighteen genes (three of which are ion carriers) are upregulated by Rab25 in a matrix specific fashion

Having identified genes whose expression was regulated by the presence of Rab25, I wished to refine my data set to highlight genes that were upregulated by Rab25 in a matrix specific fashion. Genes that were differentially expressed in A2780-Rab25 cells on CDM as compared to A2780-DNA3 cells on CDM, which also showed differential expression on plastic surfaces, of at least 1.5 fold, were removed from the primary list. This was done to prevent false positive discoveries and to exclude any genes that showed expression variation on 2D in the same direction as they did in 3D. This resulted in the identification of 18 genes that were upregulated in a Rab25 and CDM specific manner and that could potentially be components of Rab25 driven invasive phenotype (Fig. 3.7).

To identify the most promising target genes from the list of 18, I decided to apply two additional statistical filters. Firstly, I looked at the Bonferroni p-value, which provides a conservative test of significance when comparing three or more groups of conditions and is derived from the unadjusted p-value by the multiplication of the later by the number of observations. Such a statistical analysis protects against 'overdiscovery' of significant events, but poses a big risk of false negatives. When Bonferroni correction is used changes in expression of only two genes appear statistically significant; CLIC3 (Bonferroni score of $p=0.0012$), and prostaglandin-endoperoxidase synthase 2 (PTGS2) (Bonferroni score of $p=0.0197$).

When a less conservative step-up p-value that controls false discovery rates (Kwong and Wong 2002) was applied, a number of other genes appeared to be significantly upregulated, such as ADAM metallopeptidase with thrombospondin type 1 motif-5 (ADAMTS5)(step-up score of $p=0.0106$), acyl-CoA synthetase short-chain family member 3 (ACSS3)(step-up score of $p=0.0364$), and tumour protein p53 inducible nuclear protein1 (TP53INP1) (step-up score of $p=0.0425$). Importantly, step-up adjustment also identified CLIC3 as the most significantly upregulated gene in that group (step-up score of $p=0.0002$). I, therefore, decided to determine whether CLIC3 may be a genuine downstream effector of Rab25.

In addition to pursuing CLIC3, I also wanted to explore the possibility that other Rab25 upregulated genes that are thought to encode for membrane transporters and/or channels may regulate invasive migration of tumour cells, so I also selected the genes for the monocarboxylic acid transporter 7 (SLC16A6) and the potassium inwardly-rectifying channel member-2 (KCNJ2) in my validation analyses. Firstly, I looked at the fold changes in expression of CLIC3, SLC16A6 and KCNJ2 as determined by the three individual microarray hybridisation experiments. As illustrated by both the heat map (Fig. 3.8A) (on which the colour of the box and the depth of the colour represent relative expression levels) and by numerical data presented as normalised, log transformed fluorescence values (Fig. 3.8B-D), the Rab25 and CDM driven upregulation was most reproducible for CLIC3 (Fig. 3.8B) and less so for SLC16A6, which showed very high induction in the second experimental replica, but less so in the first or third hybridisation (Fig. 3.8C). On the other hand, alteration in KCNJ2 mRNA levels was not observed in the first experiment, but occurred to a similar extent in the other two experimental repeats (Fig. 3.8D).

A. *Upregulated in A2780-Rab25 on CDM (fold change \geq 3), fold change on plastic <1.5*

Gene Symbol	Probeset ID	CDM			Plastic	
		p-value CDM	bonferroni p-value	stepup p-value	Fold-Change	Fold-Change plastic
PTGS2	204748_at	3.60E-07	0.0197029	0.000802463	6.77	1.10
HTRA1	201185_at	3.81E-03	1	0.109139	5.47	-1.08
NLRC3	236295_s_at	6.25E-04	1	0.0521152	5.16	1.45
SLC16A6	230748_at	1.07E-03	1	0.063257	4.75	-1.45
CLIC3	219529_at	2.25E-08	0.00123207	0.000215605	4.73	1.10
ALDH6A1	221589_s_at	1.60E-03	1	0.07539	4.02	1.43
ADAMTS5	229357_at	2.36E-05	1	0.0106548	3.85	1.21
GLT8D2	227070_at	6.54E-04	1	0.052965	3.80	1.20
TRIM2	202342_s_at	9.49E-04	1	0.06053	3.62	1.04
C1orf25	233750_s_at	6.74E-03	1	0.139397	3.58	1.38
GRK5	204396_s_at	6.71E-03	1	0.139185	3.54	1.24
ACSS3	229222_at	2.51E-04	1	0.0364138	3.25	1.25
ADAMTS5	235368_at	3.71E-03	1	0.108384	3.24	1.12
GNPMB	201141_at	3.10E-03	1	0.100301	3.23	1.50
SYTL1	227134_at	4.53E-03	1	0.117668	3.16	1.41
KCNJ2	206765_at	1.00E-02	1	0.164811	3.08	1.15
TP53INP1	225912_at	3.78E-04	1	0.0425706	3.06	1.34
FAM49A	209683_at	8.42E-04	1	0.0580347	3.00	-1.12

B.

Gene Symbol	Gene Title
PTGS2	prostaglandin-endoperoxide synthase 2
HTRA1	HtrA serine peptidase 1
NLRC3	NLR family, CARD domain containing 3
SLC16A6	solute carrier family 16, member 6 (monocarboxylic acid transporter 7)
CLIC3	chloride intracellular channel 3
ALDH6A1	aldehyde dehydrogenase 6 family, member A1
ADAMTS5	ADAM metalloproteinase with thrombospondin type 1 motif, 5
GLT8D2	glycosyltransferase 8 domain containing 2
TRIM2	tripartite motif-containing 2
C1orf25	chromosome 1 open reading frame 25
GRK5	G protein-coupled receptor kinase 5
ACSS3	acyl-CoA synthetase short-chain family member 3
ADAMTS5	ADAM metalloproteinase with thrombospondin type 1 motif, 5
GNPMB	glycoprotein (transmembrane) nmb
SYTL1	synaptotagmin-like 1
KCNJ2	potassium inwardly-rectifying channel, subfamily J, member 2
TP53INP1	tumor protein p53 inducible nuclear protein 1
FAM49A	family with sequence similarity 49, member A

Figure 3-7 Eighteen genes are differentially expressed in a Rab25 and CDM-dependent fashion.

This list contains genes that are regulated by Rab25, but only when cells are plated onto CDM. From left to right are: gene symbols, microarray probe numbers, p-values, Bonferroni p-values and step-up p-values for changes on CDM (in red and green very highly and highly significant p-values, respectively), fold changes on CDM and fold changes on plastic. Highlighted in yellow boxes are three genes whose upregulation I chose to validate; SLC16A6, CLIC3 and KCNJ2 and in the black box is CLIC3 – the main candidate gene (A). Gene names corresponding to gene symbols listed above (B).

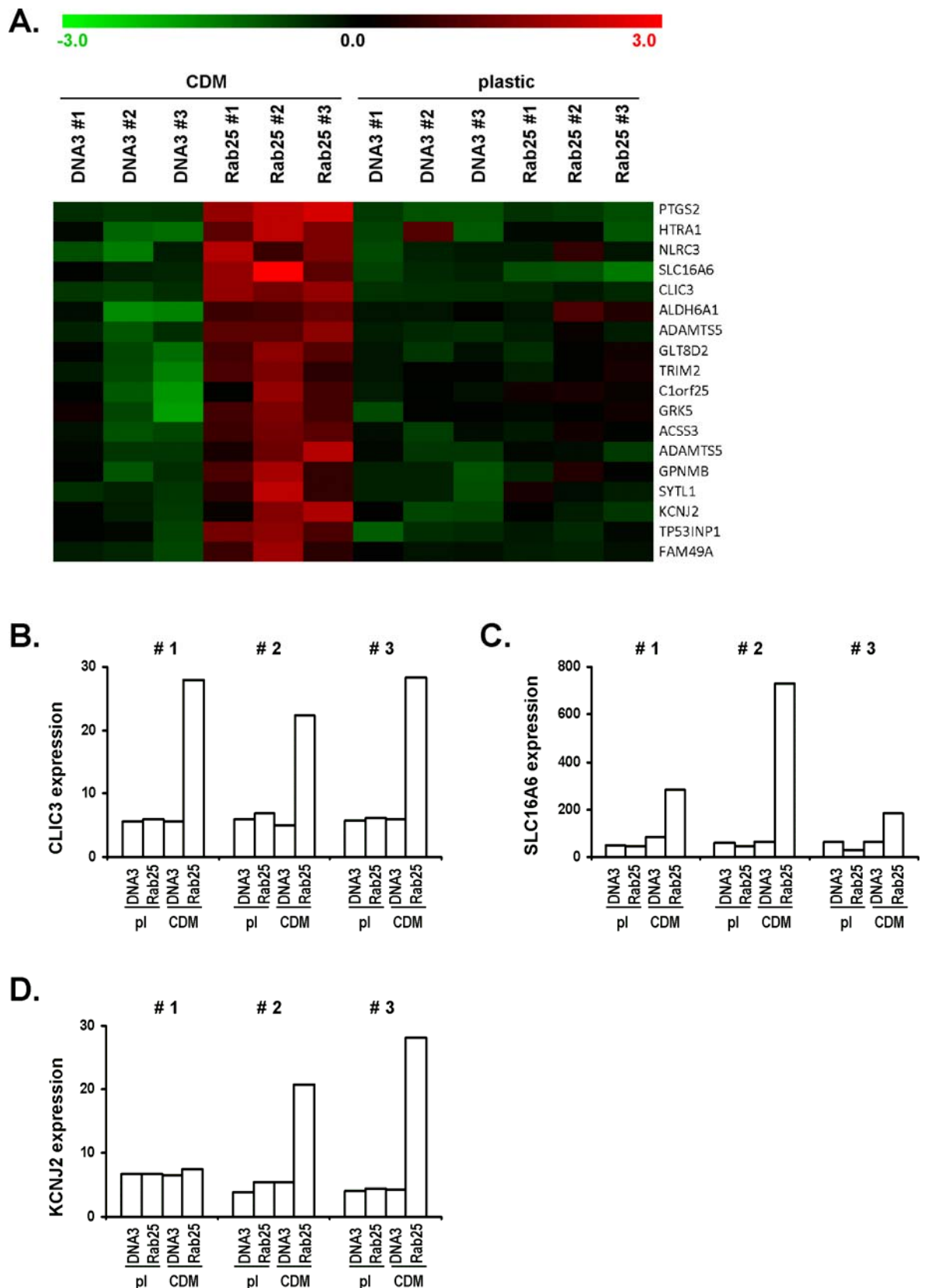


Figure 3-8 Of the 18 genes that are upregulated in a Rab25 and CDM-dependent manner, three are transporters.

The heat map shows 18 transcripts upregulated in A2780-Rab25 cells grown on CDM. The columns represent triplicate sets of samples, with the A2780-DNA3 (DNA3) and A2780-Rab25 (Rab25) cells on CDM to the left and the same cell lines on plastic to the right. The 18 rows denote the 18 transcripts and the colour and intensity of the boxes allocated to each data point represent the log₂ expression level: low expression (green), high expression (red) (A). Linear fluorescence values from each replica experiment (#1, #2 and #3) corresponding to probe sets recognising CLIC3 (B), SLC16A6 (C) and KCNJ2 (D) were extracted from the microarray data set.

3.2.2 Use of qPCR to validate CLIC3, SLCA16A6 and KCNJ2 upregulation

3.2.2.1 qPCR primer pairs amplify a single product and they do so in a linear manner over a range of cDNA concentrations

Reverse transcription followed by quantitative polymerase chain reaction (qPCR) is a method of quantifying the initial amount of template DNA molecules for a gene of interest. The quantity of the template in an experimental sample is most commonly expressed relative to its amount in a control sample, and equal template loading for both samples is ensured by normalisation against a housekeeping gene. Unlike the conventional RT-PCR, qPCR allows 'real time' observation of amplicon accumulation, which is reflected by proportional fluorescence accretion as the amplification cycles proceed. The qPCR reaction consists of four stages characterised by different kinetics. Initially, in the lag phase the product is being amplified, but fluorescence generated in that process is beyond the detection threshold. Secondly, the exponential amplification phase occurs and the copy number of the template doubles with each amplification cycle. This stage is the most crucial for the quantification process as it allows the determination of the threshold cycle (C_T), which is the point at which the amplification curve crosses the threshold and it is used for subsequent relative quantification. C_T is inversely proportional to the log initial template quantity, which means that the more starting template there is the lower the C_T value. Thirdly, in the retardation phase, the amplification inhibitory factors accumulate and the reaction constituents become limiting, which decreases the reaction rate. Finally, the process reaches a steady state and the amplification ceases (Scheffe, Lehmann et al. 2006).

One very important consideration for a successful and accurate template measurement in qPCR is the choice of suitable primers. I therefore confirmed that the primer pairs targeting CLIC3, SLC16A6, KCNJ2 and two housekeeping/reference genes - β -actin and GAPDH, respectively, were specifically amplifying a single product, as illustrated by the ethidium bromide stained agarose gel on which qPCR reaction mixes were resolved (Fig. 3.9A). The generation of a single product was also analysed by the inspection of the

dissociation (melting) curve of each amplification product, as generated by the Opticon Monitor Software. The melting curve analysis of the 5 amplicons of interest confirmed the presence of a single spike each (Fig. 3.9B), indicative of a single amplification product. Additionally, '-cDNA' reaction (Fig. 3.9C), in which cDNA is replaced by water and '-RT' reaction, for which a mock RT mix is used and no cDNA synthesis is possible (Fig. 3.9D), yield no template amplification confirming the purity of qPCR reaction components and the lack of amplification of possible genomic contaminants, respectively.

Having confirmed that the qPCR reagents were suitable for validation of the candidate genes, I wanted to ensure that all the primer pairs were amplifying in a linear manner over a range of concentrations. This was achieved by performing qPCR reactions on serial dilutions of cDNA templates and plotting C_T values against the logarithmic values of standard cDNA amounts, which were expressed as dilution factors of the cDNA preparation (i.e. 2x, 1x, 0.5, 0.25, 0.125, 0.0625, 0.03215). The correlation coefficient (R^2) values are 0.9955, 0.995, 0.992, 0.9915 and 0.997 for CLIC3 (Fig. 3.10A), SLC16A6 (Fig. 3.10B), KCNJ2 (Fig. 3.10C), β -actin (Fig. 3.10D) and GAPDH (Fig. 3.10E), respectively, indicating a near perfect linear relationship between the C_T value and cDNA concentration and confirming that the amount of fluorescence measured is proportional to the amount of starting material. Additionally, the amplification efficiencies were calculated from the formula $E=10^{(-1/-a)}-1$, where 'a' represents the gradient of the linear fit (Arezi, Xing et al. 2003) and amounted to: 0.97, 0.87, 1.26, 1.07 and 1.06 for CLIC3, SLC16A6, KCNJ2, β -actin and GAPDH, respectively.

There are two ways of expressing changes in mRNA level following qPCR analysis. One is in absolute template concentrations and relies on the incorporation of previously generated standard curves for known concentrations of the template. However, the more commonly used method for qPCR data quantification describes changes in target gene expression in one sample relative to another, without measuring the absolute quantities of the template. A variation of such relative quantification method is the $\Delta\Delta C_T$ model (Livak and Schmittgen 2001), which also takes into account the possible variation in initial mRNA content between the samples that may arise from unequal total RNA input by incorporating the relevant content of housekeeping genes for each of the analysed conditions and therefore allows for normalisation to an endogenous

reference gene. The $\Delta\Delta C_T$ quantification requires near equal amplification efficiencies and was therefore suitable for the evaluation of changes in the levels of CLIC3 and SLC16A6, but not KCNJ2 mRNA levels with β -actin and GAPDH being used as reference genes.

Given that the amplification efficiency for KCNJ2 primers differed significantly from the others, I decided to use a different mathematical model to calculate relative alterations in the expression of this gene; one that incorporates efficiencies of both the reference and target gene amplification in the calculation (Pfaffl 2001). Additionally, to confirm the suitability of the $\Delta\Delta C_T$ method for the quantitative assessment of CLIC3 and SLC16A6 transcript levels, I have compared the results generated by the $\Delta\Delta C_T$ method and by the model described by Pfaffl for 3 different data sets and observed no discrepancies in relative expression levels (not shown), confirming that $\Delta\Delta C_T$ model is indeed suitable for analysing the expression of these two genes and that slight discrepancies in the amplification efficiencies are negligible and will not obscure the results.

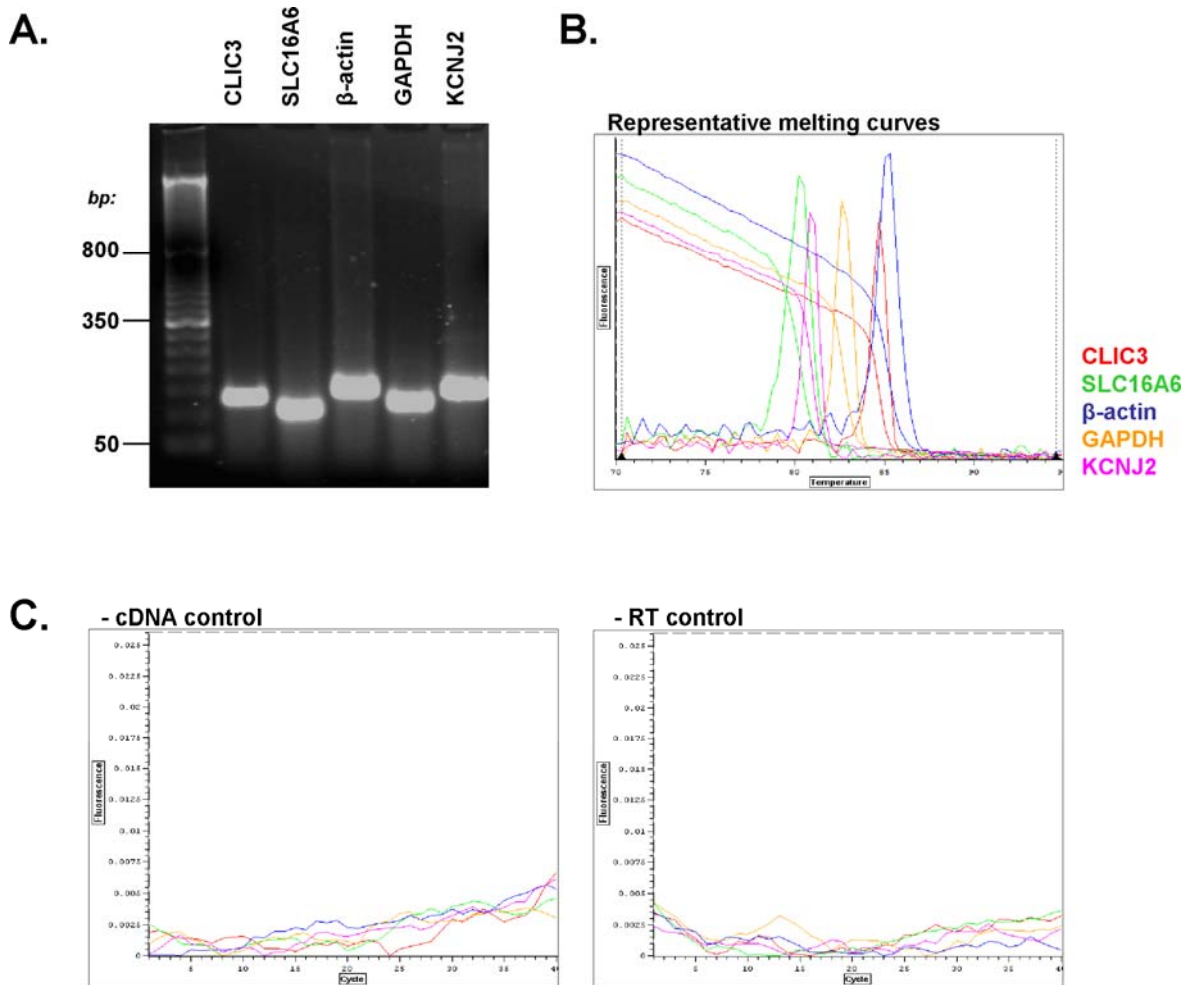


Figure 3-9 Primers for quantitative PCR (qPCR) amplify a single product.

Primer pairs targeting CLIC3 (red), SLC16A6 (green), KCNJ2 (pink) and two housekeeping genes; β -actin (blue) and GAPDH (orange) each amplify a single product as shown by electrophoretic separation on a 2% agarose gel (A) and by representative melting curves of each amplicon, which were generated using Opticon Monitor software (B). qPCR reactions run with the omission of cDNA (-cDNA control) or run on cDNA mix in which cDNA could not have been synthesised due to omission of reverse transcriptase (-RT control), yield no amplicon as shown on the plots derived from Opticon Monitor software (C).

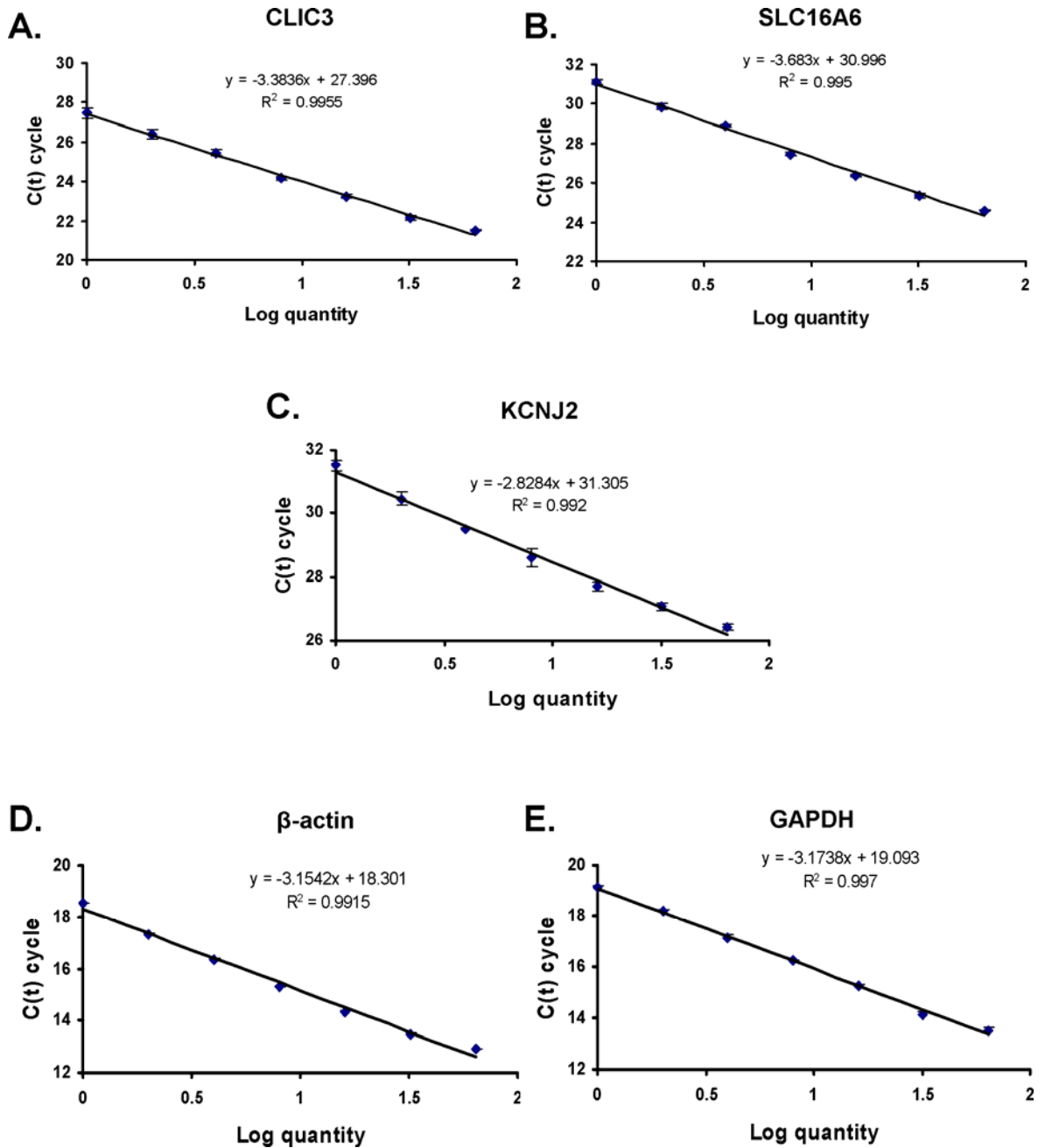


Figure 3-10 Q-PCR primer pairs amplify a product in a linear manner over a range of cDNA concentrations.

cDNA was synthesised from RNA isolated from A2780-Rab25 cells grown on cell derived matrices for 18 hours. Serial dilutions of cDNA were used in a series of triplicate q-PCR reactions to test the efficiency of the above primer-sets, in the presence of the SYBR Green dsDNA-specific fluorescent dye. Standard curves representing a plot of C(t) against the initial log quantity of the template and corresponding Rsq values are shown for CLIC3 (A), SLC16A6 (B), KCNJ2 (C) β -actin (D) and GAPDH (E).

3.2.2.2 CLIC3, SLC16A6 and KCNJ2 mRNA levels increase when A2780-Rab25 cells are seeded onto CDM

To validate the Rab25 and CDM driven upregulation of CLIC3, SLC16A6 and KCNJ2, I seeded A2780-DNA3 and A2780-Rab25 cells onto plastic or CDM for 16 hours and subsequently harvested and purified total RNA. Furthermore, to assure that the contribution of the 3D-like matrix to the upregulation of the genes in question was not limited to one type of matrix, I employed two different types of CDM. Firstly, one that was prepared using primary cultured human dermal fibroblasts (HDF) (and previously utilised for the microarray samples) and secondly, one which was produced from telomerase immortalised human foetal foreskin fibroblasts (Tif).

After having synthesised cDNA from the purified total RNA samples I performed qPCR analyses on triplicate sets of samples using two independent housekeeping genes; β -actin and GAPDH. When compared, the numerical data generated independently by normalisation to the two reference genes shows no or very little divergence regardless of which housekeeping gene was used (Fig. 3.11 & 3.12). Preliminary visual inspections of the amplification curves indicated that the magnitude and specificity of Rab25 and CDM-driven upregulation was greater for CLIC3 than for SLC16A6 and KCNJ2. Indeed, CLIC3 mRNA levels increased approximately 5 fold following expression of Rab25 when cells were plated onto plastic surfaces, and about 22 fold when attached to HDF-derived CDM (Fig. 3.11A). SLC16A6 and KCNJ2 expression displayed little or no response to Rab25 expression on plastic, and approximately 5-6 fold increments when cells were plated onto CDM (Fig, 3.11B&C). Moreover, there was little noticeable difference in the mRNA levels of CLIC3 (Fig. 3.12A), SLC16A6 (Fig. 3.12B) or KCNJ2 (Fig. 3.12C) when cells were plated onto CDMs derived from either HDFs or Tif fibroblasts.

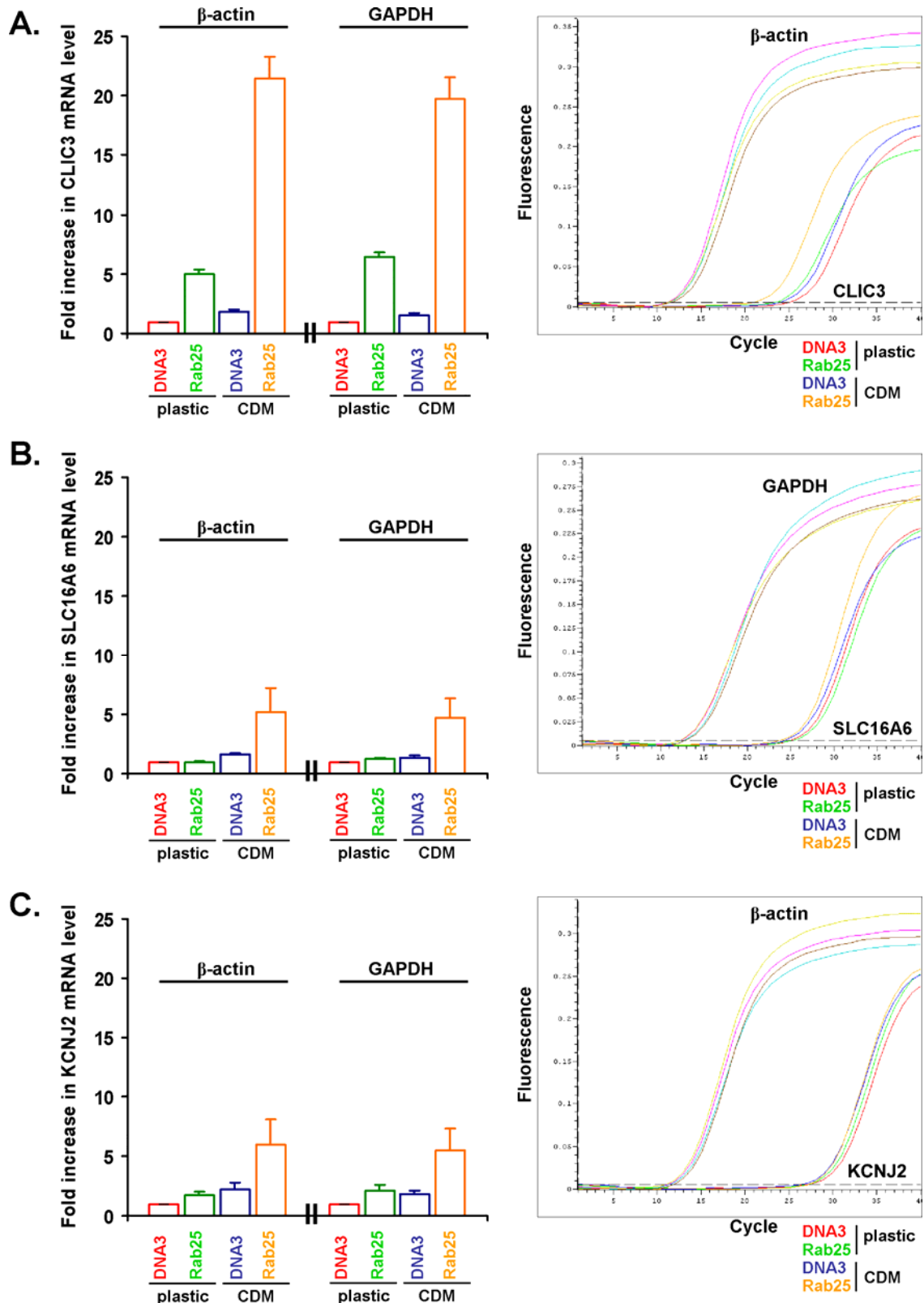


Figure 3-11 Validation of three microarray hits by q-PCR when cells are grown on HDF-derived CDM.

A2780-DNA3 (DNA3) and A2780-Rab25 (Rab25) cells were plated onto plastic surfaces and onto human dermal fibroblast (HDF) derived CDM substrates for 18 hours, RNA was then harvested and purified. cDNA was synthesised and used for quantitative PCR (q-PCR). Expression of CLIC3 (A), SLC16A6 (B) and KCNJ2 (C) was analyzed in the four experimental samples: DNA3 plastic (red), Rab25 plastic (green), DNA3 CDM (blue) and Rab25 CDM (orange). On the right shown are representative amplification plots for genes in question as well as housekeeping genes. The panel on the left shows relative abundance of the target genes, normalised to two independent housekeeping genes; β -actin and GAPDH. Data are mean \pm SEM of three independent experiments, within which three technical replicas were performed.

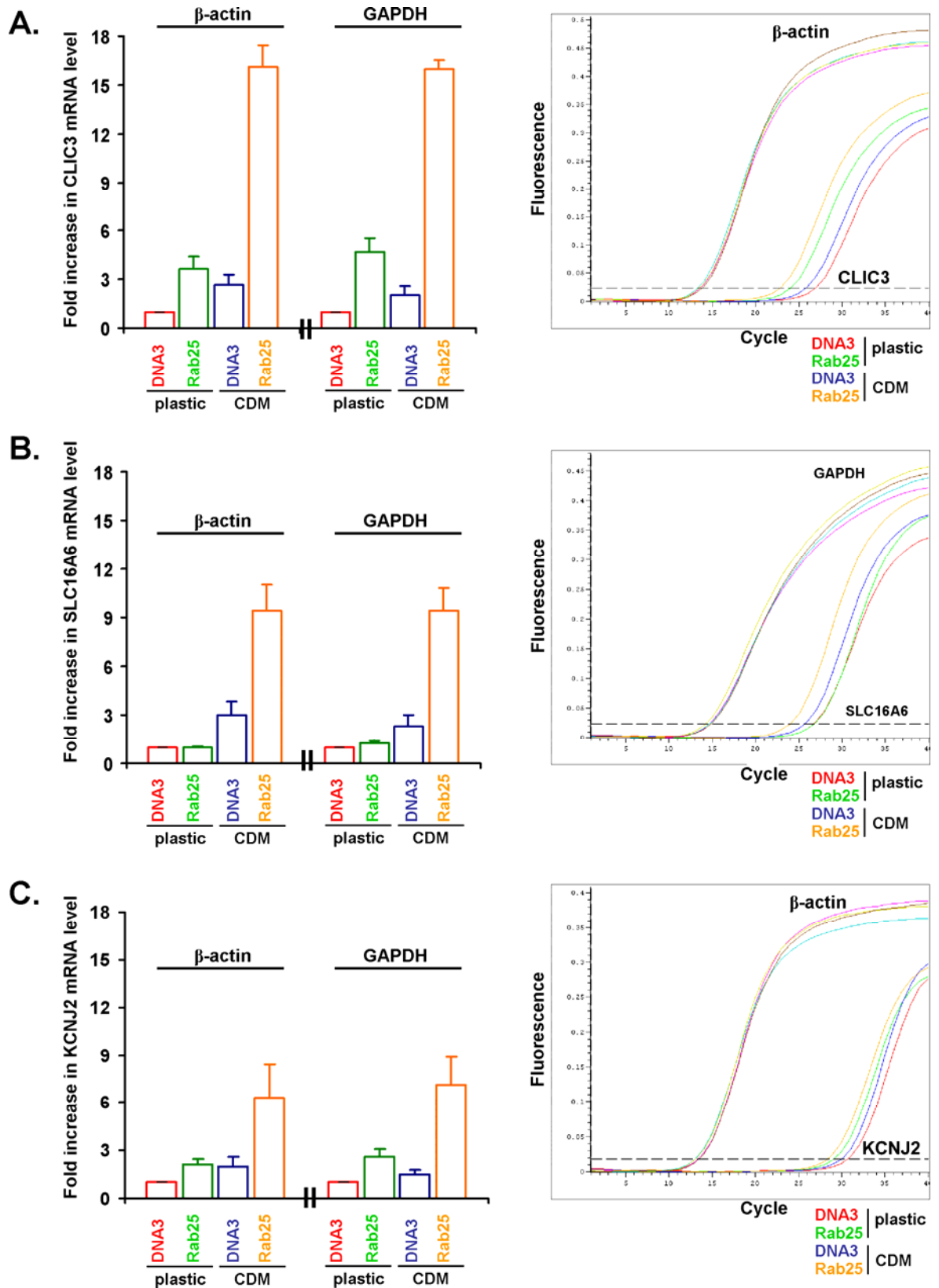


Figure 3-12 Validation of three microarray hits by q-PCR when cells are grown on Tif-derived CDM.

Q-PCR amplification plots and quantification of three independent experiments are shown as in the previous figure. The HDF-derived matrices were here replaced with telomerase immortalised fibroblast (Tif)-derived matrices.

3.2.3 The role of Rab25 in upregulation of CLIC3 expression

3.2.3.1 Upregulation of CLIC3 mRNA but not SLC16A6 or KCNJ2 is opposed by RNAi of Rab25

To determine whether the differences in levels of CLIC3, SLC16A6 and KCNJ2 between A2780-DNA3 and A2780-Rab25 cells were owing primarily to expression of Rab25 and not to coincidental clonal variations between these two cell lines, I decided to use two approaches. Firstly, I transiently overexpressed Rab25 in A2780 cells plated on both plastic and CDMs and assessed levels of the transcripts in question. Secondly, I suppressed Rab25 levels in A2780-Rab25 cells with a short hairpin RNAi vector (shRNAi), seeded the cells onto plastic and CDMs and subsequently determined the levels of CLIC3, SLC16A6 and KCNJ2 mRNA. Additionally, in both cases I looked at possible effects of Rab25's nearest homolog Rab11, on the expression levels of the three candidate genes.

When transiently overexpressed (Fig. 3.13A&B), neither Rab11 nor Rab25 had any discernable and reproducible effects on the expression of CLIC3, SLC16A6 or KCNJ2, regardless of whether cells are seeded onto plastic or CDM (Fig. 3.13C). This inability of transiently expressed Rab25 to upregulate these three candidate genes is consistent with the observation that A2780 clones that stably express Rab25 are more invasive than cells transiently expressing the GTPase.

I then suppressed levels of Rab11 GTPases and Rab25 with shRNAi (Fig. 3.14B) in A2780-Rab25 cells and plated them onto plastic or CDM (Fig. 3.14A). No reduction in SLC16A6 or KCNJ2 transcript levels was observed upon shRNAi of either Rab11A&B or Rab25, but suppression of Rab25 (but not Rab11s) substantially reduced levels of CLIC3 mRNA by about 40%, when cells were plated onto either substrate. These data indicate that continued expression of Rab25 (but not Rab11A&B) is necessary to maintain CLIC3 mRNA at high levels in A2780 cells, whereas the differences in expression of SLC16A6 and KCNJ2 between A2780-DNA3 and A2780-Rab25 cells was likely owing to clonal variation between these two ovarian carcinoma lines.

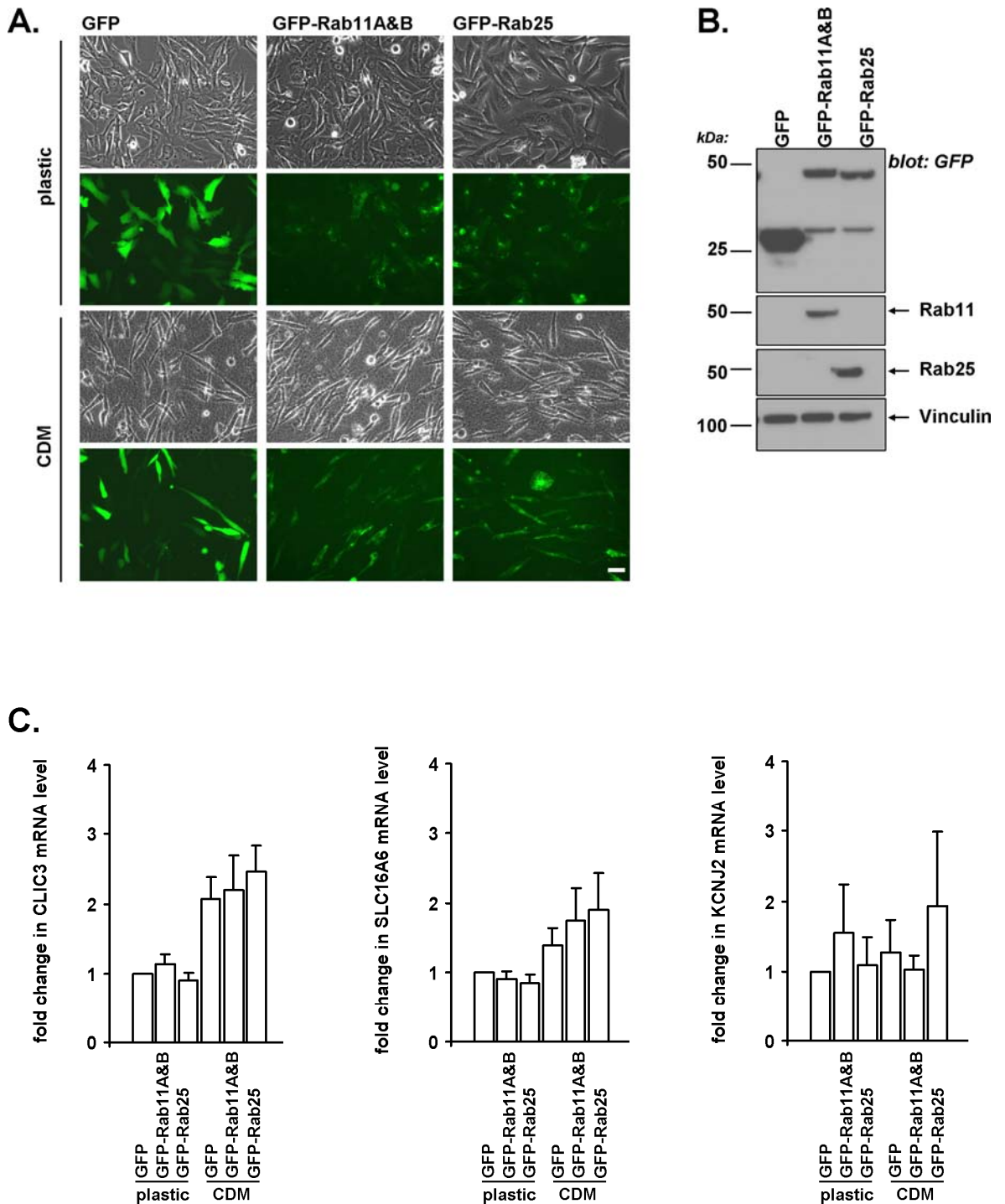


Figure 3-13 CLIC3, SLC16A6 and KCNJ2 expression following transient overexpression of Rab25.

A2780-DNA3 cells were transiently transfected with 3 μ g of GFP, GFP-Rab11 or GFP-Rab25 and were seeded onto either plastic surfaces or CDMs. After 16 hours overexpression was verified by fluorescence microscopy; scale bar, 50 μ m (A). Protein and RNA were then harvested and overexpression on CDM was also analysed by Western Blotting with GFP, Rab11 and Rab25 specific antibodies (B). Changes in CLIC3, SLC16A6 and KCNJ2 transcript levels were analysed by qPCR. From left to right shown are relative expression levels of CLIC3, SLC16A6 and KCNJ2 (C). Data are mean \pm SEM of three independent experiments, within which three technical replicas were performed.

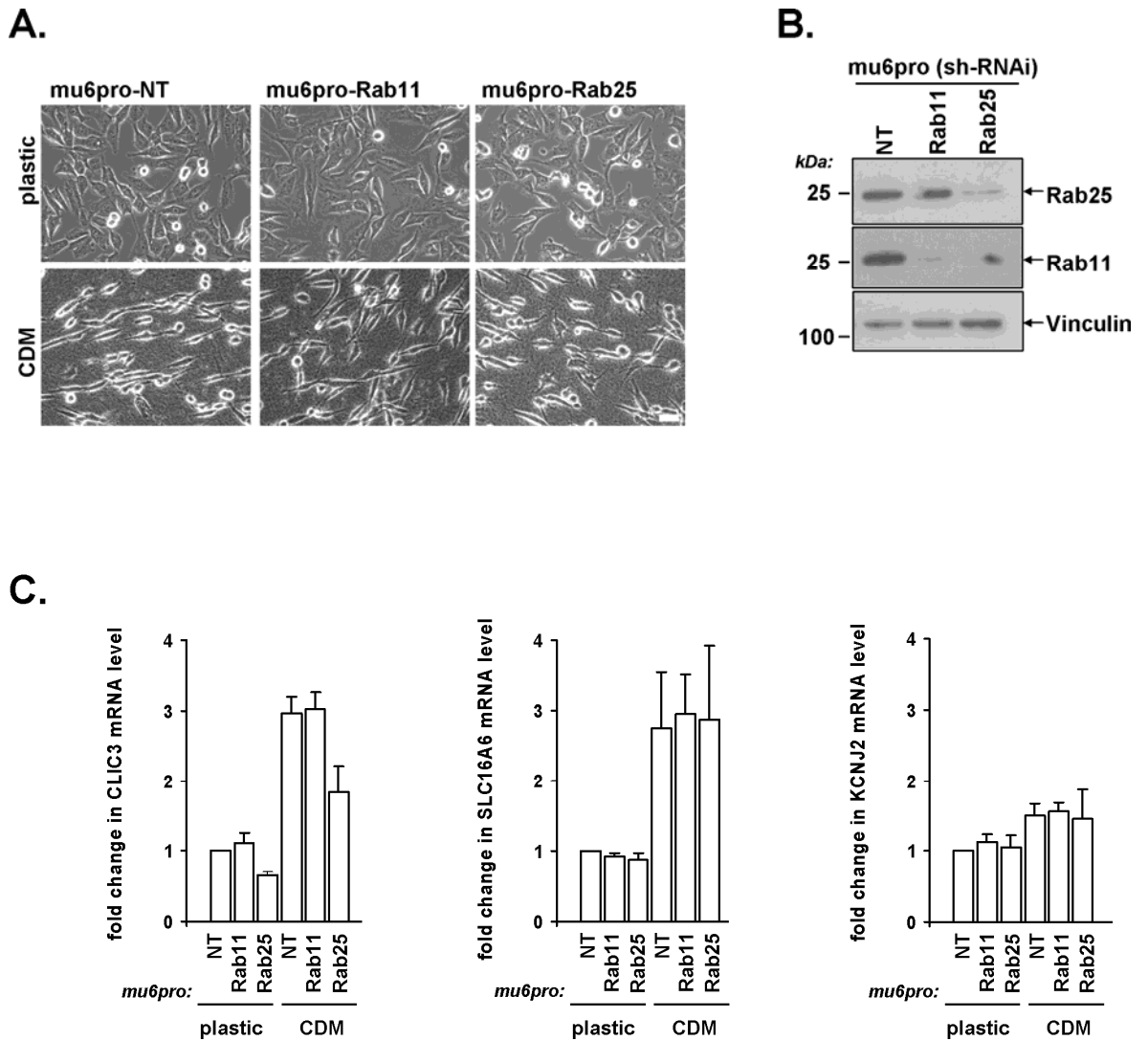


Figure 3-14 CLIC3, SLC16A6 and KCNJ2 expression following Rab25 suppression.

A2780-Rab25 cells were transfected with 3 μ g of short hairpin vectors, containing non targeting control (mu6pro-NT) and targeting Rab11A&B (mu6pro-Rab11A&B) and Rab25 (mu6pro-Rab25), respectively. 24 hours after nucleofection cells were seeded onto either plastic or CDM for 16 hours and bright field images were taken; scale bar, 50 μ m (A). RNA and protein lysates were collected and the suppression of Rab11A&B and Rab25 was analysed by Western-blotting (B). Changes in CLIC3, SLC16A6 and KCNJ2 mRNA levels were investigated by q-PCR. From left to right shown are relative expression levels of CLIC3, SLC16A6 and KCNJ2 (C). Data are mean \pm SEM of three independent experiments, within which three technical replicas were performed.

3.2.3.2 CLIC3 protein levels increase following Rab25 expression and even more so with Rab25 expression and exposure to a three-dimensional matrix

It was next important to determine whether the previously described alterations in CLIC3 gene expression were also reflected by changes in the levels of CLIC3 protein. To do this I plated A2780-DNA3 and A2780-Rab25 cells on plastic and CDM surfaces for 16 hours, harvested protein samples, resolved them by SDS-PAGE and determined CLIC3 proteins levels by Western blotting (Fig. 3.15). CLIC3 protein was largely undetectable in A2780-DNA3 cells, and allowing these cells to attach to CDM did not noticeably alter this. On the other hand, A2780-Rab25 cells expressed detectable quantities of CLIC3 protein when cultured on plastic and this was only slightly increased when these cells were plated onto CDM. This indicated that the levels of CLIC3 protein did not accurately reflect the alterations in CLIC3 mRNA that were described in previous sections.

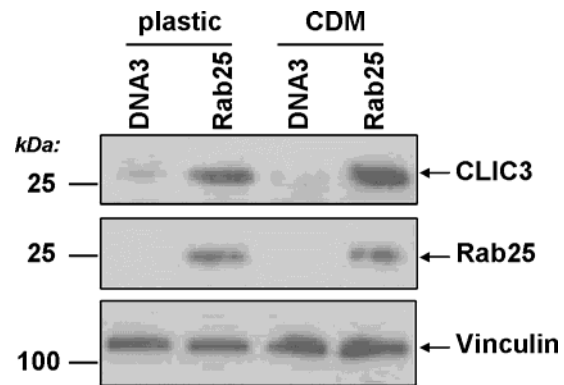


Figure 3-15 CLIC3 protein is upregulated in a Rab25 and CDM-dependent manner.

A2780-DNA3 and A2780-Rab25 cells were plated onto either plastic or CDM substrates for 18 hours, at which point protein lysates were collected and 40 μ g were analysed by Western-blotting using antibodies against HA-tag (recognising Rab25) and against CLIC3. Protein loading was verified by immunoblotting against vinculin.

3.2.3.3 Expression of CLIC family members other than CLIC3 is not affected by Rab25 or CDM

The family of human chloride intracellular channel proteins (CLICs) comprises six closely related homologues; CLIC1, CLIC2, CLIC3, CLIC4, CLIC5 and CLIC6 (Littler, Harrop et al.). To determine whether more than one CLIC family member was regulated by Rab25 I reviewed the microarray data with respect to the expression of other CLICs in the A2780 cell line upon expression of Rab25 and cultivation on CDM. CLIC1 and CLIC4 were expressed by A2780 cells (Fig. 3.16A), whereas CLICs 2, 5, & 6 were undetectable (Fig. 3.16B). Furthermore, no significant changes in the levels of CLIC2 1 & 4 were detectable either following Rab25 expression or exposure to the CDM (Fig. 3.16A). These data indicate that CLIC3 is the sole member of the CLIC family whose expression is regulated by Rab25 in A2780 cells.

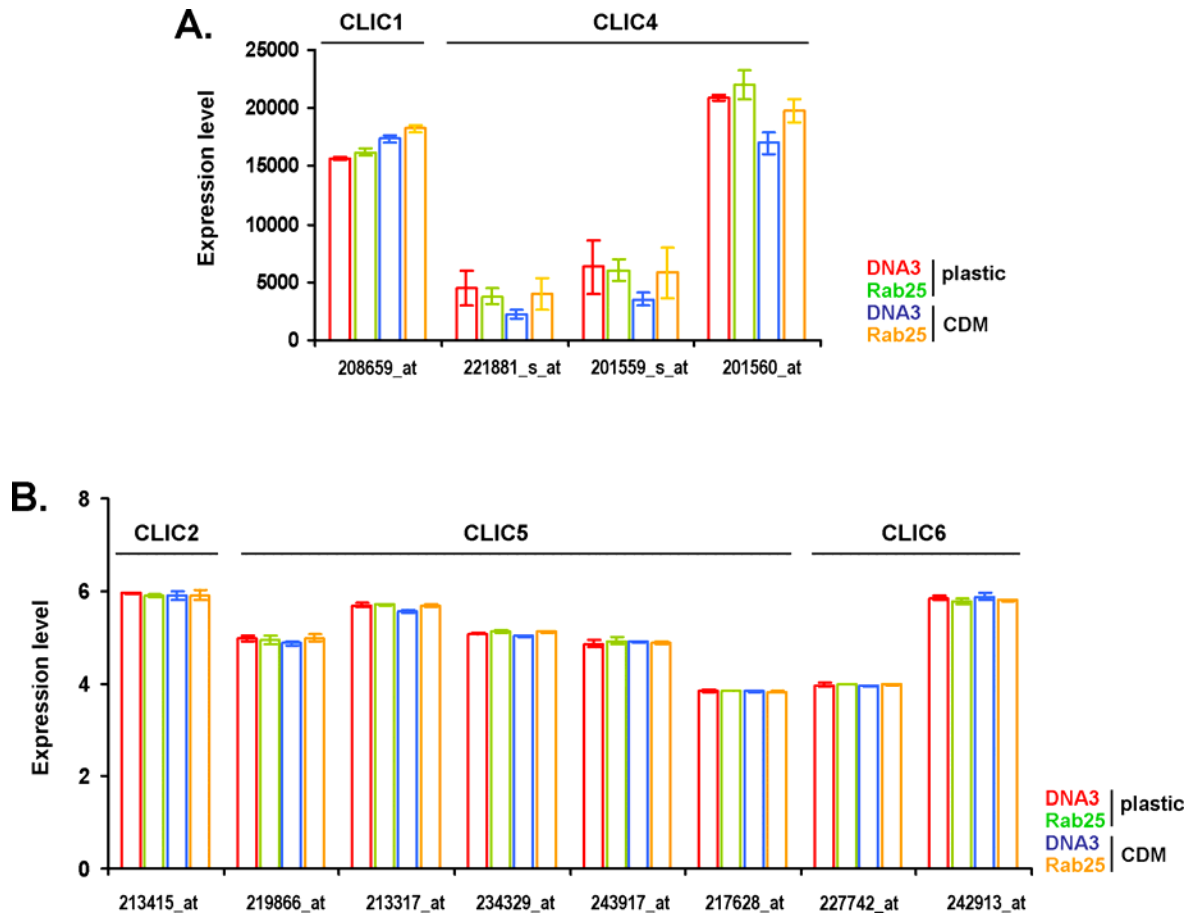


Figure 3-16 Expression of the other CLIC family members in A2780 cells.

Absolute fluorescence values were derived from the microarray data sets, averaged and plotted on the graphs (mean of 3 experiments \pm SEM). In (A) shown are mRNA levels of the CLIC family members, which are expressed in A2780 cells: CLIC1 and CLIC4. In (B) shown are mRNA levels of CLICs that are not expressed: CLIC2, CLIC5 and CLIC6. Affymetrix chip probe numbers recognising the said genes are listed at the bottom of the graphs. A2780-DNA3 cells on plastic (DNA3 plastic) in red, A2780-Rab25 on plastic (Rab25 plastic) in green, A2780-DNA3 cells on CDM (DNA3 CDM) in blue, A2780-Rab25 on CDM (Rab25 CDM) in orange.

3.2.3.4 Suppressing the function of β 1 integrin with blocking antibodies increases CLIC3 mRNA level

Given the previously established physical association between Rab25 and α 5 β 1, and the role that this integrin plays in Rab25-driven invasion, I wished to determine its requirement in Rab25's ability to upregulate CLIC3. To oppose α 5 β 1 function I used antibodies which bind to the extracellular portion of the integrin or to the integrin binding site (RGD) in fibronectin and they have been shown to inhibit Rab25-driven invasion into three dimensional matrices (Caswell, Spence et al. 2007). As a control I utilised an antibody that blocks the function of an unrelated α v integrin. To confirm the efficacy of these antibodies I used immunofluorescence to assess the fibronectin fibril network, which is known to rely upon the continued presence of active α 5 β 1 for its integrity. Indeed, antibodies that blocked α 5, β 1 or the RGD site in fibronectin (but not those that targetted α v β 3) reduced fibronectin fibrillogenesis (Fig. 3.17A). I then seeded cells onto plastic and CDM coated substrates, allowed them to adhere and hindered α 5 β 1 function with the blocking antibodies (Fig. 3.17B). It quickly became apparent that the function of β 1 integrin is imperative to the cells' ability to form contacts with the extracellular matrix and to adhere to the substratum, as exemplified by a large number of rounded cells and impaired cell spreading. Q-PCR analysis of CLIC3 mRNA levels following blocking antibody treatment revealed no alterations in CLIC3 expression when cells were grown on plastic surfaces. However, β 1 integrin blocking antibodies lead to a significant increase in CLIC3 mRNA levels when cells were plated onto CDM (Fig. 3.17C), indicating that the activity of β 1 integrins play a role in the maintenance of CLIC3 levels in A2780 cells.

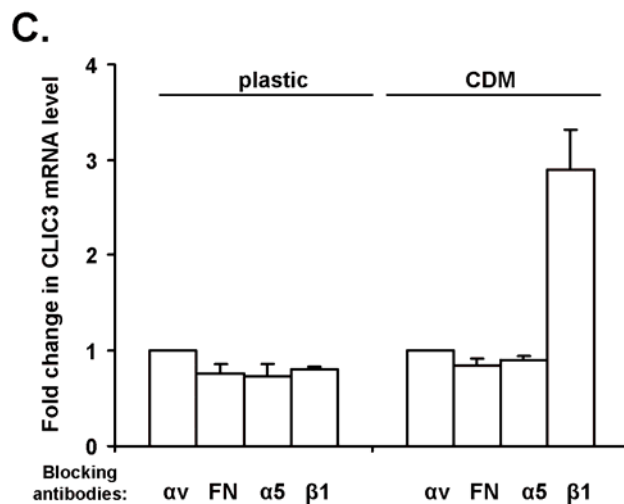
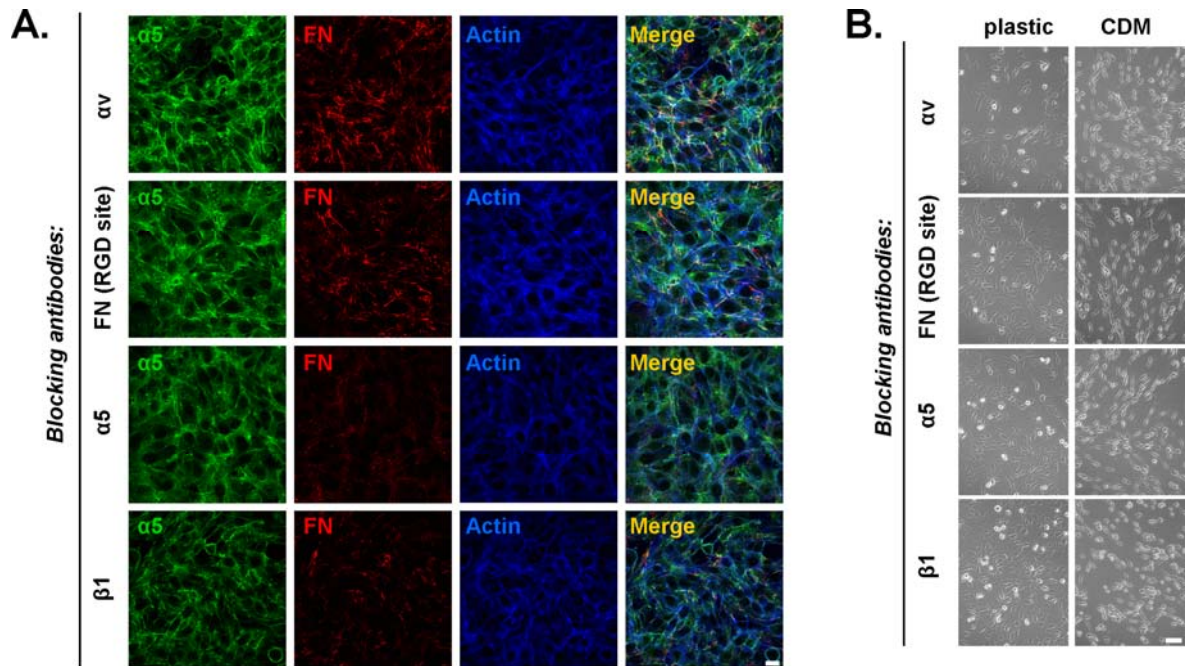


Figure 3-17 Suppressing $\beta 1$ integrin function increases CLIC3 mRNA levels.

A2780-Rab25 were seeded either onto glass cover slips (A), plastic surfaces or CDMs (B). Cells were allowed to adhere for 2 hours and then were incubated overnight with 1 μ g/ml of αv integrin, fibronectin (FN), $\alpha 5$ integrin and $\beta 1$ integrin blocking antibodies, respectively. Cells on cover slips were fixed in 4% PFA, fibrillar fibronectin (FN) was visualised with a rabbit antibody and Cy-3 conjugated secondary antibody (red), $\alpha 5$ with a mouse antibody and Cy-2 conjugated secondary antibody (green) and Phalloidin –Texas Red was used to visualise F-actin (blue). Scale bar, 20 μ m (A). Cells plated onto plastic or CDM were imaged using a bright field microscope, scale bar 100 μ m (B). RNA was then harvested and changes in CLIC3 level were analysed by qPCR. Q-PCR data are mean \pm SEM of three independent experiments and were normalised to β -actin (C).

3.3 Discussion

3.3.1 Summary

Here, I have performed a gene expression analysis, which identified candidate genes that have the potential to act downstream of Rab25 and $\alpha 5\beta 1$ integrin to drive invasive migration of ovarian adenocarcinoma cells. I have characterised the gene signature of Rab25 expressing cells to be composed of 18 genes and confirmed the upregulation of three of them; CLIC3, SLC16A6 and KCNJ2 on mRNA level by qPCR. I also showed that, even though the expression of all three validated genes appeared to be Rab25 and CDM mediated, only the upregulation of CLIC3 was reversed by Rab25 suppression. Furthermore, I demonstrated that CLIC3 amplification occurred on protein level.

3.3.2 *How could upregulation of CLIC3 mRNA occur?*

In this chapter I provide a clear demonstration of the augmentation of CLIC3 mRNA levels following Rab25 expression and the extracellular matrix involvement in this process. Due to my primary interest in tumour invasion and progression I chose not to investigate the reasons for CLIC3 transcript upregulation and to instead focus on the cellular role of CLIC3 and its possible implication in human disease. Nonetheless, there are a number of processes that likely are affected by the Rab25 and extracellular matrix axis, which confer changes in CLIC3 mRNA levels. Here, I will briefly discuss a few stages at which gene expression regulation could occur.

Gene expression is a multistep process which results in information from a DNA sequence being transformed into a functional gene product. Any stage of this cascade can be regulated and lead to changes in the levels of the protein. Gene expression is controlled by gene copy number and amplifications of chromosomal regions have been reported to be responsible for upregulation of transcript levels and to be implicated in tumour aggressiveness and progression. Indeed, Rab25 has been shown to be a component of 1q22 amplicon whose copy number increases in 54% of advanced serous epithelial ovarian carcinomas. Linear regression analysis of 21 epithelial ovarian cancers, for which both comparative

genomic hybridisation (CGH) and expression data were compiled has revealed a direct relationship between Rab25 gene copy number and mRNA levels (Cheng, Lahad et al. 2004). The increase in CLIC3 mRNA levels could result from amplified 9q34.3 chromosomal region in which it resides. However, examination of the chromosomal locations of the remaining 17 Rab25 and matrix-specific hits did not reveal any convergences with the chromosomal site of CLIC3, hence contravening the possible regulation of its expression at the gene copy level. Interestingly, the other two Rab25 and matrix upregulated transcripts, namely SLC16A6 and KCNJ2 occupy neighbouring loci, 17q24.2 and 17q23.1-24.2, respectively. This, in concert with the inability of Rab25 suppression to diminish their expression, could indicate chromosomal amplification as the mechanism of upregulation of these transporters.

The second level at which gene expression can be modulated is the accessibility of DNA for transcription, which is controlled by epigenetic modifications of DNA and its associated histones (Zhang and Meaney). There is mounting evidence that epigenetic control of gene expression is employed by cancer cells and it can contribute to tumour invasion and progression (Kim, Jang et al. 2008; Moncada-Pazos, Obaya et al. 2009). Additionally, there is evidence that the engagement of cancer cells with the extracellular matrix can orchestrate changes in gene expression by epigenetic mechanisms (Kim, Lee et al. 2007). Given the regulatory role that epigenetic regulation can exert on gene transcription, it is tempting to speculate that the ligation of $\alpha 5\beta 1$ integrin to its ligand fibronectin and its interaction with Rab25 could drive cancer cell invasion by exerting epigenetic regulation on gene expression. The next layer of transcriptional regulation encompasses the transcription process itself, as well as mRNA processing. The levels of a given cytoplasmic mRNA are a balance between nuclear synthesis rates, processing and cytoplasmic degradation and it is thought that mRNA decay is the major orchestrator of gene expression (Guhaniyogi and Brewer 2001). Indeed, eukaryotic messenger RNA is subject to cotranscriptional processing which involves three events that affect transcript stability; 5' capping, 3' polyadenylation and splicing (Proudfoot, Furger et al. 2002). Further investigation will be required to determine whether Rab25 and $\alpha 5\beta 1$ integrin axis affect one or more of these processes thus increasing the half live of CLIC3 mRNA.

It has been recently shown that about 95% of multiexon transcripts are alternatively spliced (Pan, Shai et al. 2008). During splicing, the non-coding introns are removed from the pre-mRNA, which results in the maturing of the transcript and generation of exon-only containing mRNA. Alternative splicing can be an important regulatory step and it can affect the coding sequence, change the reading frame and even lead to nonsense mediated decay of the gene product (Kim, Jang et al. 2008). Alternative splicing of tumour protein p53 inducible nuclear protein 2 (TP53INP2) has been implicated in ovarian tumour cell invasion into three dimensional matrices (Moran-Jones, Grindlay et al. 2009). Interestingly, one of the CLIC3 homologues, CLIC5, exists in two splice forms, as CLIC5A and CLIC5B. My preliminary data demonstrates that a novel alternative splice variant of CLIC3, with a 81 nucleotide intronic insertion prevails in A2780-DNA3 cells when plated on plastic, but is absent in A2780-Rab25 cells cultured on CDMs, in which the well-characterised variant lacking the insertion predominates (data not shown). One possibility could be that the intron-containing transcript arises as a result of inefficient splicing and is destined for degradation, whereas the combination of Rab25 expression and the appropriate 3D microenvironment favours correct splicing and the generation of a functional transcript. The above observations suggest that fluctuations in splicing events could contribute to the variation in functional CLIC3 mRNA levels.

It is also worth considering the role of $\alpha 5\beta 1$ integrin in the regulation of CLIC3 expression. Given the requirement for the ligation of the integrin with the ECM and Rab25 in invasive cell migration and the prerequisite for the collaboration between the GTPase and the matrix in the upregulation of CLIC3, it was surprising to detect an augmentation in CLIC3 levels following the obstruction of $\beta 1$ integrin function. This was unexpected because if the integrin were to act as part of the Rab25 and CDM axis, the suppression of its function would have likely resulted in a decrease in CLIC3 mRNA similar to that seen upon inhibition of Rab25 levels. The $\beta 1$ -block induced augmentation of CLIC3 mRNA hints at an alternative scenario, where blocking $\beta 1$ integrin function and thus disabling cancer cell adherence and invasion through a three dimensional matrix leads to a compensatory increase in CLIC3 mRNA. By increasing the levels of CLIC3, a potentially pro-invasive gene that might be acting downstream of the integrin, the cell might be attempting to counteract the dysfunctionality of the integrin

and maintain its migratory potential. Interestingly, $\alpha 5$ integrin blockade doesn't result in alterations in CLIC3 mRNA, which could be suggestive of $\beta 1$ ligation with more than just $\alpha 5$ subunit being needed for CLIC3 induction.

3.3.3 What is the source of discrepancy between CLIC3 mRNA and protein level?

When measured by qPCR, Rab25 alone drives an approximately 5 fold increase in CLIC3 mRNA on plastic, but when cells are plated onto CDM this is increased to nearly 20 fold. However, although Rab25 is clearly able to drive the expression of CLIC3 protein in A2780 cells, the ability that CDM has to augment this is not as great as when CLIC3 expression is assessed by measuring mRNA levels. Lack of concordance in the expression between mRNA and protein levels of a given gene product is not uncommon. Lichtinghagen and colleagues found no correlation between the mRNA expression and protein levels of MMP-2, MMP-9 and TIMP-1, respectively, in 17 prostatic adenocarcinoma patients (Lichtinghagen, Musholt et al. 2002). Moreover, a study of 76 lung adenocarcinomas and 9 normal lung tissues has revealed that mRNA abundance of only 21% genes could be significantly correlated with protein concentrations (Chen, Gharib et al. 2002).

These discrepancies are likely attributable to mRNA turnover, protein synthesis regulation, post-translational modifications and protein degradation. These processes are not mutually exclusive and could all affect protein accumulation in the cell and its half live. It is therefore conceivable that introduction of the interaction between a cell and cell-derived matrix in the presence of Rab25 alters the synthesis or stability of CLIC3 protein thus making protein abundance an inaccurate reflection of CLIC3 transcription.

3.3.4 Other potentially interesting hits

Although I only chose three genes from the list of 18 that I identified as potential downstream effectors of Rab25 driven invasion, and only proved that one of them, CLIC3, was specifically upregulated by Rab25, it is highly likely that more than one effector contributes to the effects of Rab25 and $\alpha 5 \beta 1$ integrin on invasive tumour cell migration. Amongst the other candidate genes are some

that are still poorly characterised, such as NLRC3, TRIM2 or FAM49A. Others have been extensively studied and their role in cancer is well established. Cyclooxygenase (COX2), also known as prostaglandin-endoperoxide synthase 2 (PTGS2) has been implicated in the metastasis of breast cancer to bone (Li, Schem et al. 2008; Lucci, Krishnamurthy et al. 2009) and brain (Bos, Zhang et al. 2009). HtrA serine peptidase1 (HTRA1) has been implicated in ovarian (Chien, Staub et al. 2004; Narkiewicz, Klasa-Mazurkiewicz et al. 2008), and endometrial cancers (Bowden, Di Nezza-Cossens et al. 2006). Intriguingly, these studies suggest that this serine protease is a candidate tumour suppressor and that it correlates inversely with tumour progression and grade.

Two genes, ADAMTS5 and SYTL1, stand out from the list due to their role in extracellular matrix degradation and their indirect connection to vesicle trafficking, respectively. ADAMTS5 encodes a secreted extracellular matrix degrading enzyme, which is a member of a disintegrin and metalloproteinase with thrombospondin motifs family. ADAMTS5 (aggrecanase 2) has been implicated in aggrecan cleavage and it has been shown to be activated by syndecan 4. Syndecans are transmembrane heparan sulphate proteoglycans that interact with a plethora of growth factors and extracellular matrix proteins. Syndecan 4 has been implicated in the regulation of ADAMTS5 activation through both a direct interaction with this protease and via activation of ERK1/2-mediated synthesis of matrix metalloproteinase-3 (MMP-3) (Echtermeyer, Bertrand et al. 2009). ADAMTS5 like other aggrecanases is inhibited by binding to tissue inhibitor of matrix metalloproteinases -3 (TIMP-3) (Kashiwagi, Tortorella et al. 2001; Troeberg, Fushimi et al. 2009). Interestingly, TIMP-3 is amongst one of the most prominent Rab25-downregulated genes in my microarray screen.

Even though the contribution of ADAMTS family of proteases to cancer progression and metastasis remains unclear, there has been an indication of ADAMTS-1,5,8,9 and 15's implication in the invasiveness of head and neck cancer, as exemplified by their higher expression in the metastatic foci when compared to the primary tumours (Demircan, Gunduz et al. 2009). In light of the potential involvement of ADAMTS5 in tumour metastasis and its regulation by the syndecan 4 axis, which can exert modulatory effects on the persistence of tumour cell migration on cell derived matrix (Bass, Roach et al. 2007) and which collaborates with $\alpha 5 \beta 1$ integrin in the formation of focal adhesions (Bass, Morgan

et al. 2008), it is tempting to speculate that ADAMTS5 might also confer Rab25 and CDM driven invasive phenotype.

Another Rab25 and CDM upregulated gene with interesting implications is synaptotagmin-like 1 (SYTL1, also SLP1). It specifically and directly binds a GTP-occupied form of Rab27A, but not other Rab proteins (Kuroda, Fukuda et al. 2002). More recently, SLP1 has been shown to form a trimeric complex with Rap1GAP2, the GTPase activator of Rap1 and with Rab27A and to control platelet granule secretion (Neumuller, Hoffmeister et al. 2009). Rab27A is a component of the membrane trafficking machinery and SLP1 is thought to collaborate with Rab27A in the secretion of lysosomes from cytotoxic T lymphocytes (CTL) (Holt, Kanno et al. 2008). Given the role of Rab27A in vesicle traffic and the involvement of Rab25 in integrin trafficking and its contribution to invasive migration, it might be worth investigating the potential role that SLP1 could play in these processes. It is even more tempting to examine SLP1's role in tumour invasion in view of the parallelisms between SLP's connection to lysosomal secretion and CLIC3's localisation and function, which will be described in the following chapter.

4 CLIC3 is a late endosomal/lysosomal protein and controls the return of lysosomally-targeted active-conformation integrins to the plasma membrane

4.1 Introduction

In the previous chapter I have identified chloride intracellular channel 3 (CLIC3) as a gene that is upregulated in A2780 cells stably expressing Rab25, and I have described the contribution that the ECM makes to its expression. Although proteins of the CLIC family have been named for their reported ability to transport chloride ions across artificial lipid bilayers, there is little consensus in the literature as to the biochemical and cellular function of these proteins. In this chapter, I will therefore introduce what is known about the structure and function of the CLICs and the controversies surrounding their cellular role. I will then present data examining CLIC3's involvement in tumour cell invasion into three dimensional matrices and describe imaging experiments that delineate the subcellular localisation of CLIC3 and how it acts to traffic $\alpha 5\beta 1$ integrin.

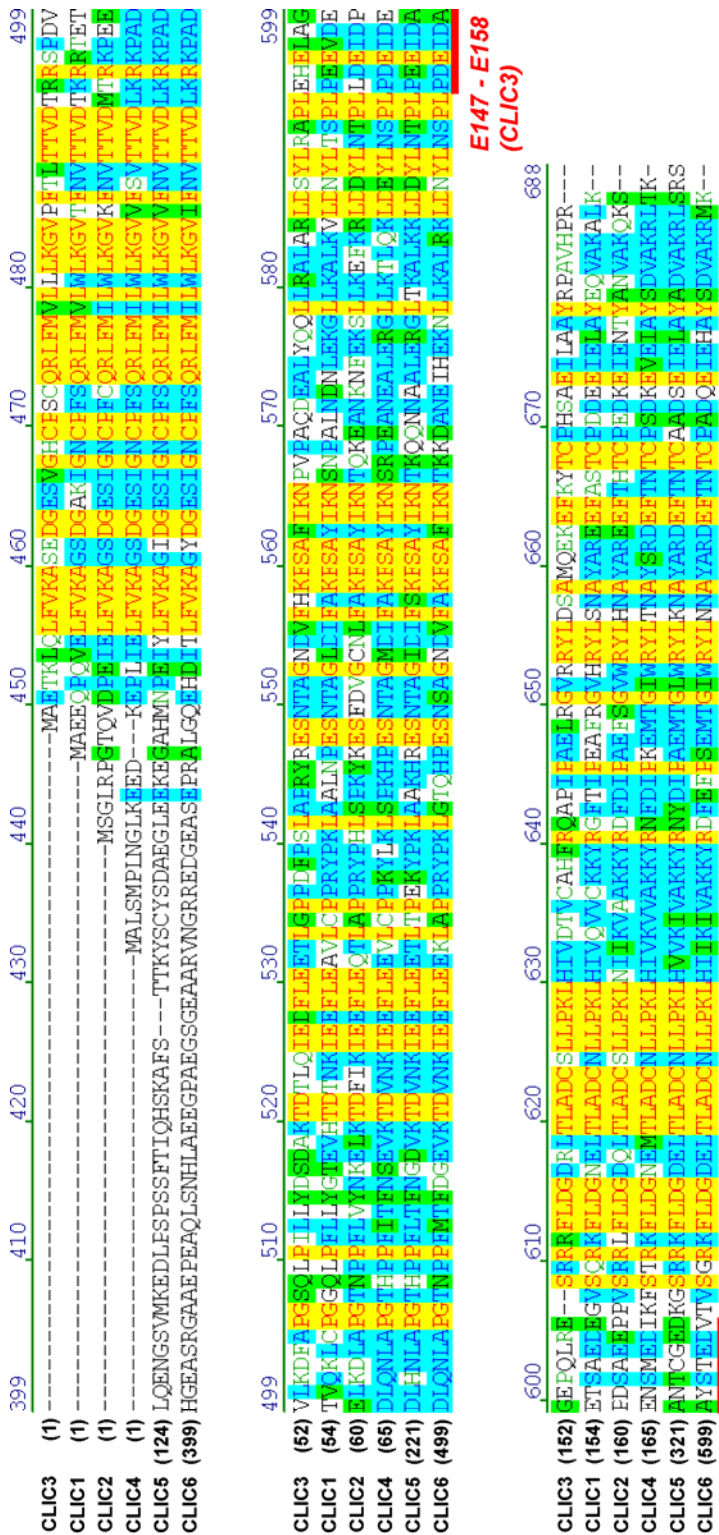
4.1.1 Phylogeny and structural conservation of CLICs

Chloride intracellular channel (CLIC) proteins constitute a new and still poorly characterised family of chloride ion channels, whose structure contains a GST omega class family fold. All known CLIC paralogues share a high degree of sequence conservation and CLIC-like proteins appear already at early evolutionary stages. A single CLIC protein paralogue is already present in lower organisms such as *Hydra magnipapillata* (phylum Cnidaria), *Schistosoma mansoni* (phylum Platyhelminthes), *Drosophila melanogaster* (phylum Arthropoda) or *Ciona intestinalis* (phylum Chordata). In the Nematodes, such as *Caenorhabditis elegans*, CLIC-like family members share approximately 35% sequence identity with their vertebrate counterparts and are represented by two proteins: EXC-4 and EXL-1. The vertebrate CLIC family of proteins encompasses six paralogues

(CLIC1-CLIC6), with CLIC2, CLIC5 and CLIC6 existing in alternative splice forms (Littler, Harrop et al.).

All six mammalian family members are highly conserved and share between 47 and 76% sequence identity. Human CLICs contain a well-conserved 240 amino acid stretch, which forms a glutathione S-transferase (GST) fold (Fig. 4.1A&B). CLIC5B and CLIC6 are significantly longer than the remaining CLICs in that they possess an N-terminal domain attached to the conserved GST fold. To date, crystal structures of four vertebrate CLICs: CLIC1, CLIC2, CLIC3 and CLIC4, in their soluble state, have been determined and show strong homology. They comprise 10 α -helices and 4 β -sheets, and between helix 5 and helix 6 they contain a highly negatively charged loop, which extrudes from the globular domain and is positioned between Pro147 and Gln164 in CLIC1 (Fig. 4.2). This loop, which appears to be the sole region of structural divergence, constitutes the putative site protein interactions involving CLIC1, and could account for varying cellular roles of different CLICs (Singh).

The high degree of sequence and structural conservation between the six CLIC family members indicates that they may have arisen through duplication events from a single protein in an ancient organism. In favour of that notion is the high homology (45% sequence identity) between the *Ciona intestinalis*'s CLIC-like protein and the vertebrate paralogues (Littler, Harrop et al.).



B.

	Identity with CLIC3 (%)	Similarity with CLIC3 (%)
CLIC1	50	57.4
CLIC2	47	57.5
CLIC4	45.8	57.7
CLIC5	29	35.4
CLIC6	16.9	21.1

Figure 4-1 The human CLICs share a high level of sequence conservation.

CLIC protein sequences were derived from the NCBI protein data bank and aligned using Vector NTI (Invitrogen) software. Yellow boxes indicate amino acids conserved throughout the family, blue correspond to residues common for some, but not all CLICs, amino acids highlighted in green show the same properties. Regions that are not shaded are those of highest divergence. Highlighted in red is the divergent region of CLIC3. The first 124 and 399 amino acids from CLIC5 and CLIC6 sequences respectively were omitted from the alignment (A). CLIC3 is most identical with CLIC1, CLIC2 and CLIC4 and less identical to CLIC5 or CLIC6 (B).

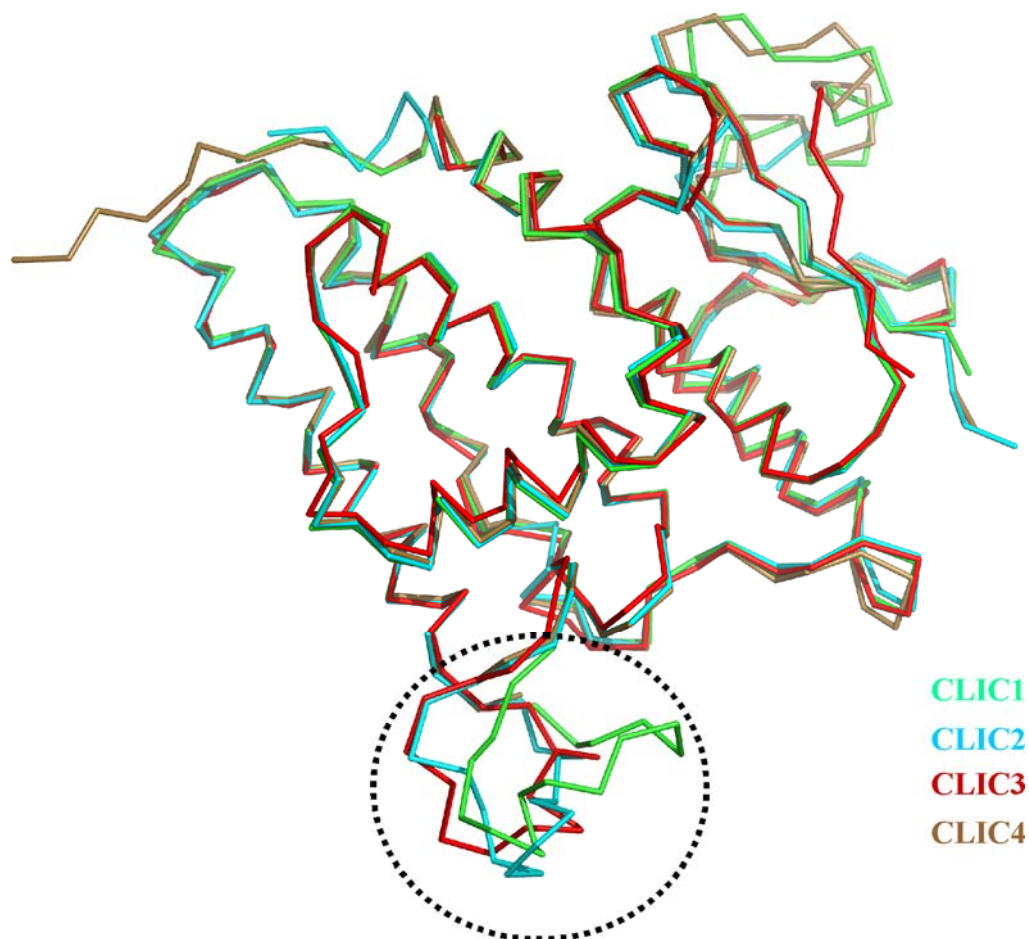


Figure 4-2 X-ray crystal structures of human CLICs: CLIC1, CLIC2, CLIC3 and CLIC4.

The atomic coordinates were retrieved from the RCSB Protein Data Bank (www.rcsb.org/pdb/), the structures were superimposed in COOT software and graphical representations of tertiary structures were generated in PYMOL. Shown in green, blue, red and brown are structures of CLIC1, CLIC2, CLIC3 and CLIC4 respectively. Encircled is the divergent loop.

4.1.2 CLICs as membrane-inserted proteins

Since CLICs do not appear to contain a stretch of hydrophobic residues that could conform to a canonical transmembrane domain, it is clear that non-orthodox models must be invoked to account for their apparent ability to transport chloride ions across membranes.

CLIC1 is thought to exist in two forms, soluble cytoplasmic and membrane-associated, and to be capable of switching between the two. Exactly how the translocation from the aqueous milieu into phospholipid membranes occurs is not clear, but Litter and colleagues have proposed a possible mechanism of membrane insertion. Upon oxidation CLIC1 can undergo a structural transition from a soluble, monomeric and globular state to a non-covalent dimeric form. This transition forces an altered conformation of the entire N-terminal domain, which contains the thioredoxin motif. The thioredoxin β -sheet, which in a reduced state comprises four strands, is now transformed into helices and loops. This process is reversible and relies on the formation of an intramolecular disulfide bond between Cys-24 and Cys-59, which then exposes a large hydrophobic region on the dimer interface. The acquisition of the dimeric oxidised conformation is then utilised for membrane anchorage and chloride ion channel activity (Littler, Harrop et al. 2004). Consistent with this, there is mounting evidence that CLIC family members can undergo a structural transition that allows their N-terminus to insert into membranes. A recent study employing fluorescence resonance energy transfer (FRET) has observed differences in the distance between an N-terminally located tryptophan 35 (Trp35) and C-terminal cysteine residues (Cys89, Cys178 and Cys223) upon addition of lipid membranes, suggestive of conformational changes being induced in parallel to the transition of the protein from an aqueous to membrane interactive state (Goodchild, Howell et al.). Furthermore, studies in EXC-4 null *C.elegans* have identified a 66 amino acid N-terminal domain, so called PTM domain, whose name derives from 'putative transmembrane' amphipatic helix within it, to be responsible for targeting of distinct CLIC-like proteins to distinct subcellular localisations (Berry, Bulow et al. 2003; Berry and Hobert 2006).

It is still not entirely clear what controls the structural transition of CLICs and their membrane insertion. As it was mentioned earlier, some CLICs can undergo structural transition and membrane insertion under oxidising conditions, but CLIC4 has been shown to insert into lipid bilayers under both reducing and oxidising conditions (Singh and Ashley 2007). To add more complexity to the mechanism of structural transition, CLIC2 has been reported to be insensitive to the redox state, but instead its ion conducting properties are promoted by low pH (Cromer, Gorman et al. 2007). Thus, further work will be necessary to unravel the exact mechanism of CLICs' insertion into lipid bilayers, and to determine whether this process contributes to chloride ion conductance across cellular membranes.

4.1.3 Biochemical diversity

4.1.3.1 Ion conductance

The discovery of a 64kDa bovine chloride channel protein, p64, which is homologous to human CLIC5B (Landry, Akabas et al. 1989), has biased the view of the potential role of CLIC family of proteins by directing investigators towards characterising their ion channel activity. The proposed ion channel role has since been studied in electrophysiological assays upon CLIC protein incorporation into lipid bilayers, in patch clamp experiments and in whole cell current approaches performed on mammalian cells. In spite of numerous efforts to characterise ion conductivity of this family of proteins, their role in this process is still a subject of debate (Table 4.1).

In a study performed by Tulk and colleagues, a pure and detergent free preparation of water-soluble CLIC1 protein was mixed with preformed vesicles and this led to an enhanced chloride permeability of the vesicle membranes. Also, addition of CLIC1 protein to preformed planar lipid bilayers resulted in increased chloride ion conductance as measured in an efflux assay, consistent with a role for CLICs in specific anion permeability (Tulk, Kapadia et al. 2002). In addition to the above mentioned studies with isolated membrane systems, there are some limited indications that CLICs may play a role in chloride transport in living cells. Studies in osteoclasts indicate that CLIC5B may contribute to the acidification of the osteoclasts bone resorption compartment

by allowing a passive flow of Cl^- ions to short-circuit the electrogenic gradient generated by an ATP-dependent proton pump. Consistent with this, CLIC5B demonstrates affinity for the SH2 and SH3 domains of c-Src, and this tyrosine kinase appears to be necessary for the functional colocalisation of the proton pump and the chloride channel in the osteoclasts (Edwards, Cohen et al. 2006).

Although it is possible that CLIC proteins can act as selective chloride ion transporters, recent reports indicating that CLIC2 may act to suppress cardiac ryanodine receptor (RyR2) Ca^{2+} channels (Board, Coggan et al. 2004; Jalilian, Gallant et al. 2008), call their role as primary and selective transporters of chloride into question. Indeed there are numerous reports that argue against the chloride selectivity of CLIC-mediated ion transport, or even against any role for CLICs in ion permeability. For instance CLIC4, although capable of inserting into lipid bilayers, can not specifically promote chloride transport, rather it mediates increased non-specific ion permeability (Singh and Ashley 2007). Also, CLIC5 even though capable of inserting into lipid bilayers is only able to form poorly selective, multiconductance ion channels that are equally permeable to Na^+ , K^+ as they are to Cl^- (Singh, Cousin et al. 2007). Furthermore, despite attempts to characterise its potential chloride conducting ability, no channel activity could be assigned to CLIC6 when tested in voltage clamp assay performed on *Xenopus* oocytes (Friedli, Guipponi et al. 2003). CLIC5A, in spite of inducing chloride channel activity when reconstituted into liposomes, fails to drive increased anion permeability when exogenously expressed in mammalian cells (Berryman, Bruno et al. 2004). Moreover, in contradiction to the reports linking CLIC4 to ion conductance, the recent study of Ponsioen indicates clearly that although CLIC4 is recruited to the plasma membrane, it does not span the bilayer, nor does it modulate chloride ion currents (Ponsioen, van Zeijl et al. 2009).

In summary, it is beyond doubt that some CLIC proteins can insert into lipid bilayers and promote anion permeability *in vitro*. However, the specificity of CLIC-mediated ion conductance, its relevance to ion transport *in vivo* and its contribution to cell biological and physiological function of CLICs is still under debate.

Protein	Length (AA)	Channel activity	Method	Reference
CLIC1	241	Anion channel activity, pH sensitive	Lipid bilayer, efflux assay	Tulk et al, 2002
CLIC2	247	Chloride conductivity, pH and redox dependent	Lipid bilayer, efflux assay	Cromer et al, 2007
CLIC3	236			
CLIC4	253	Poorly selective, redox modulated	Lipid bilayer, efflux assay	Singh & Ashley, 2007
		Chloride conductance, redox regulated	Artificial liposomes, efflux assay	Littler et al, 2005
		No channel activity, probable transferase activity	Whole cell, patch clamp	Ponsioen et al, 2009
		Chloride conductance	Patch clamp	Proutski et al, 2002
CLIC5A	251	Multiconductance (Na, K, Cl)	Lipid bilayer	Singh et al, 2007
		No permeability	Whole cell, iodide efflux	Berryman et al, 2004
CLIC5B	410	Chloride conductance	Lipid bilayer	Edwards et al, 1998
CLIC6	704	No chloride conductivity	Voltage clamp on <i>Xenopus</i> oocytes	Friedli et al, 2003

Table 4-1 Biophysical properties of CLICs based on the available literature.

4.1.3.2 CLICs as glutathione transferases?

The CLIC family of proteins has an approximately 15% sequence identity with Omega class glutathione transferases (GSTs) and belongs to the GST structural fold superfamily (Dulhunty, Gage et al. 2001). It has therefore been proposed that they can fulfil, amongst a plethora of other roles, an enzymatic one.

Typically, GST proteins catalyse the conjugation of reduced tripeptide (glutamine, cysteine, glycine) glutathione (GSH) to electrophilic regions of other molecules. This occurs through the activation of the thiol group of the GSH, which then allows for high-affinity non-covalent binding to its substrates. The GST module consists of two domains: an all-helical domain at the C-terminus, and a thioredoxin domain at the N-terminus. The latter is well-conserved amongst multiple families of redox-active proteins, whose active sites frequently centre around a cysteine, which is a component of the Cys-X-X-Cys motif. This motif has been shown to be present in the redox-active site of CLIC1 resembling glutaredoxin (Harrop, DeMaere et al. 2001) and all CLICs are thought to contain a cysteine residue (approximately Cys24), which becomes activated by the protein itself and forms a disulfide bridge with GSH. (Littler, Harrop et al.). Indeed, Ponsioen and colleagues suggest that the conserved Cys-35 in CLIC4, which is necessary for membrane translocation of that CLIC, might be responsible for its yet unidentified transferase activity and might serve as a catalytic residue to bind and process potential substrates (Ponsioen, van Zeijl et al. 2009).

4.1.4 Functional diversity

4.1.4.1 CLICs in membrane remodelling and tubulogenesis

Morphogenesis of highly-ordered endothelial tubes is a prerequisite for the formation of functional excretory, respiratory and vasculatory systems. The creation of vascular lumen, also sometimes referred to as cell-hollowing tubulogenesis, is thought to be driven by coordinated intracellular and intercellular fusion events. It has been proposed that this process necessitates signalling downstream of integrin-ECM interaction and is initiated by the integrin- and cdc42/Rac1-dependent formation of pinocytic intracellular

vesicles. This is followed by the fusion of multiple pinocytic vacuoles into a large intracellular vacuole, which then fuses with its counterparts in the neighbouring cells leading to the formation of an extracellular lumen of a multicellular tube. Each step of the intercellular lumen formation is thought to require efficient intracellular membrane trafficking and vacuolar acidification events (Kamei, Saunders et al. 2006).

A *C.elegans* CLIC-like protein, EXC-4, has been implicated in establishing and maintaining tubular architecture during and after cell hollowing. The excretory canal of this nematode consists of a single cell which extends four long and narrow canals along the length of the body. These canals contain a lumen, which is thought to collect fluids and waste that are later transferred to the excretory duct. In the *exc-4* null animals the morphology of the excretory tube is altered in that it presents with cyst-like swelling and enlargement of the canal's lumen. Ectopic introduction of GFP-tagged EXC-4 into *exc-4* null animals rescues the mutant phenotype and localises EXC-4 to the membrane of the excretory cell and the duct. Interestingly, EXC-4 has been shown to act during early stages of lumen formation, when the vacuole is being formed, rather than during subsequent tubule flattening and lumen remodelling. Moreover, expression of GFP-EXC-4 in *exc-4* null animals at different larval stages reveals continuous requirement for that CLIC-like protein in the maintenance of the tubular architecture even following the development and outgrowth of the excretory canal. The only other CLIC-like protein orthologue thought to be present in the *C.elegans* genome is termed EXL-1 (for EXC-4-like) and localisation studies performed with fluorescently-labelled EXL-1 revealed its abundance in lysosomal membranes and the Golgi apparatus, thus also implicating it in membrane dynamics and remodelling (Berry, Bulow et al. 2003).

Work of Ulmasov and colleagues performed on *Clic4^{-/-}* mice have implicated CLIC4 in the tubulogenic pathway in mammals. Mice deprived of CLIC4 show strong angiogenic defects as exemplified by *in vivo* matrigel assays, and by decreased spontaneous development of retinal blood vessels as well as an attenuated vascular response to oxygen challenge in the retina. Additionally, endothelial cells derived from the *Clic4*-null mice exhibit defects in the cell-hollowing tubulogenic pathway *in vitro*, as measured by the extent of vacuolisation. Moreover, vacuolar acidification in these cells is impaired. The

authors show similar defects in endothelial cells derived from wild-type mice by the application of a generic chloride channel inhibitor, IAA-94, and by the inhibition of vacuolar type ATPase with bafilomycin A1. Based on these observations, they propose that CLIC4 may play a role in a short-circuiting anion conductance, which permits vacuolar proton ATPase-mediated acidification along the cell-hollowing pathway. These data lend support to the proposed role for CLICs in tubulogenesis, but should be interpreted with caution owing to the broad spectrum of processes that the non-specific chloride channel inhibitor and a very potent proton pump inhibitor may impinge on (Ulmasov, Bruno et al. 2009).

Angiogenesis is a process of new vasculature formation from pre-existing vessels and requires the activation of endothelial cells by angiogenic factors such as the vascular endothelial growth factor-A (VEGF-A), which binds to and activates the VEGF receptor-2. This in turn allows capillary sprouting or splitting, both of which result in the formation of new vasculature. Human CLIC4 has been shown to be regulated in the process of angiogenesis in a proteomic screen, which utilised VEGF for the induction of endothelial cell tubulogenesis. CLIC4 suppression by siRNA revealed its requirement for efficient tube formation and extension. Interestingly, whilst CLIC4 expression is high in resting vessels, it is decreased at later stages of tubular morphogenesis in collagen gels and during pathological angiogenesis in tumour vessels, thus indicating the need for tight regulation of CLIC4 levels throughout multiple stages of tubule morphogenesis. (Bohman, Matsumoto et al. 2005).

Finally, in a study performed by Suginta and colleagues, CLIC4 has been shown to partially coexist with caveolin and has been implicated in caveolar endocytosis (Suginta, Karoulias et al. 2001), thus further substantiating the notion that CLIC family of proteins may indeed play a role in membrane dynamics and remodelling.

4.1.4.2 Cell growth and survival

CLIC family members, in particular CLIC4 have also been implicated in apoptosis and nuclear signalling processes. Indeed, in keratinocytes, CLIC4 has been observed in the nucleus and induction of apoptosis by etoposide, a DNA

damaging agent, or overexpression of tumour suppressor protein p53, increases expression of CLIC4. Not only does induction of apoptosis augment CLIC4 expression, but also its ectopic expression can drive alterations in the mitochondrial membrane potential and the initiation of apoptosis (Fernandez-Salas, Suh et al. 2002). This is supported by another study, which links CLIC4 to nuclear transport complexes and reports its translocation from the cytoplasm to the nucleus where it might contribute to the initiation of the apoptotic cascade (Suh, Mutoh et al. 2004). In contrast to the above studies, which ascribe a pro-apoptotic role to CLIC4, is a report by Sue and colleagues that argues an anti-apoptotic role for CLIC4. Their findings show that tumour necrosis factor (TNF α)-induced apoptosis leads to a decrease in CLIC4 protein levels and that off-target inhibition of CLIC1, CLIC4 and CLIC5 proteins by antisense expression in osteosarcoma lines, results in TNF α -induced apoptosis. Additionally, suppressing the above CLIC proteins in tumour grafts inhibits tumour growth and leads to apoptosis (Suh, Mutoh et al. 2005).

CLIC4 has also been implicated in sustaining nuclear signalling downstream of transforming growth factor β (TGF- β). CLIC4 and transcription factor that participates in TGF- β signalling, Schnurri-2, associate in the cytoplasm and cooperatively translocate to the nucleus in a TGF- β dependent fashion. Once in the nucleus, CLIC4 interacts with phospho(p)-Smad2 and p-Smad3 and acts as a shield against nuclear phosphatases such as protein phosphatase 1a (PPM1a), thus stabilizing these transcription factors and maintaining nuclear signalling downstream of TGF- β (Shukla, Malik et al. 2009). Consistent with a role for CLIC4 in prolonging nuclear signalling events is the ability of TGF- β 1 to induce the upregulation of CLIC4 mRNA levels (Ronnov-Jessen, Villadsen et al. 2002).

4.1.4.3 Other functions

Multiple physiological functions other than membrane trafficking and cell survival have been ascribed to CLIC family members, and these include their ability to function as scaffolds, their contribution to maintaining cell polarity during cell division as well as a role in cell migration (Table 4.2).

CLICs have been shown to be enriched at sites comprising large complexes of scaffold and signalling molecules, suggestive of their role as adaptor proteins in

the context of a plethora of cellular processes. Indeed, CLIC4 interacts with protein kinase A-anchoring protein 350 (AKAP350) at the centrosome, midbody and in the apical region of polarized epithelial cells and is enriched in a variety of subcellular sites such as mitochondria, nuclear matrix and cytoskeletal, actin-based structures at the cell cortex (Berryman and Goldenring 2003). Not only does CLIC4 interact with AKAP350, CLIC4 amino acids 121-253 have been shown to mediate its interaction with the C-termini of one of the G protein-coupled receptors (GPCRs), histamine H3 receptor (H3R) (Maeda, Haraguchi et al. 2008). Moreover, CLIC5B also associates at the Golgi apparatus with AKAP350 (Shanks, Larocca et al. 2002), further strengthening the notion that CLIC proteins could act primarily as adaptors or scaffolding proteins. Another member of CLIC family, CLIC5A, acts as a cytoskeletal component or regulator. When expressed in bacteria, it recruits actin, α -actinin, ezrin and IQ-GAP1 complexes from placental microvilli extracts. In line with that finding, ectopic expression of CLIC5A in JEG-3 choriocarcinoma cells confirms its coincidence with the cortical actin cytoskeleton (Berryman, Bruno et al. 2004).

CLICs have also been implicated in cell movement. Indeed, CLIC4 has been demonstrated to alter the alignment of myosin heavy chain IIA and actin filaments. Suppression of its levels opposes the activation of small GTPases, RhoA and Rac1, that are necessary for cell retraction and formation of protruding processes in moving cells, whilst also affecting the cellular distribution of the latter (Spiekerkoetter, Guignabert et al. 2009).

Given the plethora of cellular localisations and physiological functions of CLIC proteins, further studies will be required to interrogate their ability to form chloride channels *in vivo* and to determine whether the resultant ion conductance contributes to the roles played by these proteins in the cells and organisms.

Protein	Function	Reference
CLIC1	Proliferation and invasion	Li et al, 2010
	CLIC1 null mice platelet dysfunction	Qiu et al, 2010
	Regulates osteoblast differentiation	Yang et al, 2009
	Cell motility and invasion	Wang et al, 2009
	Apoptosis	Kang MK & Kang SK, 2008
	Modulation of amyloid-beta phagocytosis	Paradisi et al, 2008
	Cell cycle regulation	Valenzuela et al, 2000
CLIC2	Interacts with RyR1 And modulates its activity	Meng et al, 2009
	Modulates RyR2 channel activity	Board et al, 2004; Dulhunty et al, 2005
CLIC3	Associates with ERK7/cell growth control	Qian et al, 1999
CLIC4	Myofibroblast conversion	Ronnov-Jessen et al, 2002
	Association with Schnurri-2, apoptosis	Shukla et al, 2009
	Regulated by RhoA	Ponsoen et al, 2004
	Affects RhoA and Rac1 activation, cell motility	Spiekerkoetter et al, 2009
	Endothelial proliferation, capillary sprouting, angiogenesis	Tung et al, 2009
	Tubulogenesis	Ulmasov et al, 2009
	Keratinocyte differentiation	Suh et al, 2007
	Localises to actin cytoskeleton, contribution to cell cycle	Berryman & Goldenring, 2003
CLIC5A	Associates with actin cytoskeleton	Berryman et al, 2004
CLIC5B	Interacts with AKAP350	Shanks et al, 2003
	Regulates myoblast proliferation and differentiation	Li et al, 2010
	Role in osteoclast bone resorption	Edwards et al, 2006
CLIC6	Interacts with dopamine D(3) receptor	Griffon et al, 2003

Table 4-2 Diversity in the cellular functions fulfilled by CLIC family members.

4.1.5 CLIC3

CLIC3 was first identified by Qian et al in a yeast two hybrid screen with the C-terminal tail of a member of mitogen-activated protein kinase family, ERK7, used as bait. Northern blot analysis of a panel of tissues revealed very high expression of CLIC3 in human placenta, lung and heart tissues. The association between ERK7 and CLIC3 has been confirmed by co-immunoprecipitation and CLIC3 has been localised mainly to the nucleus, but also to the cytoplasm and its ectopic expression has been linked to enhanced chloride conductance (Qian, Okuhara et al. 1999). Almost a decade later, the placental abundance of CLIC3 was confirmed in a gene expression profiling study, which identified CLIC3 to be highly expressed in placenta-derived trophoblast cells at two different gestational stages. Also, when probed with anti-CLIC3 antibody, placental extracts showed evidence of high CLIC3 distribution. When analysed by immunohistochemistry, CLIC3 expression was most prevalent in the apical membrane and the cytoplasm, but also in the nucleus (Money, King et al. 2007).

Interestingly, stimulation of explanted normal breast fibroblasts with 20% fetal calf serum, which is known to drive fibroblast to myofibroblast transition, resulted in transcriptional upregulation of CLIC3 and CLIC4, but not other CLIC family members. When their levels were investigated upon TGF- β 1 stimulation, only the levels of CLIC4 were augmented, which could be indicative of CLIC3 upregulation in differentiated fibroblast by a component of the serum, other than TGF- β 1 (Ronnov-Jessen, Villadsen et al. 2002).

The crystal structure of CLIC3, lacking the 5 C-terminal amino acids has been resolved at the resolution of 1.95Å, in both reduced and oxidised states (Fig. 4.3). Even though CLIC3 is monomeric in solution, the crystal form comprises two molecules, suggesting that it adopts a similar fold to the other CLICs. It presents with a more open and polar GST-like active site than that of other CLICs, which opens the possibility for this member of the family to form distinct interactions with other proteins and to play unique cellular roles. Also, the foot-loop region, which in other family members is flexible, seems well ordered in CLIC3, yet again suggesting that this member of the family might be functionally divergent (Littler, Brown et al.).

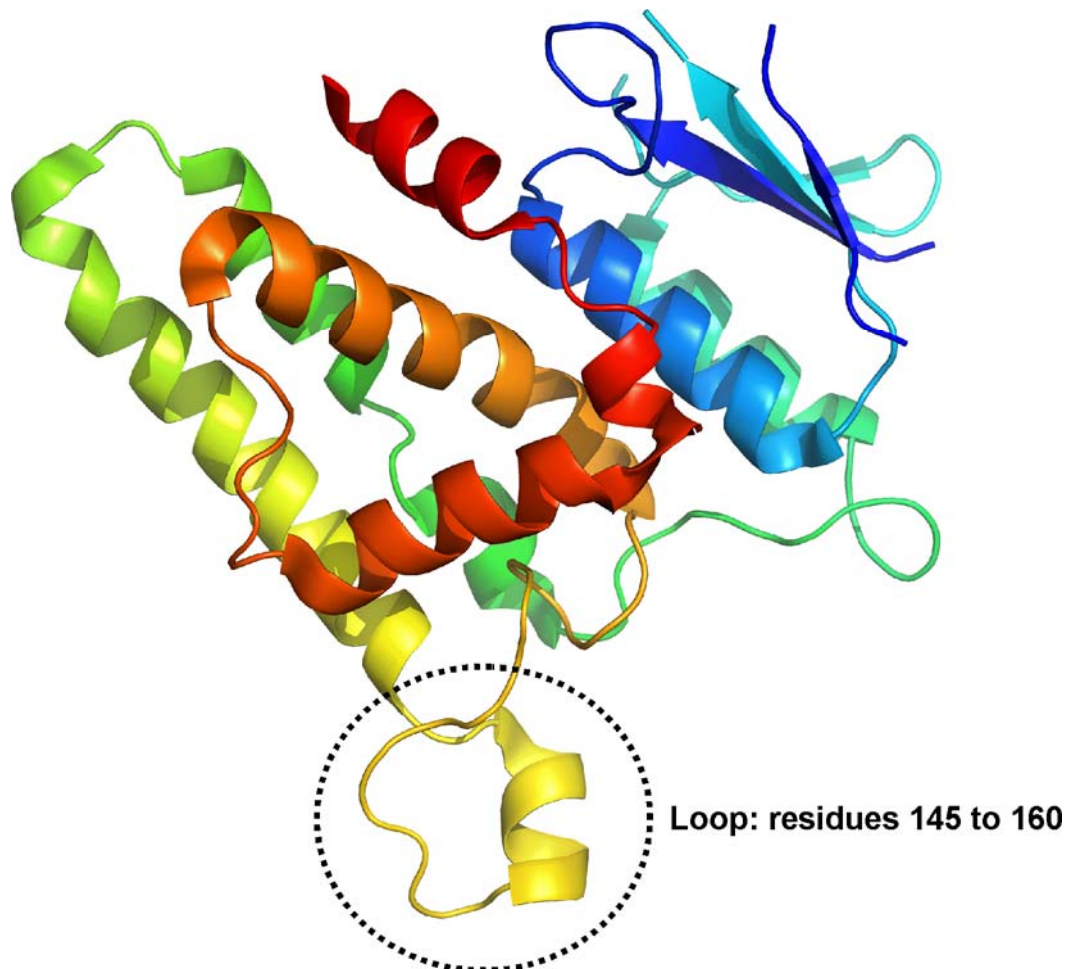


Figure 4-3 X-ray crystal structure of CLIC3

Molecular representation of the crystal structure of human CLIC3 protein shows α -helices and β -sheets, with N-terminal elements of the structure in blue and C-terminal in red. Encircled is the region of sequence and structural diversity.

4.2 Results

4.2.1 CLIC3 is necessary for Rab25-driven invasion into fibronectin-supplemented matrigel

Rab25 has been previously shown to drive tumour cell invasion into three-dimensional matrices and this process relies on the binding of this GTPase to $\alpha 5 \beta 1$ integrin and the ligation of the heterodimer to its ligand, fibronectin (Caswell, Spence et al. 2007). Given the Rab25 and CDM-mediated upregulation of CLIC3 expression (which was described in the previous chapter), I wanted to investigate the possible involvement of CLIC3 in tumour cell invasion. To that end, I developed reagents for the suppression and enhancement of CLIC3 levels. I tested the efficacy of four individual short interfering RNA oligonucleotides (siRNAs) as well as a SMART pool siRNA, which is a pool of the four individual sequences. I transfected A2780-Rab25 cells with the above mentioned preparations, as well as with non targetting (NT siRNA) oligonucleotides and examined the levels of CLIC3 mRNA (upper panel) and protein (lower panel) 48 (Fig. 4.4A) and 72 (Fig. 4.4B) hours after transfection. When mRNA expression was analysed, both β -actin and GAPDH served as internal loading controls and relative transcript levels were calculated using the $\Delta\Delta C_T$ method, as described in the previous chapter. It became apparent that siRNA SMART Pool and oligonucleotides #3 and #4 were most effective at reducing levels of the CLIC3 transcript, irrespective of which housekeeping gene was used for normalisation. After 48 hours of siRNA introduction, the suppression reached an average of about 75% for the three siRNA preparations in question, when compared to NT siRNA. Extending that period to 72 hours further decreased CLIC3 mRNA levels to about 20% for siRNA SMART Pool and to approximately 10% for siRNAs #3 and #4 when compared to NT siRNA.

The ability of these siRNAs to suppress CLIC3 levels was mirrored at the protein level, as illustrated by the Western blot analysis of CLIC3 protein expression, where vinculin was used to ensure equal loading. Indeed, 48 hours after transfection of cells with siRNA SMART Pool or oligonucleotides #3 or #4, the CLIC3 protein levels were substantially reduced, and 72 hours following

transfection, oligos #3 and #4 abrogated CLIC3 protein expression virtually completely.

Having confirmed the efficacy of CLIC3 suppression in A2780-Rab25 cells, I tested whether suppressing its expression would affect tumour cell invasion into three dimensional matrices. I employed an inverse invasion assay (Hennigan, Hawker et al. 1994), in which tumour cells were plated on the underside of a matrigel plug that was supplemented with 25µg/ml fibronectin (N.B. The inclusion of fibronectin has previously been shown to be necessary for Rab25-driven invasion (Caswell, Spence et al. 2007)). The cells were allowed to migrate through the porous membrane of the inset that separates them from the matrigel. Subsequently, the ECM plugs were placed in a chemoattractant gradient, which in the case of the present study was provided by the inclusion of 10% serum and 25ng/ml epidermal growth factor (EGF) in the upper chamber (Fig. 4.5A). 48 hours later, living cells were stained using a fluorescent label (calcein-AM) and imaged with a confocal microscope. Optical sectioning was performed in a step-wise fashion, every 15µm, starting at the porous membrane and moving upwards in the direction of cell invasion. Since the SMART Pool siRNA and oligo #3 and #4 siRNAs proved to be most efficient at suppressing CLIC3 expression, I used them to examine the role of CLIC3 in Rab25-driven invasion. Figure 4.2B shows representative strips of matrigel, which were assembled from individual images obtained during optical sectioning of the ECM plug. Cells are stained green and their migration from left to right on the matrigel strips, as indicated by the arrow, corresponds to their upward migration through the ECM. Quantification of at least three independent experiments, within which each experimental condition was represented by three ECM plugs and three regions (corresponding to different x,y positions) of each plug were imaged, was performed using Image J software. The invasive potential of the cells was expressed as the percentage of the cells that migrated beyond 45µm relative to the total number of cells in the ECM plug. Suppression of CLIC3 with SMART Pool, oligo #3 and oligo #4 siRNA resulted in a marked reduction in invasiveness of A2780-Rab25 cells and is shown in figure 4.5C. CLIC3 suppression was validated by Western blotting at the end point of the assay and vinculin was used to confirm equal loading (Fig. 4.5D).

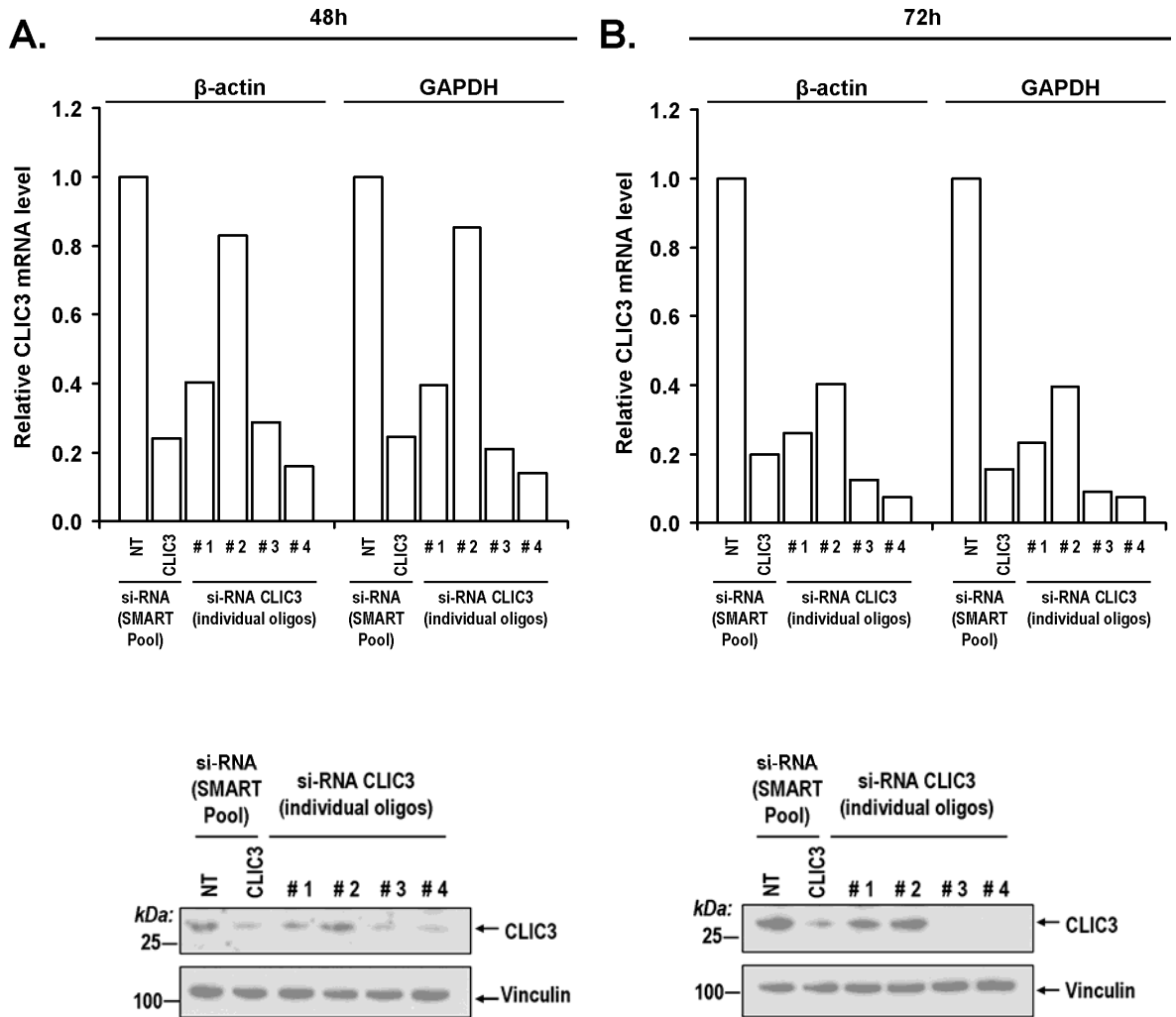


Figure 4-4 Suppression of CLIC3 with siRNA smart pool and individual oligonucleotides.

A2780-Rab25 cells were nucleofected with $1\mu\text{M}$ of the indicated siRNA duplexes and cells were harvested at 48h (A) and 72h (B) following transfection. CLIC3 mRNA suppression was verified by quantitative PCR (qPCR) and expression levels were normalised to two housekeeping genes; β -actin and GAPDH (top panel). The efficiency of CLIC3 suppression was also validated on protein level by Western blotting (bottom panel).

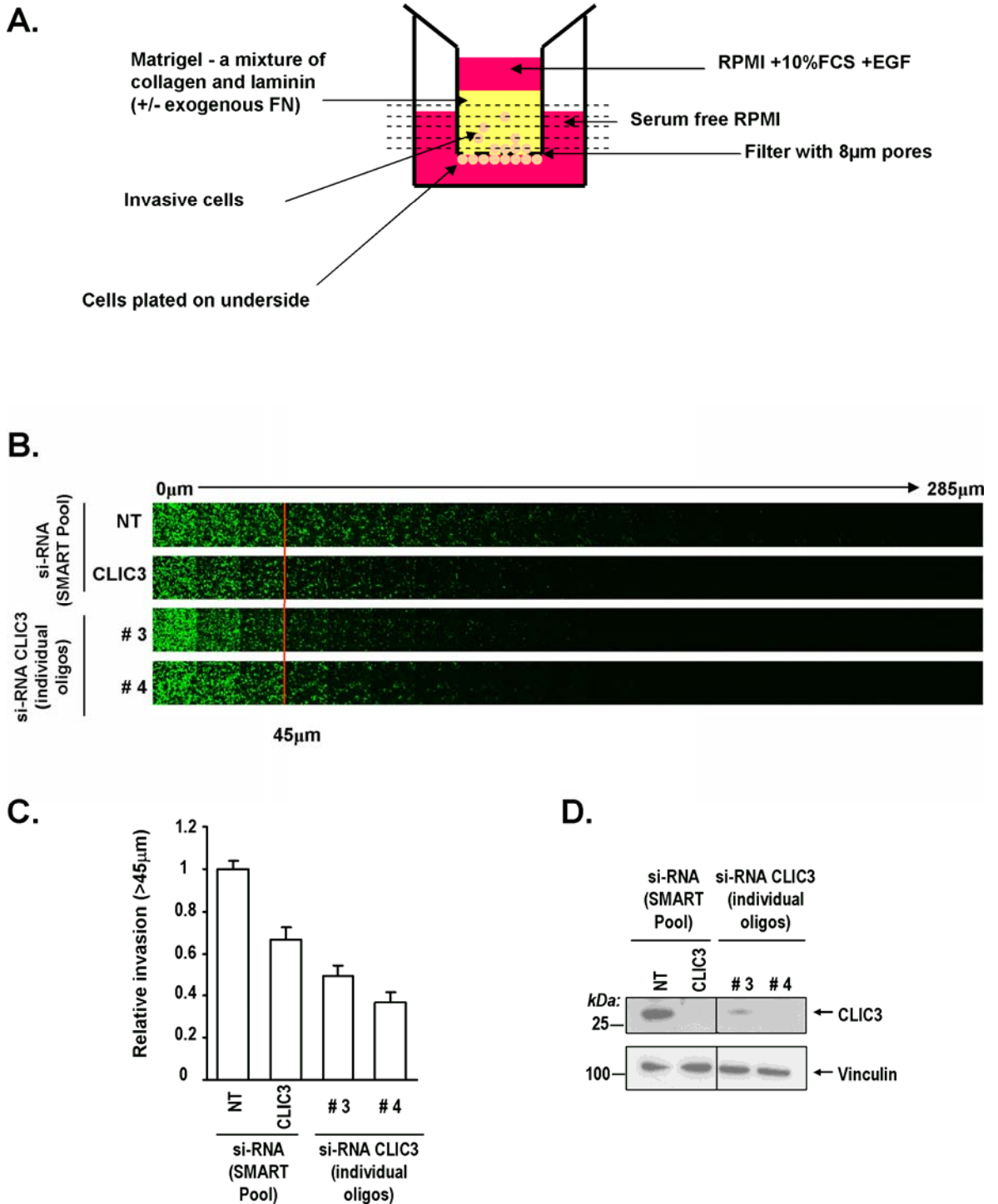


Figure 4-5 Suppression of CLIC3 levels reduces invasiveness of A2780-Rab25 cells.

A schematic explaining inverse invasion assays (A). Matrigel plugs were enriched with 25µg/ml fibronectin and 4×10^4 cells were plated onto the underside of each transwell 24h post-nucleofection with smart pool siRNA and two individual oligonucleotides. Following a 48h period cells were stained with calcein-AM and visualised by confocal microscopy. For each condition three series of optical sections were captured every 15µm. The consecutive images were assembled into a sequence in which the depth of the matrigel increases from left to right (B). The invasive migration is expressed as the percentage of cells that migrate further than 45µm. Data are mean \pm SEM from at least three individual experiments, each performed in triplicate (C). CLIC3 suppression was assessed by Western blotting at the end point of the invasion assay (D).

Having demonstrated a requirement for CLIC3 in Rab25-driven invasion, I wanted to establish whether it is on its own sufficient to drive invasion in cells lacking Rab25 expression. To that end, I constructed a Flag-tagged CLIC3 expression vector (Appendix 4.1A) and confirmed that its transfection into A2780 cells yielded high CLIC3 protein expression levels (Fig. 4.6C). I then overexpressed CLIC3 in A2780-DNA3 cells and allowed them to invade for 72 hours into matrigel plugs that were either supplemented with fibronectin or in which fibronectin was omitted (Fig. 4.6A). The quantification of the invasive capacity beyond 45 μ m indicated that CLIC3 increased invasiveness by approximately 50% (Fig. 4.6B). Strikingly, the invasive capacity of CLIC3 was strongly dependent on fibronectin, and in the absence of this component of the extracellular matrix CLIC3 had no effect on the invasiveness of cancer cells. Interestingly, it appears that fibronectin itself hinders A2780-DNA3 cell invasion.

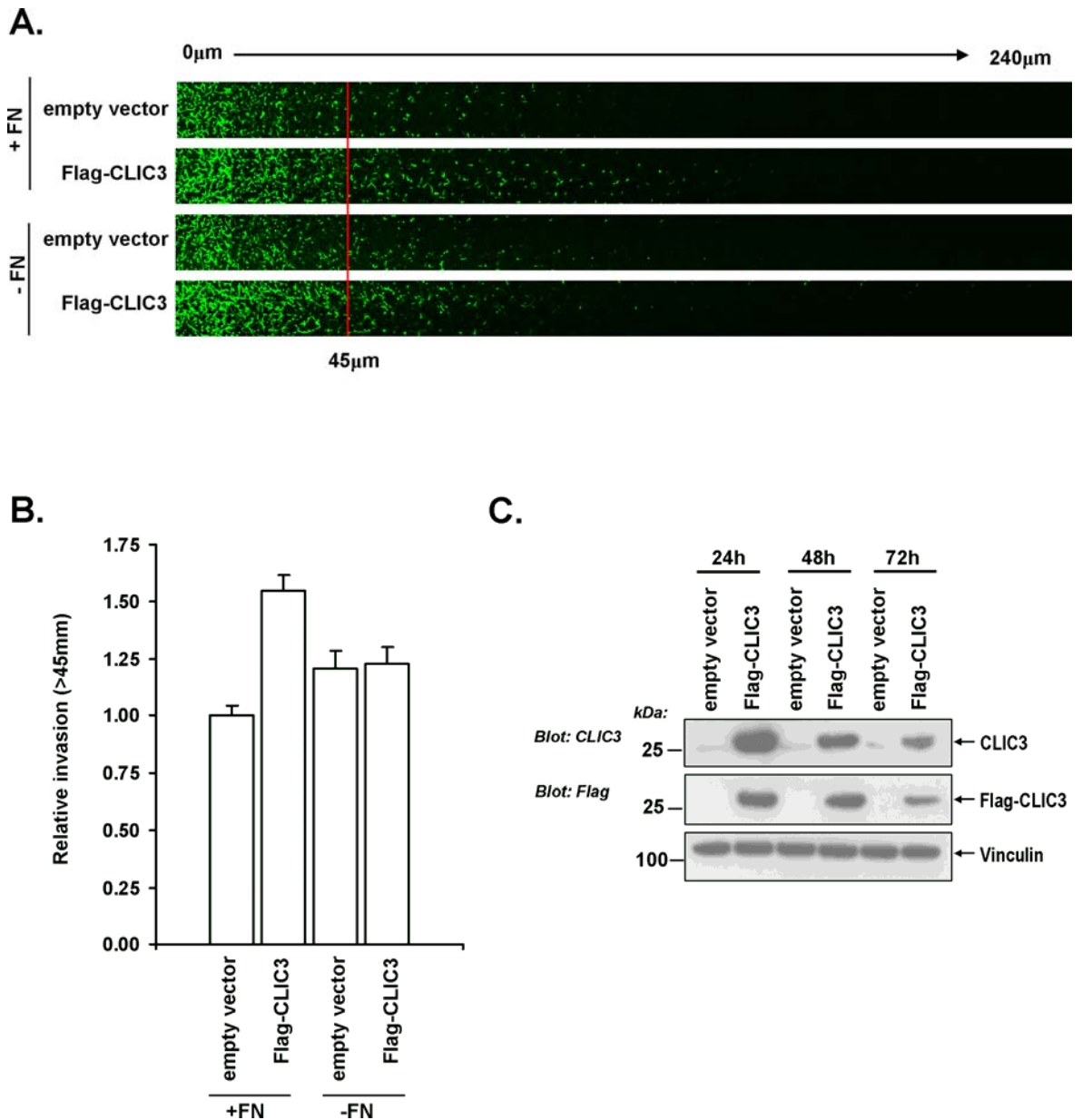


Figure 4-6 CLIC3 drives invasion of A2780-DNA3 cells into fibronectin-rich matrigel.

Four hours after nucleofection with Flag-CLIC3, 4×10^4 cells were plated onto the underside of a transwell containing fibronectin-enriched (25 $\mu\text{g}/\text{ml}$) matrigel. Cells were allowed to invade for 72 hours and were then stained with calcein-AM and visualised by confocal microscopy. For each condition three series of optical sections were captured every 15 μm . The consecutive images were assembled into a sequence in which the depth of the matrigel increases from left to right (A). The invasive migration of cells is expressed as the percentage of cells that migrate further than 45 μm . Data are mean \pm SEM from three experiments, each performed in triplicate (B). The overexpression of CLIC3 was verified by Western blotting 24, 48 and 72 hours after transfection (C).

4.2.2 CLIC3 is localised to vesicular-like structures but not to early or recycling endosomes

To study the localisation and dynamics of CLIC3 in live cells it was necessary to tag the CLIC3 protein with a fluorescent reporter. To this end, I introduced the gene sequence for the red fluorescent protein, mCherry, into a mammalian expression vector for CLIC3, such that the fluorescent tag would be attached to the N-terminus of CLIC3 (Appendix 4.1B). Western blotting confirmed that transfection of this construct into A2780 cells led to the production of a Cherry-CLIC3 fusion protein of the appropriate molecular weight, and its expression persisted for at least 72h following transfection (Fig. 4.7A). Live cell imaging using a fluorescence confocal microscopy indicated that, although a small fraction of the fusion protein was diffusely distributed within the cytoplasm and the nucleus, the bulk of the ectopically expressed Cherry-CLIC3 localised to vesicular-type structures that were dynamic and in constant movement both within the cell body, as well as travelling into and out of an extended pseudopod (Fig. 4.7B & Movie1).

As outlined previously, CLIC3 is expressed in A2780 cells in response to expression of a GTPase, Rab25, which is known to be involved in controlling the dynamics of endosomal membranes and the recycling of $\alpha 5\beta 1$ integrin in the context of cell migration. I therefore investigated the possibility that the vesicular-type distribution adopted by Cherry-CLIC3 may represent an endosomal compartment, or other element of the endomembrane trafficking system that may be involved in integrin transport. I therefore co-expressed Cherry-CLIC3 with markers of early (GFP-EEA1 and GFP-Rab4, Fig. 4.8A&B) or recycling (GFP-Rab11A, Fig. 4.9A) endosomes and also with GFP-Rab25 (Fig. 4.9B) and assessed their distribution using confocal microscopy. However, there was no clear colocalisation between Cherry-CLIC3 and these endosomal markers indicating that CLIC3 is not recruited to early or recycling endosomal membranes.

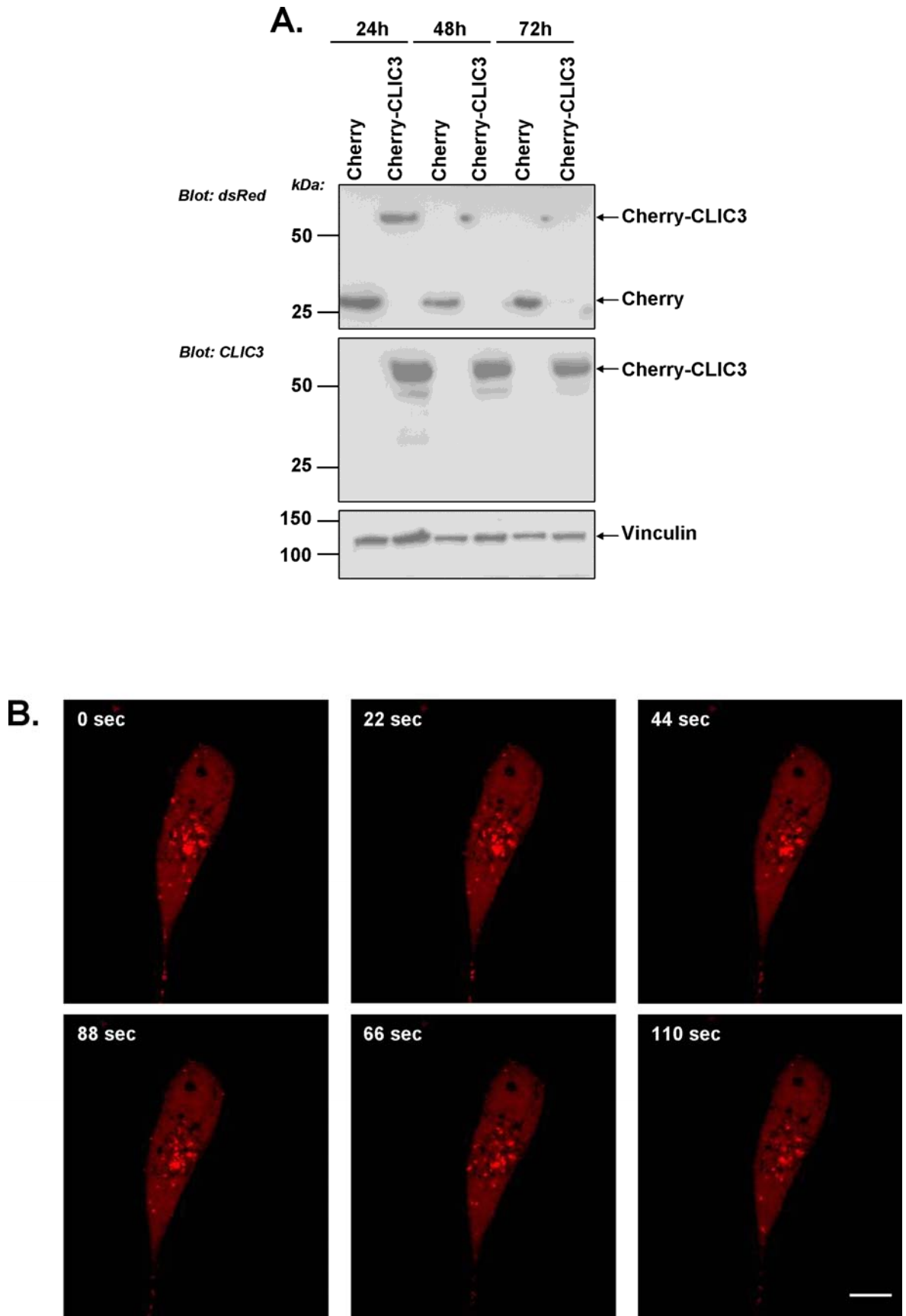


Figure 4-7 Cherry-CLIC3 expression and localisation in A2780-Rab25 cells.

A2780-Rab25 cells were transfected with 3 μ g of Cherry or Cherry-CLIC3 and expression assessed by Western blotting 24, 48 and 72 hours after transfection (A). A2780-Rab25 cells transfected with Cherry-CLIC3 were seeded sparsely onto CDMs. 24 hours after transfection Cherry-CLIC3 was directly visualised in living cells using a confocal microscope. Time-lapse movies were recorded over a period of 120 seconds. Stills from a movie corresponding to 22 second intervals are presented. Scale bar, 10 μ m (B).

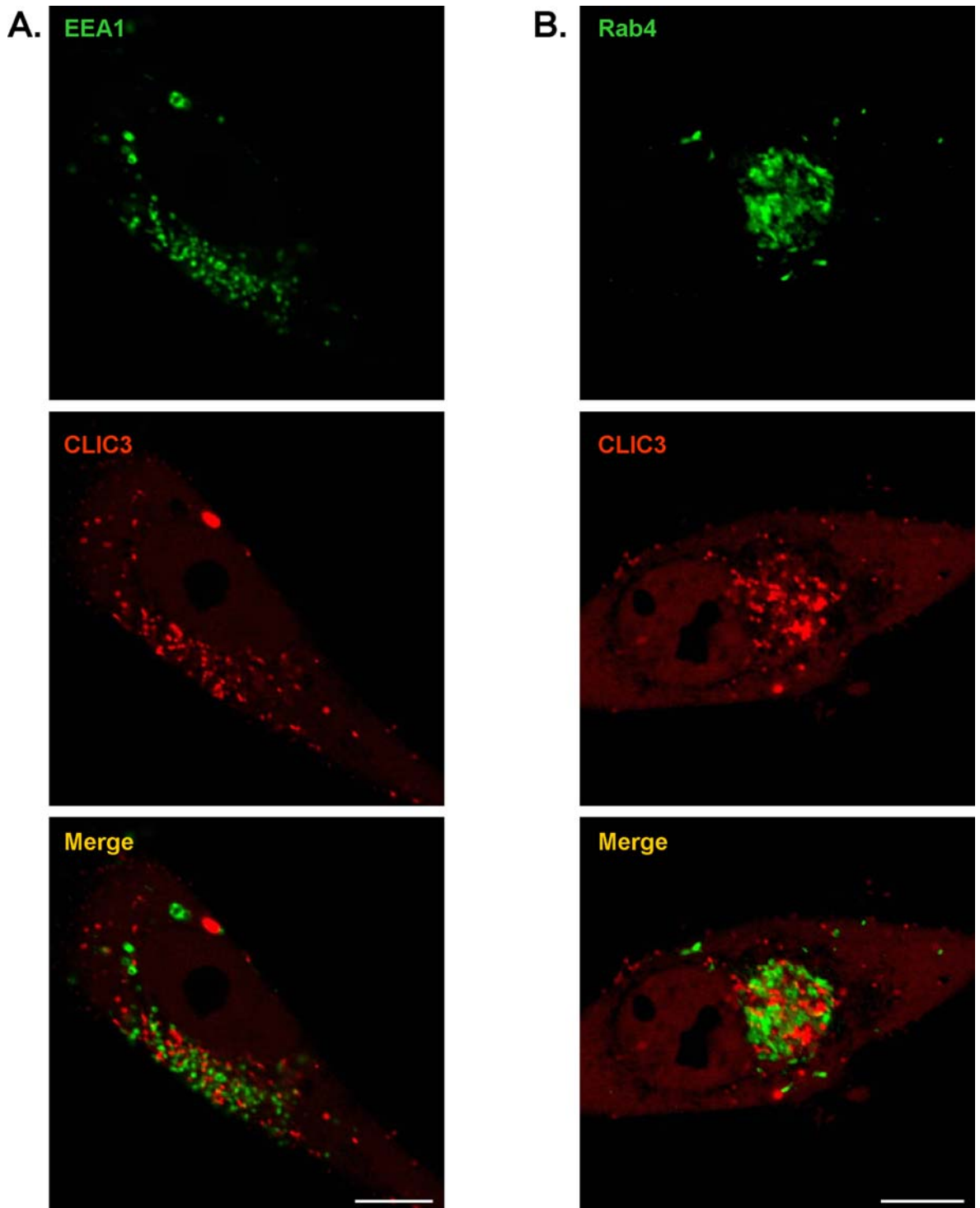


Figure 4-8 CLIC3 does not colocalise with early endosomal markers: EEA1 or Rab4.

A2780-Rab25 cells were co-transfected with 1.5 μ g of Cherry-CLIC3 (red) and 1.5 μ g GFP-EEA1 (green) (A) or with 1.5 μ g of Cherry-CLIC3 (red) and 1.5 μ g GFP-Rab4 (green) (B). 24 hours after transfection the overexpressed fluorescent proteins were directly visualised in living cells using a confocal microscope. Scale bars, 10 μ m.

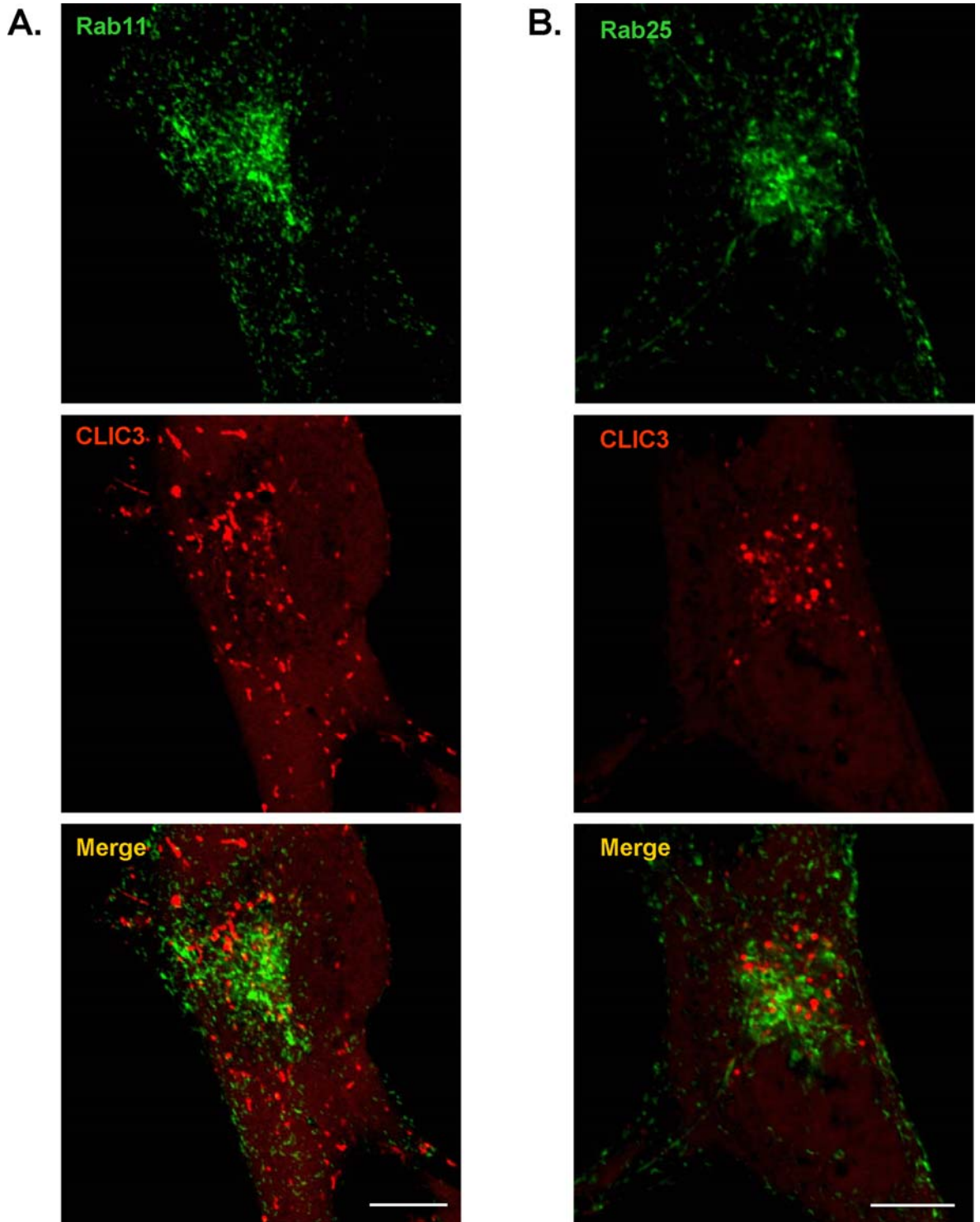


Figure 4-9 CLIC3 does not colocalise with recycling endosomal markers: Rab11 or Rab25. A2780-Rab25 cells were co-transfected with 1.5 μ g of Cherry-CLIC3 (red) and 1.5 μ g GFP-Rab11 (green) (A) or with 1.5 μ g of Cherry-CLIC3 (red) and 1.5 μ g GFP-Rab25 (green) (B). The fluorescent proteins were directly visualised in living cells after 24 hours with a confocal microscope. Scale bars, 10 μ m.

4.2.3 CLIC3 is localised to late endosomes/lysosomes

To determine whether CLIC3 was localised to other elements of the endosomal pathway, I transfected Cherry-CLIC3 in combination with GFP-Rab7, a GTPase that is present on late endosomes and plays a role in the maturation of this compartment and ultimate delivery of endocytosed material to lysosomal compartments (Chavrier, Parton et al. 1990; Meresse, Gorvel et al. 1995). Clearly, there was a marked colocalisation between Cherry-CLIC3 and Rab7 (Fig. 4.10A), indicating that CLIC3 is recruited to late, rather than early endosomes. To further substantiate CLIC3's presence at later endosomal elements, I examined its distribution with respect to lysosomal markers such as Lysosomal-associated membrane protein 1 (LAMP1, Fig. 4.11A) (Rohrer, Schweizer et al. 1996), sialin (Fig. 4.12A) (Morin, Sagne et al. 2004), and the acidotropic dye LysoTracker-Green (Fig. 4.13A) (MacIntyre and Cutler 1988) that is known to accumulate in the highly acidic environment of lysosomes. Indeed, there was a near complete colocalisation between CLIC3 and these markers, indicating that CLIC3 is localised primarily to late endosomes/lysosomes.

As mentioned previously, the ability of CLIC3 and Rab25 to increase invasion is dependent on the presence of fibronectin within the extracellular matrix. Cell movement through the ECM is known to be accompanied by remodelling and degradation of the fibronectin within the matrix, which is followed by its subsequent internalisation via an $\alpha 5\beta 1$ -dependent mechanism. Following internalisation fibronectin is routed to lysosomes and degraded within this compartment (Sottile and Chandler 2005). To determine the intracellular fate of the internalised fibronectin with respect to CLIC3, I conjugated the Alexa647 fluorophore to soluble fibronectin and allowed its internalisation by A2780-Rab25 cells that had been transfected with Cherry-CLIC3 (Fig. 4.13B) alone or in combination with GFP-tagged markers of late endosomes/lysosomes (Fig. 4.10B, 4.11B, 4.12B). Consistent with previous reports, internalised fibronectin accumulated within late endosomes/lysosomes and therein colocalised closely with CLIC3 and other markers of this compartment.

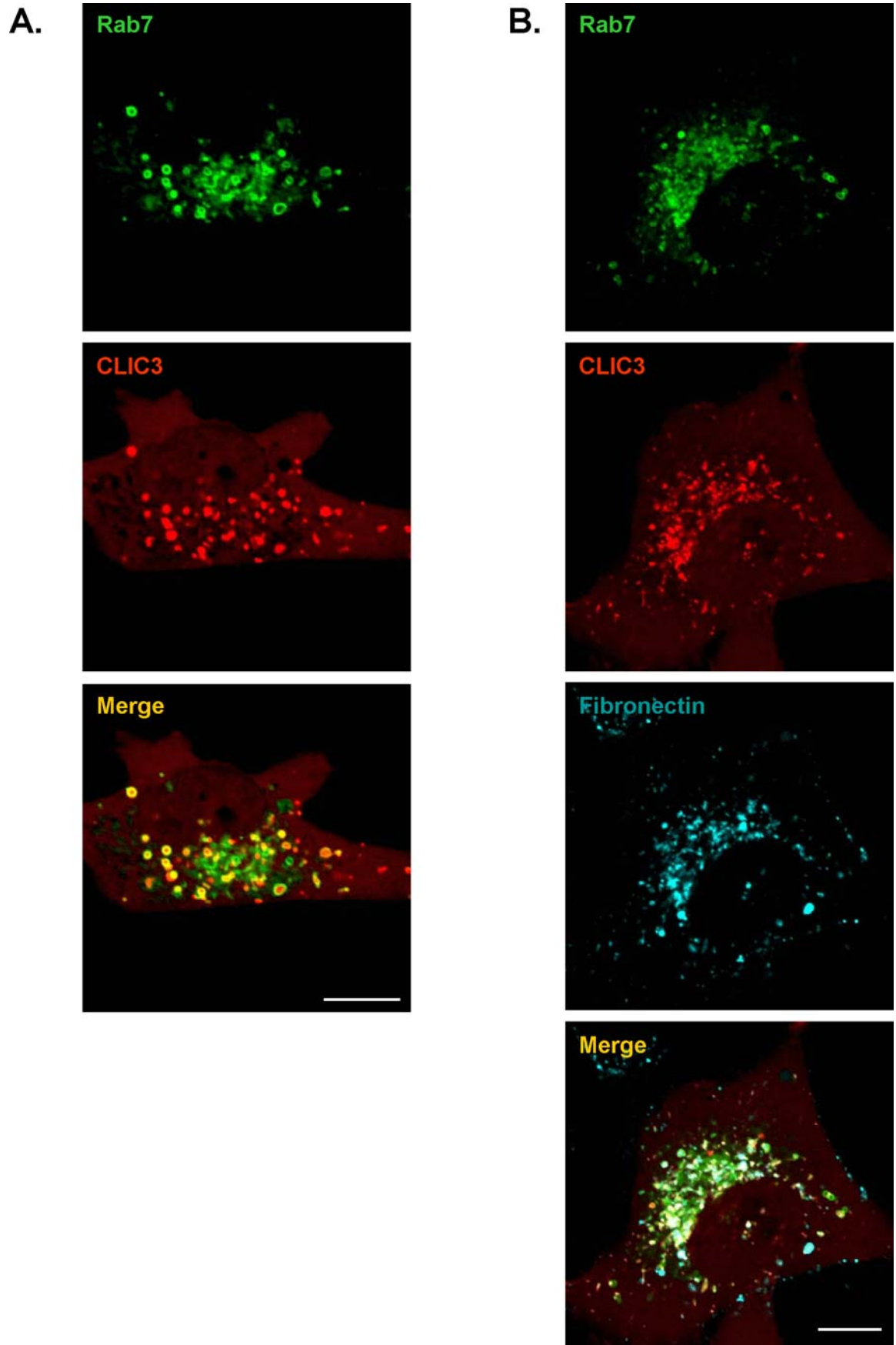


Figure 4-10 CLIC3 colocalises with a late endosomal/lysosomal marker, Rab7.

A2780-Rab25 cells were co-transfected with 1.5 μg of Cherry-CLIC3 and 1.5 μg of GFP-Rab7. 24 hours after transfection Rab7 (green) and CLIC3 (red) were visualised directly in living cells using a confocal microscope (A). Alternatively, cells were incubated with soluble fibronectin-Alexa-647 for 3 hours (2.5 μg/ml) prior to visualisation. Rab7 (green), CLIC3 (red) and fibronectin (cyan) were visualised directly in living cells using a confocal microscope (B). Scale bars, 10 μm.

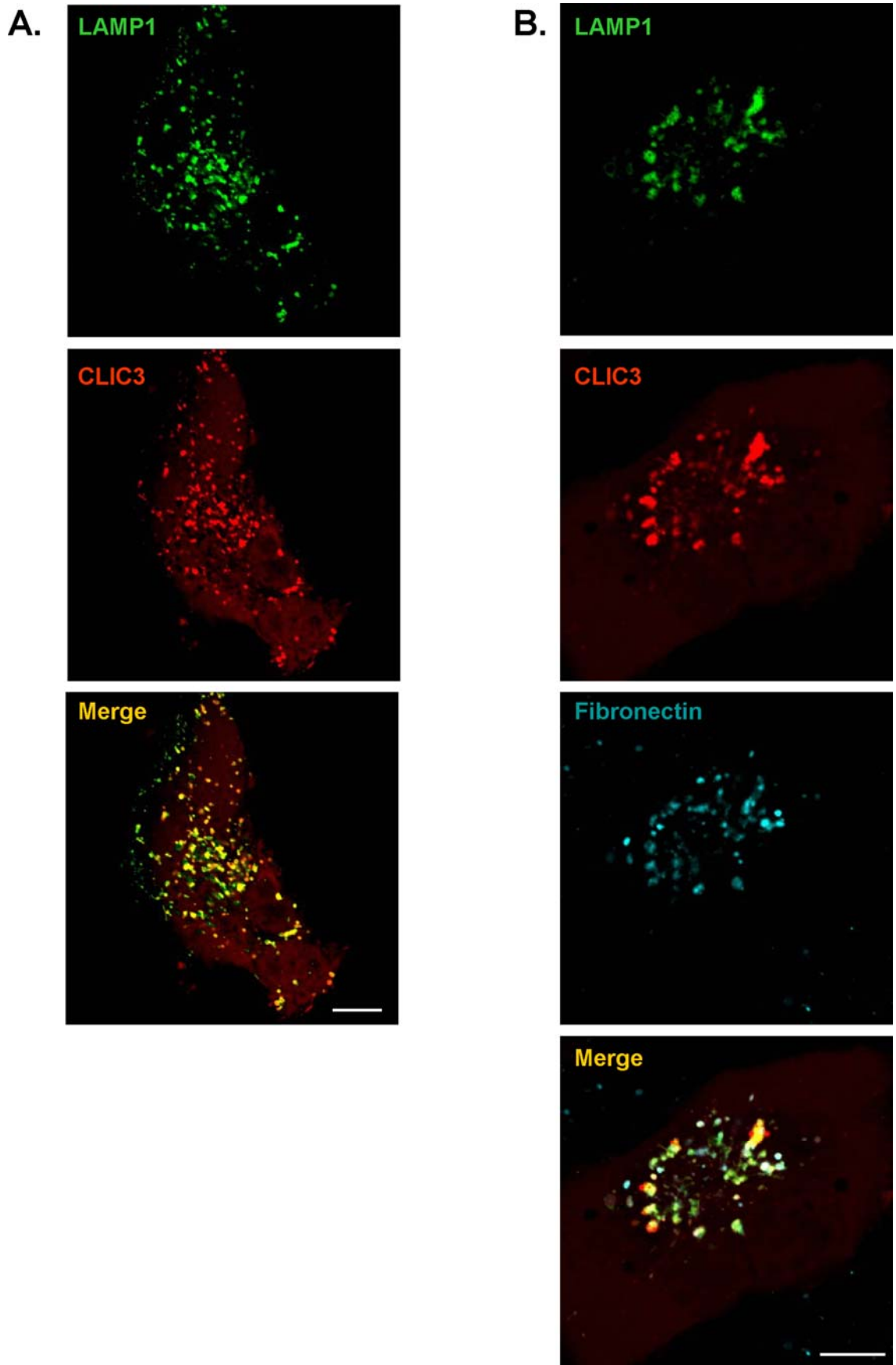


Figure 4-11 CLIC3 colocalises with a lysosomal marker, LAMP1.

A2780-Rab25 cells were co-transfected with 1.5 μ g of Cherry-CLIC3 and 1.5 μ g of YFP-LAMP1. 24 hours after transfection LAMP1 (green) and CLIC3 (red) were visualised directly in living cells using a confocal microscope (A). Cells were transfected as in (A) and after 24hours were incubated with soluble fibronectin conjugated to Alexa-647 fluorophore for 3 hours (2.5 μ g/ml) prior to visualisation. LAMP1 (green), CLIC3 (red) and fibronectin (cyan) were visualised directly in living cells using a confocal microscope (B). Scale bars, 10 μ m.

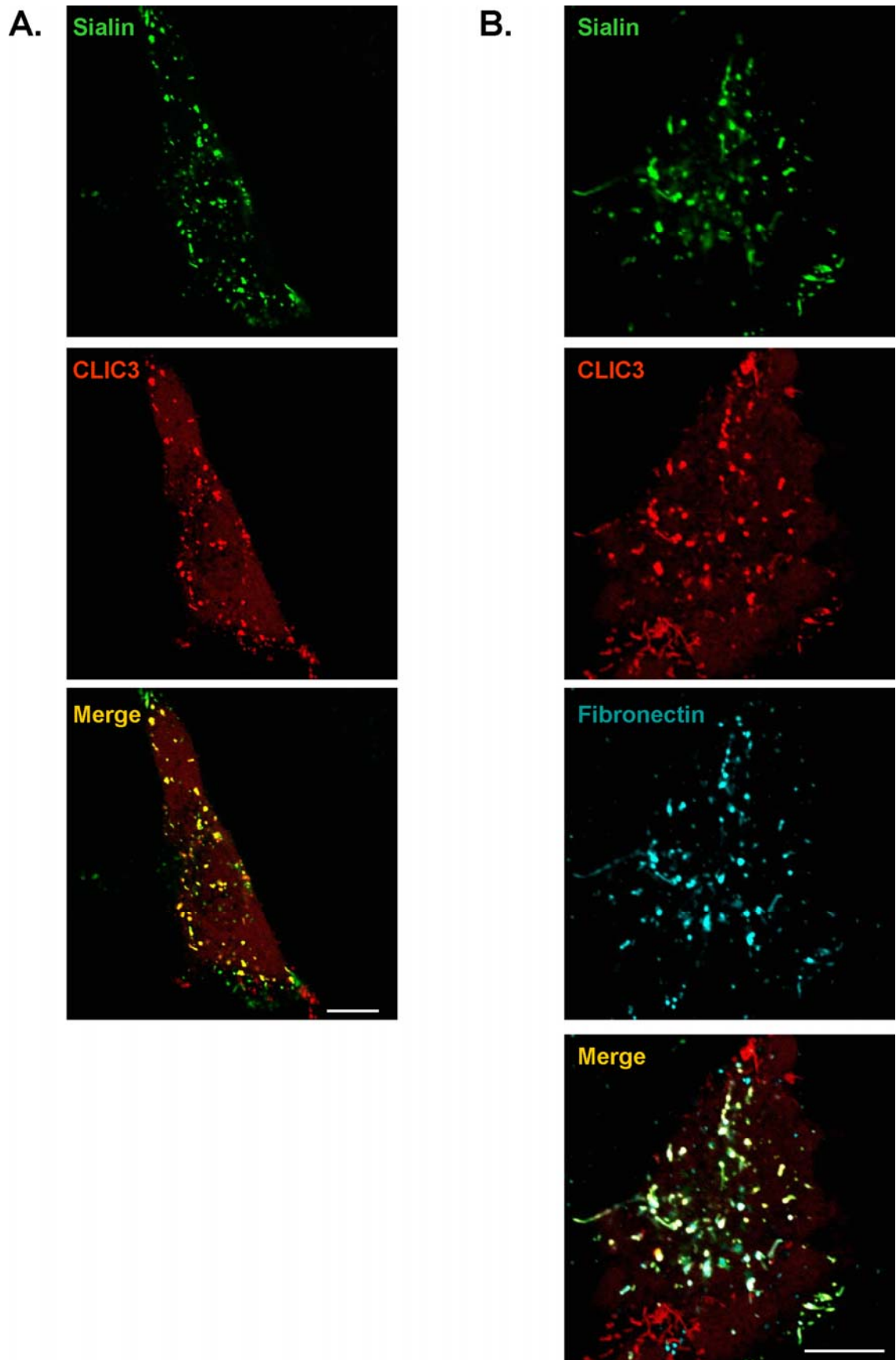


Figure 4-12 CLIC3 colocalises with a lysosomal protein, sialin.

1.5 μ g of Cherry-CLIC3 (red) and 1.5 μ g of GFP-sialin (green) were introduced into A2780-Rab25 cells and after 24 hours they were visualised directly in living cells using a confocal microscope (A). Cells were transfected as in (A) and after 24hours were incubated with soluble fibronectin conjugated to Alexa-647 fluorophore for 3 hours (2.5 μ g/ml) prior to visualisation. Sialin (green), CLIC3 (red) and fibronectin (cyan) were visualised directly in living cells using a confocal microscope (B). Scale bars, 10 μ m.

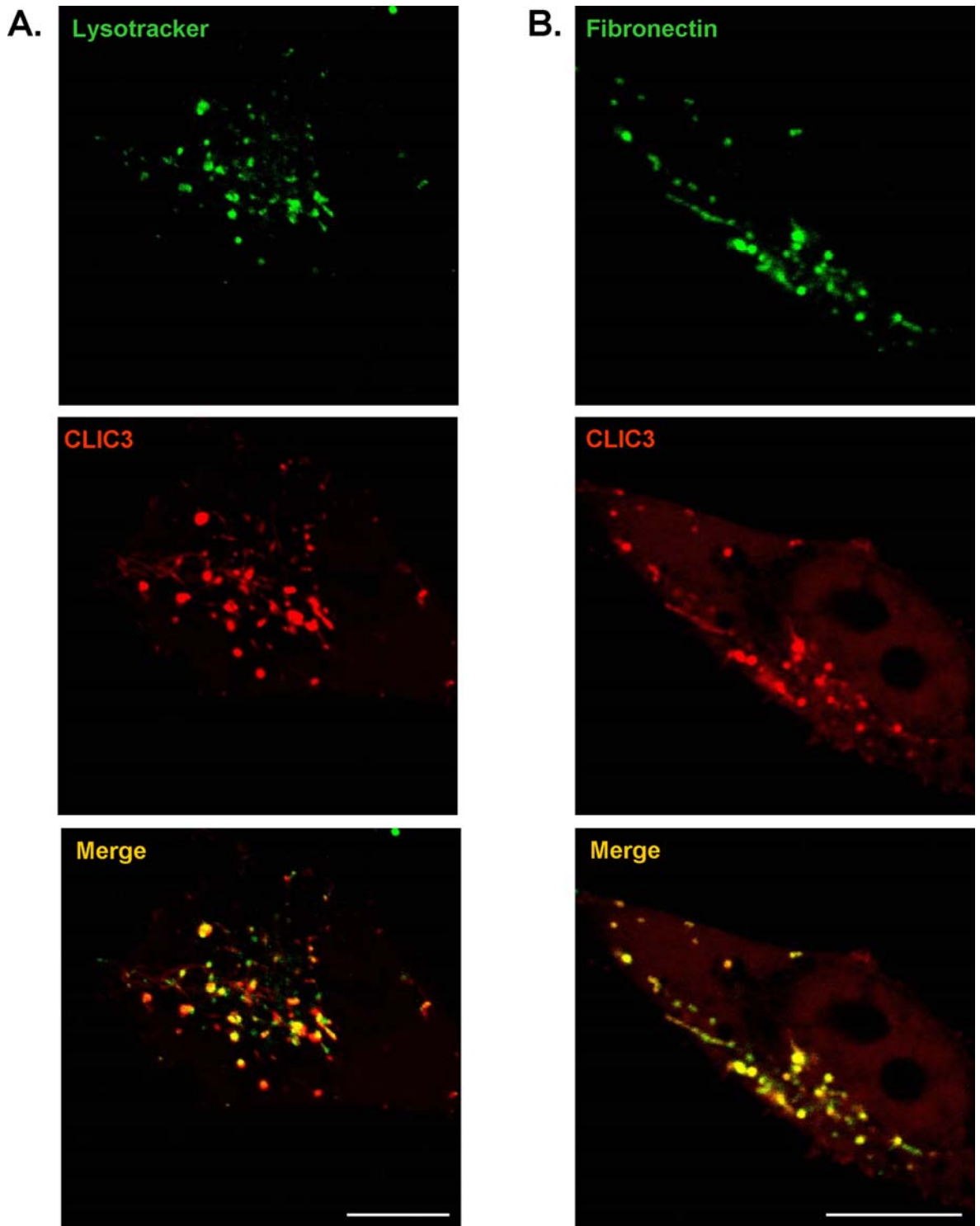


Figure 4-13 CLIC3 colocalises with internalised fibronectin and lysotracker.

A2780-Rab25 cells were transfected with 3 μ g of Cherry-CLIC3. 24 hours after transfection cells were incubated with 100nM Lysotracker -FITC for 20 minutes prior to visualisation. Lysotracker (green) and CLIC3 (red) were directly visualised in living cells using a confocal microscope (A). Fibronectin-Alexa-647 (2.5 μ g/ml) was added 24 hours after nucleofection for a period of 3 hours prior to visualisation. Fibronectin (green) and CLIC3 (red) were directly visualised in living cells using a confocal microscope (B). Scale bars, 10 μ m.

A remaining issue that I wished to address was whether CLIC3's ability to localise to lysosomes was dependent on the presence of Rab25. I therefore expressed Cherry-CLIC3 in A2780 cells lacking Rab25 expression and looked at its distribution with respect to GFP-sialin and internalised fibronectin (Fig. 4.14 A&B). This indicated clearly that the ability of CLIC3 to be recruited to late endosomes/lysosomes is independent of the cell's Rab25 status.

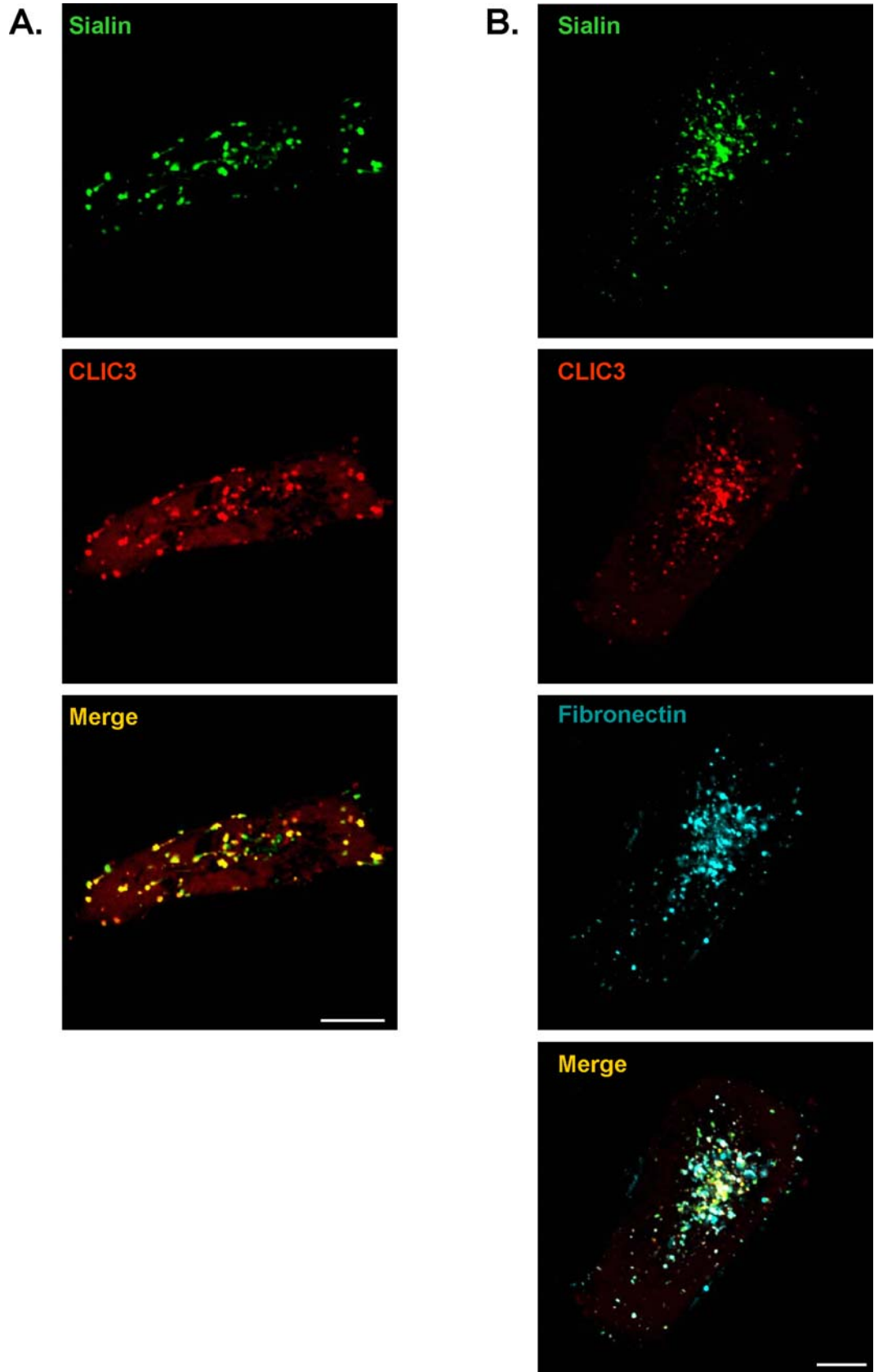


Figure 4-14 Late endosomal/lysosomal localisation of CLIC3 is independent of Rab25 expression.

A2780-DNA3 cells were co-transfected with 1.5 μ g of Cherry-CLIC3 and 1.5 μ g of GFP-sialin. 24 hours after transfection sialin (green) and CLIC3 (red) were visualised directly in living cells using a confocal microscope (A). Cells were transfected as in (A) and after 24hours were incubated with soluble fibronectin conjugated to Alexa-647 fluorophore for 3 hours (2.5 μ g/ml) prior to visualisation. Sialin (green), CLIC3 (red) and fibronectin (cyan) were visualised directly in living cells using a confocal microscope (B). Scale bars, 10 μ m.

4.2.4 Active $\alpha 5$ integrin is routed to CLIC3-positive late endosomes/lysosomes in a Rab25-dependent manner

Given the colocalisation of CLIC3 with internalised fibronectin, I investigated the possibility that $\alpha 5$ B1 integrin may be trafficked to the CLIC3-positive compartment. However, under basal conditions, there was clearly little colocalisation between CLIC3 and $\alpha 5$ integrin in A2780-Rab25 (Fig. 4.15A). Integrins are transmembrane heterodimeric molecules that adopt active and inactive conformations. Ligand binding to integrins can favour their active conformations and this leads to the transduction of signals into the cell, which can lead to enhancement of a number of intracellular signalling axes; this is termed outside-in signalling (Schwartz, Schaller et al. 1995). $\alpha 5$ B1 integrin can bind to its ligand, fibronectin, not only when the latter is present as a component of a well-organised fibrillar extracellular matrix, but it also shows affinity for soluble fibronectin monomers (Huveneers, Truong et al. 2008). I therefore decided to use soluble fibronectin as a tool to activate surface $\alpha 5$ B1 and thus determine whether active conformation integrins are preferentially trafficked to lysosomes that are CLIC3-positive. Indeed, live cell imaging showed that addition of fibronectin to A2780-Rab25 cells increased the colocalisation of internalised $\alpha 5$ B1 integrin with CLIC3 (Fig. 4.15A&B). I then deployed an image analysis approach to obtain a quantitative estimate of the degree to which fibronectin can increase delivery of $\alpha 5$ B1 to the CLIC3 compartment. Confocal images from at least 4 independent experiments and of at least 30 cells were subjected to a series of manipulations using the Image J software. Briefly, images in both the green ($\alpha 5$ integrin) and the red (CLIC3) channel were contrast-enhanced and threshold adjustment was performed. The images were then merged and colocalisation between CLIC3 and $\alpha 5$ was expressed as the ratio of yellow versus red pixels. These analyses revealed that occupation of $\alpha 5$ B1 with its ligand, fibronectin, led to >2-fold increase in the appearance of $\alpha 5$ within the CLIC3 compartment (Fig. 4.15D).

Not only can the conformation of integrins be altered by occupation of their ligand-binding site, it can also be induced from within the cell. This is mediated by interaction of cytoplasmic proteins, such as talin, with the intracellular portions of the integrin, and can also be artificially promoted by introduction of

point mutations that weaken intermolecular associations, which are established by a salt-bridge that forms between the α and β integrin cytotails. Indeed, it is well-established that mutation of the juxtamembrane salt-bridge promotes inside-out activation of the platelet integrin, α IIb β 3 (Hughes, Diaz-Gonzalez et al. 1996), and this has also been reported to be achievable for α 5 β 1. In α 5 β 1 the membrane proximal salt-bridge is thought to be formed by a GFFKR sequence in the α subunit. Mutation of this sequence to GAFKR (F1025A) has been shown to induce the phosphorylation of focal adhesion kinase (FAK) and paxillin when cells are in suspension (Webb, Zhang et al. 2007), thus indicating that this mutation can lock α 5 β 1 into an active conformation and induce downstream signalling, irrespective of ligand occupancy. The F1025A mutant of α 5, may therefore be considered to be constitutively active (CA α 5). I therefore used GFP-tagged CA α 5 (GFP-CA α 5) to determine whether fibronectin's ability to promote the delivery of α 5 β 1 to lysosomes may be due to alterations in the heterodimer conformation. Indeed, GFP-CA α 5 integrin colocalised with CLIC3, to a much higher extent than wild type integrin (wt- α 5) (Fig. 4.15A&C). Quantification revealed an almost 2-fold increase in the routing of the constitutively active α 5 to the CLIC3 compartment when compared to wild type integrin (Fig. 4.15D). This indicated that it is the active conformation of the integrin that dictates α 5 β 1's routing to late endosomes/lysosomes.

To determine whether there was a requirement for Rab25 for the lysosomal routing of active α 5 integrin, I looked at the distribution of GFP- α 5 in A2780-DNA3 cells, which lack Rab25 expression. In contrast to the observations in Rab25-expressing cells, no discernable colocalisation between GFP- α 5 and Cherry-CLIC3 was seen in A2780-DNA cells, and this was not augmented by addition of soluble fibronectin (Fig. 4.16A,B&C). This suggested that Rab25 is necessary for the routing of active α 5 integrin to the late endosomal/lysosomal CLIC3-positive compartment.

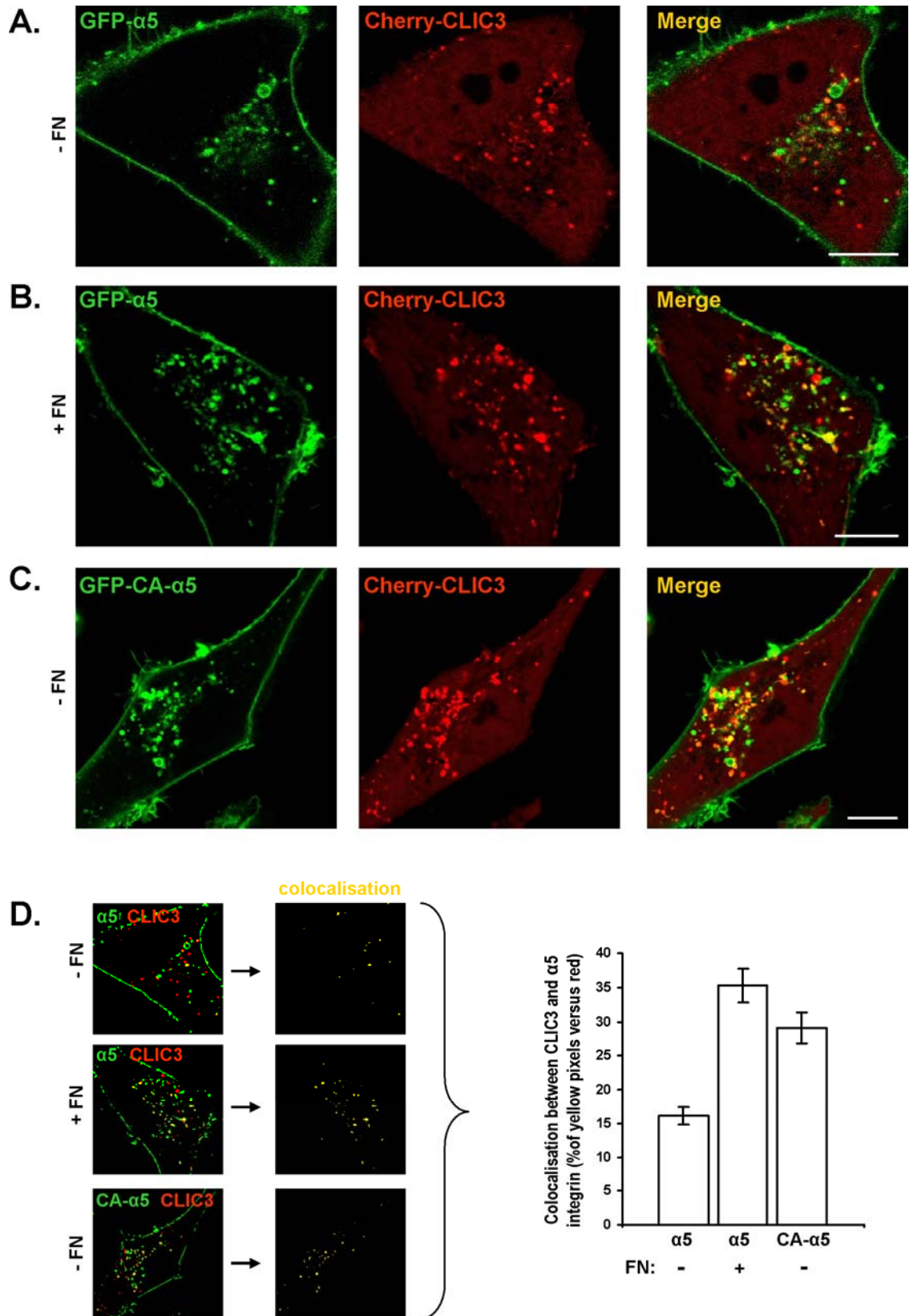


Figure 4-15 Addition of soluble fibronectin and expression of a constitutively active mutant of $\alpha 5$ integrin enhances colocalisation between CLIC3 and $\alpha 5$ integrin vesicles.

A2780-Rab25 cells were transfected with 1.2 μ g of Cherry-CLIC3 in combination with 4.8 μ g of GFP- $\alpha 5$ (A&B) or with 4.8 μ g of constitutively active integrin; GFP-CA $\alpha 5$ (C). 24 hours after transfection $\alpha 5$ integrin (green) and CLIC3 (red) were visualised directly in living cells without fibronectin (FN) treatment (A&C) or after cells were treated with 2.5 μ g/ml of soluble FN for 3 hours (B). Scale bars, 10 μ m. Shown in (D) are representative images, corresponding to these in (A-C), as obtained in Image J software, where colocalisation between CLIC3 (red) and $\alpha 5$ integrin (green) was quantified and expressed as percentage of yellow pixels versus red pixels (D). Data are mean \pm SEM from at least 4 experiments, $n > 30$ cells.

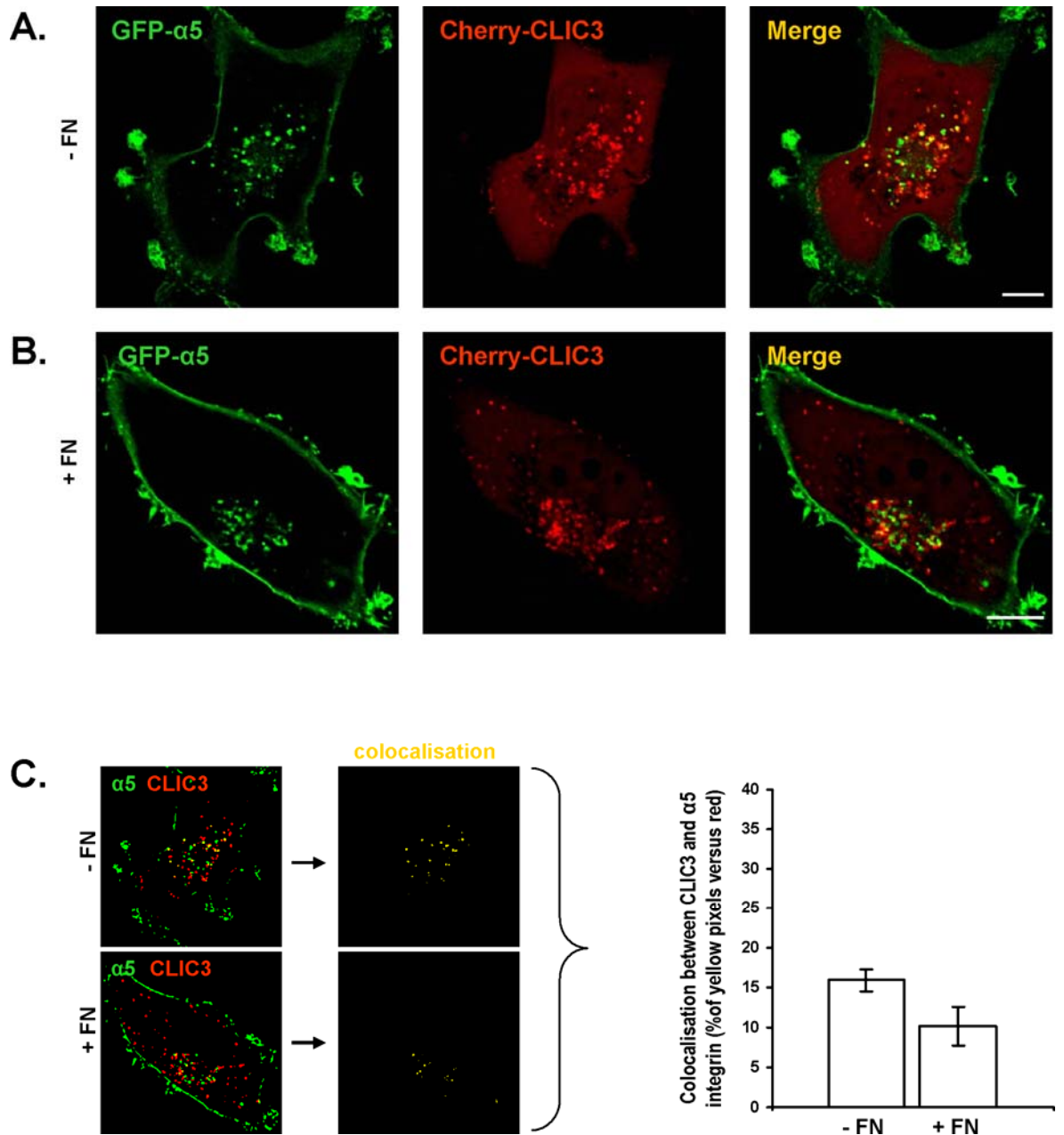


Figure 4-16 Fibronectin-induced enhancement of colocalisation between CLIC3 and $\alpha 5$ integrin vesicles requires Rab25.

A2780-DNA3 cells were co-transfected with 1.2 μ g of Cherry-CLIC3 and 4.8 μ g of GFP- $\alpha 5$. 24 hours after transfection $\alpha 5$ integrin (green) and CLIC3 (red) were visualised directly in living cells without fibronectin (FN) treatment (A) or after cells were treated with 2.5 μ g/ml of soluble FN for 3 hours (B). Scale bars, 10 μ m. Shown in (C) are representative images, corresponding to these in (A&B), generated with Image J software, where colocalisation between CLIC3 (red) and $\alpha 5$ integrin (green) was quantified and expressed as percentage of yellow pixels versus red pixels (C). Data are mean \pm SEM from 2 experiments, n=13 cells.

I then wished to test the hypothesis that lysosomally-routed $\alpha 5 \beta 1$ would come into close physical proximity with CLIC3 within this compartment, and to this end I used a fluorescence resonance energy transfer (FRET) approach. Fluorescence is a process initiated by the absorption of a photon, which takes the molecule into an excited state, and is then followed by the emission of a photon with a longer wavelength, which in turn brings the molecule back to its ground state. The time required for the return to the ground state is referred to as the fluorescence life time (τ) and can be used as a determinant of interaction between proteins. This is due to the ability of a fluorescent donor molecule to return to its ground state by transferring its energy to the acceptor molecule, which resides nearby (within 10 nm distance), a process referred to as FRET. The fluorescence lifetime of the donor will be shorter when FRET occurs, because the donor can lose its surplus energy and exit the excited state faster by comparison with a donor that is not within a FRET-able distance of an acceptor molecule. The FRET efficiency (E) therefore depends on the distance between the donor and the acceptor molecule and can be deduced from the comparison of the lifetime of the donor in the presence of acceptor (τ_{DA}) and the lifetime of the donor alone (τ_D), according to the following formula: $E = 1 - \tau_{DA}/\tau_D$ (Lambert instruments manual).

I transfected A2780-Rab25 cells with GFP- $\alpha 5$ integrin (to act as the fluorescence donor), either alone or in combination with Cherry-CLIC3 or Cherry (potential fluorescence acceptors), and measured the lifetime of the GFP donor both in the absence of added fibronectin and also following addition of 2.5 $\mu\text{g}/\text{ml}$, 25 $\mu\text{g}/\text{ml}$ and 50 $\mu\text{g}/\text{ml}$ soluble fibronectin (Fig. 4.17A). When Cherry-CLIC3 was used as the acceptor, a dose-dependent decrease in the lifetime of GFP- $\alpha 5$ was observed following fibronectin addition (Fig. 4.17C). However, when unconjugated Cherry was used as the acceptor, the fluorescence lifetime of GFP- $\alpha 5$ remained unchanged following the addition of fibronectin, thus indicating that the alterations in the fluorescent integrin's lifetime were specifically owing to its proximity to Cherry-CLIC3 and not simply to the presence of the Cherry protein in the cell. By using these lifetime measurements to calculate the FRET efficiency, I found that addition of fibronectin was able to drive an approximately 8-fold increase in FRET between GFP- $\alpha 5$ and Cherry-CLIC3 (Fig. 4.17D). I then used the same approach to determine the FRET between GFP-

CA α 5 and Cherry-CLIC3 and found that this constitutively active mutant had an approximately 5-fold greater FRET efficiency with CLIC3 than did the wild-type integrin and that this was not affected by the addition of fibronectin. In the previously outlined immunofluorescence colocalisation experiments, it appeared that α 5B1 was not routed to CLIC3-positive late endosomes/lysosomes in cells that lacked expression of Rab25. To confirm this result using the FRET approach, I expressed GFP- α 5 or GFP-CA α 5 (donors) and Cherry-CLIC3 or Cherry (acceptors) in A2780-DNA3 cells and measured the lifetime of GFP following addition of 25 μ g/ml soluble fibronectin (Fig. 4.18A). Expression of Cherry-CLIC3 did not suppress the lifetime of GFP- α 5 or GFP-CA α 5 (in the presence or absence of fibronectin) indicating that the integrin and CLIC3 do not come into close proximity in cells that do not express Rab25. Taken together, these data indicate that active-conformation α 5B1 heterodimers are transported to late endosomes/lysosomes via a mechanism that requires Rab25. Then, upon arrival at this compartment, active α 5B1 comes into close proximity with CLIC3 in a way that can be detected by FRET.

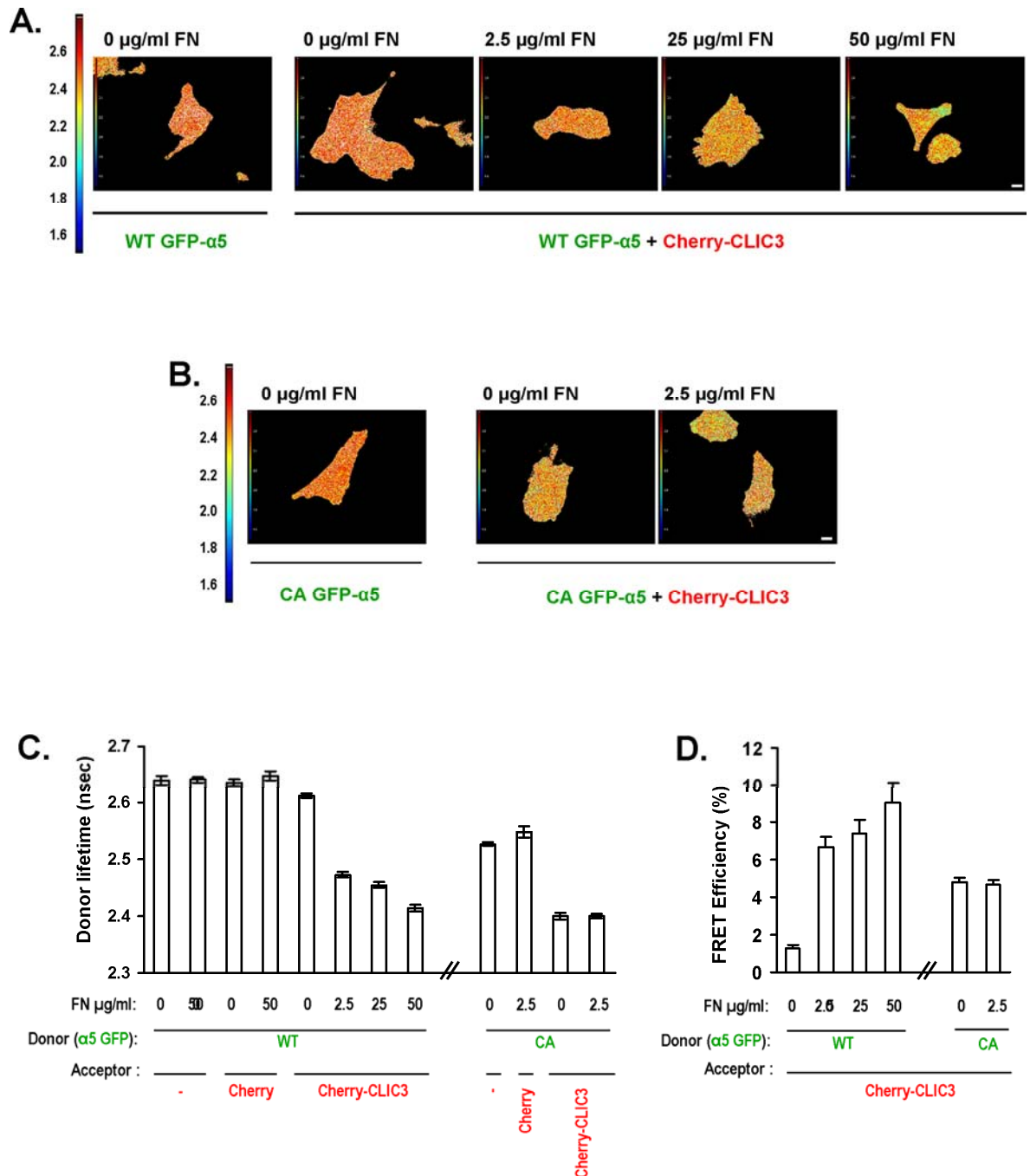


Figure 4-17 FLIM-FRET analysis of the proximity of $\alpha 5$ integrin and CLIC3 in Rab25 expressing cells.

A2780-Rab25 cells were transfected with 4.8 μg of GFP- $\alpha 5$ (donor) alone or in combination with 1.2 μg of Cherry-CLIC3 (acceptor) (A) or with 4.8 μg of constitutively active integrin (GFP-CA $\alpha 5$, donor) alone or together with 1.2 μg of Cherry-CLIC3 (acceptor) (B). Cells were either left untreated or treated with indicated concentrations of fibronectin (FN) for 3 hours and donor lifetime was recorded. Shown in pseudocolor are GFP life time maps, with low life time in blue and high life time in red, as indicated on the colour gradient bar. Scale bar, 10 μm . Donor life times are shown in (C). In (D) shown are FRET efficiencies. Life time and FRET efficiency values are mean \pm SEM from three independent experiments, $n > 45$.

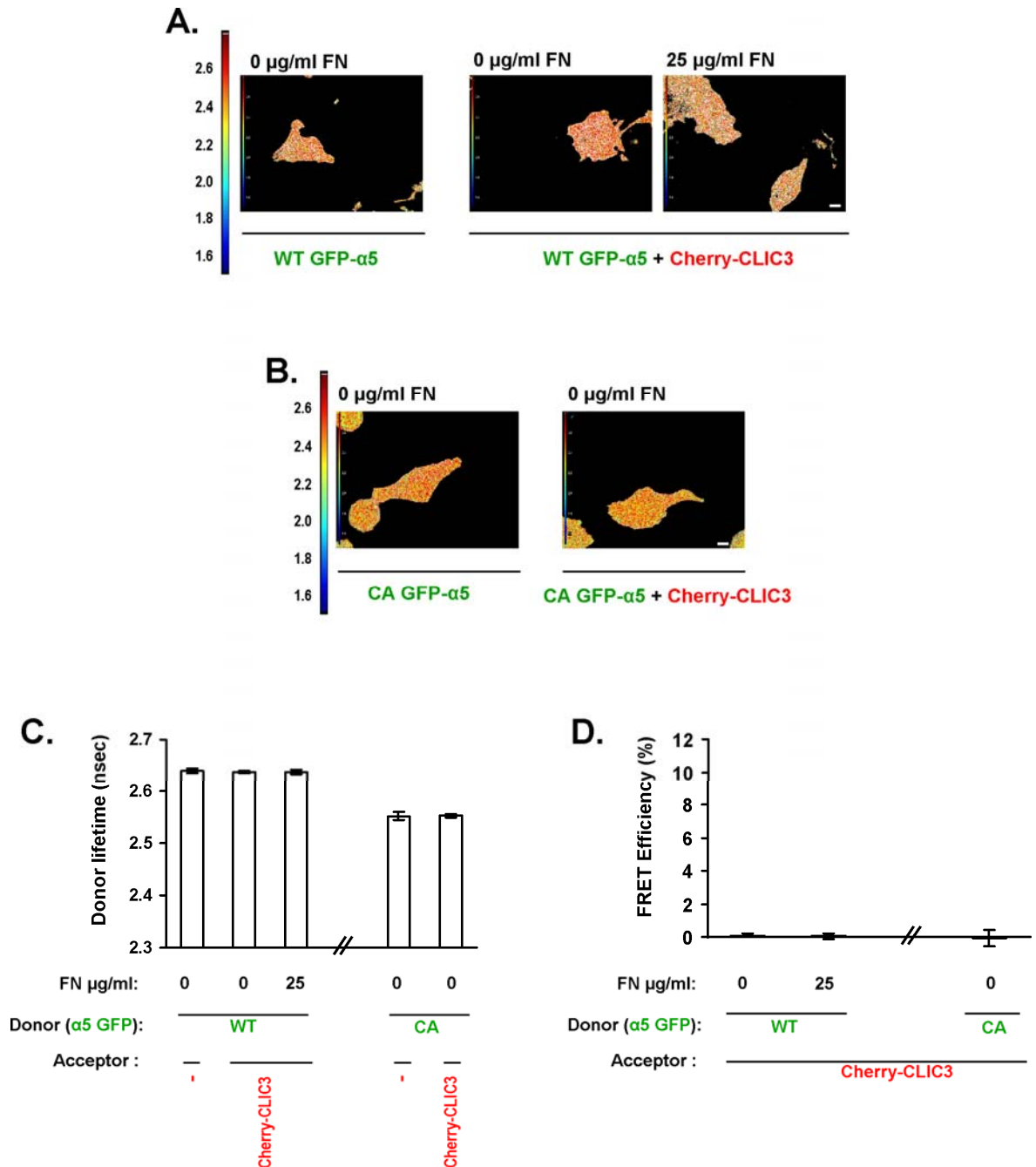


Figure 4-18 FLIM-FRET analysis of the relationship between $\alpha 5$ integrin and CLIC3 in A2780-DNA3 cells.

A2780-DNA3 cells (lacking Rab25 expression) were transfected with 4.8 μg of GFP- $\alpha 5$ (donor) alone or in combination with 1.2 μg of Cherry-CLIC3 (acceptor) (A) or with 4.8 μg of constitutively active integrin (GFP-CA $\alpha 5$, donor) alone or together with 1.2 μg of Cherry-CLIC3 (acceptor) (B). Cells were either left untreated or treated for 3 hours with 25 $\mu\text{g/ml}$ fibronectin (FN) and then donor life time measurements were taken. Shown in pseudocolor are GFP life time maps, with low life time in blue and high life time in red. Scale bar, 10 μm . Donor life times are shown in (C). In (D) shown are FRET efficiencies. Life time and FRET efficiency values are mean \pm SEM from three independent experiments, $n > 45$.

4.2.5 $\alpha 5\beta 1$ integrin is trafficked from CLIC3-positive late endosomes/lysosomes to the plasma membrane

Lysosomes are thought to be the final destination for proteins that are intended for degradation. I therefore used a membrane-impermeant biotinylation reagent to label $\alpha 5\beta 1$ at the cell surface. I then allowed the integrin to be internalised in the presence and absence of fibronectin and used a capture-ELISA to measure the quantity of labelled integrin remaining in the cells over a 60 min period (Appendix 4.2). Surprisingly, $\alpha 5\beta 1$ was not degraded within this period, suggesting the possibility that lysosomally-targetted integrins are being returned to the plasma membrane from the CLIC3 compartment for reengagement with the extracellular matrix. To test this hypothesis I utilised a photoactivatable mutant of $\alpha 5$ integrin (paGFP- $\alpha 5$). This mutant is engineered by the substitution of histidine to threonine, H203T and it exhibits very little emission under basal conditions. However, upon irradiation with violet light (390-415nm), it undergoes conformational change that leads to a 70-fold increase in fluorescence emission at 504nm (green) (Lippincott-Schwartz and Patterson 2009). The combination of photostability of the paGFP and the ability to ‘switch on’ the fluorescence of the fusion protein in a specific region allow for a spatio-temporal dissection of the route taken by labelled cargo from defined subcellular compartments.

I therefore expressed paGFP- $\alpha 5$ integrin in A2780-Rab25 cells in combination with Cherry-CLIC3, and added soluble fibronectin to induce targetting of the integrin to the CLIC3-positive late endosomes/lysosomes. I then aimed a pulse of 405nm laser light at a ‘single point’ corresponding to a Cherry-CLIC3-positive vesicle, and this led to photoactivation of late endosomally/lysosomally-localised integrin within the confines of this structure. During the following couple of minutes, green fluorescence of $\alpha 5$ integrin was rapidly lost from the photoactivated vesicles, and this was accompanied by increased green fluorescence at an adjacent region of the plasma membrane (Fig. 4.19A&D, Movie 2).

As indicated in the previous section, it is the activated conformation of $\alpha 5\beta 1$ that dictates its routing to CLIC3-positive late endosomes/lysosomes. It is

possible that the integrin must return to the inactive conformation to return to the plasma membrane. To address this issue, I utilised a photoactivatable version of the constitutively active mutant of $\alpha 5$ (paGFP-CA $\alpha 5$). Interestingly, CA $\alpha 5$ traffics from the CLIC3 late endosomal/lysosomal compartment to the adjacent region of the plasma membrane (Fig. 4.19B, Movie 3), and quantification of images from at least 8 independent experiments indicated that both wild-type and constitutively active $\alpha 5$ integrin recycled at rates that were indistinguishable from one another (Fig. 4.19D). Conversely, when photoactivation of a single-point adjacent, but not overlapping with the CLIC3 compartment was performed it resulted in negligible photoactivation within the confocal section in question (although subsequent activation of a larger region confirmed the expression of paGFP- $\alpha 5$), and did not yield the accumulation of green fluorescence at the plasma membrane. This suggested that integrin activated in figure 4.19A and B did indeed traffic to the membrane from the photoactivated CLIC3-positive structures and did not simply translocate from the plasma membrane above and below the imaged confocal sections (Appendix 4.3). It is also interesting to note that upon arrival at the cell surface, the photoactivated integrin did not disperse in a way that would be expected if it was freely diffusible in the plasma membrane. This indicates that recycled $\alpha 5$ remains spatially-restricted within a region of the cell surface that is near to the site of exocytosis.

To confirm whether photoactivated integrin appeared at the plasma membrane by following a defined recycling pathway, rather than simply by consequence of non-specific diffusion of the fluorophore from the lysosomal membrane I employed bafilomycin A1, which blocks V-type ATPase and thus also acidification of the endosomal system. Due to its ability to perturb pH gradients within the endosomes, bafilomycin A1 is also believed to block endosomal trafficking events. Indeed, upon bafilomycin A1 treatment I observed no delivery of photoactivated integrin to the plasma membrane, nor did I find decay in the fluorescence the integrin within the photoactivated CLIC3 compartment (Fig. 4.19C&D, Movie 4).

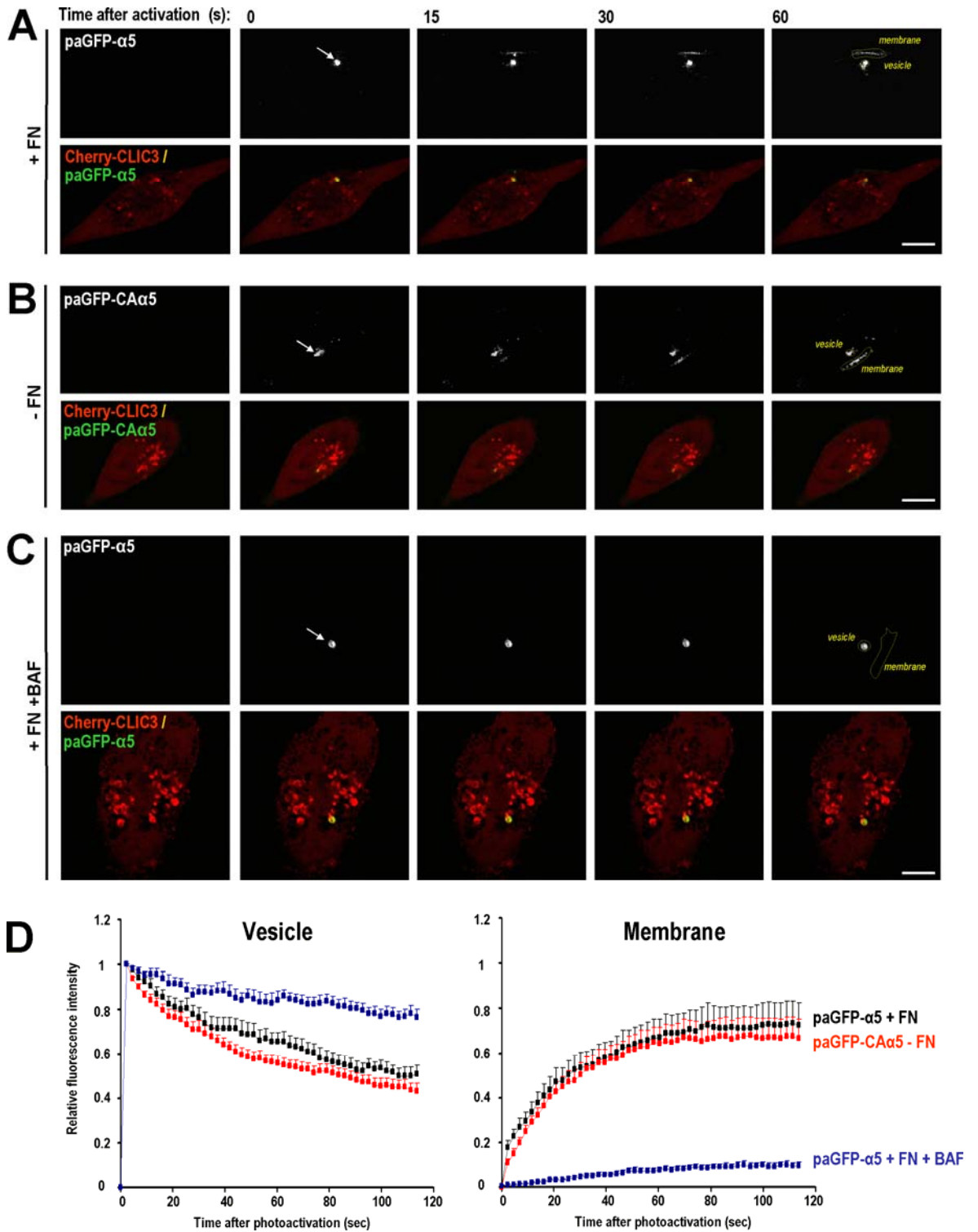


Figure 4-19 Photoactivation shows that $\alpha 5$ integrin returns to the plasma membrane from CLIC3 vesicles.

Figure legend continues on the following page.

Figure 4.19 Photoactivation shows that $\alpha 5$ integrin returns to the plasma membrane from CLIC3 vesicles. A2780-Rab25 cells were co-transfected with 1.2 μ g of Cherry-CLIC3 and 4.8 μ g of photoactivatable wild type $\alpha 5$ integrin; paGFP- $\alpha 5$ (A&C) or with 1.2 μ g of Cherry-CLIC3 and 4.8 μ g of photoactivatable, constitutively active integrin; paGFP-CA- $\alpha 5$ (B). Photoactivation was aimed at CLIC3-positive vesicles, as indicated by the white arrows. Images were then captured with a confocal microscope every 2 seconds over a period of 120 seconds and movies were generated. Still images from a representative movie are presented and include a frame prior to photoactivation, one immediately after photoactivation (0 sec) and subsequent ones at 15 second intervals. Top panels show $\alpha 5$ integrin in grey, bottom panels are merged images with $\alpha 5$ in green and CLIC3 in red. In (A) 2.5 μ g/ml of soluble fibronectin (FN) was used for 1.5 hours prior to photoactivation to increase colocalisation between CLIC3 and $\alpha 5$ integrin. In (C) 2.5 μ g/ml of soluble FN and 100nM Bafilomycin A1 (BAF) were used for 2 hours to block endosomal recycling. Scale bars, 10 μ m. The integrated fluorescence intensities of the photoactivated region and adjacent plasma membrane were plotted against time (D). Shown is loss of fluorescence in the activated region (vesicle) and its gain in the proximal plasma membrane region (membrane), both regions indicated by yellow shapes in (A, B, C). Values are mean fluorescence \pm SEM from 8 individual experiments, n=14 for paGFP- $\alpha 5$ +FN (A, black), n=43 for paGFP-CA $\alpha 5$ (B, red), n=8 for paGFP- $\alpha 5$ +FN +BAF (C, blue).

4.2.6 CLIC3 facilitates the recycling of active $\alpha 5\beta 1$ integrin back to the plasma membrane

I then used a modification of the recycling assay described by Roberts and colleagues (Roberts, Barry et al. 2001) to determine whether recycling of lysosomally-routed $\alpha 5\beta 1$ might require the presence of CLIC3. When surface-labelled $\alpha 5\beta 1$ was endocytosed in the absence of added fibronectin, it returned to the plasma membrane with largely single order kinetics, and this was unaffected by knockdown of CLIC3 (Fig.4.20A). However, following inclusion of fibronectin during the internalisation period, or expression of CA $\alpha 5$ - two situations under which transport of $\alpha 5\beta 1$ to late endosomes/lysosomes is promoted - the integrin recycled with altered kinetics. Under these circumstances, there was an initial, rapid component to $\alpha 5\beta 1$'s return to the plasma membrane which was reduced either by suppression of CLIC3 levels with siRNA (Fig.4.20B, 4.22A), or by addition of bafilomycin (Fig. 4.21A); a drug that opposes endosomal acidification.

Given the importance of $\alpha 5\beta 1$ activity status in its delivery to late endosomes/lysosomes, I performed recycling assays using the 9EG7 antibody, which specifically recognises the extracellular inducible epitope of $\beta 1$ integrin heterodimers (Wennerberg, Fassler et al. 1998), so as to detect recycling of only the active $\beta 1$ heterodimers. This revealed that active $\beta 1$ integrins were returned to the plasma membrane with kinetics that corresponded to the rapid, CLIC3-dependent component of recycling. Moreover, recycling of active integrin was strongly opposed by knockdown of CLIC3 (Fig.4.20C) or by addition of bafilomycin (Fig. 4.21B), and this was particularly apparent following expression of CA $\alpha 5$ (Fig. 4.22B).

Taken together, these data indicate a requirement for CLIC3 in the recycling of active conformation, lysosomally-targetted $\alpha 5\beta 1$ heterodimers and corroborate the observation from the previous section, that active integrin can return to the cell surface from the late endosomal/lysosomal compartment.

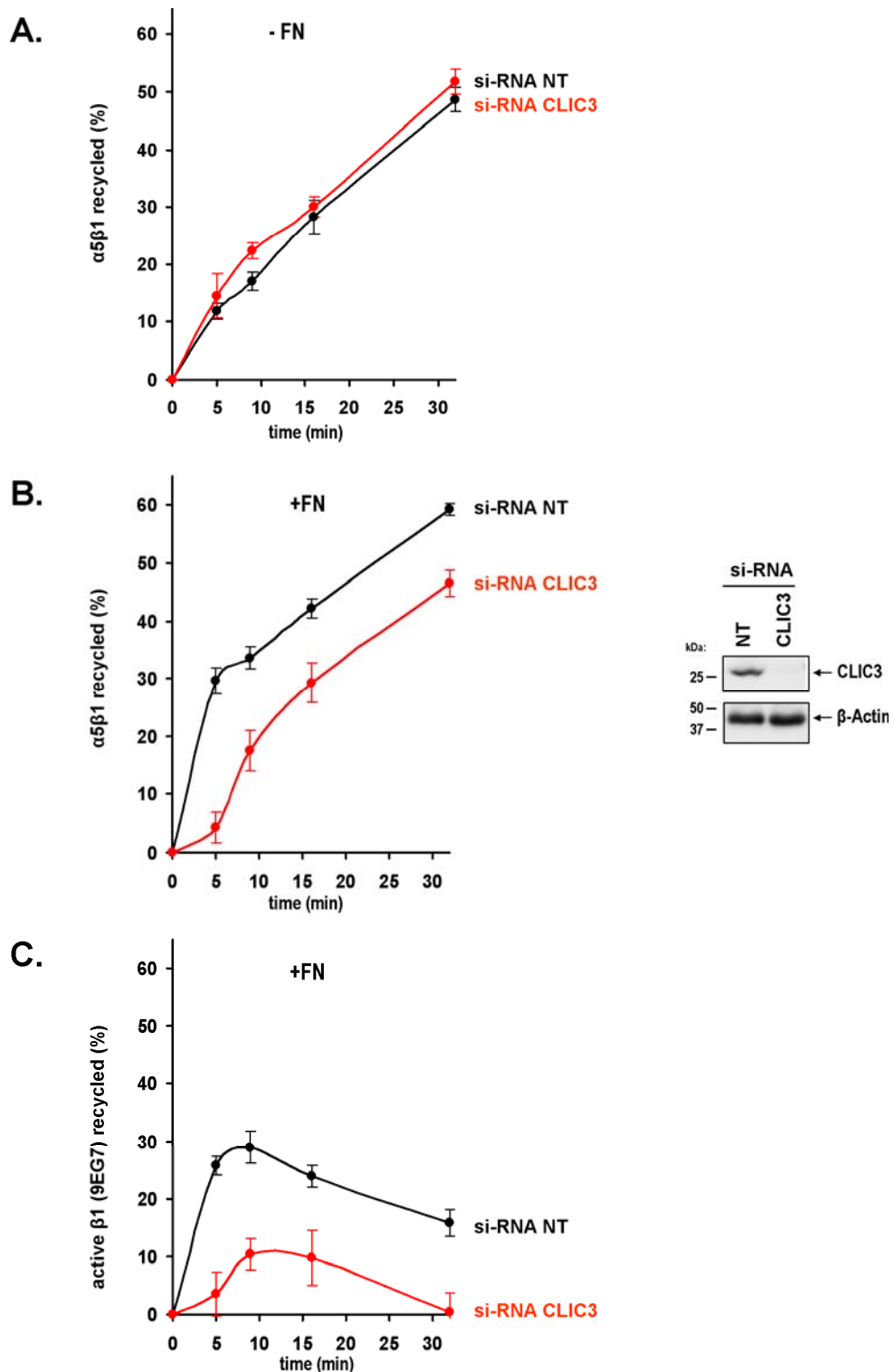


Figure 4-20 Inhibition of CLIC3 suppresses recycling of lysosomally-targetted $\alpha 5\beta 1$.

A2780-Rab25 cells were co-transfected with GFP- $\alpha 5$ and either non-targetting siRNA (siRNA-NT, black) or with smart pool siRNA targeting CLIC3 (siRNA-CLIC3, red). 48 hours after transfection cells were serum starved, surface labelled with 0.2mg/ml NHS-S-S-Biotin at 4°C and internalisation was then allowed to proceed for 30min at 37°C in the presence of serum, and the presence (B&C) or absence (A) of soluble fibronectin (FN, 2.5 μ g/ml). Biotin remaining at the cell surface after internalisation was removed by treatment with MesNa at 4°C and internalised integrin was allowed to return to the cell surface at 37°C for the indicated times. Cells were then re-exposed to MesNa, lysed and biotinylated integrin was determined by ELISA-capture on microtitre plates previously coated with antibodies recognising GFP (A&B), or active $\beta 1$ integrin (9EG7) (C). The proportion of integrin recycled to the plasma membrane is expressed as a percentage of the internal pool. Values are mean \pm SEM from three independent experiments.

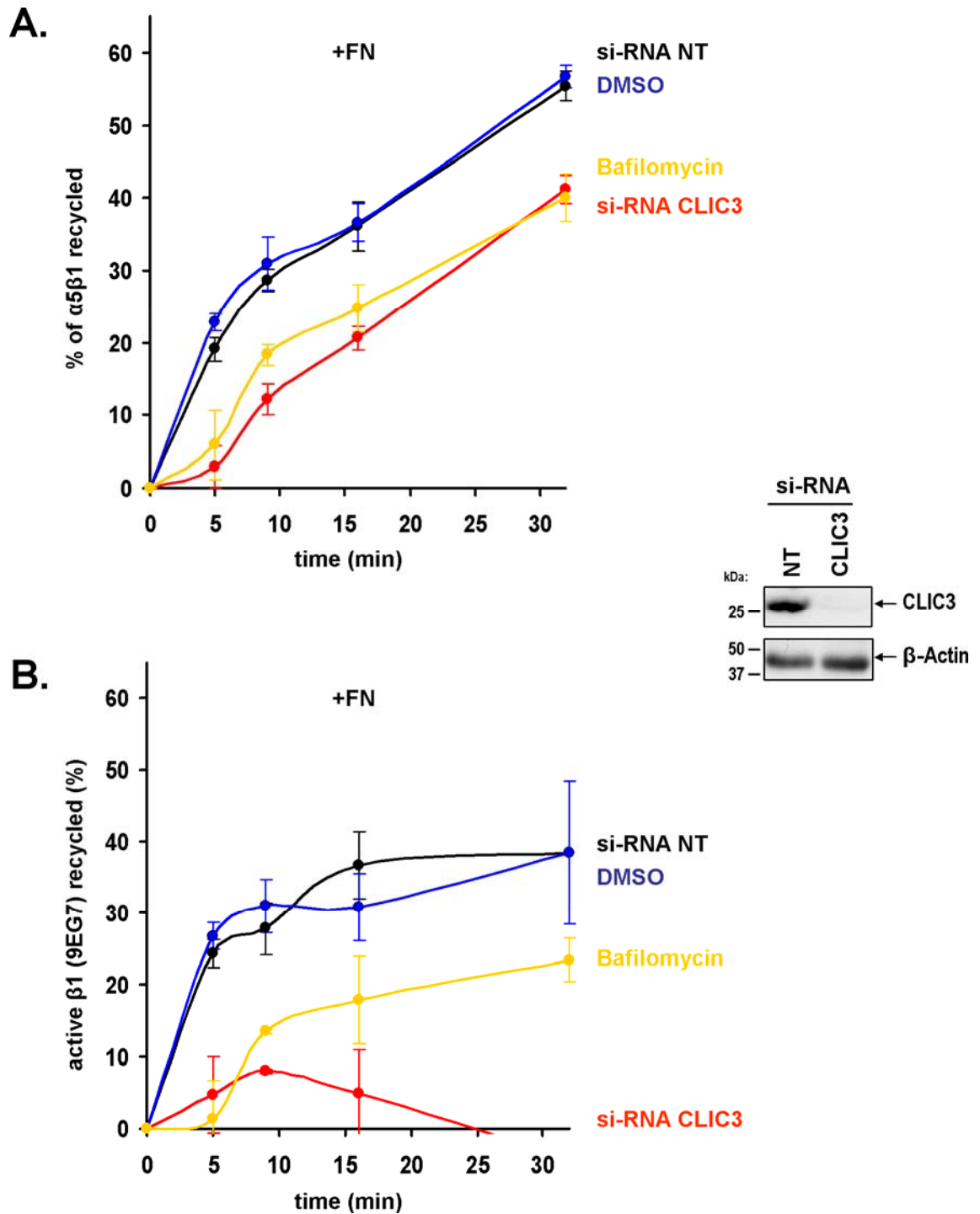


Figure 4-21 Inhibition of CLIC3 or addition of bafilomycin A1 suppress recycling of lysosomally-targetted $\alpha 5\beta 1$.

A2780-Rab25 cells were transfected with non-targeting siRNA (siRNA-NT, black) or with smart pool siRNA targeting CLIC3 (siRNA-CLIC3, red) or left untransfected. 48 hours after transfection cells were serum starved, surface labelled with 0.2mg/ml NHS-S-S-Biotin at 4°C and internalisation was then allowed to proceed for 30min at 37°C in the presence of serum and additional soluble fibronectin (FN, 2.5 μ g/ml). The untransfected cells were treated with either 0.001% DMSO (blue) or 100nM bafilomycin A1 (yellow) during the internalisation stage. Biotin remaining at the cell surface after internalisation was removed by treatment with MesNa at 4°C and internalised integrin was allowed to return to the cell surface at 37°C for the indicated times. Cells were then re-exposed to MesNa, lysed and biotinylated integrin was determined by ELISA-capture on microtitre plates previously coated with antibodies recognising $\alpha 5$ integrin (A), or active $\beta 1$ integrin (9EG7) (B). The proportion of integrin recycled to the plasma membrane is expressed as a percentage of the internal pool. Values are mean \pm SEM from three independent experiments.

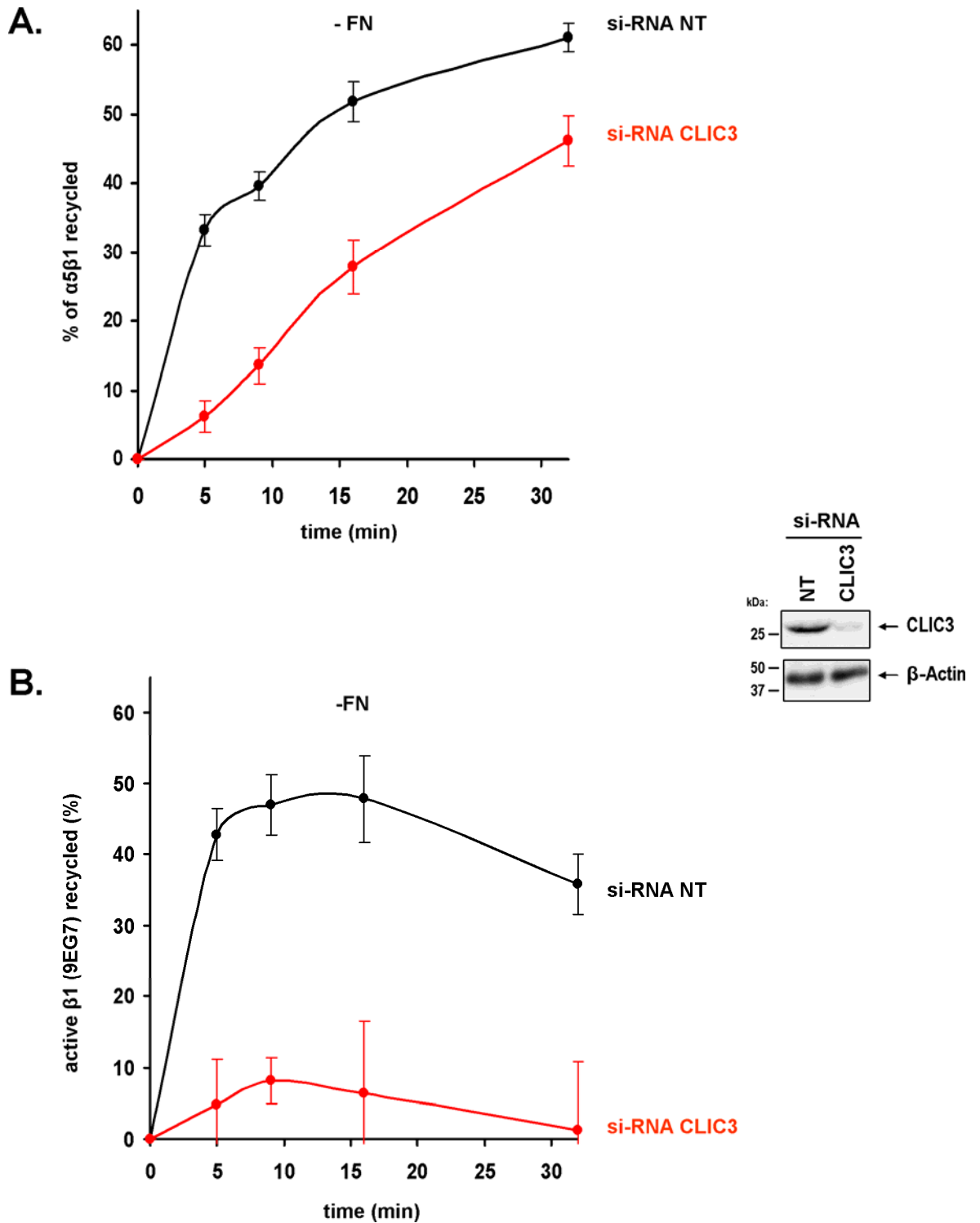


Figure 4-22 Inhibition of CLIC3 suppresses recycling of constitutively active $\alpha 5 \beta 1$.

A2780-Rab25 cells were co-transfected with GFP-CA $\alpha 5$ and either non-targeting siRNA (siRNA-NT, black) or with smart pool siRNA targeting CLIC3 (siRNA-CLIC3, red). 48 hours after transfection cells were serum starved, surface labelled with 0.2mg/ml NHS-S-S_Biotin at 4°C and internalisation was then allowed to proceed for 30min at 37°C in the presence of serum. Biotin remaining at the cell surface was removed by treatment with MesNa at 4°C and internalised integrin was allowed to return to the cell surface at 37°C for the indicated times. Cells were then re-exposed to MesNa, lysed and biotinylated integrin was determined by ELISA-capture on microtitre plates previously coated with antibodies recognising GFP (A), or active $\beta 1$ integrin (9EG7) (B). The proportion of integrin recycled to the plasma membrane is expressed as a percentage of the internal pool. Values are mean \pm SEM from three independent experiments.

4.3 Discussion

4.3.1 Summary and general points

Here I describe a novel role for CLIC3 in Rab25-driven and $\alpha 5\beta 1$ -dependent invasion of ovarian adenocarcinoma cells into fibronectin-rich, three dimensional matrices. Using live cell imaging I localised CLIC3 to a vesicular compartment, which coincided with markers of late endosomes/lysosomes. Moreover, I have found that both Rab25 and the conformation of the integrin determine the targetting of the former to the CLIC3-positive late endosomes/lysosomes, and that these heterodimers can return to the plasma membrane in a CLIC3-dependent fashion (Fig. 4.23).

The experiments addressing subcellular localisation of CLIC3 were performed with ectopically expressed and fluorescently tagged protein. This approach offers the advantage of enabling visualisation of live cells and bypasses the need for cell fixation and permeabilisation and obviates problems of artefacts resulting from uneven epitope exposure. On the other hand, studies carried out with overexpressed proteins pose a risk of distorting the correct localisation of the endogenous protein. At the outset of the project, I attempted to determine the localisation of endogenous CLIC3 in cultured cells using immunofluorescence (IF). However, in spite of employing a number of different fixing and permeabilisation reagents, varying blocking solutions and antibody concentrations, the antibodies I developed were not suitable for IF. Nevertheless, there is some evidence supporting endosomal localisation of CLIC3. Firstly, another group has independently identified CLIC3 whilst searching for endosome-associated proteins (personal communication with Jean Gruenberg). Secondly, immunohistochemical staining of ovarian and pancreatic tumour sections (see next chapter) and of peritoneal and subcutaneous tumour xenografts generated using A2780-Rab25 cells indicate that endogenous CLIC3 is localised to punctuate structures within the cytoplasm, which are reminiscent of endosomes.

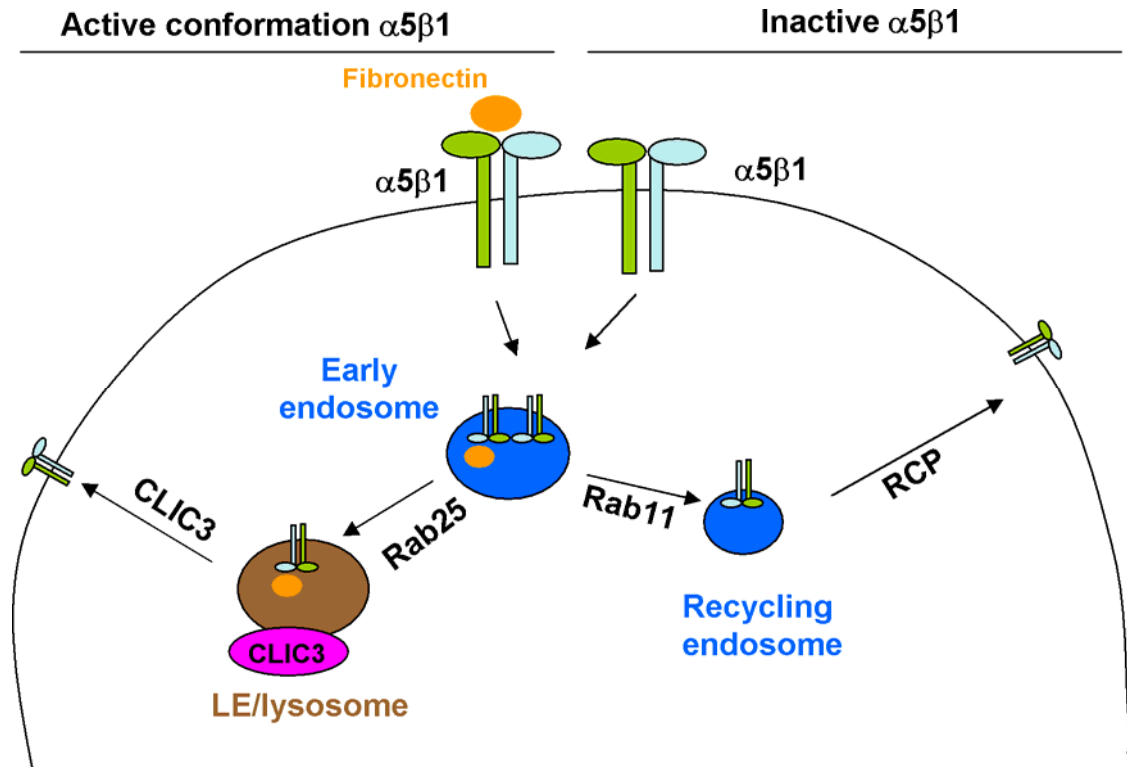


Figure 4-23 Working paradigm.

Having observed an augmentation in the colocalisation of CLIC3 and $\alpha 5$ integrin endosomal fractions by confocal microscopy and having quantified those changes, I wanted to support that observation using FRET. Even though the FRET map does not spatially resolve the distribution of donor-acceptor proximity, the observed changes in donor life time corroborate lysosomal targeting of active integrins. Ideally, I would like to supplement the FRET data, where the donor life time was measured, with ratiometric FRET data, whereby changes in emission intensities of both donor and acceptor are recorded. During FRET the emission intensity from the donor decreases, whilst the amount of photons emitted from the acceptor increases. FRET efficiency is therefore calculated as a ratio of emission intensities from both entities. This method however, requires a plethora of optimisation steps prior to data acquisition, due to the measurements being affected by fluorophore intensities and local concentrations as well as bleed through problems originating from overlapping emission and excitation spectra for the two fluorophores. Moreover, the close proximity of CLIC3 and $\alpha 5$, as determined by FRET, may indicate that the two proteins interact physically. I therefore attempted to test this using immunoprecipitation protocols. I performed experiments where I tried to co-immunoprecipitate CLIC3 with both endogenous and ectopically expressed integrin from cells that underwent treatments, which were seen to lead to the accumulation of $\alpha 5\beta 1$ in the CLIC3 compartment (fibronectin and/or bafilomycin A1 addition). Also, the reversible crosslinking agent DTBP, which had been found to stabilise weak intermolecular associations was used. Additionally, I coupled GST-CLIC3 to sepharose beads and incubated these with lysates from cells expressing Rab25. Notwithstanding these measures, I have been unable to demonstrate co-immunoprecipitation or pulldown of $\alpha 5\beta 1$ with CLIC3. Taken together these findings indicate that although the integrin and CLIC3 come into very close proximity within the same endosomal niche, they do not necessarily physically interact with one another.

4.3.2 Fibronectin uptake and sorting of $\alpha 5\beta 1$ integrin to late endosomes/lysosomes

An important step in the metastatic cascade is the breaching of tissue barriers by invasive tumour cells. Cancer cells migrate through the extracellular matrix (ECM) by degrading its components, such as collagen or fibronectin. ECM degradation may be mediated by extracellular proteases (such as MMPs) and by endocytosis of matrix proteins and their intracellular degradation by lysosomal proteases. In regard of fibronectin, these two routes to ECM turnover are likely to occur in sequence, with extracellular proteolysis liberating soluble fibronectin fragments from the insoluble, cross-linked ECM, which are then internalised for destruction within cellular lysosomes (Sottile and Chandler 2005). The main transmembrane receptor that binds fibronectin is $\alpha 5\beta 1$ integrin and it is through the endocytosis of this heterodimer that fibronectin can enter the endocytic pathway (Shi and Sottile 2008). The internalisation of integrin heterodimers can occur via clathrin-dependent and non-clathrin dependent pathways. Indeed, even though $\alpha 5\beta 1$ integrin is thought to be normally endocytosed into clathrin coated structures, it has been shown that overexpression of Rab21 can activate alternative caveolar routes to increase clathrin-independent endocytosis of this integrin (Pellinen, Tuomi et al. 2008). Moreover, it has recently become apparent that divergent endocytosis pathways could be employed for internalisation of integrins in different conformations and that both inactive and active conformation integrins can be endocytosed. For instance, disabled 2 (Dab2) has been implicated in clathrin-mediated endocytosis of inactive $\beta 1$ integrins (Teckchandani, Toida et al. 2009). On the other hand, clathrin and disabled 2 (Dab2) have also been shown to control the internalisation of ligand-activated $\beta 1$ integrins (12G10 epitope) at sites of focal adhesion disassembly (Chao and Kunz 2009). Additionally, a recent study by Valdembri and colleagues supports proposed separate internalisation routes of active and inactive integrins. It has been shown in endothelial cells, that active $\alpha 5\beta 1$ integrin (SNAKA51 epitope) is endocytosed from fibrillar adhesions via a neuropilin 1 (Nrp1)-dependent route, whereas internalisation of inactive integrin shows no requirement for Nrp1 in the same cell type (Valdembri, Caswell et al. 2009).

My data indicate that an important factor in the delivery of fibronectin to late endosomes/lysosomes is the differential sorting of active and inactive $\alpha 5\beta 1$ heterodimers within the endosomal pathway. Here I show that, in an ovarian adenocarcinoma cell line, fibronectin occupancy or mutation of the 'salt-bridge' sequence in the $\alpha 5$ cytodomain - two manipulations which favour the active conformation of $\alpha 5\beta 1$ integrin - promote late endosomal/lysosomal routing of the active receptor and, presumably, its fibronectin ligand. This is consistent with the findings that a fraction of the internalised $\alpha 5\beta 1$ integrin is sorted, together with its ligand fibronectin, to multivesicular bodies, to then be trafficked to lysosomes (Lobert, Brech et al.). However, these authors show that fibronectin occupancy of the heterodimer results in the ubiquitination of the latter and this serves as a cue for integrin degradation, a process that involves the endosomal sorting complex required for transport (ESCRT). They therefore propose that whilst inactive integrins are trafficked via the perinuclear recycling compartment back to the cell surface, active conformation integrins are routed for degradation. In contrast to these observations, my data indicate that late endosomal/lysosomal active conformation integrins are not degraded, but can rapidly return to the plasma membrane. Lobert and colleagues report that the half life of integrin degradation in fibroblasts is of the order of several hours and is fully dependent on fibronectin having been added to the cells for at least 24 hours (Lobert, Brech et al.). The fact that, in the course of my studies I added fibronectin to the cultured cells for much shorter periods (1.5-3h) and at lower concentrations (2.5 μ g/ml instead of 10 μ g/ml), could account for the inability to detect integrin ubiquitination. It is therefore possible that a small proportion of active, fibronectin-bound integrin is subject to lysosomal degradation in ovarian adenocarcinoma cells, but this is beyond detection under the experimental conditions that I employed.

Given that $\alpha 5\beta 1$ integrin is not ubiquitinated in A2780 cells, it is likely that other signals mediate its Rab25-dependent sorting to lysosomes. Previous work has shown that Rab25, when in GTP-bound form, directly associates with $\beta 1$ cytoplasmic tail, and FRET/FLIM analyses of living cells indicate that this interaction is markedly enhanced when cells are plated on fibronectin-rich CDMs (Caswell, Spence et al. 2007). This may indicate that Rab25 preferentially binds to $\alpha 5\beta 1$ upon its engagement with its ligand (thus when in an active

conformation) and suggests that active conformation integrins are routed to the lysosomes by the virtue of their association with Rab25. It is not completely clear how non-ubiquitinated receptors are sorted to the limiting membrane of late endosomes, but one school of thought is that they arrive there by default because they lack signals for sorting to the recycling pathway. $\alpha 5\beta 1$ integrin is known to recycle via the Rab coupling protein (RCP)-regulated and Rab11 dependent pathway. It has also recently been found that RCP and Rab25 interact with the same portion of the $\beta 1$ cytoplasmic tail (P.Caswell, personal communication), indicating the possibility that the two proteins compete for integrin binding. Thus, when $\alpha 5\beta 1$ is in its active conformation, Rab25 may preferentially bind to the heterodimer and oppose its RCP-mediated recycling, and therefore promote its delivery to the late endosomal/lysosomal pathway.

4.3.3 Return of $\alpha 5\beta 1$ to the plasma membrane

As early as in 1987 it was suggested that lysosomes should not be considered to exclusively be a degradative compartment for endocytosed material. Indeed, the integral membrane glycoprotein, LEP100, has been shown to be present at three cellular locations; lysosomes, endosomes and at the plasma membrane. Constant transport of LEP100 between endosomes and lysosomes as well as lysosomes and the cell surface has been reported, and this suggests the existence of a considerable bi-directional flux between these compartments. Moreover this flux has been reported to be refractory to inhibition by lysosomotropic agents, such as chloroquine (Lippincott-Schwartz and Fambrough 1987). Almost a decade later, a pathway mediating the direct transport of MHC class II receptors from lysosomes to the plasma membrane, without passage through early endosomes, was characterised in B-cells (Wubbolts, Fernandez-Borja et al. 1996).

Exocytosis of late endosomes and lysosomes is known to lead to the release of their luminal contents from the cell (Idone, Tam et al. 2008). It has been proposed that tumour endosomal exocytosis results in the release of matrix-degrading enzymes and can therefore contribute to cancer metastasis (Bernacki, Niedbala et al. 1985). During lysosome exocytosis, the limiting membrane fuses with the plasma membrane and the contents of lysosomal lumen is *en masse* released from the cell. However, it is unlikely that lysosome exocytosis

accompanies the recycling of integrins, since the CLIC3-positive compartment from which $\alpha 5\beta 1$ returns to the cell surface, seems relatively immobile and does not visibly undergo incorporation into the plasma membrane. Also, preliminary experiments indicate that fluorescently-labelled fibronectin does not exocytose from lysosomes, from which integrins are actively recycling.

It is possible that the retromer complex may be involved in the return of late endosomal/lysosomal fraction of $\alpha 5\beta 1$ to the cell surface. The cytoplasmic domain of the cation-independent mannose 6-phosphate receptor (CI-MPR) has been shown to interact with a subunit of the endosomally-resident heteropentameric retromer complex. The retromer complex forms tubular-vesicular extensions along the endocytic pathway, into which the CI-MPR can be sequestered and in that way rescued from lysosomal degradation and delivered to the Trans Golgi Network (TGN) for further sorting and the return to the cell surface (Arighi, Hartnell et al. 2004). However, upon photoactivation, $\alpha 5\beta 1$ seems to travel directly from late endosomes/lysosomes to the plasma membrane, without passing through other subcellular domains, such as the TGN. It is therefore unlikely that it follows the same route to the cell surface as does the CI-MPR. Nonetheless, this does not necessarily exclude the involvement of a retromer-like complex in the transport of lysosomally-targeted $\alpha 5\beta 1$ to the plasma membrane. Retromer has been implicated in transcytosis of polymeric immunoglobulin receptor (pIgR) and its cargo, a process of transporting endocytosed material from apical to basolateral surface of epithelial cells (Verges, Luton et al. 2004), which does not proceed via the TGN, but involves tubular endosomes (Bonifacino and Hurley 2008). I have often observed CLIC3 to be present in tubular membraneous structures that protrude from late endosomes/lysosomes and which could be analogous to endosomal tubes formed by the action of the retromer. Further investigation will be required to establish whether a retromer-like complex is involved in the transport of integrins between components of the endocytic pathway and the plasma membrane.

As it was mentioned in more detail in the introduction to this chapter, CLICs have been named for their ability to transport chloride ions across lipid membranes (Littler, Harrop et al.). They are thought to contribute to the acidification of subcellular compartments by short-circuiting the electrogenic gradients generated by the vacuolar type proton pump (Edwards, Cohen et al.

2006). I therefore considered the possibility that CLIC3 may be regulating intracellular membrane dynamics and trafficking events by affecting the pH of the lysosomal compartment in which it resides. However, I did not detect alterations in the pH of the lysosomal niche following CLIC3 overexpression (Fig. 4.24A) or suppression (Fig. 4.24B). This suggested that even though CLIC3 might be contributing to small local pH changes within endosomal subdomains, it does not control the acidification of the lysosomal compartment as such and further investigations will be required to determine biochemical processes that underlie CLIC3-mediated membrane dynamics regulation.

Furthermore, a more detailed investigation of the relation between $\alpha 5\beta 1$ /CLIC3 and Rab27 and its effector, SLP1 (which was identified alongside CLIC3 to be upregulated by Rab25 and CDM) might shed some light onto the mechanism by which $\alpha 5\beta 1$ recycles from late endosomes/lysosomes. Other CLIC family members have been reported to act as scaffolds and it is possible that CLIC3 also acts to recruit the recycling machinery to integrin-containing lysosomes. Indeed, preliminary experiments indicate a relationship between CLIC3 and Rab27, which is a constituent of membrane trafficking machinery and is known to regulate exocytosis of secretory lysosomes (Izumi, Gomi et al. 2003).

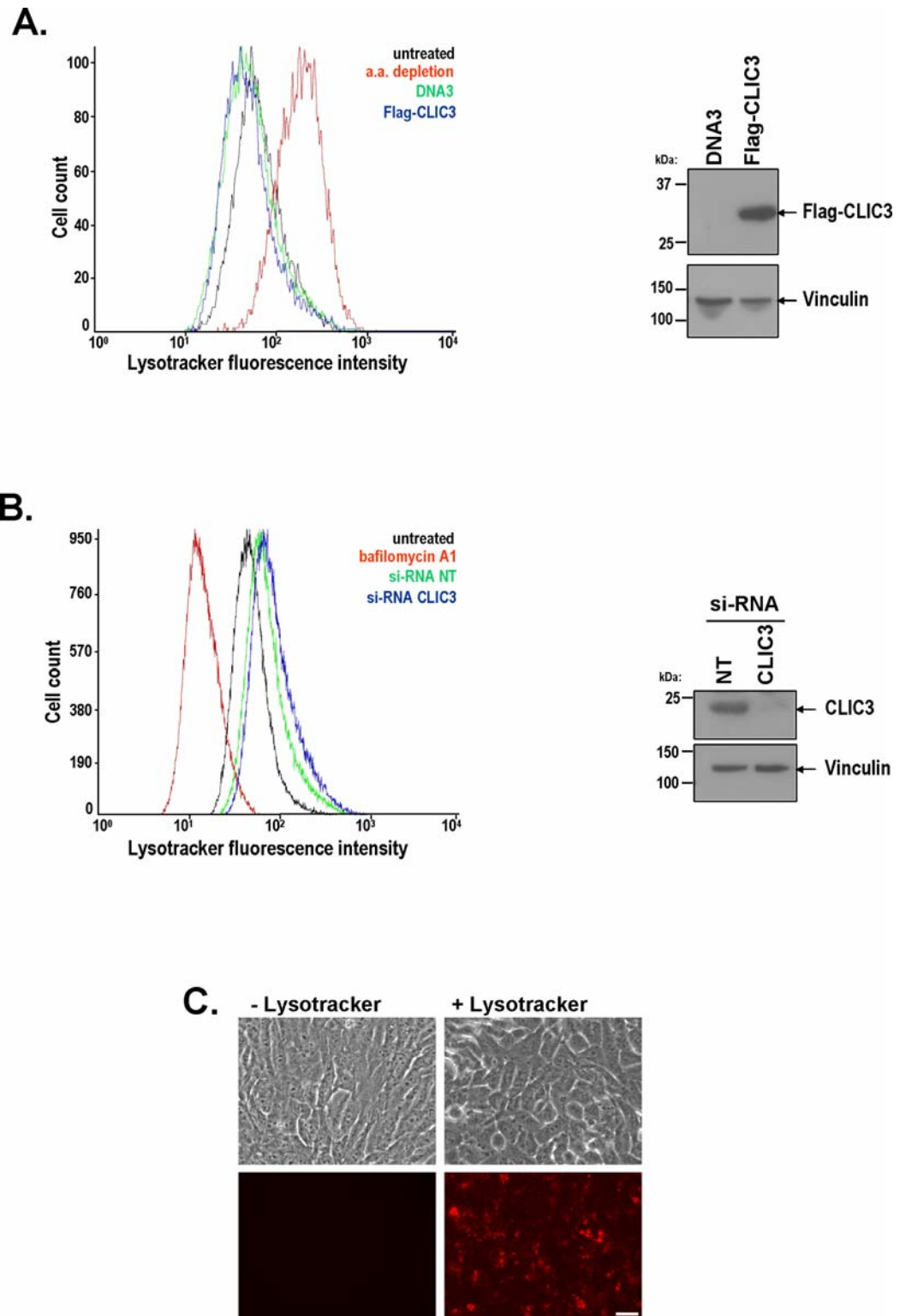


Figure 4-24 CLIC3 does not affect lysosomal pH.

A2780-Rab25 cells were transfected with 3 μ g of an empty vector (DNA3, green) or 3 μ g of Flag-tagged CLIC3 (Flag-CLIC3, blue) and overexpression was assessed by immunoblotting. Untreated cells were either left untreated (black) or subjected to autophagy-inducing amino acid withdrawal (red) for 3 hours (A). Alternatively, non-targetting siRNA (siRNA-NT, green) or siRNA targeting CLIC3 (siRNA-CLIC3, blue) was introduced and CLIC3 suppression was analysed by immunoblotting. Untreated cells were either treated with 0.001% DMSO (untreated, black) or challenged with 100nM bafilomycin A1 (red), to oppose acidification of lysosomes (B). Cells were allowed to take up acidotropic agent; Lysotracker-Red (100nM) for 20 minutes, the uptake was confirmed by fluorescence microscopy, scale bar, 50 μ m (C) and cells were then trypsinised and analysed by Fluorescence Assisted Cell Sorting (FACS). Representative histograms show the distribution of fluorescence for each cell population obtained after lysotracker staining.

A further interesting aspect of my work is that $\alpha 5\beta 1$ returns to the cell surface from the late endosomal/lysosomal compartment in its active conformation, and it would be interesting to speculate how this may occur. Although it appears that fibronectin and the integrin dissociate prior to the return of the receptor to the cell surface, the experiments with paGFP-CA $\alpha 5$ indicate that return to an inactive conformation is not a prerequisite for $\alpha 5\beta 1$ recycling. How does the integrin maintain its active conformation in the absence of its ligand? It is possible that the association of the β integrin cytoplasmic tail with talin and/or kindlin persists upon the internalisation of the receptor and is sufficient to maintain its active conformation, even following disengagement of fibronectin (Moser, Legate et al. 2009). It is also conceivable that lysosomal targeting of active integrins would perturb their interaction with hypothetical and yet unidentified integrin deactivators, thus locking them in an active state. More experimental work will be needed to determine how integrins maintain their active conformation when recycling to the cell surface from the late endosomal/lysosomal compartment.

5 CLIC3 drives tumour progression *in vivo* and is an independent prognostic factor in PDAC

5.1 Introduction

5.1.1 CLICs in cancer

There have been a number of reports connecting CLIC family members, in particular CLIC1, to carcinomas *in vivo* and indicating their potential suitability to serve as cancer biomarkers. In a proteomic study performed on 56 patients, CLIC1 has been identified to be upregulated by 1.95 fold in 67.9% of gastric cancers when compared to matched non-cancerous adjacent mucosa. Increased expression of CLIC1 correlated with lymph node metastasis, perineural invasion and tumour staging as well as with lower 5-year survival (Chen, Wang et al. 2007). A small study of 6 colorectal cancer patients confirmed tumour-associated upregulation of CLIC1 when cancerous tissue was compared to its healthy neighbouring counterpart (Petrova, Asif et al. 2008). The above observations can influence the management of the disease and can be informative in terms of patients' prognosis, but do not offer the advantage of early disease detection and prompt medical intervention. From the early diagnostic point of view, it is more imperative to identify novel plasma tumour biomarkers, which offer the opportunity of early stage disease detection through a simple blood test, in contrast to tissue biomarkers, which can be assayed following a biopsy or surgical resection and therefore do not bear such a high diagnostic potential. The release of cancer specific proteins during the disease progression into the tumour microenvironment and the bloodstream, such as for example secretion of the glycoprotein CA-125 by ovarian epithelial cancers, has been successfully used for post-operative monitoring and also partially for cancer screening. Interestingly, CLIC1 has been observed to be secreted by cancer cells and to be detectable in serum and plasma samples of cancer patients. In a study performed by Chang and colleagues this chloride intracellular channel has been indicated to be a potential plasma marker for nasopharyngeal carcinoma (NPC). Three quarters of the analysed NPC samples have shown CLIC1 positivity when assessed by IHC and in line with that the

plasma levels of CLIC1 were significantly higher in NPC patients than in healthy individuals. When CLIC1 plasma concentration cut-off of 2.58 μ g/ml was applied, CLIC1 was capable of discriminating between NPC patients and healthy subjects, thus suggesting it could be applicable for early detection of NPC (Chang, Wu et al. 2009). Also, the analysis of tumour interstitial fluids and normal interstitial fluids identified CLIC1, amongst 25 other likely markers, to be potentially applicable for early serological detection of breast carcinomas (Gromov, Gromova et al.).

Two independent lines of evidence implicate CLIC1 in tumour metastasis. Liu and co-workers have identified CLIC1 as a potential tissue biomarker for lymphatic metastasis of mouse hepatocarcinoma in a study performed on two murine cell lines, Hca-F and Hca-P, both derived from mouse hepatocarcinoma but displaying high (75%) and low (25%) lymphatic metastatic potentials, respectively (Liu, Sun et al. 2008). A similar approach was used by Wand and colleagues to identify the upregulation of CLIC1 in highly metastatic gallbladder carcinoma line GBC-SD when compared to its low metastatic counterpart (Wang, Peng et al. 2009).

In addition to cell biological studies, which suggest that CLIC4 may contribute to signalling in cancer (as outlined in the introduction to chapter 4), CLIC4 has also been correlated with cancer progression *in vivo*. The level of CLIC4 protein is significantly decreased in tumours and its predominantly nuclear localisation in normal tissue is replaced by mostly cytoplasmic abundance in tumours. Interestingly, its expression in normal stromal tissue is low, but elevated in tumour-activated stroma (Suh, Malik et al. 2007). Additionally, immunochemical staining of breast carcinoma myofibroblasts revealed CLIC4 expression, which was absent in normal breast stroma (Ronnov-Jessen, Villadsen et al. 2002).

5.1.2 Ovarian and pancreatic cancer

Ovarian cancer is the fifth most common cancer in women in the UK and the fourth most common cause of cancer-related death. In the last three years, 6850 women have been diagnosed with ovarian cancer annually and 4370 died each year. Worldwide, over 204,000 new cases are diagnosed each year and there is a steep increase in the incidence in women who have been through menopause

with 80% of cases in females age 50 or older. Over the last three decades, ovarian cancer incidence rate has been increasing, peaked in 2001, and is currently 17% higher than it was in 1975. Interestingly, the mortality rate has decreased by approximately 20% from 1975 to 2008. In line with this, the 5 year survival rates have been gradually increasing from 20% in the 1970s to almost 40% in 2006. As with most cancers, the main discriminator of survival is the stage of the disease at diagnosis. Indeed, 5 year survival rates reach 70% when diagnosed early, but drop to 15% when patient presents with distant metastases at diagnosis, which is the case for a third of the ovarian cancer patients. Amongst risk factors predisposing an individual to developing ovarian cancer are mutations in BRCA1, BRCA2 and HNPCC genes, but this group of ovarian cancer patients only constitutes 10% of the cases (Cancer Stats, Cancer Research UK, <http://info.cancerresearchuk.org/cancerstats/index.htm>).

There are four main stages of ovarian cancer: stage I, with the tumour confined to one or both ovaries, stage II, when the tumour extends to other pelvic organs, stage III presents with peritoneal micrometastases beyond the pelvis and/or local lymph node involvement and stage IV is determined by the presence of distant metastases. Early stage ovarian cancer is amenable to non-radical surgical intervention whilst advanced carcinoma requires surgical debulking combined with chemotherapy. Epithelial ovarian cancer comprises a heterogeneous group of tumours according to their histological differentiation. The most prevalent histological subtype, serous, is histologically similar to cancers of fallopian tubes and accounts for approximately 50% of cases. The less common types of ovarian cancer encompass endometrioid (15-20% cases), characterised by the presence of glandular structures and mucinous (10% cases), which are composed of glands and cysts lined by mucin-rich cells as well as even less common clear cell cancers. Generally, the prognosis for patients with the latter three types is much better than for women with serous cancers (Naora 2007). The most prevalent subtype, serous carcinoma is subdivided into low grade (Type I pathway) and high grade (Type II pathway). Low grade serous carcinomas arise from adenofibromas or serous cystadenomas and have frequent mutations in the K-Ras, B-Raf and ErbB2 genes, which are upstream regulators of the mitogen-activated protein kinase (MAPK), whilst lacking p53 mutations. Their progression to invasive carcinomas occurs slowly and in a step-wise

fashion, which entails progression to an atypical proliferative serous tumour (APST), also sometimes referred to as typical serous borderline tumour, then to non-invasive micropapillary serous borderline tumour (MPSC) and then to invasive MPSC. This gradual development determines a better outcome of these tumours than that of high grade cancers. High grade serous carcinomas develop rapidly, making the identification of precursor lesions challenging. These tumours have been thought to originate from the single layer of cells in the surface epithelium or from epithelial inclusions in the ovary, but it has been suggested that a significant proportion of such carcinomas could originate from intraepithelial lesions in the fallopian tube. Approximately 80% of high-grade tumours harbour mutations in p53 and are characterised by high level of chromosomal instability and high proliferative index but lack mutations in the K-Ras, B-Raf and ErbB2 genes (Vang, Shih le et al. 2009).

Pancreatic cancer is the eleventh most common cancer in the UK with 7800 people diagnosed each year and is the fifth most common cause of cancer-related death. The incidence rates increase drastically over the age of 45 and 80% of cases are diagnosed in people aged 60 and over. In 2002 more than 230,000 people were diagnosed worldwide. Interestingly, over the last three decades the incidence in males has decreased, whilst the incidence in females remained unchanged. This is in agreement with the decline in smoking in men, which is thought to account for 20% of pancreatic tumours. The prognosis for pancreatic cancer patients is poor, owing to its mostly late detection and its hardly accessible localisation in the body (Fig. 5.1A). Due to the very poor prognosis the mortality rates closely reflect the incidence rates and unfortunately the mortality trend hasn't improved in the past decades (Fig. 5.1B & C). The one year survival has almost doubled since the 1970s, but still remains low at 16%, with the five year survival being as low as 3% and ten year survival at 2%. Median survival for patients whose disease was detected early enough to qualify them for surgical resection amounts to 11-20 months whilst patients with irresectable, stage III pancreatic carcinoma, whose disease has locally spread show median survival of 6-11 months and those with metastatic disease only survive for 2-6 months (Cancer Stats, Cancer Research UK, <http://info.cancerresearchuk.org/cancerstats/index.htm>).

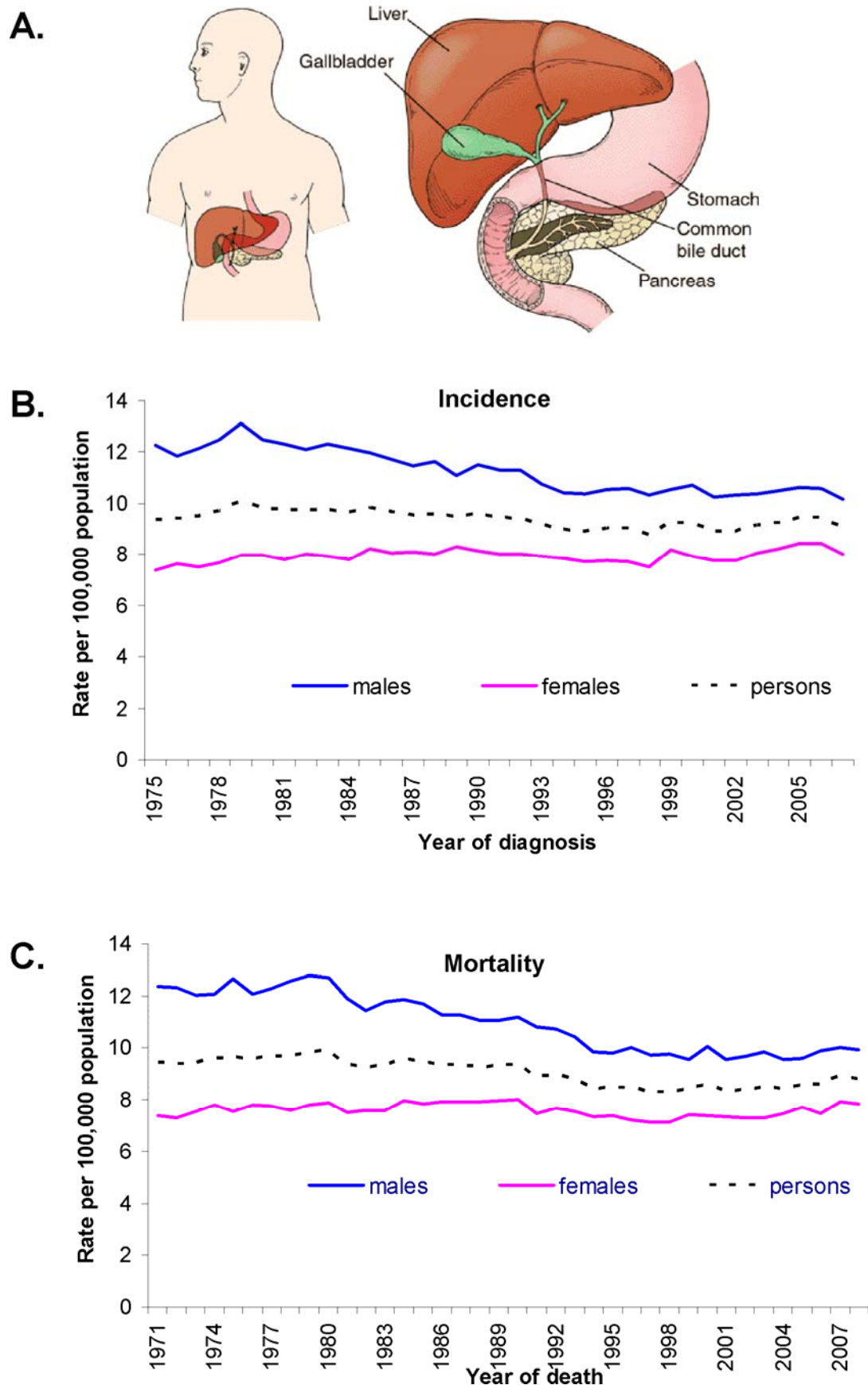


Figure 5-1 Incidence and mortality rates for pancreatic cancer.

Location of pancreas in the human body (<http://faculty.ksu.edu.sa/1877>) (A). Age standardised incidence rates of pancreatic cancer by sex in Great Britain between 1975 and 2007 (Cancer Stats, <http://info.cancerresearchuk.org/cancerstats/index.htm>) (B). Age standardised mortality rates for pancreatic cancer by sex in the UK, 1971-2008 (Cancer Stats, <http://info.cancerresearchuk.org/cancerstats/index.htm>) (C).

The pancreatic parenchyma can be divided into two distinct parts, exocrine tissue, which is composed of ducts and acini, and endocrine portion made of Langerhans islets which harbour hormone-secreting cells. Most commonly pancreatic cancer originates from the exocrine part of the gland through the de-differentiation of the epithelial lining of the duct, and ductal adenocarcinoma accounts for 85% of diagnosed pancreatic cancers (Coppola 2000). Because this disease is almost always diagnosed at an advanced stage it is difficult to identify lesions from which it arises. It is however thought that pancreatic ductal adenocarcinoma arises from precursor lesions called pancreatic intraepithelial neoplasia (PanIN), which harbour similar genetic abnormalities as invasive pancreatic carcinoma. A proposed definition of PanIN describes it as a microscopic papillary or flat non-invasive epithelial neoplasm originating from the pancreatic ducts, usually smaller than 5mm in diameter and composed of cells with varying amounts of mucin and degrees of cytoarchitectural atypia. PanINs are divided into three grades depending on the severity of the epithelial atypia, PanIN 1 (minimal atypia with retained nuclear polarity), which is further subdivided into 1A (flat lesions) and 1B (papillary lesions), PanIN2 (moderate atypia with multitude of nuclear abnormalities) and PanIN3, also designated 'carcinoma in situ' (marked atypia with marked nuclear atypia, loss of nuclear polarity and frequent mitoses). The three step classification system reflects their histological progression to an invasive neoplasia, whereupon the hyperplastic cells breach the basement membrane (Fig. 5.2). PanIN lesions are very common and their incidence increases with age. They not only exist in pancreas affected by invasive carcinoma but are also associated with chronic pancreatitis. Even though PanINs are considered to be precursory to pancreatic ductal adenocarcinoma, the frequency and rate of their conversion into invasive carcinoma has not been determined (Hruban, Maitra et al. 2007; Koorstra, Feldmann et al. 2008)

Pancreatic cancers, similarly to other epithelial cancers, such as those of the ovary, do not arise *de novo* but rather as a consequence of a sequential histological and genetic progression of precursor hyperplasia. Activating mutations on the K-Ras oncogene, particularly in codon 12, are the most common genetic abnormality in pancreatic cancer and occur with a high frequency of approximately 90-95%. They are also thought to be one of the earliest changes to occur in the progressive PanIN cascade, as they have been observed in 36%, 44% and 87% of cancer-related PanIN-1A, PanIN-1B and PanIN-2/3, respectively and therefore to be an initiating event in the formation of carcinoma (Maitra and Hruban 2008). Also, the accumulation of mutations in TP53, MADH4/SMAD4/DPC4 has been implicated in the step-wise progression from PanINs to aggressive ductal carcinoma (Takaori 2007).

It seems that the best strategy to improving pancreatic cancer patients' outcome is the early identification of curable pancreatic neoplasms before they develop into incurable invasive cancer. However, the current imaging technology does not allow detection of these tiny lesions, further underscoring the need for the identification of molecular markers predicting the invasive disease in order to allow early detection in asymptomatic patients who are still amenable to treatment.

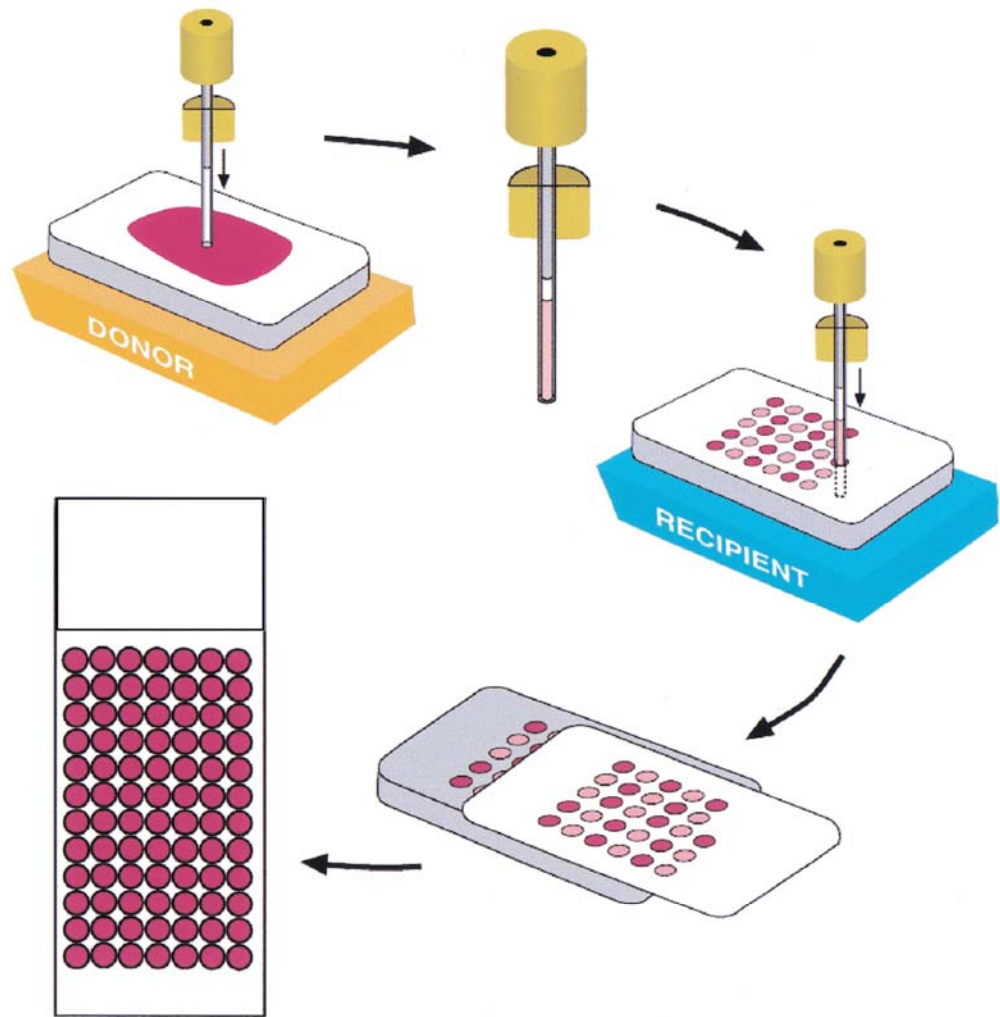
5.1.3 Tissue microarrays

Tissue microarray (TMA) technology was first introduced in 1987 by Wan and colleagues (Wan, Fortuna et al. 1987) and 10 years later further developed into a technique that allowed rapid and reproducible generation of high quality TMA and simultaneous analysis of up to 1000 samples (Kononen, Bubendorf et al. 1998). TMAs are an ordered array of cylindrical tissue cores mounted onto a glass slide, which allow the analysis of protein and gene expression of numerous biomarkers under identical experimental conditions. During TMA generation, a core of tissue (0.6-2mm in diameter) is lifted from a formalin-fixed and paraffin embedded whole section and placed in a pre-prepared hole in a recipient paraffin block. A resulting block can contain a multitude of histospots with known coordinates allowing easy linkage to clinicopathological data and it can be sectioned up to hundreds of times for multiple analyses (Fig. 5.3A & B). TMAs

are ordinarily used for immunohistochemical evaluation of biomarkers in various tumour types and present a number of benefits over standard whole-section studies. Firstly, examination of the tissue section by the pathologist occurs only once and prior to core sampling, ensuring that appropriate and representative areas of the tumour are being arrayed on the recipient paraffin block. Secondly, each histologic section on the TMA uses only a small fraction of the donor tumour block, which can therefore be used for the construction of numerous TMAs. Another advantage of analysing a cohort of tumours on a TMA is the internal consistency of immunohistochemical staining, which occurs under the same conditions and with the same antibody concentration for each core. Moreover, the portability of TMA slides encourages their sharing with other research centres thus allowing multifaceted analysis of the same cohort of tumours. However, in spite of clear benefits, there are also a number of pitfalls associated with the use of TMAs, which are mostly shared with the weaknesses of whole section analysis, such as the dependency on good quality tissue and the availability of suitable antibodies or potentially detrimental effects of tissue oxidation on antigenicity. An additional concern arises when intra-tumour heterogeneity is taken into account. The analysis of a single core might not yield a representative result or allow for the detection of varying levels of biomarker in the different locations within the tumour. To tackle the heterogeneous nature of carcinomas, multiple histospots should be sampled from each tissue in order to improve the significance of the study. One other limitation in the application of TMAs for biomarker validation is the analysis of the TMA, which requires a trained eye to discriminate tumour from stromal tissue and a rigorous linking of the histospot score to the correct coordinate and patient information. Furthermore, the scoring process itself is subjective and semi-quantitative, regardless of whether definite score of 0 to 3 is assigned or whether a continuous value ranging from 0 to 300 is calculated based on the percentage of cells showing different staining intensities. (Rimm, Camp et al. 2001; Camp, Neumeister et al. 2008). Despite their possible limitations, TMAs are widely applied not only to immunohistochemical or immunofluorescent analysis of protein levels or localisation, they can also be employed for *in situ* hybridization, which allows the detection of gene expression or chromosomal abnormalities (Mobasher, Airley et al. 2004). TMAs have the potential to accelerate translational research by serving as a platform for validation of the

involvement of novel genes in tumour progression. Such Progression Model TMAs utilise tumour samples collected during the clinical progression of the disease and allow the assessment of gene expression at various disease stages. Outcome TMAs on the other hand contain tumour samples which are linked to clinicopathological data of the patient that they were derived from thus facilitating the evaluation of the marker as a potential prognostic factor, molecular target or therapeutic response determinant (Henshall 2003).

A.



B.



Figure 5-3 Construction of tissue microarrays (TMAs).

Schematic illustration of TMA generation from donor paraffin embedded tissue sections (Rimm et al. 2001) (A). Example of immunohistochemically-stained TMA (B).

5.2 Results

Thus far, CLIC3 has not been associated with tumour progression or metastasis *in vivo* and has not been suggested as a diagnostic or prognostic marker for any types of carcinoma. Due to my identification of CLIC3 in an ovarian adenocarcinoma cell line, and owing to the contribution of Rab25 to the aggressiveness of ovarian tumours (Cheng, Lahad et al. 2004) I sought to evaluate its involvement in that type of cancer as well as in pancreatic cancer, which shares a number of similarities to its ovarian counterpart.

5.2.1 Generation of a CLIC3 specific antibody

In light of the lack of commercially available CLIC3 specific antibody, I had to generate one myself in order to evaluate the expression of CLIC3 in tumour samples, and its correlation with disease progression and patient survival. As it was mentioned in the introduction to the previous chapter, alignment of the protein sequences and crystal structures for CLIC family members revealed high level of sequence and structural similarity between CLIC3 and CLIC1, CLIC2 and CLIC4 (Fig. 4.1 & 4.2). The high level of sequence conservation makes it difficult to produce antibodies that specifically recognise individual members of the family. I therefore searched for a region that would be divergent in the CLIC3 sequence and identified a 12 amino acid stretch from glutamic acid 147 to glutamic acid 158 (E147-E158) that displayed different properties to the corresponding sequences in the remaining CLICs (Fig. 4.1). Interestingly, a close inspection of overlaid crystal structures revealed that this divergent region in CLIC3 and its counterparts in the other CLICs form a loop that extrudes from the globular domain (Fig. 4.2 & 4.3). The ability of this unique region to form a highly ordered fold on the surface of the molecule suggested its potential high antigenicity and suitability for the generation of a CLIC3-specific antibody. However, the utilisation of that peptide as the antigen failed to yield antibodies which would efficiently recognize CLIC3 (data not shown). Consequently, I attempted antibody generation using a full length CLIC3 protein. To that end I constructed a pGEX-6P-1-CLIC3 vector in which CLIC3 is fused to GST and separated from it by a protease cleavage site (Appendix 4.1C). BL21(DE3)pLysS *E.coli* cells are engineered in such a way that they lack *lon* and *ompT* proteases

that can degrade proteins during the purification process and they also allow a controlled induction of exogenous protein expression with Isopropyl-1-thio- β -D-galactopyranoside (IPTG). I therefore transformed these competent cells with pGEX-6P-1 and grew the bacterial culture in LB medium supplemented with 100 μ g/ml ampicillin. When the density of the culture reached OD₆₀₀ of 0.8, protein expression was induced with 1mM IPTG and expression verified one, two and three hours later. Both soluble and insoluble protein fractions appeared to contain GST-CLIC3, which runs as a 50kDa band on an SDS-PAGE gel. Subsequently, GST-CLIC3 was purified on a GST-resin and collected in three elution fractions (Fig. 5.4A). The three fractions were pooled and the resulting GST-CLIC3 preparation was subjected to PreScission Protease treatment, which removed the GST-tag from the recombinant protein. The CLIC3 protein was then purified in two consecutive affinity purification steps on a GST-resin, whereby GST-tagged protease and GST itself were trapped on the column whilst CLIC3 was collected in the flow-through as the final, near homogenous solution at 1.35mg/ml concentration (Fig. 5.4B). The absence of GST and the presence of pure CLIC3 in the final preparation was confirmed by Western blotting with a GST specific and commercially available CLIC3 specific antibody, respectively (Fig. 5.4C). The CLIC3 protein solution was then dispatched to Eurogentec for the inoculation of two rabbits that were used for the production of antibodies targetting that antigen and the resulting sera were affinity purified on a GST-resin column coupled with GST-CLIC3.

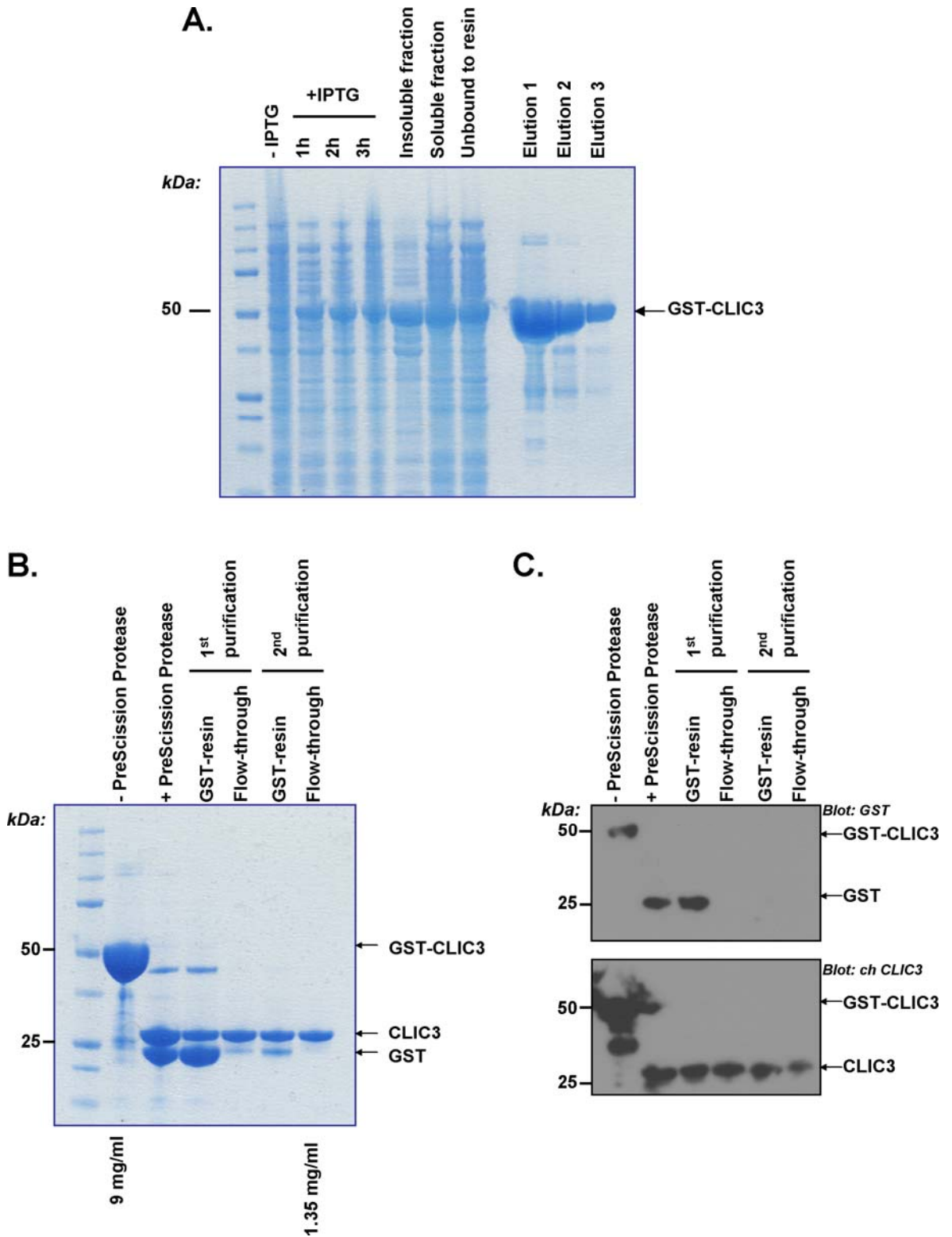


Figure 5-4 Bacterial expression and affinity purification of GST-CLIC3.

Pelleted BL21(DE3)pLysS bacterial cells were resuspended in PBS and resolved by SDS-PAGE and Coomassie stained. Soluble GST-CLIC3 was affinity purified on GST-resin and collected in three elution fractions (A). A Coomassie stain of GST-CLIC3 prior to PreScission protease cleavage and of CLIC3 after digestion and two consecutive purification steps (B). Western Blotting of the same samples as in (B) with a commercially available chicken antibody against CLIC3 and an antibody against GST (C).

5.2.2 CLIC3 antibody specifically recognises CLIC3, but not other members of the CLIC family

To validate the two batches of anti-CLIC3 antibody, each originating from an immunised rabbit, designated 1543 and 1544 respectively, I produced GST-CLIC1, GST-CLIC4 and GST-CLIC3 (Fig. 5.5A & B). 500ng of these preparations along with GST and CLIC3 proteins were analysed by Western blotting with the 1543 antibody batch, at 1:1000, 1:5000, 1:10 000 and 1:20 000 dilutions. The 1543 antibody showed very high affinity for both recombinant GST-CLIC3 and CLIC3, but also bound to GST and GST-CLIC1 and GST-CLIC4 (Fig. 5.6A). When the same antibody dilutions were tested on lysates derived from A2780-DNA3 and A2780-Rab25 cells, which were confirmed to either lack or express CLIC3 by immunoblotting with a commercial chicken anti-CLIC3 antibody (Fig. 5.6C), and failed to recognise CLIC3 (Fig. 5.6B). 1544 antibody batch was then tested in the same manner and revealed high affinity for both GST-CLIC3 and CLIC3, whilst showing no binding to either GST-CLIC1, GST-CLIC4 or GST (Fig. 5.7A). Importantly, when applied at 1:5000 dilution, 1544 antibody specifically recognised a band of approximately 27kDa in A2780-Rab25 cell lysates, which was absent in A2780-DNA3 lysates (Fig. 5.7B).

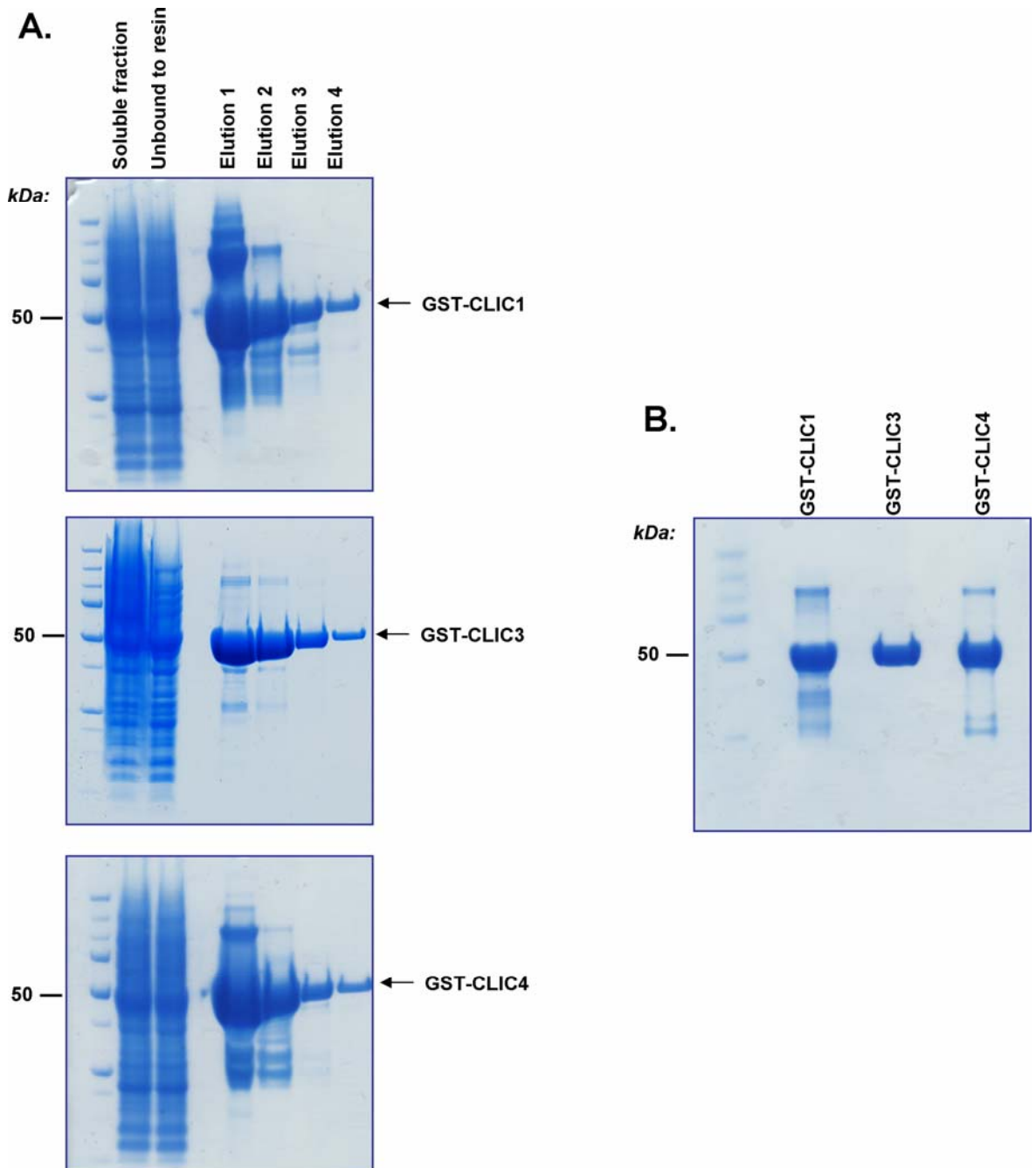


Figure 5-5 Bacterial expression of GST-CLIC3, GST-CLIC1 and CLIC4 for antibody purification and validation.

BL21(DE3)pLysS bacterial culture, transformed with pGEX-6P-1-CLIC3, pGEX-2T-CLIC1 and pGEX-2T-CLIC4 respectively was grown in LB medium with 100 μ g/ml ampicillin. At $OD_{600} = 0.8$ protein expression was induced with 1mM IPTG. At 4 hours cells were pelleted, resuspended in PBS, resolved by SDS-PAGE and Coomassie stained. Soluble GST-CLICs were captured on GST-resin, eluted in four steps (A), elution fractions were pooled and subjected to a subsequent affinity purification step, which led to the production of highly homogenous GST-CLIC1, GST-CLIC3 and GST-CLIC4 protein solutions (B).

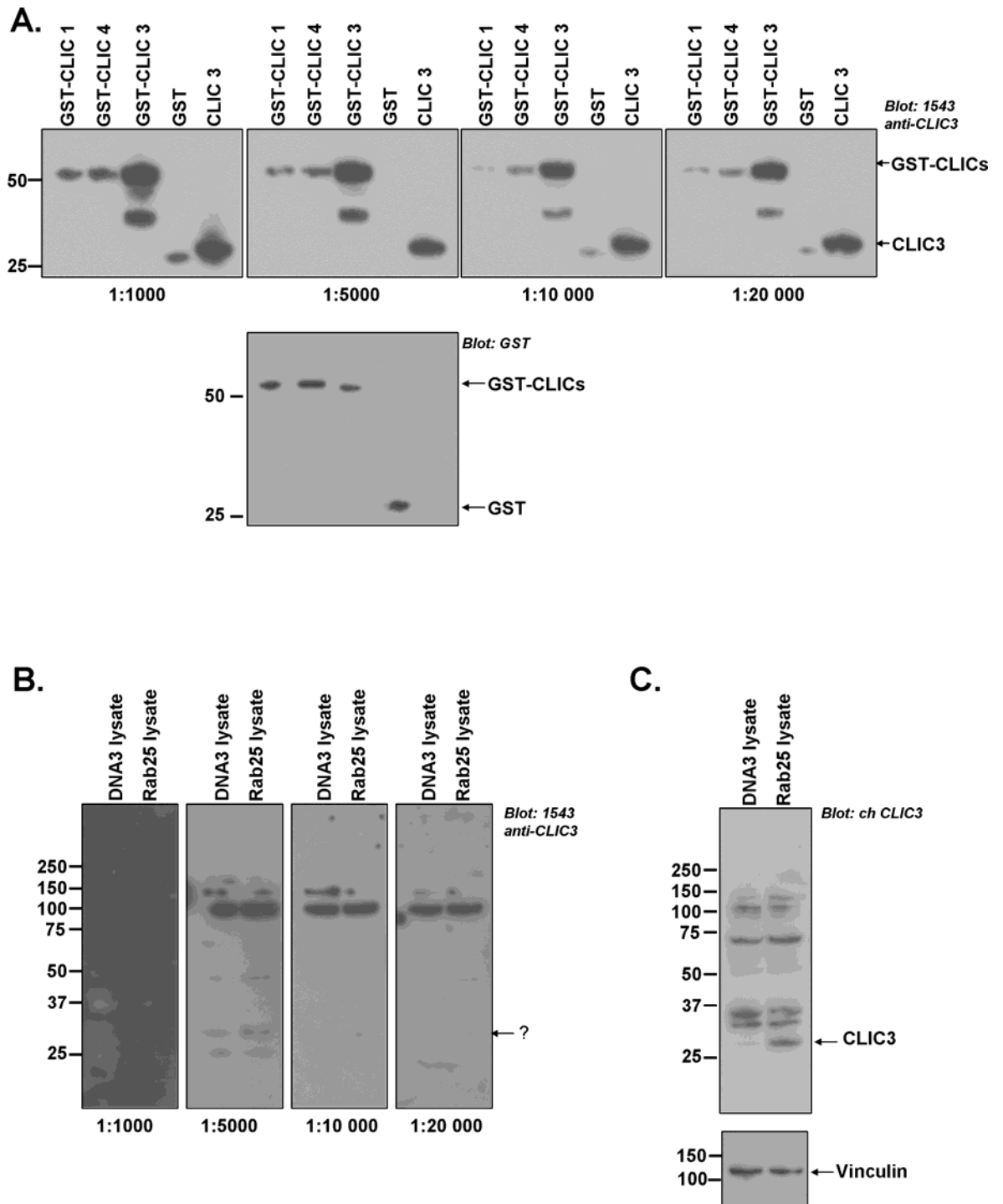


Figure 5-6 Validation of the antibody from 1543 serum.

500ng of recombinant GST-CLIC1, GST-CLIC4, GST-CLIC3, GST and CLIC3 were subjected to Western blotting and probed with 1543 anti-CLIC3 antibody at the indicated antibody dilutions. Protein loading was confirmed by probing with GST-HRP antibody at 1:5000 dilution (A). 40 μ g of A2780-DNA3 and A2780-Rab25 cell lysates were analysed by Western Blotting with the 1543 anti-CLIC3 antibody at the same dilutions as for the recombinant proteins. Equal lysate loading verified by probing for Vinculin (B). The same lysates were subjected to Western blotting with commercial chicken anti-CLIC3 antibody at 1:2500 dilution (C).

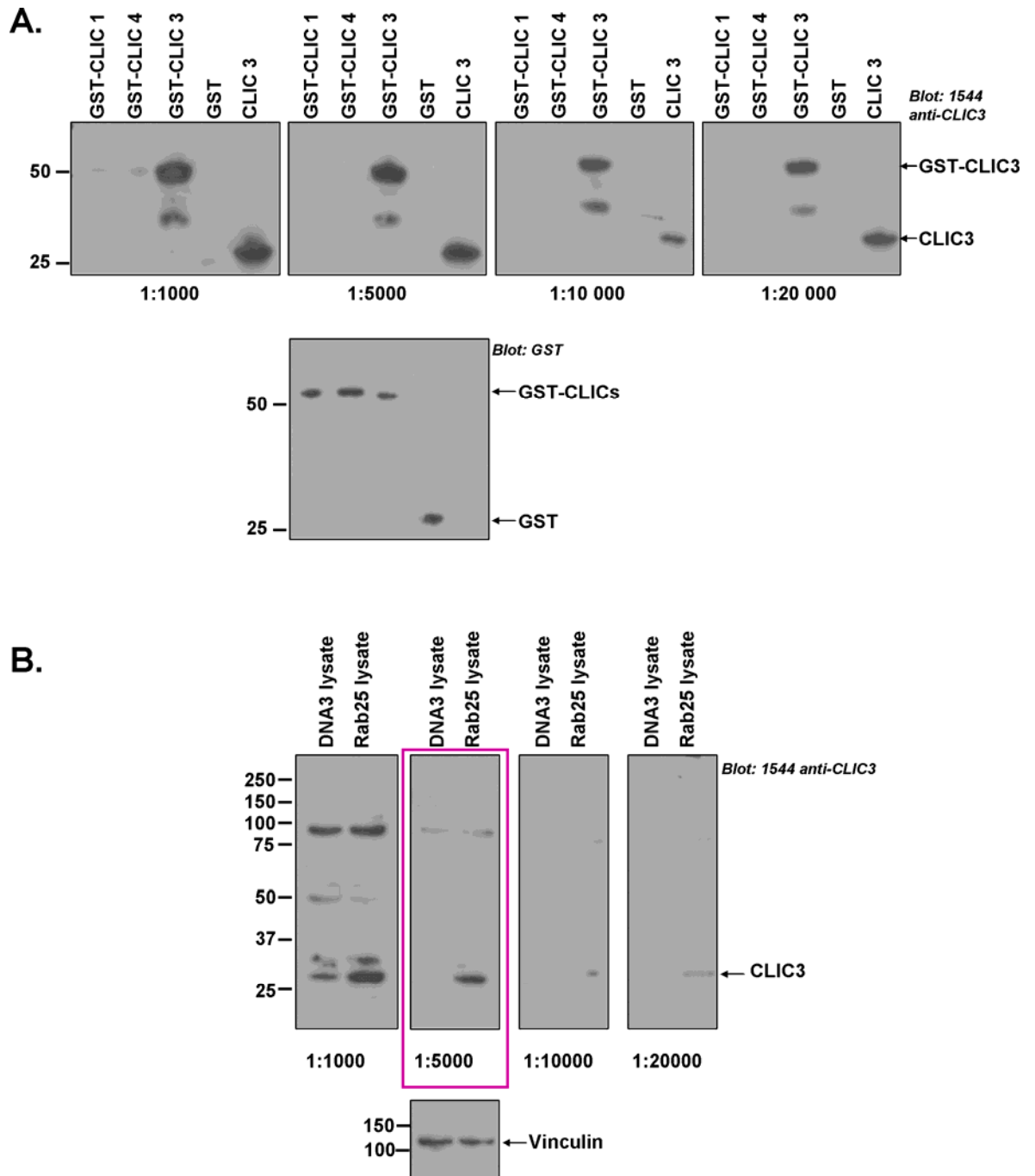


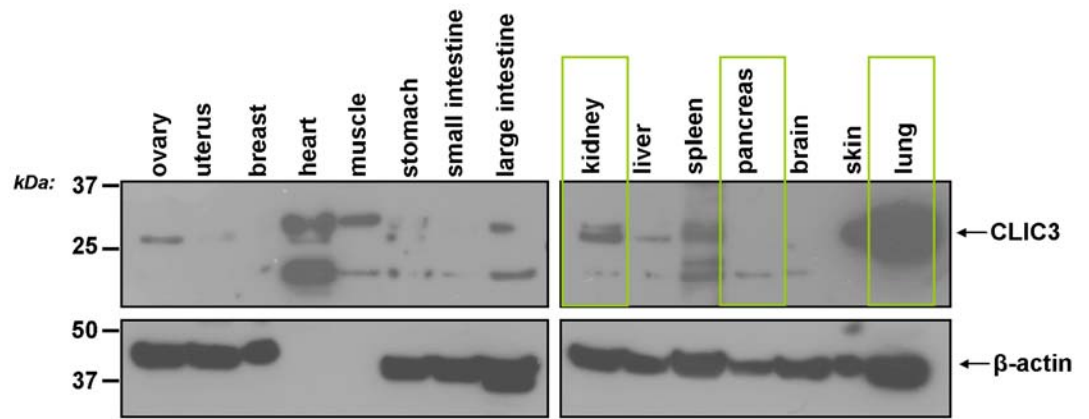
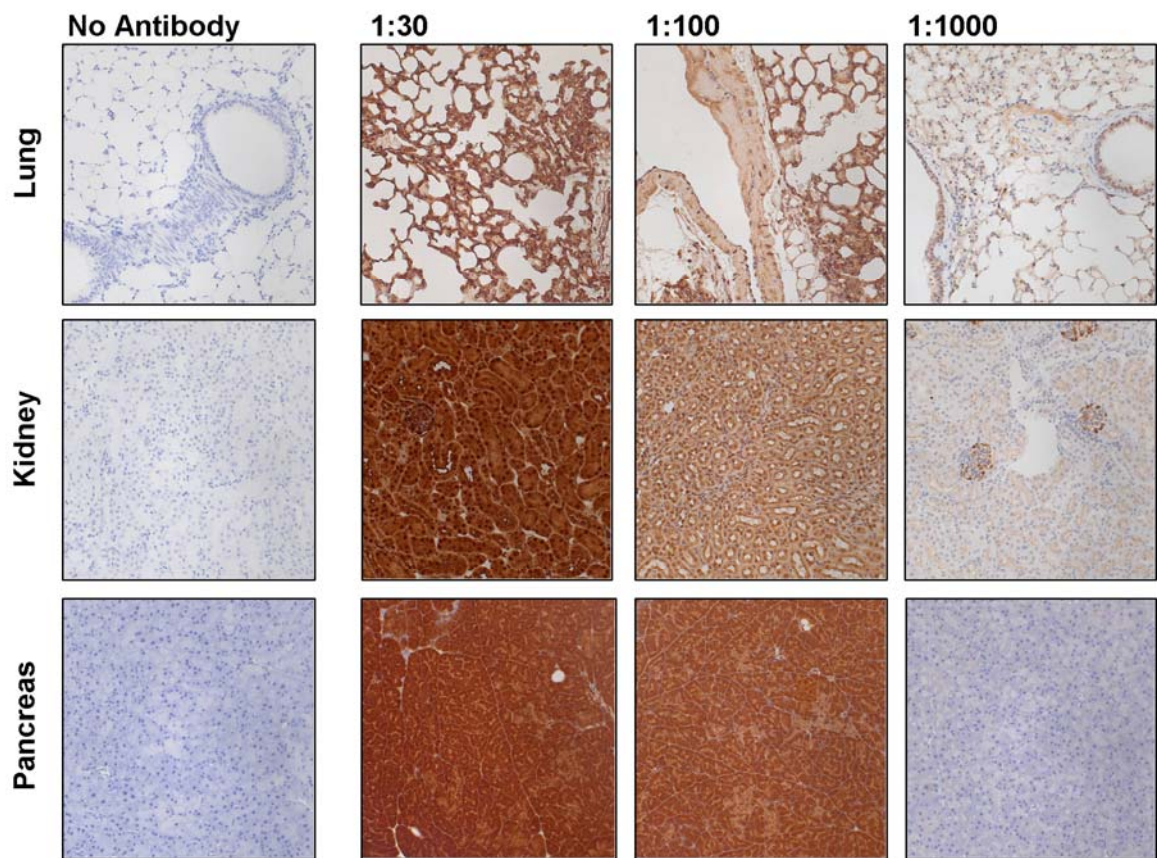
Figure 5-7 Antibody from 1544 serum specifically recognises CLIC.
The same protein preparations and antibody dilutions were used as in Fig. 5.6.

5.2.3 Optimisation of the antibody for immunohistochemistry

To identify the most suitable conditions for performing immunohistochemical staining with the 1544 CLIC3-specific antibody in tissue samples, I performed a number of optimisation steps on mouse tissue, which is more readily available than human specimens. Firstly, I used Western blotting to confirm that the 1544 antibody was able to recognise the mouse CLIC3 protein and this was possible due to very high degree of sequence homology between the human and murine CLIC3 protein. To that end, I harvested various tissue from 3 month old FVB female mice. Mouse tissue samples were then either fixed in 10% Neutral Buffered Formalin (NBF) and paraffin embedded, or homogenised and subjected to Western blotting with the CLIC3 antibody at 1:5000 dilution. This allowed me to identify three tissues: pancreas, kidney and lung, which respectively exhibited low, moderate and high CLIC3 protein abundance, and which I subsequently utilised to determine antibody dilution and antigen retrieval method to be used for IHC (Fig. 5.8A). Antigen retrieval is required to expose epitopes that have been masked by the tissue fixation process. Most commonly, heat induced epitope retrieval (HIER) in combination with a buffer of choice is successfully used to break protein cross-links on formalin fixed and paraffin embedded tissue. A trial IHC was performed in 10mM Na citrate buffer (pH6), with the omission of primary antibody or with the antibody at 1:30, 1:100 and 1:1000. The lowest antibody concentration revealed CLIC3 expression pattern in fixed tissue similar to that observed by Western blotting (Fig. 5.8B). When the antigen retrieval step was omitted (Fig. 5.9A) or when Proteinase K (Fig. 5.9B) was applied to induce enzymatic epitope recovery, no CLIC3 staining was observed. I then exploited another antigen retrieval agent, namely ethylenediaminetetraacetic acid (EDTA) buffer (pH8) and found that it enhanced the CLIC3 epitope exposure more efficiently than did citrate buffer, even at dilutions as high as 1:2000. Importantly, CLIC3 IHC performed under these conditions yielded expression patterns largely comparable to that seen by Western blotting; i.e. lung exhibited very high CLIC3 abundance, kidney displayed some CLIC3-positivity, while pancreas lacked expression (Fig. 5.10). CLIC3 IHC on human placental tissue confirmed the unsuitability of Proteinase K retrieval method and validated efficient epitope recovery with both citrate and

EDTA buffers, with the latter in combination with 1:500 antibody dilution being the most optimal condition (Fig. 5.11A).

I had previously established that the 1544 CLIC3 antibody recognises CLIC3 by Western blotting and shows no affinity for its near homologues, CLIC1 or CLIC4. To be certain that the staining pattern obtained in human tissue was specific to CLIC3, I performed preabsorption experiments. Prior to probing the tissue with CLIC3 antibody, I pre-incubated the latter with 5-fold excess of recombinant CLIC3, CLIC1 or CLIC4. Whereas pre-incubation of the antibody with either CLIC1 or CLIC4 did not reduce the intensity of immunostaining, the signal was lost when the antibody was preabsorbed with CLIC3, thus confirming the specificity of the antibody for that family member only (Fig. 5.11B). To gain further support for the specificity of CLIC3 antibody and its suitability for tumour tissue analysis, I decided to stain sections from a range of tumours and to compare the staining intensity obtained with the antibody with the tumour's CLIC3 mRNA content, as determined by qPCR analysis of matching RNA and tissue block samples. I selected four pancreatic ductal adenocarcinomas (PDAC), designated 112T, 110T, 11PD and 21PD, which had previously been determined in an independent microarray screen, to have low and high CLIC3 expression, respectively (data not shown, Nigel Jamieson). Using qPCR I confirmed very low CLIC3 transcript levels in the 112T and 110T patients, and high CLIC3 mRNA abundance in the 11PD and 21PD samples (Fig. 5.12A). CLIC3 IHC performed on matching tumour sections confirmed very low CLIC3 protein abundance in 112T and 110T tumours and very high and high expression in 11PD and 21PD patients, respectively, thus further substantiating the specificity of the antibody (Fig. 5.12B). This correlation between the mRNA levels and tissue content of CLIC3 lent further support to the antibody-specificity studies presented earlier in this section.

A.**B.***Citrate Buffer pH 6***Figure 5-8 Trial CLIC3 immunohistochemistry (IHC) on mouse tissue.**

40 μ g of protein homogenates were subjected to Western blotting with anti-CLIC3 antibody at 1:5000 dilution. Protein loading was verified by probing with anti β -actin antibody, 1:10 000 (A). CLIC3 IHC was performed on mouse lung, kidney and pancreas tissue, in 10mM Na Citrate buffer (pH6) with the omission of primary antibody (no antibody) as well as with the antibody at 1:30, 1:100 and 1:1000 dilutions (B).

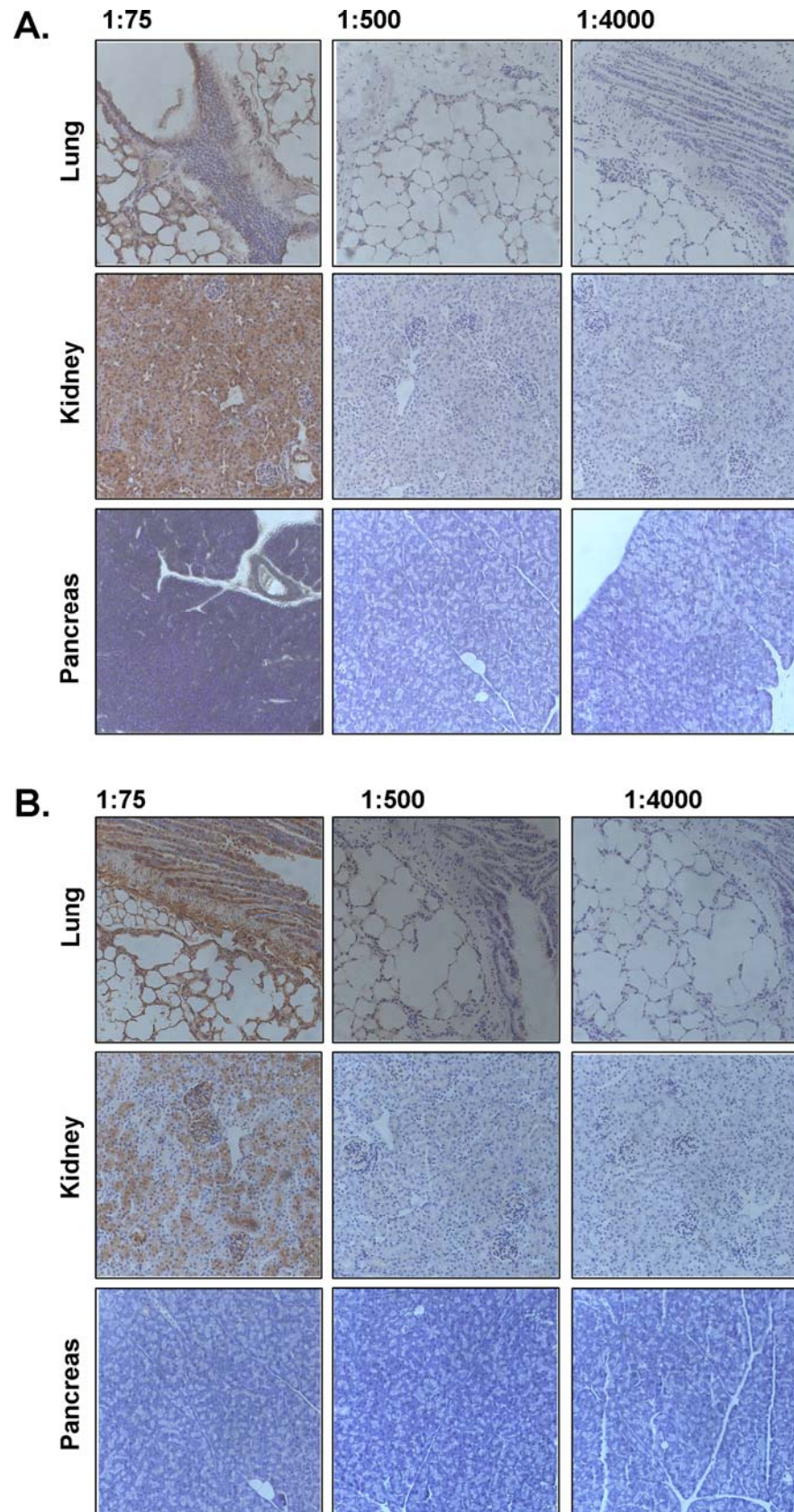


Figure 5-9 CLIC3 IHC with no antigen retrieval and with Proteinase K retrieval on mouse tissue.

Mouse tissue was fixed in 10% Neutral Buffered Formalin (NBF), paraffin embedded and processed as per IHC protocol, with the omission of antigen retrieval step (A) or antigen retrieval was performed with Proteinase K (B). The CLIC3 antibody was used at 1:75, 1:500 and 1:4000 dilutions on mouse lung, kidney and pancreas tissue.

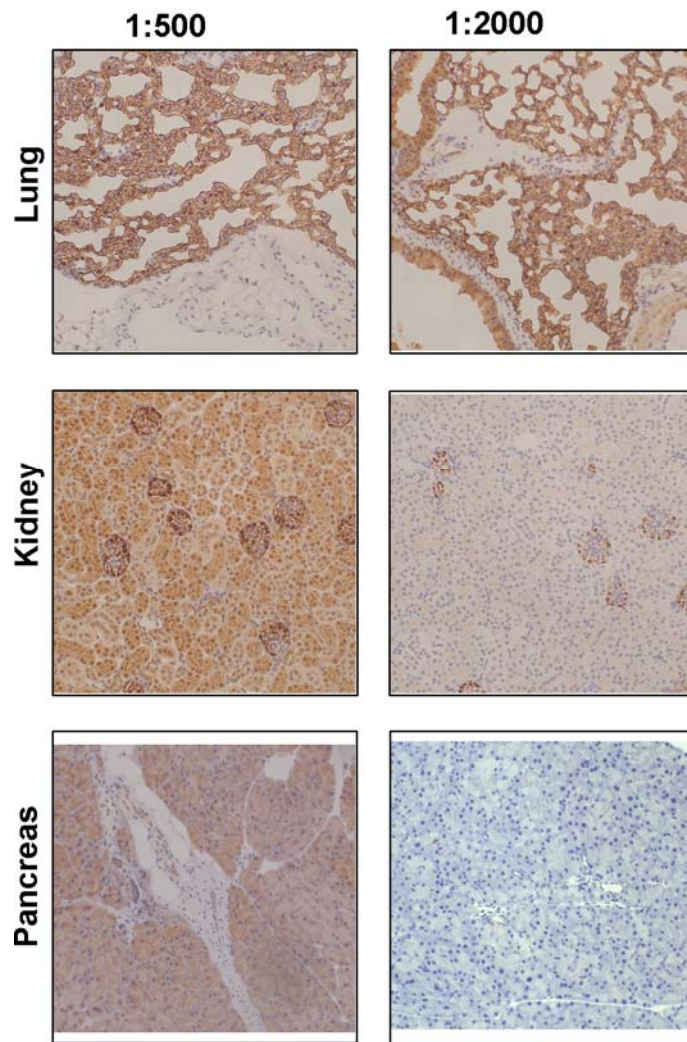
EDTA buffer pH8

Figure 5-10 CLIC3 IHC on mouse tissue using EDTA buffer (pH8).

Heat-induced epitope retrieval in conjunction with EDTA buffer (pH8) was used to expose the antigen. The CLIC3 antibody was used at 1:500 and 1:2000 dilutions on mouse lung, kidney and pancreas tissue.

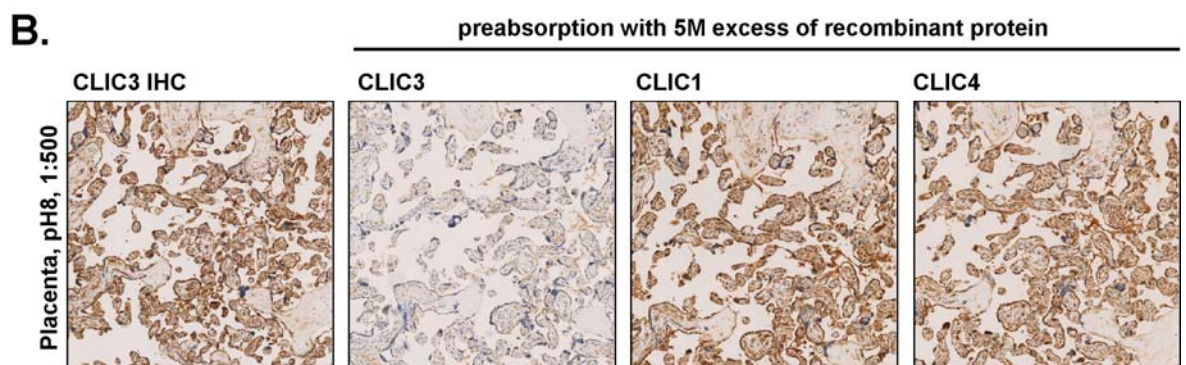
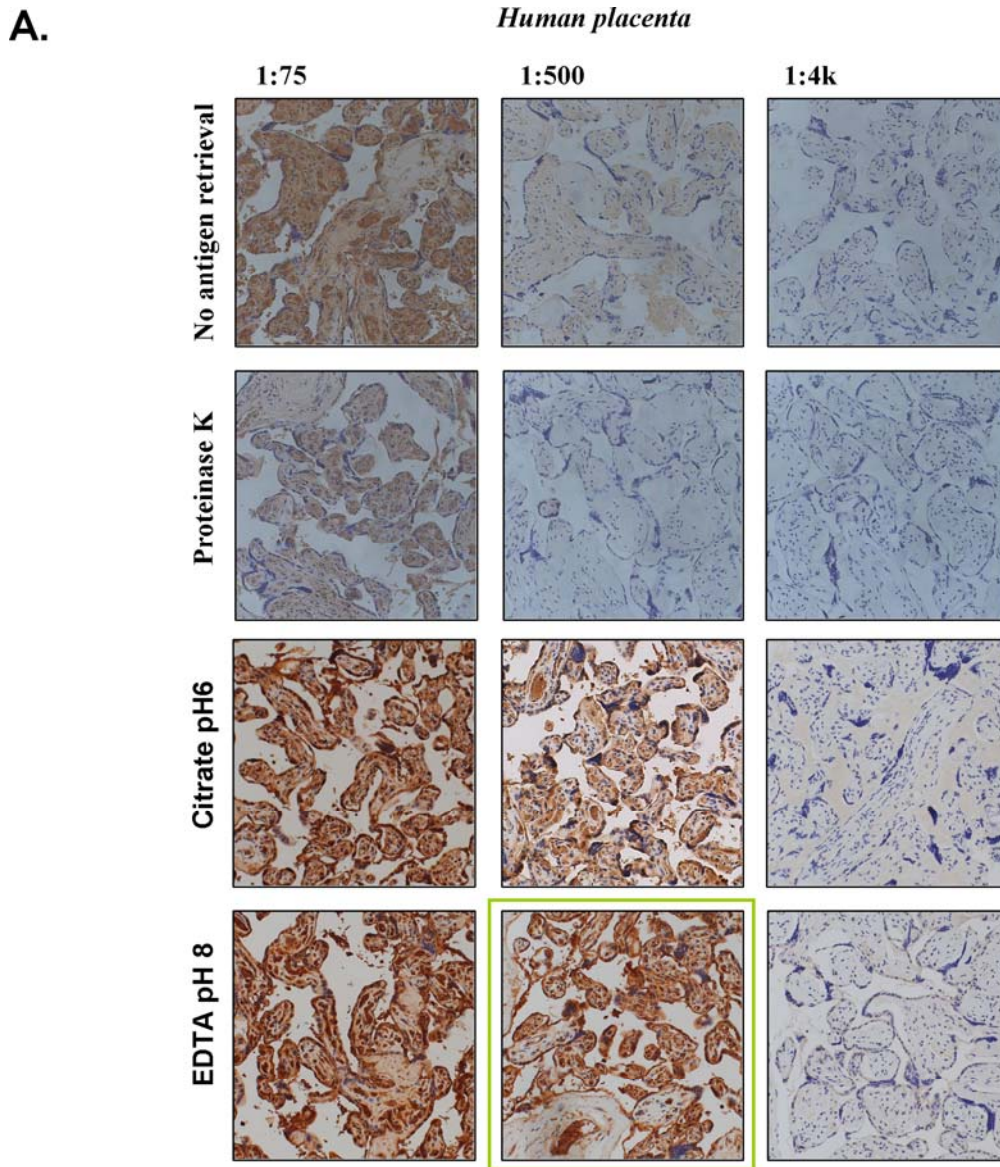


Figure 5-11 CLIC3 IHC on human placenta.

No retrieval, Proteinase K, Citrate buffer (pH6) or EDTA buffer (pH8) were used respectively to reveal the antigen. CLIC3 antibody was applied at 1:75, 1:500 and 1:4000 dilutions (A). Antigen retrieval was performed with EDTA buffer (pH8). Prior to probing the tissue with the antibody, the antibody was pre-incubated with 5M excess of recombinant GST-CLIC3, GST-CLIC1 and GST-CLIC4, respectively. The antibody-protein complex was used instead of the neat antibody at 1:500 dilution (B).

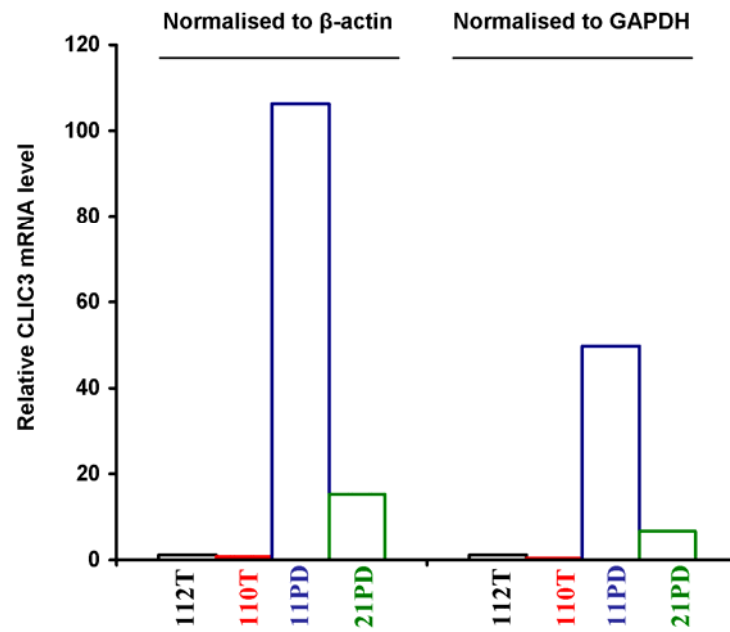
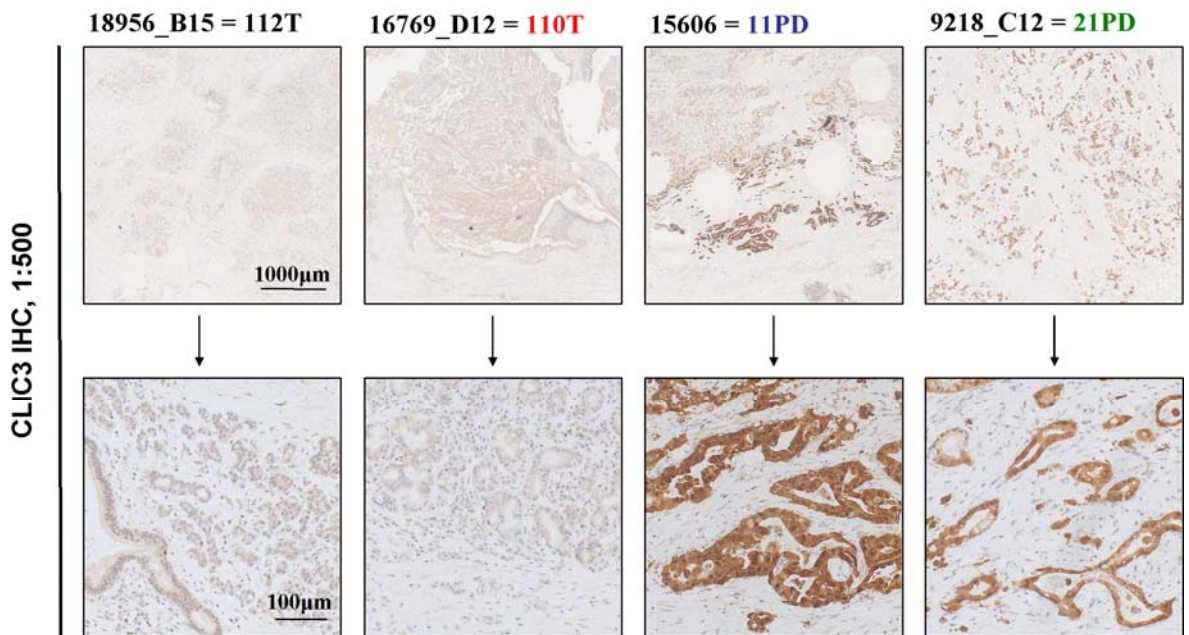
A.**B.**

Figure 5-12 CLIC3 mRNA and protein in matching pancreatic tumour samples.

Relative CLIC3 mRNA expression was validated by qPCR for two low CLIC3 expressors; patients 112T (black) and 110T (red), and two high expressors, patients 11PD (blue) and 21PD (green) and was normalised to either β -actin or GAPDH (A). Tissue blocks corresponding to the RNA samples from (A) were subjected to CLIC3 IHC, where the antibody was used at 1:500 dilution. In the top panel a lower and in the bottom a higher magnification of the tissue sections are shown (B).

5.2.4 CLIC3 expression in ovarian carcinomas

Prior to determining the relevance of CLIC3 in ovarian cancer progression I endeavoured to confirm the suitability of the antibody for TMA staining. It is not uncommon for the antibody concentration and antigen retrieval method to require adjustment when minute tissue cores are being immunohistochemically stained instead of whole tissue sections which had thus far been used. Therefore, I performed CLIC3 IHC on a trial TMA containing 5 tumour tissue cores, using two antigen retrieval methods, citrate pH6 and EDTA pH8, as well as two antibody dilutions, 1:500 and 1:750 (Fig. 5.13). Epitope recovery with EDTA and antibody dilution 1:500 appeared to have been unaffected by the transition from whole tissue sections to TMA cores and were therefore utilised for CLIC3 immunohistochemistry on a TMA containing 472 cases of ovarian carcinoma.

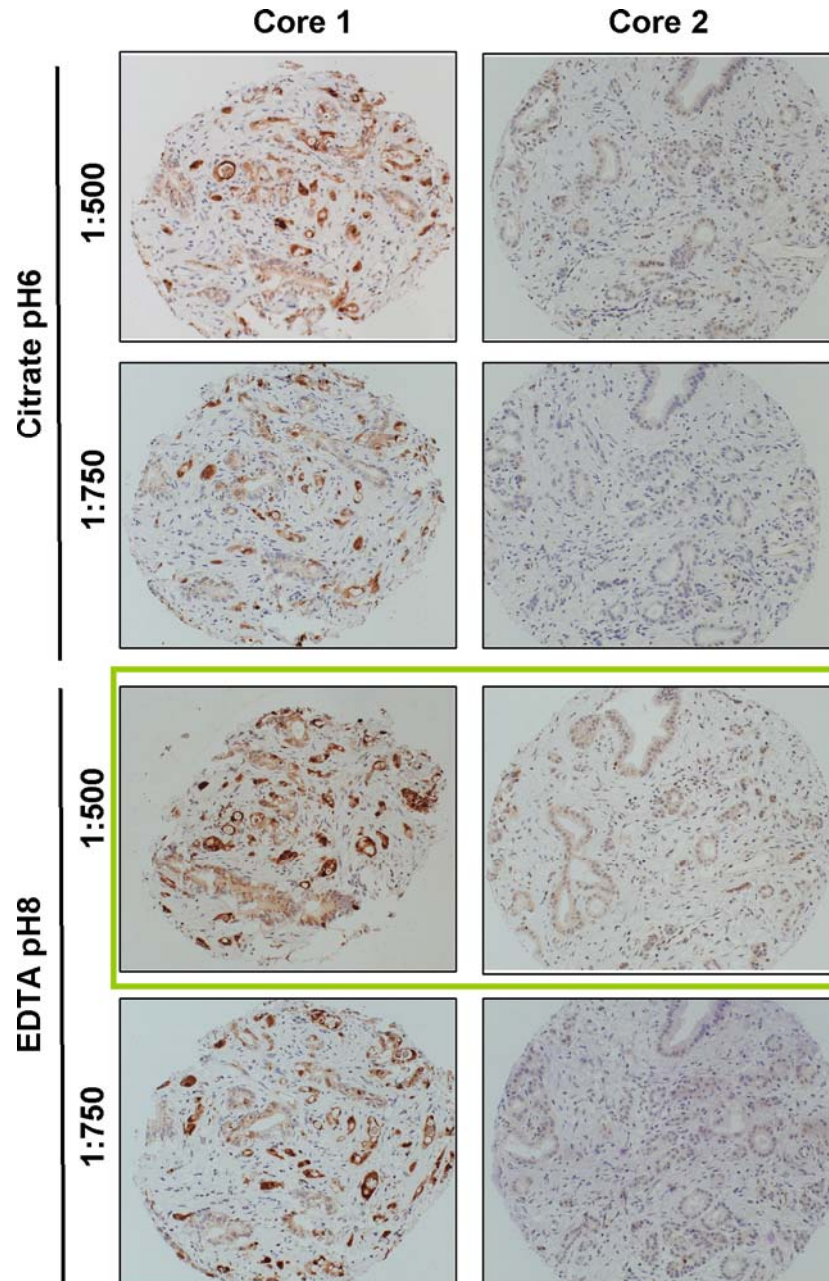


Figure 5-13 CLIC3 IHC on a practice TMA.

CLIC3 IHC was performed on a pancreatic practice TMA containing 5 cores. Antigen retrieval carried out with Citrate pH6 or EDTA pH8 buffers and CLIC3 antibody was used at 1:500 or 1:750 dilutions. Two randomly selected cores are shown and the green box is drawn around the most optimal immunohistochemical staining method.

CLIC3 was mostly observed as multiple puncta in the cytoplasm of the tumour cells, but was also evident in the nucleus, especially when CLIC3 expression was high (Fig. 5.14A). To obtain a quantitative index of CLIC3 abundance a scoring guide was devised, which aided in the determination of staining intensity throughout the TMA. A four-step score was used, where 0 corresponded to no expression, 1 to low expression, 2 to medium and 3 to high (Fig. 5.14B). Due to observed intra-tumour heterogeneity of CLIC3 abundance, a histoscore was calculated for each core. The histoscore was designed to reflect the percentage of tumour cells within the core which fell into each staining category, thus generating a continuous score ranging from 0 to 300. Even though most tumour cores displayed some CLIC3 positivity, in most cases the abundance was low and no correlation between CLIC3 expression and survival was detected, regardless of whether all ovarian tumour types were considered cooperatively or whether they were split into individual subtypes (data not shown). However, a connection between CLIC3 and tumour invasion was established by categorising ovarian tumours into Type I (which encompass low grade serous, endometrioid, clear cell and mucinous carcinomas), or Type II (comprising high grade serous tumours that are more aggressive and more likely to progress to metastatic disease). CLIC3 protein levels, as indicated by the histoscore, were significantly higher in Type II than in Type I ovarian tumours (Fig. 5.14C), thus lending support to the proposal that this chloride intracellular channel could contribute to tumour aggressiveness and invasion *in vivo*.

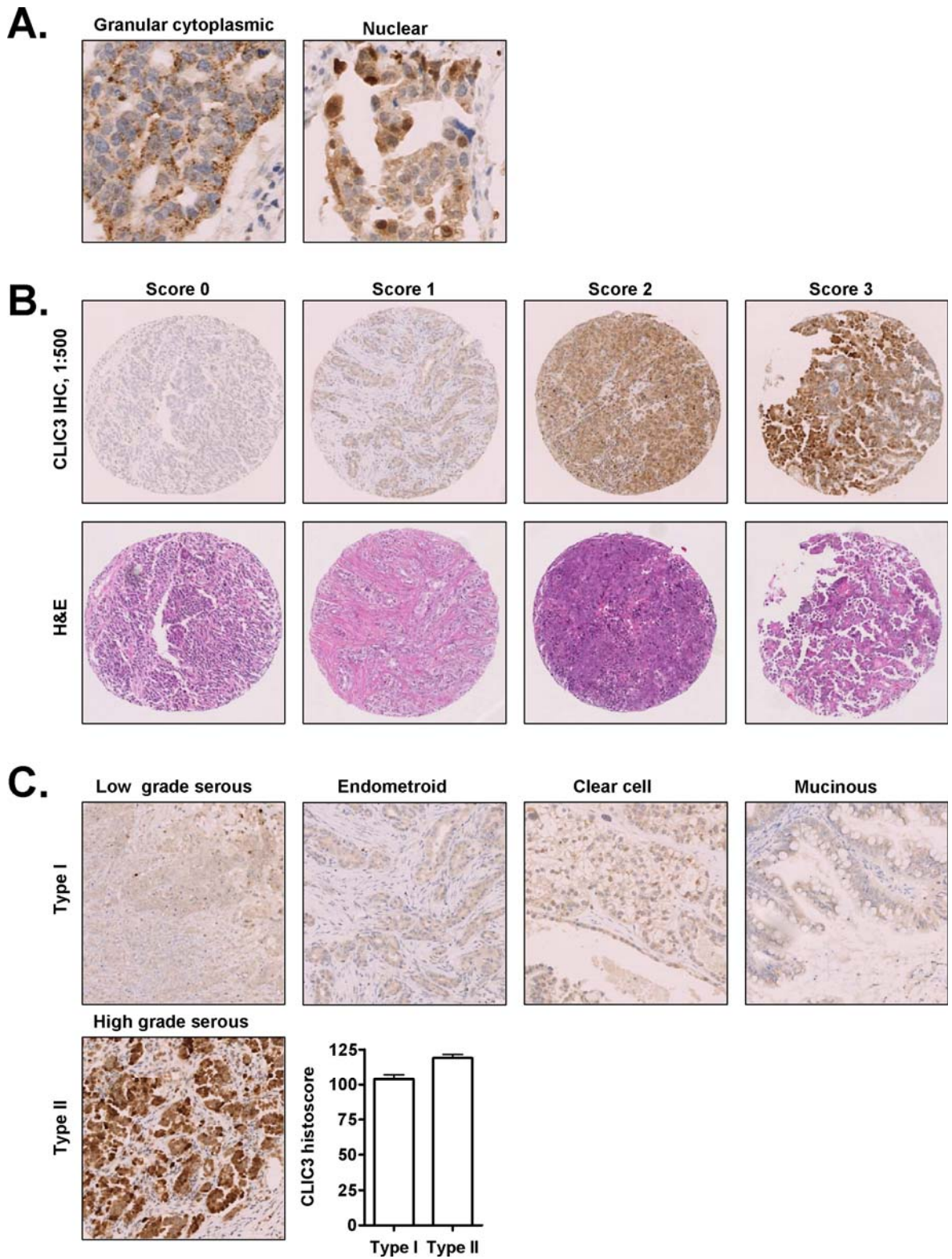


Figure 5-14 CLIC3 expression in ovarian tumours.

The ovarian TMA was stained with CLIC3 antibody at 1:500 dilution. High magnification of granular cytoplasmic and nuclear CLIC3 staining in ovarian tumours (A). Tumour cores representing CLIC3 staining intensity of 0 (no staining), 1 (weak staining), 2 (medium staining) and 3 (strong staining). Underneath shown are corresponding H&E stained sections (B). CLIC3 IHC of low grade serous, endometrioid, clear cell, mucinous (all type I) and high grade serous (type II) ovarian cancers. Graph illustrating the difference in the mean histoscore between type I and type II ovarian tumours (C). Scoring and data analysis performed in conjunction with Charlie Gourley.

5.2.5 CLIC3 is expressed in Pancreatic Intraepithelial Neoplasia (PanIN) and invasive pancreatic ductal adenocarcinomas (PDAC) but not in normal pancreatic ducts

Due to the histopathological resemblance between ovarian and pancreatic tumours, I extended the analysis of CLIC3 expression to pancreatic carcinoma. I initially performed CLIC3 immunohistochemistry on whole pancreatic tumour sections and normal human pancreatic tissue. Consistent with the observations in the mouse pancreas, CLIC3 was undetectable in normal human pancreatic ducts or acinar tissue, but was present in precursor lesions (PanINs) and high grade ductal carcinomas (Fig. 5.15A). CLIC3 was localised to cytoplasmic puncta as well as in the nucleus of those tumour cells that expressed high CLIC3 levels (Fig. 5.15B). Interestingly, in the well organised regions of PanINs, CLIC3 was at low abundance, but enriched in the more dysplastic regions of these tumour precursor lesions (Fig. 5.15A). Furthermore, CLIC3 was noticeably enriched at the invasive edge of tumours, where infiltration of the healthy tissue can be clearly observed (Fig. 5.15C).

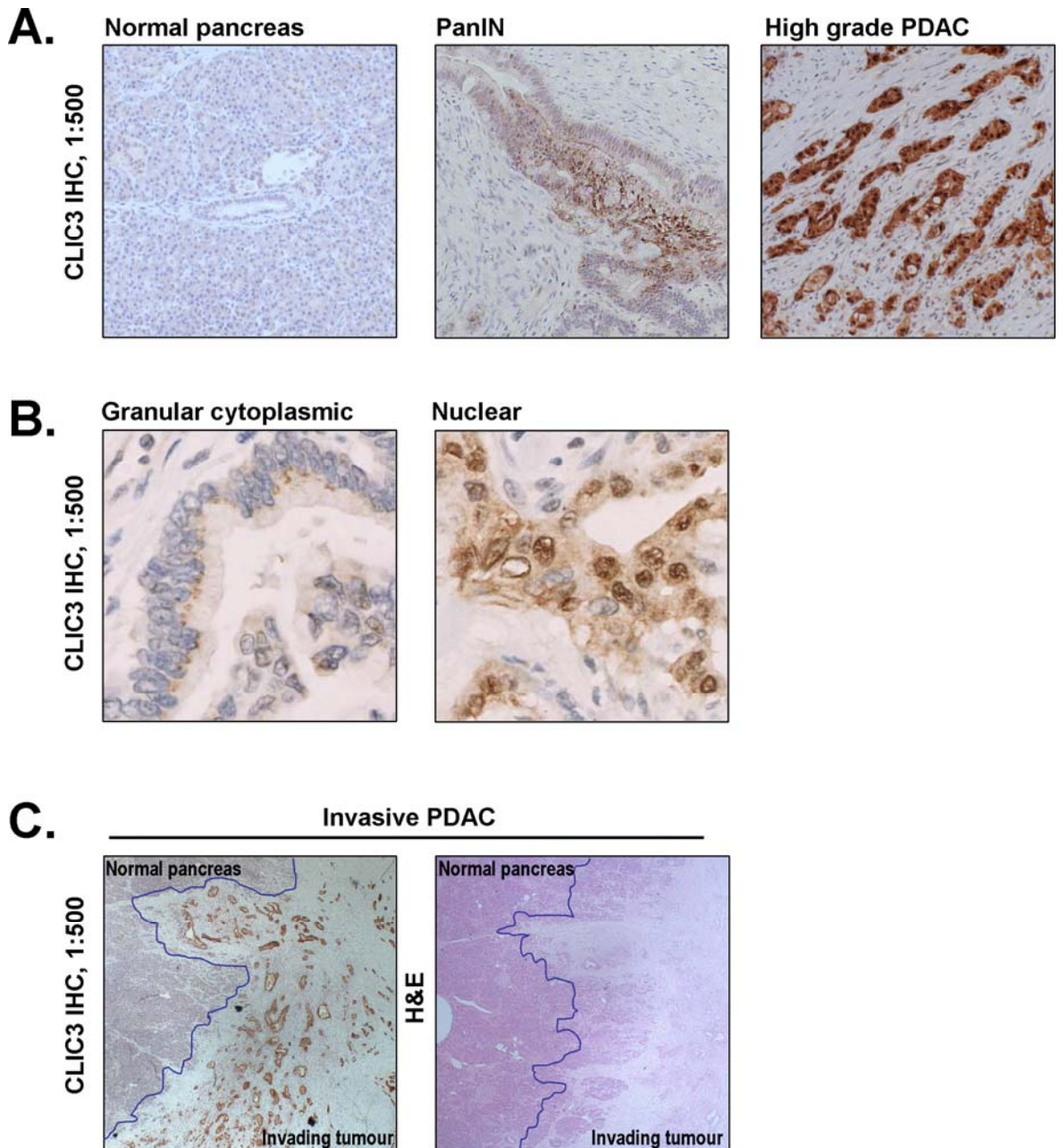


Figure 5-15 CLIC3 IHC of normal pancreatic ducts, Pancreatic Intraepithelial Neoplasia (PanIN) and high grade and invasive pancreatic ductal adenocarcinomas (PDAC).

CLIC3 IHC of the above mentioned tissues performed at 1:500 antibody dilution. Normal pancreas, PanIN and high grade PDAC in (A). Invasive PDAC was additionally Haematoxylin and Eosin (H&E) counterstained. The blue line indicates the boundary of normal and cancerous tissue (B). High magnification of CLIC3 immunostaining in PDAC shows granular cytoplasmic and nuclear abundance (C).

5.2.6 CLIC3 predicts poor PDAC patient survival

Having observed elevated CLIC3 expression in high grade and invasive pancreatic tumours, I sought to establish whether there was a relationship between CLIC3 expression and pancreatic ductal adenocarcinoma (PDAC) aggressiveness. I performed immunohistochemistry on a pancreatic TMA containing 118 cases of PDAC, each represented by 6 cores. Primary visual inspection revealed a broad spectrum of CLIC3 staining intensity; from tumours lacking CLIC3 protein to those expressing it at a very high level. For the purpose of linking the expression levels to the clinicopathological data I needed to obtain a quantitative index of CLIC3 abundance. To that end I have picked four tumour cores which represented an average score of 0 (no expression), 1 (low expression), 2 (medium expression) and 3 (high expression) (Fig. 5.16) and utilised them as a guide when calculating a continuous histoscore for each tumour sample. CLIC3 expression levels did not differ when tumour stage, size, grade, vascular invasion or resection status were considered. Univariate analysis, which divided PDAC patients into low CLIC3 expressors (histoscore<100, n=33) and high CLIC3 expressors (histoscore>100, n=85) revealed that high CLIC3 expression was associated with significantly decreased cumulative survival following PDAC resection, when compared to low expression ($p=0.01$, Fig. 5.17A). Median survival for high CLIC3 expressors amounted to 11.5 months (95% CI: 7.9-15.1) and was greatly increased to 20.1 months (95% CI: 15.6-24.6) when CLIC3 expression was low (Fig. 5.17B). Moreover, tumours presenting with no lymph node involvement (LN0, n=24) exhibited lower CLIC3 expression (mean histoscore 54.5) than those with more than 50% lymph node involvement (LN>50%, n=12, mean histoscore 125.8, $p=0.005$). Likewise, tumours with less than 50% lymph node invasion (LN<50%, n=82) had significantly lower levels of CLIC3 (mean histoscore 66.5), by comparison with the LN>50% tumours ($p=0.01$, Fig. 5.17C). More importantly, multivariate Cox proportional-hazards regression analysis identified CLIC3 expression, along with tumour stage, size, grade and margin involvement, as an independent predictor of poor survival with a hazard ratio of 1.35 (95% CI: 1.08-1.81, $p=0.028$, Fig. 5.18).

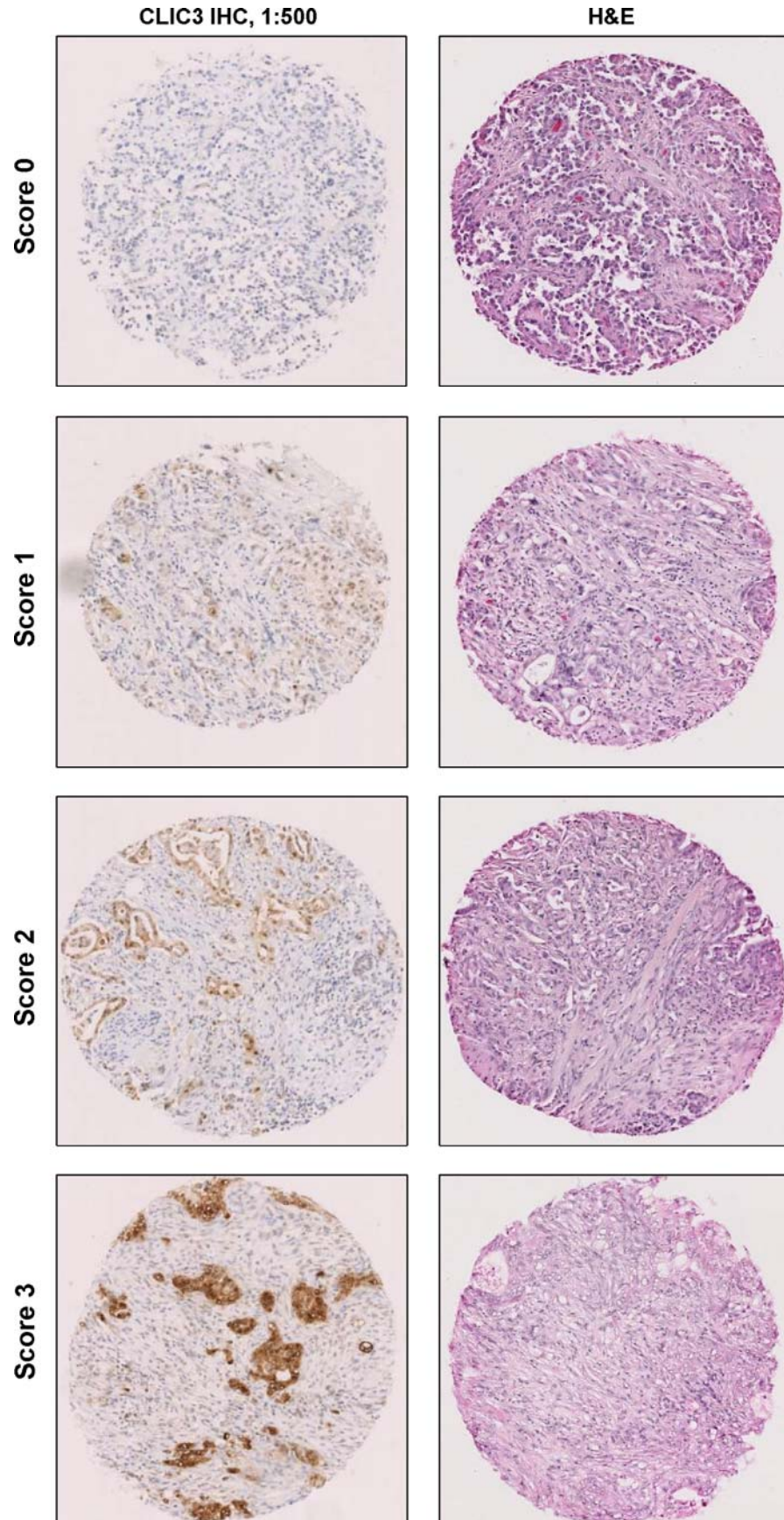


Figure 5-16 Scoring guide for the pancreatic ductal adenocarcinoma (PDAC) tissue microarray (TMA).

Shown are tumour cores selected from the TMA to represent staining intensity scores of 0 (no staining), 1 (weak staining), 2 (medium staining) and 3 (strong staining). The panel on the left shows the cores with CLIC3 immunostaining (1:500 antibody dilution), while the panel on the right shows corresponding Haematoxylin and Eosin (H&E) staining.

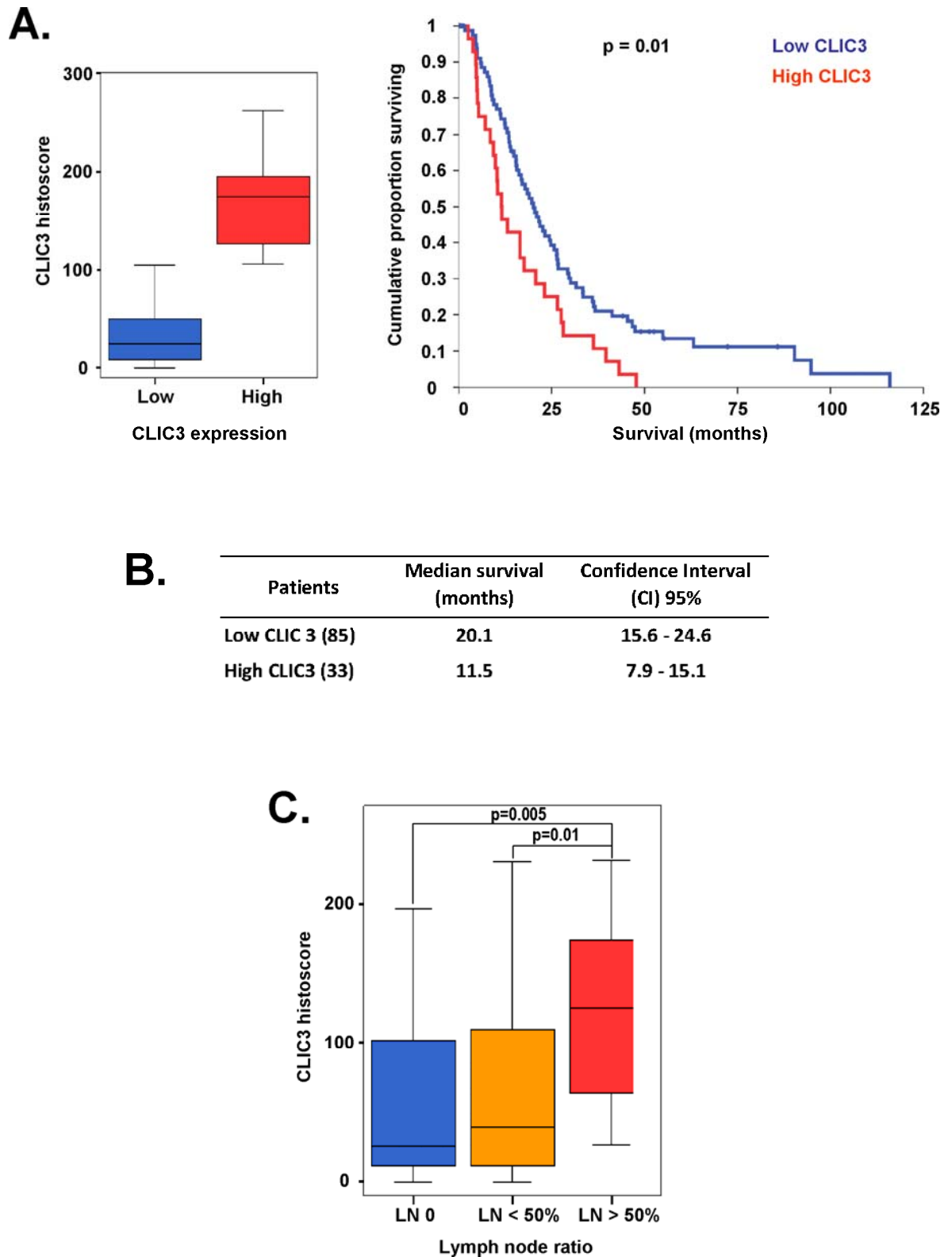


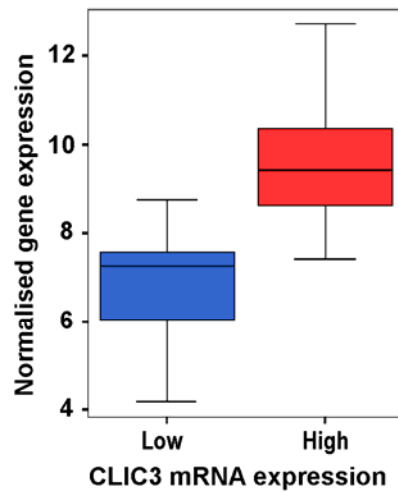
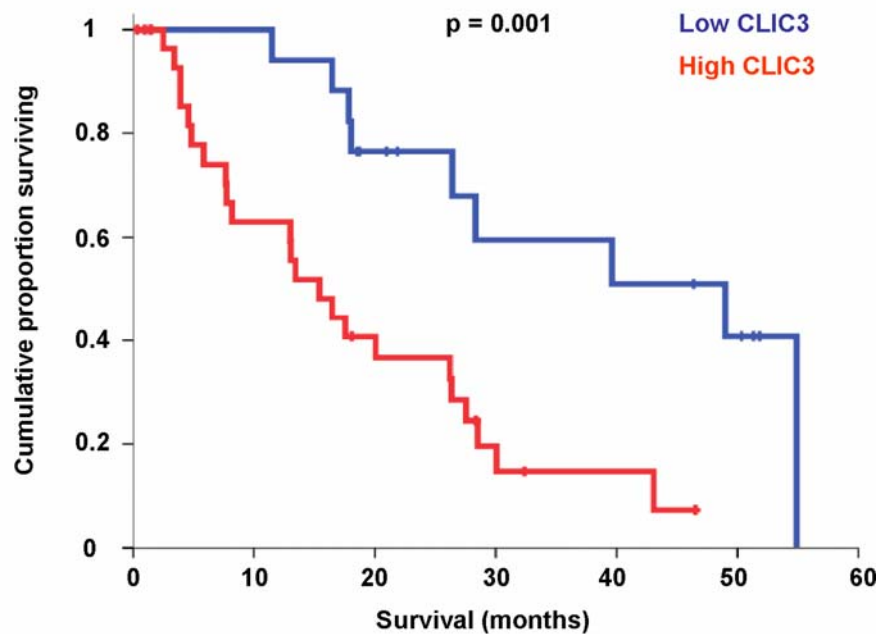
Figure 5-17 High CLIC3 protein expression renders poor survival in patients with operable pancreatic ductal adenocarcinoma (PDAC).

Box plot illustrating stratification of PDAC patients into low and high CLIC3 expressors based on the histoscore and Kaplan-Meier analysis of survival for high and low CLIC3 expressors (A). Median survival data for low and high CLIC3 expressors with 95% Confidence Interval (CI) (B). Box plot of mean CLIC3 histoscore vs. lymph node metastasis (C). TMA scoring and data analysis performed in conjunction with Nigel Jamieson.

		Overall survival	
		HR (95% CI)	P value
Age (years)	<65/ ≥65	0.83 (0.67-1.03)	0.099
Gender	Female/ Male	1.01 (0.62-1.61)	0.991
Tumor stage	T2/ T3	2.20 (1.13-4. 27)	0.019
Tumor size (mm)	<30/ ≥30	1.82 (1.19-2.79)	0.006
Lymph node status	Absent/ Present	1.71 (0.92-3.23)	0.091
Margin involvement	R0/ R1	2.23 (1.32-3.77)	0.003
Tumor grade	Low/ High	1.98 (1.25-3.14)	0.004
Perineural invasion	Absent/ Present	0.73 (0.27-1.92)	0.519
Vascular invasion	Absent/ Present	1.32 (0.89-2.09)	0.213
CLIC3	Low/ High	1.35 (1.08-1.81)	0.028

Figure 5-18 Predictors of survival in 118 patients with pancreatic ductal adenocarcinoma following pancreaticoduodenectomy according to multivariate Cox regression analysis. CLIC3 protein expression assessed by immunohistochemistry.

Given the subjectivity of TMA scoring and its semi-quantitative nature, I sought to use a more quantitative approach to validate the above correlation between CLIC3 and patient survival. A separate cohort of 48 PDAC patients that had undergone pancreaticoduodenectomy and for which outcome data was available, had previously been analysed by microarray gene expression profiling (Nigel Jamieson). Using the data from these analyses, PDAC patients were stratified into low (n=17) and high (n=31) CLIC3 expressors based on the normalised mean gene expression (log value 8.04, Fig. 5.19A). Kaplan-Meier analysis revealed that patients with low CLIC3 had a significantly increased survival by comparison with those that were high expressors ($p=0.001$, Fig. 5.19B). Median survival for high CLIC3 expressors amounted to 15.4 months (95% CI: 9.57-21.22), and this was increased over three fold, to 49 months (95% CI: 17.92-80.01), when CLIC3 expression was low (Fig. 5.19C). Furthermore, multivariate Cox proportional-hazards regression analysis identified CLIC3 mRNA expression as an independent predictor of poor survival with a hazard ratio of 4.81 (95% CI: 1.86-12.3, $p=0.001$). Other predictors of poor outcome included margin involvement, tumour stage and size (Fig. 5.20).

A.**B.****C.**

Patients	Median survival (months)	Confidence Interval (CI) 95%
Low CLIC3 (17)	49	17.92 - 80.01
High CLIC3 (31)	15.4	9.57 - 21.22

Figure 5-19 High CLIC3 mRNA expression renders poor survival in patients with operable pancreatic ductal adenocarcinoma (PDAC).

Box plot illustrating stratification of PDAC patients into low and high CLIC3 expressors based on normalised mean gene expression (A). Kaplan-Meier survival graph shows a statistically significant survival advantage for patients whose CLIC3 mRNA levels are low (blue) when compared to those whose CLIC3 mRNA levels are high (red). Log rank, $p=0.001$ (B). In (C) shown is median survival data for low and high CLIC3 expressors with 95% Confidence Interval (CI). Microarray screen and data analysis performed by Nigel Jamieson.

		Overall survival	
		HR (95% CI)	P value
Tumor stage	T2/ T3	2.29 (1.35-3.82)	0.023
Tumor size (mm)	<30/ ≥30	2.67 (1.08-6.57)	0.033
Lymph node status	Absent/ Present	2.43 (0.81-9.11)	0.199
Margin involvement	R0/ R1	2.83 (1.77-4.14)	0.002
Tumor grade	Low/ High	1.83 (0.71-4.68)	0.21
Vascular invasion	Absent/ Present	2.10 (0.78-5.68)	0.142
CLIC3	Low/ High	4.81 (1.86-12.3)	0.001

Figure 5-20 Predictors of survival in 48 patients with pancreatic ductal adenocarcinoma following pancreaticoduodenectomy according to multivariate Cox regression analysis. CLIC3 mRNA expression assessed by microarray hybridisation.

5.2.7 CLIC3 expression correlates with enhanced Src signalling in pancreatic tumour tissue

Given the contribution of CLIC3 to the recycling of active conformation $\alpha 5\beta 1$ integrin in the A2780-Rab25 tumour cell line, I sought to determine whether CLIC3 expression correlated with indicators of activated integrin signalling in pancreatic tumours. It is well established that integrin activation leads to autophosphorylation of non-receptor tyrosine kinases, such as focal adhesion kinase (FAK) and Src (Brunton and Frame 2008). Src then activates a member of the signal transducers and activators of transcription (STAT) family, STAT3, which is necessary for cell transformation and, in turn, can contribute to transcription of cell cycle regulators such as D-type cyclins, in particular cyclin D1, or p21 (Sinibaldi, Wharton et al. 2000). Interestingly, the nuclear accumulation of cyclin D1, which regulates the transition from G1 to S phase of the cell cycle leads to concurrent nuclear stabilisation of p21 (Coleman, Marshall et al. 2003). To investigate a possible correlation between CLIC3 levels and the status of signalling pathways downstream of activated integrins in the pancreatic TMA, I examined the levels of autophosphorylated, active Src (phospho-Tyr⁴¹⁶-Src) with respect to CLIC3 expression. These analyses indicated that CLIC3 histoscore correlated closely with membranous phospho⁴¹⁶-Src histoscore (Spearman's rho correlation coefficient 0.47, $p < 0.001$), which is consistent with a role for CLIC3 in integrin signalling (Fig. 5.21A). Furthermore, there was a clear correlation between CLIC3 expression and signalling downstream of Src, as evidenced by the nuclear abundance of phospho⁷²⁷-STAT3 (Spearman's rho correlation coefficient 0.539, $p < 0.0001$, Fig. 5.21B), cyclin D1 (Spearman's rho correlation coefficient 0.391, $p < 0.001$, Fig. 5.21C) and p21 (Spearman's rho correlation coefficient 0.387, $p < 0.01$, Fig. 5.21D).

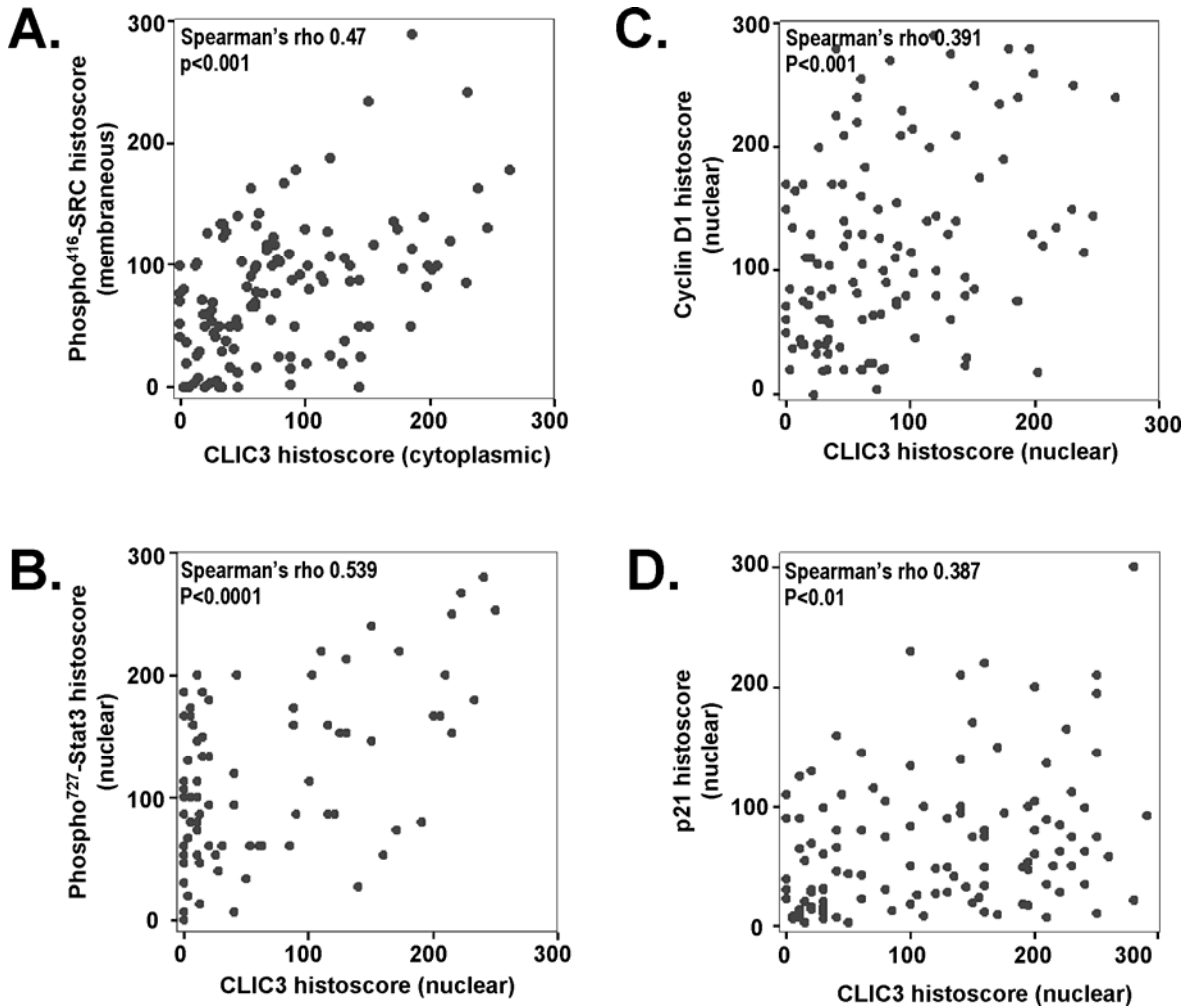


Figure 5-21 CLIC3 expression correlates with that of Phospho⁴¹⁶-Src, Phospho⁷²⁷-STAT3, cyclin D1 and p21 in pancreatic adenocarcinomas.

Shown are Spearman's correlation plots for cytoplasmic CLIC3 and membranous Phosphotyrosine⁴¹⁶-Src (A), nuclear CLIC3 and nuclear Phosphoserine⁷²⁷-STAT3 (B), nuclear cyclin D1 (C) and p21 (D), respectively. Spearman's rho correlations and p-values are indicated on the plots. Correlation plots generated in conjunction with Nigel Jamieson.

5.3 Discussion

5.3.1 Summary

Here, I generated an antibody that recognises CLIC3 but not other CLIC family members, and demonstrated that it is suitable for Western blotting and immunohistochemical staining of normal and cancerous tissues from humans and mice. I then utilised this reagent to examine CLIC3 protein expression in ovarian and pancreatic tumours. I found there to be higher CLIC3 expression in the more aggressive forms of high grade ovarian serous carcinomas, and a clear relationship between the abundance of CLIC3 and poor prognosis in operable cases of PDAC. Further analyses indicated that CLIC3 can be independently used as a predictor of poor overall survival in PDAC patients, and its expression in pancreatic tumours correlates with enhanced Src activity.

5.3.2 How does *CLIC3* contribute to tumour progression *in vivo*?

The role played by CLIC3 in Rab25-driven invasiveness and integrin trafficking *in vitro* suggest that it could contribute to metastasis *in vivo*. Indeed, the expression of this protein is higher in Type II ovarian tumours which are more likely to progress to disseminated disease. Moreover, CLIC3 is enriched at invasive tumour fronts and its expression correlates with lymph node metastasis and subsequent death from disseminated disease following surgical removal of the primary tumour. Previous studies have indicated that integrins can affect tumour cell migration and invasion not only by providing a mechanical link between the extracellular matrix and the actin cytoskeleton, but also by exerting effects on downstream signalling pathways. The recycling of $\alpha 5 \beta 1$ integrin from the Rab11 compartment in a Rab-coupling protein (RCP)-dependent manner has been shown to contribute to invasion by controlling the association of EGFR1 with RCP and by influencing signalling to protein kinase B (PKB/Akt) downstream of EGFR (Caswell, Chan et al. 2008). However, CLIC3 expression did not correlate with levels of phospho-PKB/Akt in pancreatic tumours, nor with the activity of other kinases, such as mTOR and S6 kinase, that are known to be downstream of activated PKB/Akt (data not shown). This could indicate that the signalling downstream of integrins trafficked via either

the lysosomal (CLIC3) or recycling endosome (RCP) pathways may be quite distinct. It is possible that integrins recycling via the RCP pathway communicate primarily with the PKB/Akt axis, whilst active heterodimers traversing the CLIC3 compartment exert effects on the activation of Src. Indeed, the strong correlation between CLIC3, active Src, STAT3 and cyclin D1 and poor patient survival indicates the possibility that increased cycling of active $\alpha 5\beta 1$ integrin through the CLIC3 pathway may drive spread and growth of metastases by enhancing the ability of active $\alpha 5\beta 1$ to signal through these effector pathways. Further work will be required to evaluate whether the above relationships can be reproduced in other human tumour types as well as in cancer cell lines *in vitro*.

5.3.3 Could CLIC3 explain conflicting roles of Rab25 in cancer?

There is clear evidence that Rab25 can act both to promote and to inhibit tumourigenesis, but it is as yet unclear what the reasons for this discrepancy are. It is possible that the expression of Rab25's effectors can determine whether it acts to promote or inhibit tumour progression. Indeed, a number of lines of evidence indicate that RCP could contribute to tumourigenesis (Caswell, Chan et al. 2008; Muller, Caswell et al. 2009; Zhang, Liu et al. 2009) and it has been suggested that this effector of Rab11 GTPases may alter Rab25's ability to act as tumour promoter (Luen Tang B, 2010). My data suggest the possibility that CLIC3 could also influence the way in which Rab25 acts to promote or inhibit tumorigenesis. More specifically, in the presence of CLIC3, when cells can recycle lysosomally-routed integrins, Rab25 may promote $\alpha 5\beta 1$ -dependent invasion. However, in tumours lacking the CLIC3 pathway, integrins trafficked to lysosomes will likely be retained within that compartment and this may promote their degradation. Under these circumstances, Rab25 loss may lead to unchecked $\beta 1$ -integrin expression and cause defects in polarity which could lead to tumour initiation and progression. To test this hypothesis, it will be necessary to examine the relationship between Rab25 and CLIC3 expression in a range of human tumour types. A study aimed at understanding the relationship between CLIC3, Rab25 and patient outcome in human ovarian and pancreatic tumours is currently underway in the lab, and preliminary data indicate that Rab25 is expressed in the majority of these tumours, particularly in those that show high

CLIC3 expression (Fig. 5.22). When this study is extended to cancers in which Rab25 is thought to be inhibitory to cancer progression (such as breast carcinoma), it should be possible to establish whether CLIC3 (or indeed other components of the CLIC3/lysosomal integrin recycling pathway) can determine the direction in which Rab25 pushes tumourigenesis.

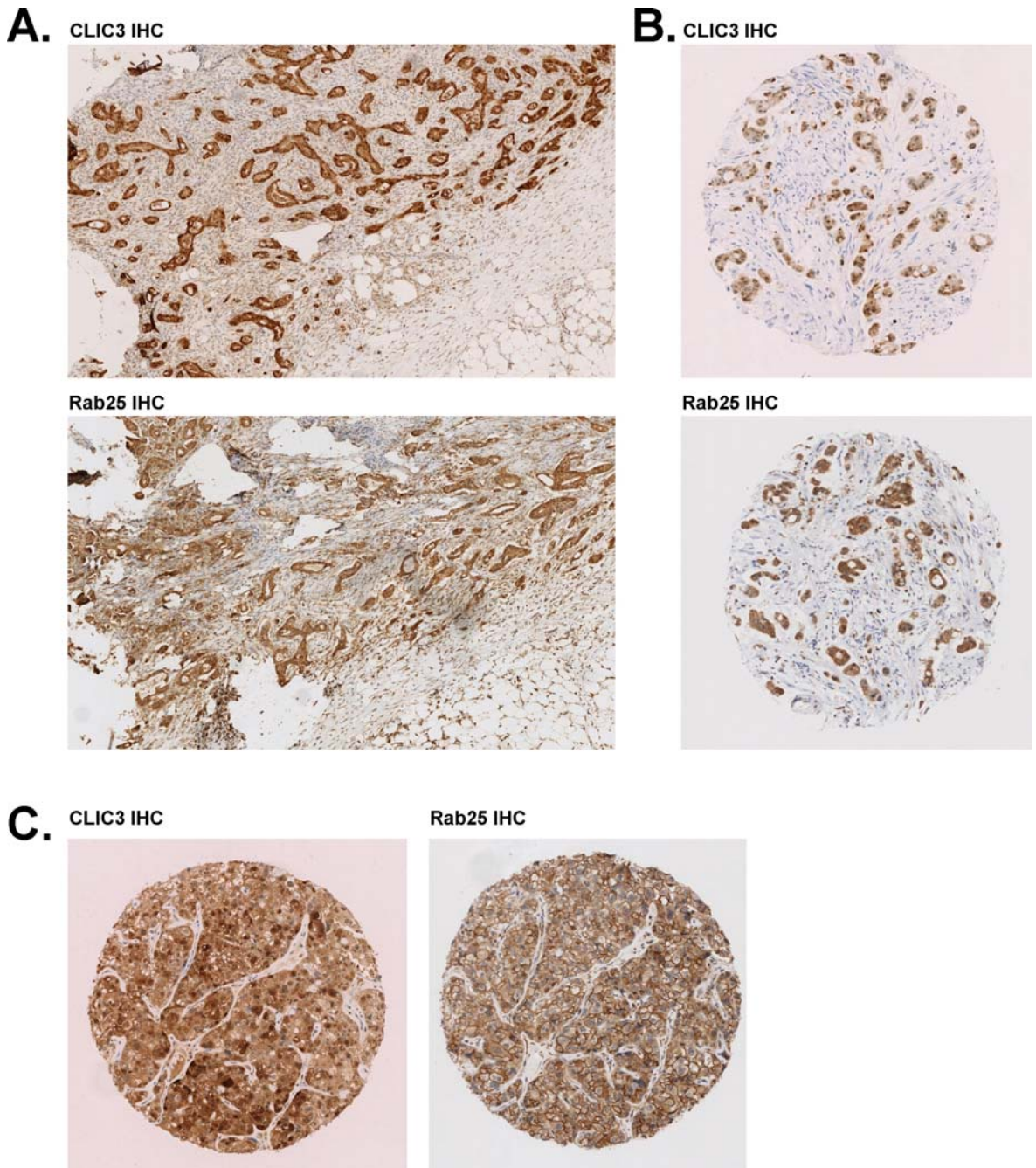


Figure 5-22 CLIC3 and Rab25 expression in PDAC and ovarian carcinoma.

(A) Immunohistochemical staining of the corresponding regions of a whole section of an invasive pancreatic ductal adenocarcinoma (B) randomly picked CLIC3-positive core from PDAC TMA (C) randomly picked CLIC3-positive core from ovarian TMA. IHC with antibodies recognising CLIC3 (pH8 retrieval, 1:750 antibody dilution) or Rab25 (pH8 retrieval, 1:1000 antibody dilution).

6 Discussion

6.1 Summary

Rab25 has been shown to promote tumour invasion and aggressiveness as well as to suppress tumour progression (Cheng, Volk et al.; Nam, Lee et al.; Wang, Wyckoff et al. 2002; Cheng, Lahad et al. 2004; Wang, Goswami et al. 2004). To gain more insight into how Rab25 may act to promote tumour cell invasion and to further explore the possible reasons for apparently opposing roles of Rab25 in human cancers, I used a microarray approach to identify genes whose expression was associated with Rab25 in a human ovarian carcinoma line. These analyses revealed a marked, Rab25-dependent increase in CLIC3 expression when cells were cultured on CDMs, by comparison with plastic surfaces. Elevated CLIC3 mRNA levels were specifically driven by Rab25 and not by other members of the Rab11 family. CLIC3 depletion in Rab25-expressing A2780 cells compromised invasion into fibronectin-supplemented matrigel, thus supporting a role for this protein in tumour invasion, and this view was reinforced by the ability of CLIC3 to drive fibronectin-dependent invasion of A2780 cells that lacked Rab25 expression. To examine the role of CLIC3 expression in human tumour progression and its correlation with patient outcome I developed an antibody that specifically recognised CLIC3, but not other members of the highly similar CLIC family, and used it in immunohistochemical staining of human ovarian and pancreatic tumour samples. Consistent with its role in tumour cell invasion *in vitro*, was high CLIC3 expression in highly metastatic Type II ovarian tumours and correlation between CLIC3 levels and poor patient outcome in operable cases of PDAC. Furthermore, CLIC3 expression correlated with the expression of active Src indicating that it is linked to activated integrin signalling in human disease.

To unravel the cellular functions of CLIC3 underlying its role in tumour progression and invasion, I investigated its cellular localisation and its relationship to the trafficking of $\alpha 5\beta 1$ integrin, a process which is controlled by a physical association of this integrin with Rab25 during tumour cell migration (Caswell, Spence et al. 2007). Live cell imaging studies indicated that CLIC3 was localised to a late endosomal/lysosomal compartment, which was positive for Rab7, LAMP1, sialin and lysotracker. Furthermore a proportion of internalised

$\alpha 5 \beta 1$ integrin colocalised with CLIC3-positive endosomes, and this colocalisation was increased when the integrin was in an active conformation, as indicated by experiments in which soluble fibronectin was used to prime the integrin, or when a constitutively active integrin mutant was employed. Moreover, this late endosomal/lysosomal routing of active integrin heterodimers required the presence of Rab25, suggesting that this GTPase facilitates its sorting to this compartment. Not only was the active $\alpha 5$ integrin shown to be trafficked to CLIC3-positive late endosomes/lysosomes, but instead of being degraded, it recycled from this cellular compartment back to the plasma membrane, as indicated by live cell photoactivation experiments. This was further substantiated by biochemical recycling experiments, which confirmed the requirement for CLIC3 in the return of active integrin to the plasma membrane.

Taken together, the data presented in this thesis outline a novel role for CLIC3 in integrin recycling, tumour cell invasion *in vitro* and cancer progression and invasion *in vivo*.

6.2 Future directions and preliminary observations

6.2.1 *CLIC3 in tumour invasion and progression*

Genetic tumour models offer a promising tool for recapitulating tumour development and progression *in vivo*, and they have been widely applied in the studies of pancreatic tumour development and progression. Pancreatic ductal adenocarcinoma (PDAC) arises from precursor lesions (PanINs), which in the course of their progression to malignancy accumulate genetic alterations, such as activation of K-Ras, loss of Ink4a, loss of p53 function or Smad4 (Hruban, Maitra et al. 2007). Recently, the loss of Lkb1 has also been shown to drive pancreatic tumour progression (Morton, Jamieson et al.). In 90% of PDAC, the progression of PanINs to invasive carcinoma is driven by the activation of the K-Ras oncogene (Almoguera, Shibata et al. 1988). Following an initiating K-Ras activating G12D mutation, a mutation in *TP53* tumour suppressor gene occurs in 50-75% cases of human pancreatic cancer (Scarpa, Capelli et al. 1993). Mutant p53 (p53(R172H)), has been shown to drive the progression of premalignant lesions harbouring the K-Ras mutation into PDAC and to promote metastasis (Morton, Timpson et al.). However, my immunohistochemical analyses of pancreatic precursor lesions and carcinomas from mice in which the *Kras*^{G12D} and *p53*^{R172H} alleles are driven by the pancreas specific Pdx-1-Cre (Hingorani, Wang et al. 2005), did not reveal CLIC3 expression. Given that mutant p53 is thought to promote invasion and metastasis through enhanced recycling of $\alpha 5\beta 1$ integrin and EGFR1 in a way that requires Rab-coupling protein (RCP) (Muller, Caswell et al. 2009), and not Rab25, it may not be surprising that these tumours lack CLIC3 expression. Genetic models of pancreatic cancer employing K-Ras mutation and Rab25 or CLIC3 overexpression might therefore be more suitable to study the contribution that these proteins make to tumour progression *in vivo*.

Cell lines derived from such genetically engineered tumours could be used to significantly strengthen the role of CLIC3 in tumour invasion. Firstly, organotypic assays more closely represent the matrix through which tumour cells invade *in vivo* than do matrigel plugs, and this is due to the collagen matrix being pre-conditioned by normal human fibroblasts, which are thought to lead the invading tumour cells *in vivo* (Gaggioli, Hooper et al. 2007). Secondly, CLIC3-driven

tumour spread, and in particular organ colonisation, could be assessed through *in vivo* approaches employing bioluminescent imaging, which evaluate metastatic spread of blood-borne cells and their subsequent population of sites, such as lungs or liver (Elkin and Vlodaysky 2001). Finally, xenograft studies, which involve subcutaneous or intraperitoneal inoculations of cultured tumour cells, offer a better opportunity of mimicking metastatic spread *in vivo*, than do tail vein injections. This is because cancer cells that form the primary tumour must escape from the cancerous mass, enter circulation and then populate secondary niches. Additionally this process can be monitored in real-time through the application of fluorescent proteins and optical imaging (Sahai 2007).

6.2.2 CLIC3 interactome

Proteins of the CLIC family share a high level of structural conservation, with the exception of an approximately 12 amino acid stretch, which forms a so called hypervariable loop that protrudes from the globular structure of CLICs. It has been speculated that this motif could serve as an adaptor site for specific protein-protein interactions (Singh). To initiate characterisation of the CLIC3 interactome I performed pull down assays, where I used GST-tagged proteins as baits and incubated them with A2780-Rab25 cell lysates. The pull-downs were then subjected to separation by SDS-PAGE and mass spectrometry analyses. Two independent experiments identified a number of proteins that specifically interacted with GST-CLIC3, but not GST alone or GST-CLIC1 or GST-CLIC4 (Fig. 6.1A&B, Appendix 6.1). One of the top hits, for which a consistently large number of peptides was identified in both mass spectrometry screens, was Tyrosine-protein phosphatase non-receptor type 14 (PTPN14). I confirmed the interaction of PTPN14 with recombinant CLIC3 by Western blotting (Fig. 6.2A). Additionally, I developed reagents for suppression and overexpression of PTPN14, which will allow functional studies (Fig. 6.2B). Interestingly, suppression of PTPN14 seemed to increase the ability of EGF to drive the phosphorylation of EGFR at Tyr 1045 (Fig. 6.2C). Phosphorylation at Tyr 1045 is required for docking of the E3 ubiquitin ligase - Cbl - to EGFR1, thus promoting ubiquitination and the ESCRT-mediated sorting of EGFR1 into luminal vesicles for degradation on the multivesicular endosomal pathway (Grovdal, Stang et al. 2004; Marmor and Yarden 2004). Thus, it is possible that PTPN14 may oppose

phosphorylation of EGFR1 at Tyr 1045 thus reducing Cbl recruitment and the consequent receptor degradation, ultimately leading to prolonged signalling downstream of EGFR1 or even recycling of the receptor from late endosomes/lysosomes, which would be likely to be pro-invasive. Indeed, PTPN14 has been observed to be enriched at the invasive fronts and in liver metastases of tumours generated with the human pancreatic tumour cell line MiaPaca2 in nude mice (Niedergethmann, Alves et al. 2007). Consistent with this, my preliminary findings have shown that suppression of PTPN14 with siRNA reduces the invasiveness of A2780-Rab25 cells into matrigel (Fig. 6.2D). Therefore these observations would suggest that PTPN14 and CLIC3 could collaborate to control the joint trafficking of $\alpha 5\beta 1$ integrin and EGFR1 and the signalling downstream of these receptors to drive tumour cell invasion.

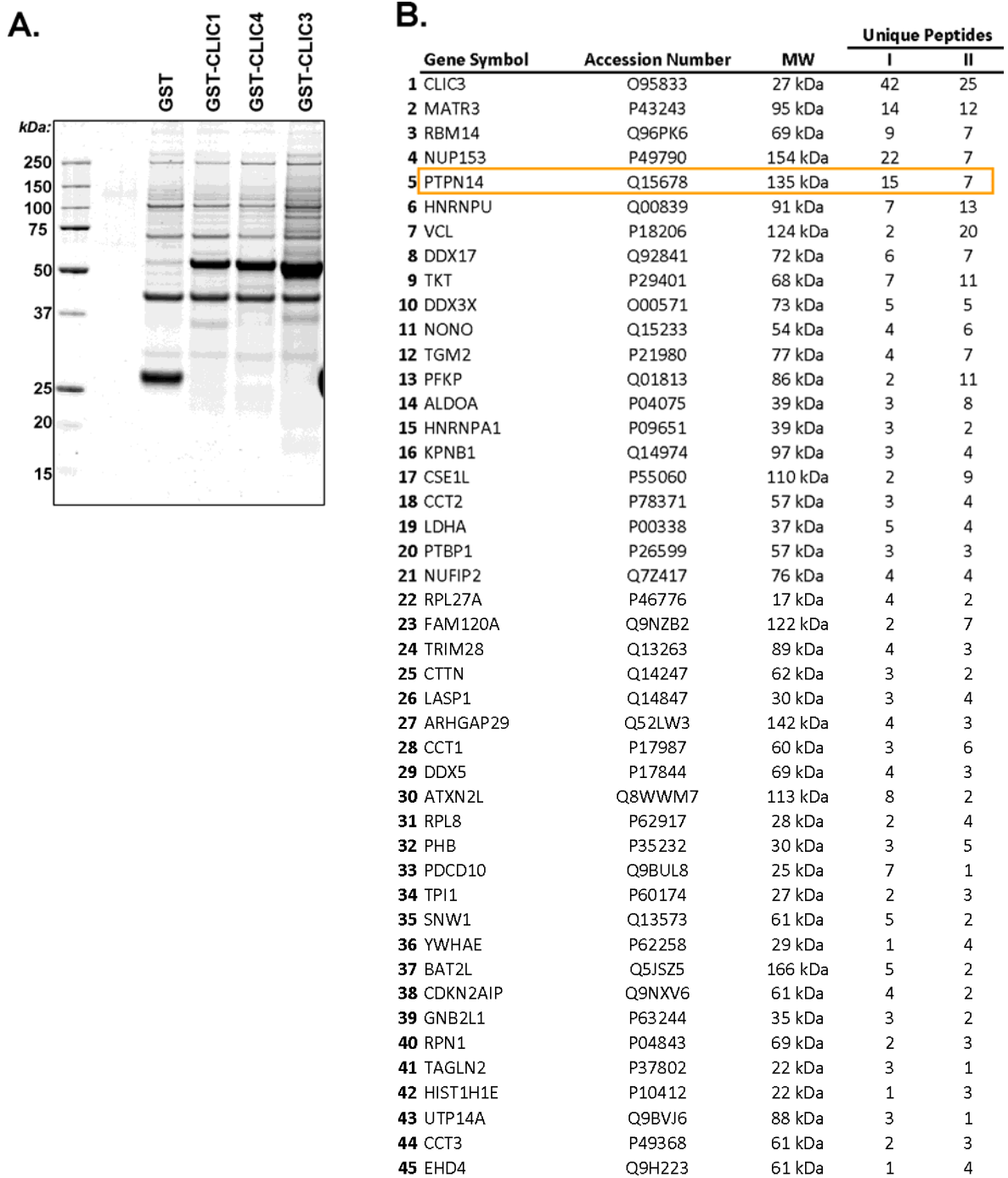


Figure 6-1 CLIC3 interactome.

A. Recombinant GST, GST-CLIC1, GST-CLIC4 and GST-CLIC3 were coupled to sepharose beads and tumbled with A2780-Rab25 cell lysates. Proteins that were pulled-down by the baits were then eluted from the column, subjected to SDS-PAGE separation and analysed by mass spectrometry. B. Proteins that specifically interacted with CLIC3 but not the other recombinant proteins are listed in the table. From left to right are: gene symbols, accession numbers, molecular weights and number of unique peptides identified in repeat 1 (I) and 2 (II)

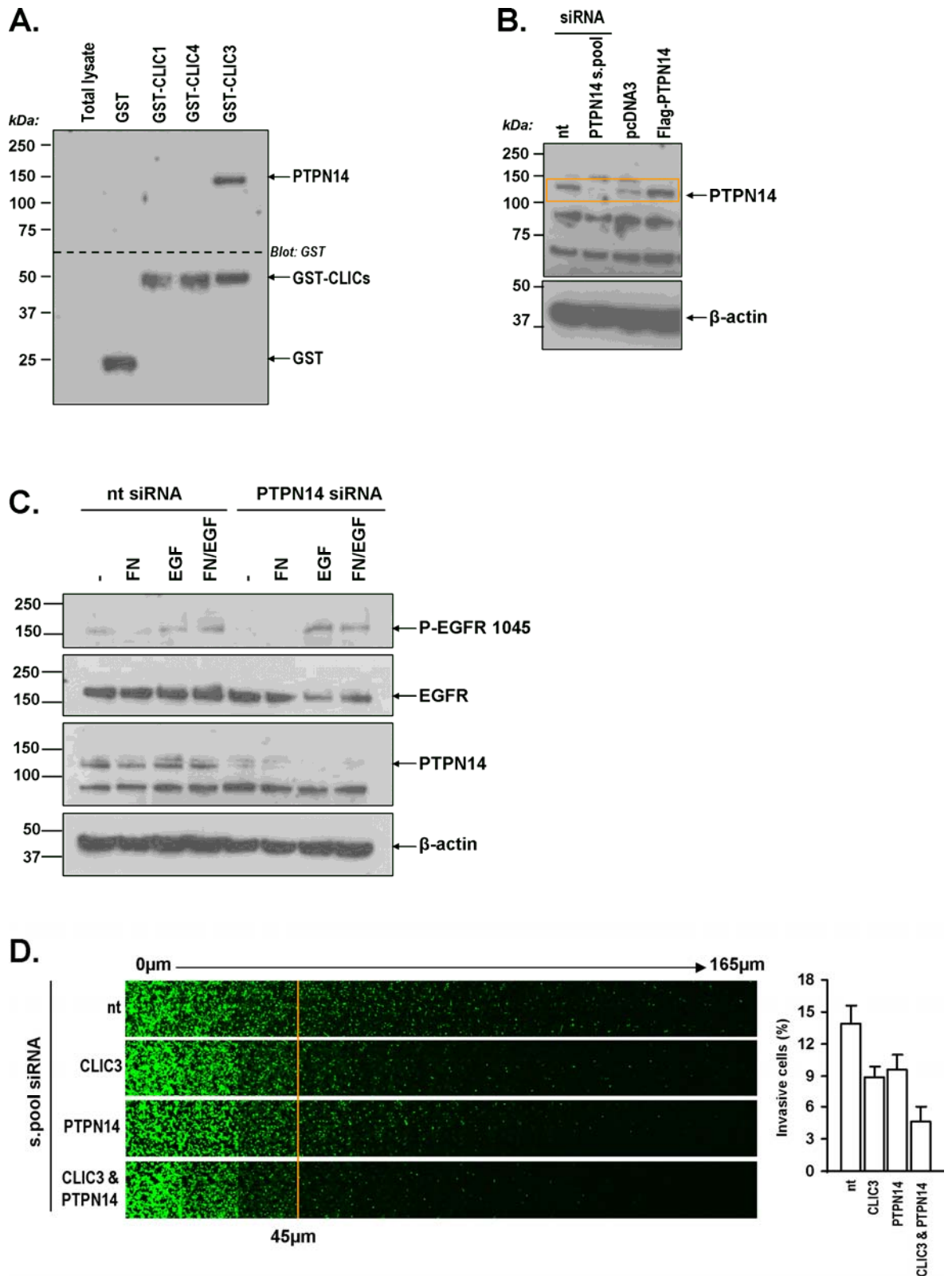


Figure 6-2 Preliminary data on PTPN14.

A. Interaction of PTPN14 with GST-CLIC3 was confirmed by Western blotting with a rabbit PTPN14 specific antibody, GST antibody was used to verify protein loading. B. PTPN14 siRNA s.pool efficiently suppresses PTPN14 protein levels 48 hours after nucleofection and ectopic expression of Flag-PTPN14 persists for 48 hours. C. Depletion of PTPN14 leads to potentiation of EGFR phosphorylation on Tyr 1045. D. PTPN14 seems to drive invasion into fibronectin-rich collagen plugs. Shown are representative collagen strips and quantification of invasion beyond 45 μ m. Data are mean from 2 experiments. All experiments in this figure were performed with A2780-Rab25 cells.

6.3 Final discussion and conclusions

6.3.1 Signalling from late endosomes/lysosomes

Endosomal vesicles are pivotal sites of receptor-initiated signal transduction and can act as scaffolds for the assembly of new signalling platforms, thus affecting signalling downstream of active transmembrane receptors following their internalisation (von Zastrow and Sorkin 2007). Indeed, EGFR remains associated with Grb2 and Shc upon its endocytosis, which allows activation of Ras residing within these endosomes (Jiang and Sorkin 2002). Additionally, internalisation of EGFR1 has been shown to be required for prolonged activation of PKB/Akt, but not MAPK signalling (Goh, Huang et al.). Moreover, G-protein-coupled receptors (GPCRs) are thought to initiate MAPK signalling cascades from endosomes and this occurs mainly through their interaction with arrestin-1 and -2, which in turn bind components of MAPK pathway (Lefkowitz and Shenoy 2005). Indeed, the stability of the GPCR and β -arrestins association determines the extent of ERK activation (Tohgo, Choy et al. 2003). Furthermore, distinct internalisation and recycling routes of $\alpha\beta 3$, $\alpha 5\beta 1$ integrin or EGFR can determine the way in which these receptors activate distinct signalling pathways (Caswell, Chan et al. 2008; Sigismund, Argenzio et al. 2008) and this is particularly evident for EGFR1. Indeed, when internalised via the CME route, this receptor is recycled to the cell surface, which prolongs signalling to Akt and ERK. On the other hand, clathrin-independent internalisation commits EGFR1 for degradation thus attenuating signalling events (Sigismund, Argenzio et al. 2008).

Lysosomes have been canonically considered to be a cul-de-sac of the endo/exocytic pathway, in which cargo proteins are degraded. However, studies of Lippincott-Schwarz reported a bi-directional flux of cargo between lysosomal and endosomal compartments as well as plasma membrane (Lippincott-Schwarz and Fambrough 1987), and those of Wubbolts suggested a direct delivery of lysosomal contents to the cell surface (Wubbolts, Fernandez-Borja et al. 1996). Recently, trafficking of internalised receptors to late endosomes/lysosomes has been connected to cellular signalling events and lysosomes have been reported to be scaffolds for the assembly of numerous protein complexes. Indeed, following NGF binding, TrkA neurotrophin receptor undergoes internalisation,

transits through early endosomes to then arrive in late endosomes. At late endosomes, a tetrameric complex is formed, which involves the TrkA receptor and this induces sustained activation of Rap1 and ERK signalling (Hisata, Sakisaka et al. 2007). Also, components of the MAPK signalling pathway, MEK1-ERK, are localised to Rab-7 and LAMP1-positive late endosomes/lysosomes through a p14-MP1 scaffold complex, and such endosomal localisation is necessary for full activation of ERK (Wunderlich, Fialka et al. 2001; Teis, Wunderlich et al. 2002). Moreover, the anchoring of MEK1-ERK signalling pathway to late endosomes requires a lipid raft adaptor protein, p18 (Nada, Hondo et al. 2009). More recently, it has become clear that the Rag proteins, which are amino acid specific regulators of the growth-regulating mTORC1 pathway (Sancak, Peterson et al. 2008), reside at the cytoplasmic face of the lysosomal membrane. The trimeric complex composed of p14, MP1 and p18 (as mentioned above with respect to MEK1-ERK signalling, but which these authors termed Ragulator), interacts with Rag GTPases and this interaction mediates the translocation of mTORC1 to the lysosomal membrane, and this is necessary for the activation of the mTORC1 pathway in response to amino acids (Sancak, Bar-Peled et al.). It is worth noting, that the mTOR pathway has been implicated in human cancers and that rapamycin, an agent antagonising mTOR signalling, has been successfully used for the treatment of several cancers, thus suggesting that signalling from lysosomal membranes plays a role in human cancer (Sudarsanam and Johnson). Late endosomes have also been shown to provide a platform for a cross-talk between signalling from Rac1, Rab7 and Arf6. A TBC domain-containing RabGAP, Armus, interacts with activated Rac1, and by integrating Rac1 activation with Rab7 function, it plays a role in Arf6 dependent disassembly of junctions and promotes E-cadherin degradation (Frasa, Maximiano et al.). This in turn can facilitate EMT and tumour progression and metastasis, thus forming a link between the lysosomal compartment and tumour progression.

K-Ras has been shown to translocate to intracellular endosomal membranes through a clathrin-mediated pathway and upon EGF stimulation. Following sorting in the early endosomal compartment, K-Ras is transported to Rab7- and LAMP1-positive late endosomes and lysosomes. This endo/lysosomal compartment acts as a platform for K-Ras activation, and K-Ras present on LAMP1-positive late endosomes/lysosomes can recruit its effector Raf1,

suggesting that it is capable of signalling from this endocytic compartment (Lu, Tebar et al. 2009). K-Ras is known to be a pivotal oncogene and to be frequently mutated in many epithelial human cancers and in mouse models of this disease. K-Ras activating G12D mutation occurs in 90% of human PDAC and it drives tumour progression (Almoguera, Shibata et al. 1988). Indeed, in a mouse model of pancreatic cancer it is G12D K-Ras that cooperates with R172H p53 to promote progression to metastatic disease (Hingorani, Wang et al. 2005). Interestingly, Singh and colleagues used pancreatic and lung cancer cell lines that harboured K-Ras mutation to deplete K-Ras with siRNA, and identified two classes of cell lines - one that relied on K-Ras for viability and one that did not. They then analysed the gene expression signature of the K-Ras dependent cell lines and identified a number of genes such as Syk or integrin $\beta 6$, whose depletion can induce EMT. More importantly, Rab25 was also shown to be a component of the K-Ras dependency signature (Singh, Greninger et al. 2009). These reports and my findings could suggest that late endosomal/lysosomal compartment is a point of convergence for K-Ras, CLIC3 and Rab25 and that this is relevant to human cancer.

The non-receptor tyrosine kinase Src localises to membraneous compartments, such as late endosomes or plasma membrane, with the active pool of Src mostly residing at focal adhesion sites (Fincham, Unlu et al. 1996). Delivery of activated Src to the cell surface has been shown to require not only Rab11, but also a late endosomal Rho family protein, RhoB (Sandilands, Cans et al. 2004). In keeping with this, the proper functioning of the late endosomal/lysosomal compartment is key for the trafficking of activated Src from endosomal compartments to the cell periphery and for its correct localisation to focal adhesions. Perturbation of ESCRT pathway or Rab7 function leads to the accumulation of active Src at aberrant late endosomes/lysosomes and this affects Src-mediated signalling and cell migration (Tu, Ortega-Cava et al.). Furthermore, depletion of a key component of the mammalian ESCRT-I complex, Tsg101, results in impaired Src-mediated activation of its downstream effectors STAT3 (Turkson, Bowman et al. 1998) and FAK (Schlaepfer and Hunter 1996), and this leads to reduced cell motility (Tu, Ortega-Cava et al.). Strikingly, the above observations share a number of parallels with my findings. Firstly, I have shown that recycling of active $\alpha 5\beta 1$ integrin requires a late endosomal/lysosomal protein, as did the

trafficking of Src. Secondly, depletion of CLIC3 affects cell migration, as did the perturbation of ESCRT pathway. Thirdly, I have shown that high expression of late endosomal/lysosomal protein, CLIC3 correlates with active Src and STAT3, and so did Tsg101 in the above mentioned study.

Taken together, the above reports suggest that late endosomal/lysosomal compartment is a key nexus point for integrating signalling from mTOR, K-Ras and Src. My findings indicate that $\alpha 5\beta 1$ integrin passes through this compartment, and the possibility that this integrin could impinge directly on these signalling pathways and this could have relevance to human cancer.

6.3.2 Exosomes and cancer

Mammalian cells can secrete proteins from their biosynthetic pathways either through controlled release of secretory granules or via constitutive exocytosis of secretory vesicles (Simpson, Jensen et al. 2008). Exocytosis is a process of cellular secretion, in which the endosomal luminal contents are released from the cell through the fusion of vesicular membrane with the plasma membrane (Idone, Tam et al. 2008). Exocytosis of multivesicular bodies (MVBs) proceeds through the fusion of their limiting membrane with the plasma membrane and can then lead to the release of their luminal contents, including exosomes, which are membrane vesicles of endocytic origin that are 40-100nm in diameter (Simpson, Lim et al. 2009).

Exosomes have been found in multiple body fluids, such as urine, blood, malignant ascites, bronchoalveolar lavage or amniotic fluid and are thought to contribute to multiple biological functions, such as the immune response, intracellular communication or RNA and protein transfer (Simpson, Lim et al. 2009). Exosomes have been reported to be secreted into the culture medium by a number of mammalian cancer cell lines and into tumour ascites by tumours *in vivo* (Wolfers, Lozier et al. 2001; Andre, Scharz et al. 2002; Hegmans, Bard et al. 2004; Mears, Craven et al. 2004; Koga, Matsumoto et al. 2005). Exosomes originating from different cell types have distinct molecular compositions, but late endosomal and lysosomal proteins have been consistently detected to be released from cells in association with exosomes. For example, the late endosomal tetraspanin CD63 is enriched in exosomes secreted by human B-

lymphocytes (Escola, Kleijmeer et al. 1998), platelets (Heijnen, Schiel et al. 1999) or mast cell lines (Valadi, Ekstrom et al. 2007). Interestingly, multiple integrin family members are common components of secreted endosomes (Fevrier, Vilette et al. 2004), and specifically, $\alpha 4$ integrin is present in B-cell-derived exosomes (Wubbolts, Leckie et al. 2003). Additionally, multiple integrin heterodimers have been detected in cancer cell-associated secretions, such as melanoma-derived exosomes (Mears, Craven et al. 2004) and those originating from colon cancer cell lines (Simpson, Jensen et al. 2008). The presence of integrins in exosomes is consistent with my observations and those of Lobert et al, that integrins can be abundant on late endosomal/lysosomal compartments. Alix, is a well established marker of exosomes and it has been detected in exosome lysates derived from melanoma cell lines (Mears, Craven et al. 2004) and in dendritic cell-associated secretions (Thery, Boussac et al. 2001). It has also been shown to promote $\alpha 5 \beta 1$ integrin-mediated cell adhesion and fibronectin matrix assembly (Pan, Wang et al. 2008), which might suggest an interesting link between integrins, exosomes and cell migration. Furthermore, an extracellular matrix protein thought to mediate adhesion of endothelial cells through $\alpha \beta 3$ integrin, DEL-1 (Hidai, Zupancic et al. 1998), has been seen in exosomes derived from mesothelioma cells (Hegmans, Bard et al. 2004). In light of all the above evidence, exosomes could be an attractive link between integrin function and recycling from late endosomes/lysosomes, and endocrine and paracrine processes involved in cancer metastasis.

Tumour-derived exosomes from malignant ascites of cancer patients may serve as an important diagnostic tool and could be used for biomarker discovery. Indeed, in some cancer types, certain tumour overexpressed proteins, have been also found in tumour-associated secretions. For example, HER2 has been seen in breast cancer exosomes (Koga, Matsumoto et al. 2005) and A33 antigen in colon cancer cell-line associated secretions (Heath, White et al. 1997). Interestingly, one of the CLIC family members, CLIC1, has been reported to be secreted by tumour cells and to be detectable in serum and plasma samples of nasopharyngeal cancer patients, suggesting it could be used as plasma biomarker of this carcinoma (Chang, Wu et al. 2009). It has also been proposed as a potential serological marker for early detection of breast carcinoma (Gromov, Gromova et al.). In preliminary experiments CLIC3 has been detected in A2780-

Rab25 ovarian carcinoma cell culture supernatants, which suggests it may be a component of tumour secretome. It is possible that CLIC3 follows the route taken by the integrins recycling from late endosomes/lysosomes to then be released in association with exosomes, and Rab27 could play a role in that process. This GTPase has been shown to govern the exosome secretion pathway, and Rab27a and Rab27b have been found to facilitate MVEs docking at the plasma membrane and subsequent exosomes secretion, in a process that depends on Rab27 effectors, such as Slp4 (Ostrowski, Carmo et al.). My identification of Slp1 as a Rab25 and CDM-upregulated gene, alongside with CLIC3 (Chapter3), and reports on its binding to Rab27A (Kuroda, Fukuda et al. 2002; Neumuller, Hoffmeister et al. 2009), further encourage exploration of this avenue.

Finally, the observations that members of the CLIC family are components of the tumour-associated secretome and the correlation between CLIC3 expression in PDAC samples and patient outcome suggest that CLIC3 could potentially be used as a secreted biomarker in the clinic for early detection of PDAC and other aggressive carcinomas.

6.3.3 Integrins in cancer progression and in the clinic

Alterations in the expression or function of integrins result in aberrant cell adhesion and migration, and have been linked to a number of diseases, such as inflammatory bowel disease, asthma, cardiovascular diseases and cancer (Huveneers, Truong et al. 2007). High expression levels of integrins have been seen to correlate with tumour progression. Indeed, genetic disruption of $\beta 1$ integrin function in the mammary epithelium of a transgenic mouse model of human breast cancer inhibits the initiation and maintenance of breast malignancy (White, Kurpios et al. 2004). Similarly, integrin signalling is required for transition of premalignant hyperplasia to carcinomas and their subsequent metastases. This is evidenced by impaired mammary tumour progression following disrupted function of FAK (Lahlou, Sanguin-Gendreau et al. 2007), a protein which is a key component of integrin focal adhesion complexes and which regulates integrin-mediated adhesion and migration (Schlaepfer, Mitra et al. 2004). Furthermore, a recent study has shown that inhibition of integrin

signalling represses invasion of a pre-malignant epithelium into ECM, whilst forced integrin clustering triggers integrin-mediated signalling and invasion (Levental, Yu et al. 2009). These authors suggest that it is enhanced signalling downstream of integrins and not necessarily increased integrin expression that is required for tumour progression. Finally, $\beta 1$ integrin has been shown to be dispensable for tumour initiation but $\beta 1$ -deficient mice have displayed lower capacity to metastasise to the lung and this was owing to abrogated adhesion signalling. These observations suggest that this integrin plays a key role in tumour progression (Huck, Pontier et al.).

Thus many experiments conducted in animal models and other *ex vivo* systems have identified integrins as promising targets for cancer therapies and have encouraged the development of integrin antagonists for use in the clinic. These molecules interfere with integrin binding to its natural ligands, thus preventing integrin-mediated signalling and potentially opposing tumour progression and metastasis (Mizejewski 1999). Integrin antagonists can be divided into three main groups: small molecule compounds, peptidomimetics and monoclonal antibodies (mAb), and for the treatment of cancer, blocking of $\alpha 5\beta 1$ and $\alpha v\beta 3$ integrin has been most widely studied (Huveneers, Truong et al. 2007).

The RGD sequence is a component of several extracellular matrix proteins, such as fibronectin, and it serves as a recognition site for many integrins (Pierschbacher and Ruoslahti 1984). Disintegrins have been discovered in snake venoms and are RGD-containing cysteine-rich peptides, which can also bind to integrins thus blocking their function, and have been seen to inhibit tumour growth and angiogenesis in xenograft tumour models (Swenson, Costa et al. 2005). However, the use of naturally occurring peptides as therapeutic agents is limited due to their relatively large size and low metabolic stability. These issues have been addressed by the use of cyclic structures, and cyclic RGD pentapeptides are commonly used to target $\alpha v\beta 3$ integrin (Ruoslahti 1996). Indeed, cyclo (RGDfV) is highly effective at antagonising $\alpha v\beta 3$ and has anti-angiogenic potency (Friedlander, Brooks et al. 1995). Further modifications to the structure of this compound have led to the generation of a more potent and selective agent, Cilengitide (c(RGDf(NMe)V)) (Goodman, Holzemann et al. 2002), which induces apoptosis in glioblastoma and medulloblastoma cells (Taga, Suzuki et al. 2002) and is being tested in clinical trials (Stupp and Rugg 2007).

Peptidomimetics are a relatively new class of non-peptide chemical RGDs, and $\alpha 5\beta 1$ -specific antagonist, ATN-161, has been shown to decrease the occurrence of liver metastases in colorectal cancer cell line xenografts and to increase survival in mice (Stoeltzing, Liu et al. 2003). Another group of integrin blocking agents encompasses monoclonal antibodies that target the extracellular domain of the heterodimers, and those directed at $\alpha 5\beta 1$ integrin have been shown to cause regression of human tumours in mouse models by acting as anti-angiogenics (Kim, Bell et al. 2000). Volociximab (M200), a chimeric humanised antibody that shows high affinity for $\alpha 5\beta 1$ (Ricart, Tolcher et al. 2008; Ng, Bai et al. 2009) has entered clinical trials as a potential anti-angiogenic therapeutic in platinum resistant ovarian cancer, but this study has been terminated due to lack of efficacy (<http://clinicaltrials.gov/ct2/home>).

Even though inhibition of $\alpha v\beta 3$ integrin in *in vitro* and *ex vivo* models has indicated that this approach may be beneficial for opposing cell migration and angiogenesis, and could serve as a potential anti-cancer therapy, clinical trials with Cilengitide have not shown extraordinary results (Stupp and Rugg 2007). This could be attributed to the recent findings demonstrating that $\alpha v\beta 3$ inhibition can be pro-invasive (Caswell, Chan et al. 2008) and can stimulate angiogenesis and tumour growth (Reynolds, Hart et al. 2009). This dichotomy in Cilengitide's effect is thought to depend on the dose of this compound, and concentrations capable of blocking angiogenesis are much higher than those that enhance tumour growth and angiogenesis (Reynolds, Hart et al. 2009). Moreover, Cilengitide has been shown to drive the coordinate recycling of $\alpha 5\beta 1$ and EGFR, which potentiates EGFR-mediated signalling and drives invasive migration of cancer cells (Caswell, Chan et al. 2008). This could suggest that the application of $\alpha v\beta 3$ blocking agents would be beneficial but only in combination with regimens that target EGFR.

The above reports of context-dependent efficacy of integrin blocking agents and the failures of integrin antagonists in clinical trials call for the determination of expression signature of individual tumours, which would help in assigning the most suitable therapeutic regimen for a particular individual. In that respect, CLIC3 may provide a powerful tool for the identification of patients that would benefit from integrin-targeting therapies.

7 Appendices

Gene Symbol	Gene Title
GDA	guanine deaminase
FKBP1B	FK506 binding protein 1B, 12.6 kDa
SULF2	sulfatase 2
FN1	fibronectin 1
NMNAT2	nicotinamide nucleotide adenylyltransferase 2
KCNK3	potassium channel, subfamily K, member 3
ODZ2	odz, odd Oz/ten-m homolog 2 (Drosophila)
EDNRA	endothelin receptor type A
AJAP1	adherens junctions associated protein 1
PTGS2	prostaglandin-endoperoxide synthase 2 (prostaglandin G/H synthase and cyclooxyge
UCA1	urothelial cancer associated 1 (non-protein coding)
NMNAT2	nicotinamide nucleotide adenylyltransferase 2
CARD16	caspase recruitment domain family, member 16
GSTT1	glutathione S-transferase theta 1
SSPN	sarcospan (Kras oncogene-associated gene)
CPS1	carbamoyl-phosphate synthetase 1, mitochondrial
AJAP1	adherens junctions associated protein 1
MT1M	metallothionein 1M
HTRA1	HtrA serine peptidase 1
BEX5	brain expressed, X-linked 5
MSLN	mesothelin
DNAJC10	DnaJ (Hsp40) homolog, subfamily C, member 10
SULF2	sulfatase 2
THSD4	thrombospondin, type I, domain containing 4
NLRC3	NLR family, CARD domain containing 3
ADAMT5	ADAM metalloproteinase with thrombospondin type 1 motif, 5
DCDC2	doublecortin domain containing 2
SLC16A6	solute carrier family 16, member 6 (monocarboxylic acid transporter 7)
CLIC3	chloride intracellular channel 3
AHNAK2	AHNAK nucleoprotein 2
NMNAT2	nicotinamide nucleotide adenylyltransferase 2
CHCHD5	coiled-coil-helix-coiled-coil-helix domain containing 5
PLA2G4A	phospholipase A2, group IVA (cytosolic, calcium-dependent)
PRKCQ	protein kinase C, theta
CDC42EP5	CDC42 effector protein (Rho GTPase binding) 5
MYO5C	myosin VC
ALDH6A1	aldehyde dehydrogenase 6 family, member A1
LPAR5	lysophosphatidic acid receptor 5
ADAMT5	ADAM metalloproteinase with thrombospondin type 1 motif, 5
GLT8D2	glycosyltransferase 8 domain containing 2
AHSA2	AHA1, activator of heat shock 90kDa protein ATPase homolog 2 (yeast)
KCNK3	potassium channel, subfamily K, member 3
DSP	desmoplakin
GPRASP2	G protein-coupled receptor associated sorting protein 2
ZNF395	zinc finger protein 395
TRIM2	tripartite motif-containing 2
C1orf25	chromosome 1 open reading frame 25
GRK5	G protein-coupled receptor kinase 5

Appendix 3.1 Genes differentially expressed in Rab25-expressing cells when plated onto CDM.

Gene names corresponding to gene symbols of transcripts differentially expressed in A2780-Rab25 cells as compared to A2780-DNA3 cells after both were seeded onto three dimensional cell derived matrices (CDM), as previously shown in figure 3.5 On the left listed are gene symbols, on the right are corresponding gene names.

Gene Symbol	Gene Title
F11R	F11 receptor
DNAJC10	Dnaj (Hsp40) homolog, subfamily C, member 10
EDNRA	endothelin receptor type A
CCND2	cyclin D2
LOC100132815	Hypothetical protein LOC100132815
FBLN7	fibulin 7
F8	coagulation factor VIII, procoagulant component
FGFBP1	fibroblast growth factor binding protein 1
CDH5	cadherin 5, type 2 (vascular endothelium)
PRDX2	peroxiredoxin 2
DCLK1	Doublecortin-like kinase 1
PLXNA2	plexin A2
C10orf58	chromosome 10 open reading frame 58
ACSS3	acyl-CoA synthetase short-chain family member 3
ADAMT55	ADAM metalloproteinase with thrombospondin type 1 motif, 5
GPNMB	glycoprotein (transmembrane) nmb
EDIL3	EGF-like repeats and discoidin I-like domains 3
PQLC3	PQ loop repeat containing 3
SYTL1	synaptotagmin-like 1
F2RL1	coagulation factor II (thrombin) receptor-like 1
ZFP90	zinc finger protein 90 homolog (mouse)
FAM129A	family with sequence similarity 129, member A
KIAA1324	KIAA1324
ZFP90	zinc finger protein 90 homolog (mouse)
KCNJ2	potassium inwardly-rectifying channel, subfamily J, member 2
C10orf58	chromosome 10 open reading frame 58
TP53INP1	tumor protein p53 inducible nuclear protein 1
PPAPDC2	phosphatidic acid phosphatase type 2 domain containing 2
EFEMP2	EGF-containing fibulin-like extracellular matrix protein 2
FAM49A	family with sequence similarity 49, member A
IL12A	interleukin 12A (natural killer cell stimulatory factor 1, cytotoxic lymphocyte
BIRC3	baculoviral IAP repeat-containing 3
TIMP3	TIMP metalloproteinase inhibitor 3
IGDCC4	immunoglobulin superfamily, DCC subclass, member 4
RAGE	renal tumor antigen
IL13RA2	interleukin 13 receptor, alpha 2
BMPRI1B	bone morphogenetic protein receptor, type IB
PTPRR	protein tyrosine phosphatase, receptor type, R
SLIT2	slit homolog 2 (Drosophila)
ITPR1	inositol 1,4,5-triphosphate receptor, type 1
PTPRR	protein tyrosine phosphatase, receptor type, R
GDF15 /// LOC100292463	growth differentiation factor 15 /// similar to growth differentiation factor 15
TGFB2	transforming growth factor, beta 2
PAG1	phosphoprotein associated with glycosphingolipid microdomains 1
DENND2D	DENN/MADD domain containing 2D
TIMP3	TIMP metalloproteinase inhibitor 3
LXN	latexin
AFF3	AF4/FMR2 family, member 3
S1PR3	sphingosine-1-phosphate receptor 3
TIMP3	TIMP metalloproteinase inhibitor 3
CDCP1	CUB domain containing protein 1
TIMP3	TIMP metalloproteinase inhibitor 3

Appendix 3.2 Genes differentially expressed in Rab25-expressing cells when plated onto CDM.

Continuation of Appendix 3.1.

Gene Symbol	Gene Title
GDA	guanine deaminase
RAB25	RAB25, member RAS oncogene family
FKBP1B	FK506 binding protein 1B, 12.6 kDa
FGFBP1	fibroblast growth factor binding protein 1
ODZ2	odz, odd Oz/ten-m homolog 2 (Drosophila)
UCA1	urothelial cancer associated 1 (non-protein coding)
NFATC2	Nuclear factor of activated T-cells, cytoplasmic, calcineurin-dependent 2
ST6GALNAC5	ST6 (alpha-N-acetyl-neuraminy-2,3-beta-galactosyl-1,3)-N-acetylgalactosaminide
CHCHD5	coiled-coil-helix-coiled-coil-helix domain containing 5
KCNK3	potassium channel, subfamily K, member 3
CCND2	cyclin D2
NMNAT2	nicotinamide nucleotide adenylyltransferase 2
CRIP1	cysteine-rich protein 1 (intestinal)
CDC42EP5	CDC42 effector protein (Rho GTPase binding) 5
DSP	desmoplakin
BEX5	brain expressed, X-linked 5
DCDC2	doublecortin domain containing 2
SULF2	sulfatase 2
MYO5C	myosin VC
NMNAT2	nicotinamide nucleotide adenylyltransferase 2
AHA2	AHA1, activator of heat shock 90kDa protein ATPase homolog 2 (yeast)
LOC100132815	Hypothetical protein LOC100132815
DNAJC10	DnaJ (Hsp40) homolog, subfamily C, member 10
PRDX2	peroxiredoxin 2
PLA2G4A	phospholipase A2, group IVA (cytosolic, calcium-dependent)
FAM129A	family with sequence similarity 129, member A
NMNAT2	nicotinamide nucleotide adenylyltransferase 2
CARD16	caspase recruitment domain family, member 16
LPXN	leupaxin
RGS4	regulator of G-protein signaling 4
IFI44	interferon-induced protein 44
TGFB2	transforming growth factor, beta 2
ITPR1	inositol 1,4,5-triphosphate receptor, type 1
TIMP3	TIMP metalloproteinase inhibitor 3
FBXO32	F-box protein 32
ARRDC3	arrestin domain containing 3
COL6A3	collagen, type VI, alpha 3
LRIG1	leucine-rich repeats and immunoglobulin-like domains 1
CXCL1	chemokine (C-X-C motif) ligand 1 (melanoma growth stimulating activity, alpha)
STC1	stanniocalcin 1
RGS4	regulator of G-protein signaling 4
HIP1	Huntingtin interacting protein 1
NF-E4	transcription factor NF-E4
PNMA2	paraneoplastic antigen MA2
CD163L1	CD163 molecule-like 1
DENND2D	DENN/MADD domain containing 2D
IGDCC4	immunoglobulin superfamily, DCC subclass, member 4
CYP2J2	cytochrome P450, family 2, subfamily J, polypeptide 2

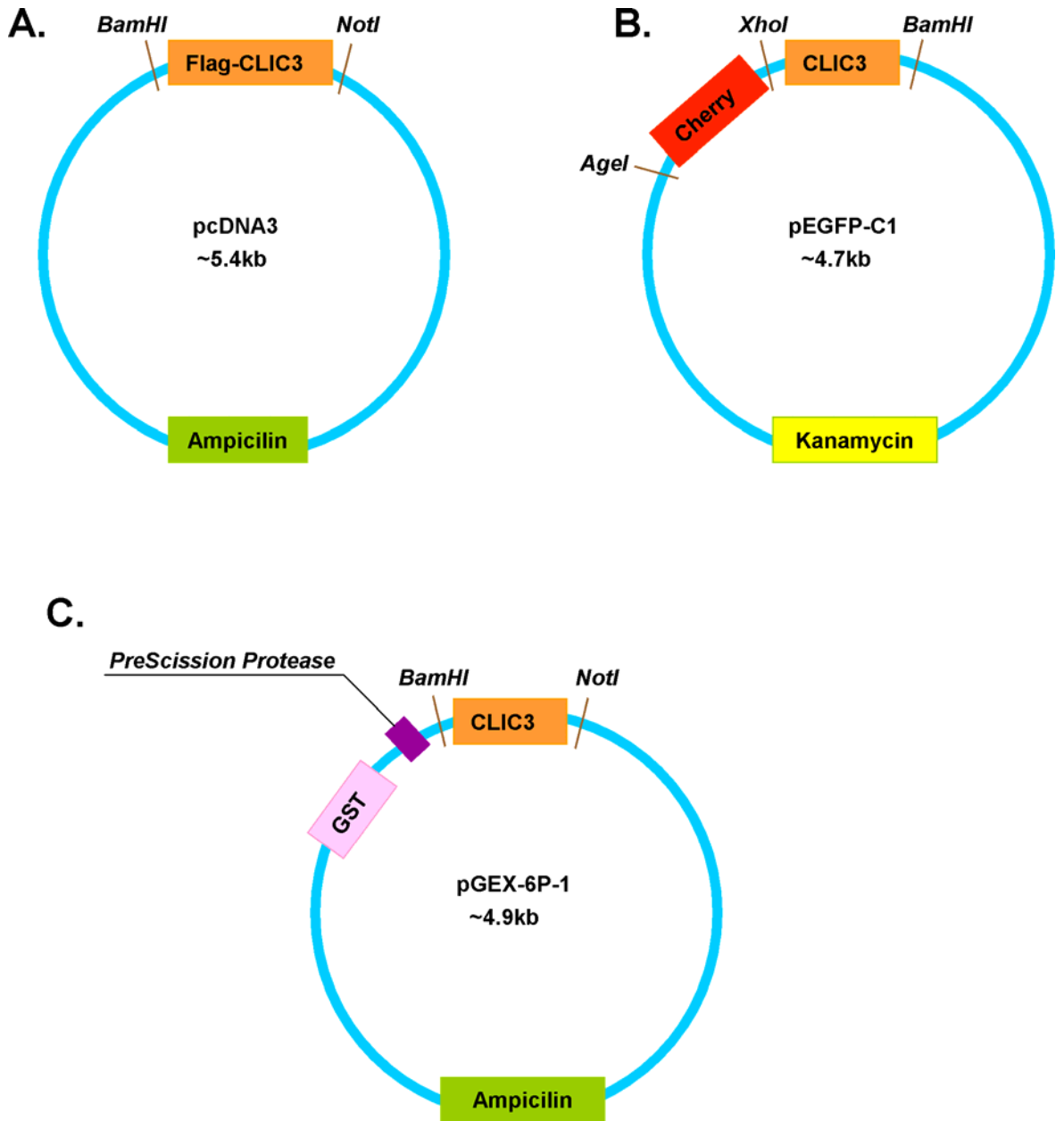
Appendix 3.3 Genes differentially expressed in Rab25-expressing cells when plated onto plastic surface.

Gene names matching the gene symbols of transcripts whose expression is regulated by Rab25 on plastic, as previously shown in figure 3.6. Gene symbols are listed on the left and corresponding gene names are on the right.

Gene Symbol	Gene Title
COL5A1	collagen, type V, alpha 1
STC1	stanniocalcin 1
RNF182	ring finger protein 182
IL13RA2	interleukin 13 receptor, alpha 2
PAG1	phosphoprotein associated with glycosphingolipid microdomains 1
LOC100288985	hypothetical protein LOC100288985
CXCL3	chemokine (C-X-C motif) ligand 3
TGFB2	transforming growth factor, beta 2
TGFB2	transforming growth factor, beta 2
LXN	latexin
GDF15 /// LOC100292463	growth differentiation factor 15 /// similar to growth differentiation factor 15
S1PR3	sphingosine-1-phosphate receptor 3
TIMP3	TIMP metalloproteinase inhibitor 3
AFF3	AF4/FMR2 family, member 3
TIMP3	TIMP metalloproteinase inhibitor 3
CDCP1	CUB domain containing protein 1

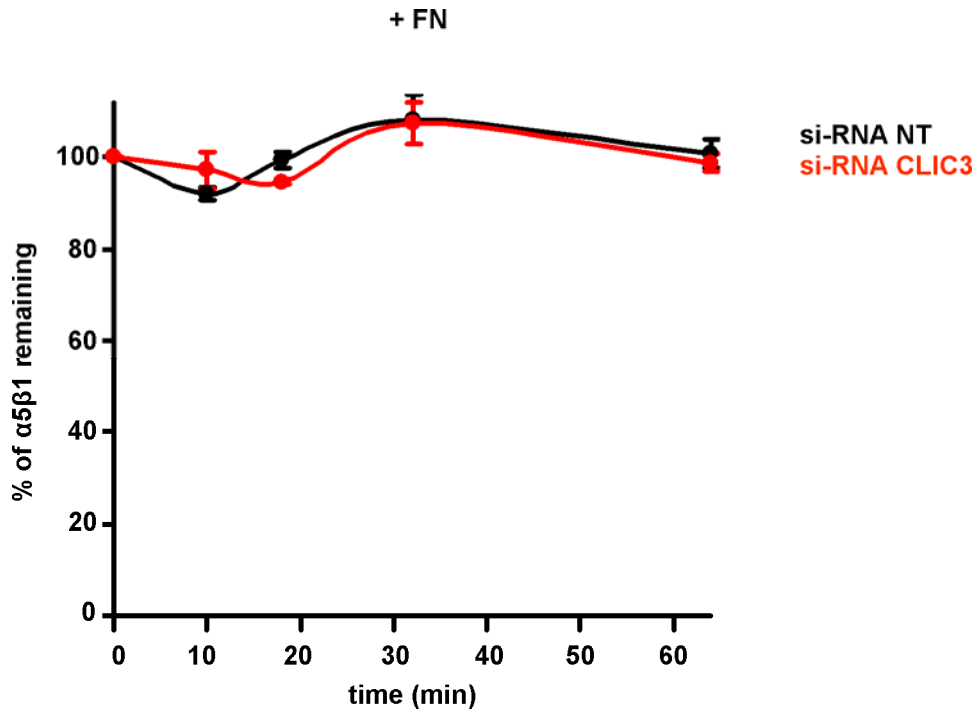
Appendix 3.4 Genes differentially expressed in Rab25-expressing cells when plated onto plastic surface.

Continuation of Appendix 3.3.



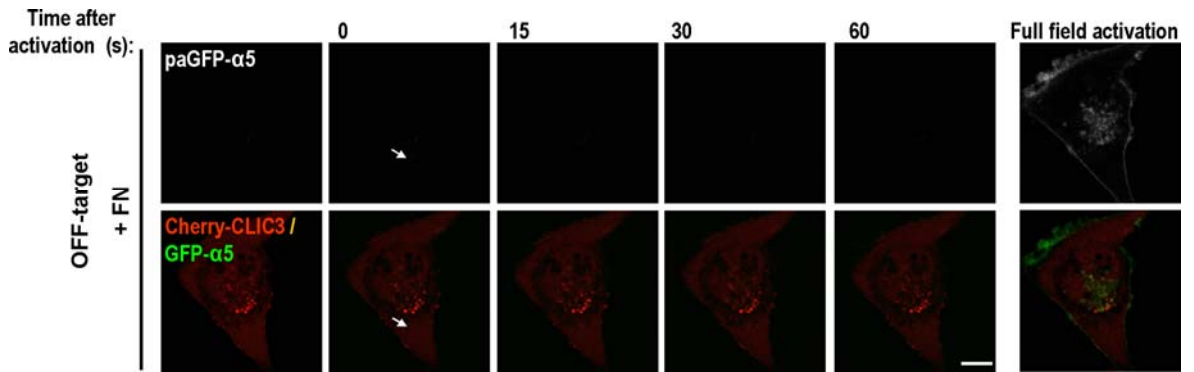
Appendix 4.1 CLIC3 expression vectors.

A. Flag-CLIC3 B. Cherry-CLIC3 C. GST-CLIC3



Appendix 4.2 $\alpha 5 \beta 1$ integrin pool is not degraded in A2780-Rab25 cells.

A2780-Rab25 cells were surface-labelled with 0.2mg/ml NHS-S-S-Biotin at 4°C and internalisation then allowed to proceed for 30 min at 37°C in the presence of 2.5 μ g/ml fibronectin. Biotin remaining at the cell surface was removed by exposure to MesNa at 4°C, then the cells were incubated for the indicated times at 37°C. The quantity of biotinylated receptor remaining within the cells was determined by capture-ELISA using microtitre wells coated with antibodies recognising $\alpha 5$.



Appendix 4.3 Photoactivation of $\alpha 5\beta 1$ in a region lacking CLIC3 vesicles.

A2780-Rab25 cells were co-transfected with 1.2 μ g of Cherry-CLIC3 and 4.8 μ g of photoactivatable wild type $\alpha 5$ integrin; paGFP- $\alpha 5$. 2.5 μ g/ml of soluble fibronectin (FN) was used for 1.5 hours prior to photoactivation to increase colocalisation between CLIC3 and $\alpha 5$ integrin. Photoactivation was performed with 405nm laser aimed at CLIC3-negative regions, as indicated by the white arrows. Images were then captured with a confocal microscope every 2 seconds over a period of 120 seconds. Movies were generated from these time-lapse images and stills corresponding to individual frames from a representative movie are presented. These include a frame prior to photoactivation, one immediately after photoactivation (0 sec) and subsequent ones at 15 second intervals after photoactivation, as well as full field activation that illuminates total pool of $\alpha 5$ integrin. Top panel shows $\alpha 5$ integrin in grey, bottom panel depicts merged images with $\alpha 5$ in green and CLIC3 in red. Scale bar, 10 μ m.

	Protein Name
1	Chloride intracellular channel protein 3
2	Matrin-3
3	RNA-binding protein 14
4	Nuclear pore complex protein Nup153
5	Tyrosine-protein phosphatase non-receptor type 14
6	Heterogeneous nuclear ribonucleoprotein U
7	Vinculin
8	Probable ATP-dependent RNA helicase DDX17
9	Transketolase
10	ATP-dependent RNA helicase DDX3X
11	Non-POU domain-containing octamer-binding protein
12	Protein-glutamine gamma-glutamyltransferase 2
13	6-phosphofructokinase type C
14	Fructose-bisphosphate aldolase A
15	Heterogeneous nuclear ribonucleoprotein A1
16	Importin subunit beta-1
17	Exportin-2
18	T-complex protein 1 subunit beta
19	L-lactate dehydrogenase A chain
20	Polypyrimidine tract-binding protein 1
21	Nuclear fragile X mental retardation-interacting protein 2
22	60S ribosomal protein L27a
23	Constitutive coactivator of PPAR-gamma-like protein 1
24	Transcription intermediary factor 1-beta
25	Src substrate cortactin
26	LIM and SH3 domain protein 1
27	Rho GTPase-activating protein 29
28	T-complex protein 1 subunit alpha
29	Probable ATP-dependent RNA helicase DDX5
30	Ataxin-2-like protein
31	60S ribosomal protein L8
32	Prohibitin
33	Programmed cell death protein 10
34	Triosephosphate isomerase
35	SNW domain-containing protein 1
36	14-3-3 protein epsilon
37	Protein BAT2-like
38	CDKN2A-interacting protein
39	Guanine nucleotide-binding protein subunit beta-2-like 1
40	Dolichyl-diphosphooligosaccharide--protein glycosyltransferase subunit 1
41	Transgelin-2
42	Histone H1.4
43	U3 small nucleolar RNA-associated protein 14 homolog A
44	T-complex protein 1 subunit gamma
45	EH domain-containing protein 4

Appendix 6.1 Proteins identified to interact with CLIC3 by mass spectrometry.

Protein names correspond to gene symbols listed in Figure 6.2.

8 Bibliography

- Almeida, E. A., A. P. Huovila, et al. (1995). "Mouse egg integrin alpha 6 beta 1 functions as a sperm receptor." *Cell* 81(7): 1095-104.
- Almeida, E. A., D. Ilic, et al. (2000). "Matrix survival signaling: from fibronectin via focal adhesion kinase to c-Jun NH(2)-terminal kinase." *J Cell Biol* 149(3): 741-54.
- Almoguera, C., D. Shibata, et al. (1988). "Most human carcinomas of the exocrine pancreas contain mutant c-K-ras genes." *Cell* 53(4): 549-54.
- Andre, F., N. E. Scharz, et al. (2002). "Malignant effusions and immunogenic tumour-derived exosomes." *Lancet* 360(9329): 295-305.
- Arezi, B., W. Xing, et al. (2003). "Amplification efficiency of thermostable DNA polymerases." *Anal Biochem* 321(2): 226-35.
- Arighi, C. N., L. M. Hartnell, et al. (2004). "Role of the mammalian retromer in sorting of the cation-independent mannose 6-phosphate receptor." *J Cell Biol* 165(1): 123-33.
- Assoian, R. K. (1997). "Anchorage-dependent cell cycle progression." *J Cell Biol* 136(1): 1-4.
- Baker, E. K., E. C. Tozer, et al. (1997). "A genetic analysis of integrin function: Glanzmann thrombasthenia in vitro." *Proc Natl Acad Sci U S A* 94(5): 1973-8.
- Balzac, F., A. M. Belkin, et al. (1993). "Expression and functional analysis of a cytoplasmic domain variant of the beta 1 integrin subunit." *J Cell Biol* 121(1): 171-8.
- Barry, W. T., C. Boudignon-Proudhon, et al. (2002). "Molecular basis of CIB binding to the integrin alpha IIb cytoplasmic domain." *J Biol Chem* 277(32): 28877-83.
- Bass, M. D., M. R. Morgan, et al. (2008). "p190RhoGAP is the convergence point of adhesion signals from alpha 5 beta 1 integrin and syndecan-4." *J Cell Biol* 181(6): 1013-26.
- Bass, M. D., K. A. Roach, et al. (2007). "Syndecan-4-dependent Rac1 regulation determines directional migration in response to the extracellular matrix." *J Cell Biol* 177(3): 527-38.
- Bernacki, R. J., M. J. Niedbala, et al. (1985). "Glycosidases in cancer and invasion." *Cancer Metastasis Rev* 4(1): 81-101.
- Bernards, A. and J. Settleman (2004). "GAP control: regulating the regulators of small GTPases." *Trends Cell Biol* 14(7): 377-85.
- Berry, K. L., H. E. Bulow, et al. (2003). "A C. elegans CLIC-like protein required for intracellular tube formation and maintenance." *Science* 302(5653): 2134-7.
- Berry, K. L. and O. Hobert (2006). "Mapping functional domains of chloride intracellular channel (CLIC) proteins in vivo." *J Mol Biol* 359(5): 1316-33.
- Berryman, M., J. Bruno, et al. (2004). "CLIC-5A functions as a chloride channel in vitro and associates with the cortical actin cytoskeleton in vitro and in vivo." *J Biol Chem* 279(33): 34794-801.
- Berryman, M. A. and J. R. Goldenring (2003). "CLIC4 is enriched at cell-cell junctions and colocalizes with AKAP350 at the centrosome and midbody of cultured mammalian cells." *Cell Motil Cytoskeleton* 56(3): 159-72.
- Board, P. G., M. Coggan, et al. (2004). "CLIC-2 modulates cardiac ryanodine receptor Ca²⁺ release channels." *Int J Biochem Cell Biol* 36(8): 1599-612.
- Bohman, S., T. Matsumoto, et al. (2005). "Proteomic analysis of vascular endothelial growth factor-induced endothelial cell differentiation reveals a role for chloride intracellular channel 4 (CLIC4) in tubular morphogenesis." *J Biol Chem* 280(51): 42397-404.
- Bolstad, B. M., R. A. Irizarry, et al. (2003). "A comparison of normalization methods for high density oligonucleotide array data based on variance and bias." *Bioinformatics* 19(2): 185-93.
- Bonifacino, J. S. and J. H. Hurley (2008). "Retromer." *Curr Opin Cell Biol* 20(4): 427-36.
- Bos, P. D., X. H. Zhang, et al. (2009). "Genes that mediate breast cancer metastasis to the brain." *Nature* 459(7249): 1005-9.

- Bowden, M. A., L. A. Di Nezza-Cossens, et al. (2006). "Serine proteases HTRA1 and HTRA3 are down-regulated with increasing grades of human endometrial cancer." *Gynecol Oncol* 103(1): 253-60.
- Bretscher, M. S. (1989). "Endocytosis and recycling of the fibronectin receptor in CHO cells." *EMBO J* 8(5): 1341-8.
- Bretscher, M. S. (1996). "Moving membrane up to the front of migrating cells." *Cell* 85(4): 465-7.
- Briesewitz, R., A. Kern, et al. (1995). "Assembly and function of integrin receptors is dependent on opposing alpha and beta cytoplasmic domains." *Mol Biol Cell* 6(8): 997-1010.
- Brooks, P. C., R. A. Clark, et al. (1994). "Requirement of vascular integrin alpha v beta 3 for angiogenesis." *Science* 264(5158): 569-71.
- Brunton, V. G. and M. C. Frame (2008). "Src and focal adhesion kinase as therapeutic targets in cancer." *Curr Opin Pharmacol* 8(4): 427-32.
- Calderwood, D. A., Y. Fujioka, et al. (2003). "Integrin beta cytoplasmic domain interactions with phosphotyrosine-binding domains: a structural prototype for diversity in integrin signaling." *Proc Natl Acad Sci U S A* 100(5): 2272-7.
- Calderwood, D. A., B. Yan, et al. (2002). "The phosphotyrosine binding-like domain of talin activates integrins." *J Biol Chem* 277(24): 21749-58.
- Calhoun, B. C. and J. R. Goldenring (1997). "Two Rab proteins, vesicle-associated membrane protein 2 (VAMP-2) and secretory carrier membrane proteins (SCAMPs), are present on immunoisolated parietal cell tubulovesicles." *Biochem J* 325 (Pt 2): 559-64.
- Camp, R. L., V. Neumeister, et al. (2008). "A decade of tissue microarrays: progress in the discovery and validation of cancer biomarkers." *J Clin Oncol* 26(34): 5630-7.
- Cary, L. A., D. C. Han, et al. (1998). "Identification of p130Cas as a mediator of focal adhesion kinase-promoted cell migration." *J Cell Biol* 140(1): 211-21.
- Casanova, J. E., X. Wang, et al. (1999). "Association of Rab25 and Rab11a with the apical recycling system of polarized Madin-Darby canine kidney cells." *Mol Biol Cell* 10(1): 47-61.
- Caswell, P. T., M. Chan, et al. (2008). "Rab-coupling protein coordinates recycling of alpha5beta1 integrin and EGFR1 to promote cell migration in 3D microenvironments." *J Cell Biol* 183(1): 143-55.
- Caswell, P. T., H. J. Spence, et al. (2007). "Rab25 associates with alpha5beta1 integrin to promote invasive migration in 3D microenvironments." *Dev Cell* 13(4): 496-510.
- Caswell, P. T., S. Vadrevu, et al. (2009). "Integrins: masters and slaves of endocytic transport." *Nat Rev Mol Cell Biol* 10(12): 843-53.
- Chang, D. D., B. Q. Hoang, et al. (2002). "Molecular basis for interaction between Icap1 alpha PTB domain and beta 1 integrin." *J Biol Chem* 277(10): 8140-5.
- Chang, Y. H., C. C. Wu, et al. (2009). "Cell secretome analysis using hollow fiber culture system leads to the discovery of CLIC1 protein as a novel plasma marker for nasopharyngeal carcinoma." *J Proteome Res* 8(12): 5465-74.
- Chao, W. T. and J. Kunz (2009). "Focal adhesion disassembly requires clathrin-dependent endocytosis of integrins." *FEBS Lett* 583(8): 1337-43.
- Chavrier, P., R. G. Parton, et al. (1990). "Localization of low molecular weight GTP binding proteins to exocytic and endocytic compartments." *Cell* 62(2): 317-29.
- Chen, C. D., C. S. Wang, et al. (2007). "Overexpression of CLIC1 in human gastric carcinoma and its clinicopathological significance." *Proteomics* 7(1): 155-67.
- Chen, G., T. G. Gharib, et al. (2002). "Discordant protein and mRNA expression in lung adenocarcinomas." *Mol Cell Proteomics* 1(4): 304-13.
- Chen, H. C. and J. L. Guan (1994). "Association of focal adhesion kinase with its potential substrate phosphatidylinositol 3-kinase." *Proc Natl Acad Sci U S A* 91(21): 10148-52.
- Chen, W. J., J. L. Goldstein, et al. (1990). "NPXY, a sequence often found in cytoplasmic tails, is required for coated pit-mediated internalization of the low density lipoprotein receptor." *J Biol Chem* 265(6): 3116-23.

- Cheng, J. M., M. Ding, et al. (2006). "Loss of RAB25 expression in breast cancer." Int J Cancer 118(12): 2957-64.
- Cheng, J. M., L. Volk, et al. "Tumor suppressor function of Rab25 in triple-negative breast cancer." Int J Cancer 126(12): 2799-812.
- Cheng, K. W., J. P. Lahad, et al. (2004). "The RAB25 small GTPase determines aggressiveness of ovarian and breast cancers." Nat Med 10(11): 1251-6.
- Chetrit, D., N. Ziv, et al. (2009). "Dab2 regulates clathrin assembly and cell spreading." Biochem J 418(3): 701-15.
- Chien, J., J. Staub, et al. (2004). "A candidate tumor suppressor HtrA1 is downregulated in ovarian cancer." Oncogene 23(8): 1636-44.
- Christofori, G. and H. Semb (1999). "The role of the cell-adhesion molecule E-cadherin as a tumour-suppressor gene." Trends Biochem Sci 24(2): 73-6.
- Coleman, M. L., C. J. Marshall, et al. (2003). "Ras promotes p21(Waf1/Cip1) protein stability via a cyclin D1-imposed block in proteasome-mediated degradation." EMBO J 22(9): 2036-46.
- Colicelli, J. (2004). "Human RAS superfamily proteins and related GTPases." Sci STKE 2004(250): RE13.
- Conner, S. D. and S. L. Schmid (2003). "Regulated portals of entry into the cell." Nature 422(6927): 37-44.
- Coppola, D. (2000). "Molecular prognostic markers in pancreatic cancer." Cancer Control 7(5): 421-7.
- Cowan, K. J., D. A. Law, et al. (2000). "Identification of shc as the primary protein binding to the tyrosine-phosphorylated beta 3 subunit of alpha IIb beta 3 during outside-in integrin platelet signaling." J Biol Chem 275(46): 36423-9.
- Criscuoli, M. L., M. Nguyen, et al. (2005). "Tumor metastasis but not tumor growth is dependent on Src-mediated vascular permeability." Blood 105(4): 1508-14.
- Cromer, B. A., M. A. Gorman, et al. (2007). "Structure of the Janus protein human CLIC2." J Mol Biol 374(3): 719-31.
- Cukierman, E., R. Pankov, et al. (2001). "Taking cell-matrix adhesions to the third dimension." Science 294(5547): 1708-12.
- Daaka, Y., L. M. Luttrell, et al. (1998). "Essential role for G protein-coupled receptor endocytosis in the activation of mitogen-activated protein kinase." J Biol Chem 273(2): 685-8.
- Danen, E. H., J. van Rheenen, et al. (2005). "Integrins control motile strategy through a Rho-cofilin pathway." J Cell Biol 169(3): 515-26.
- Davidson, B., Z. Zhang, et al. (2006). "Gene expression signatures differentiate ovarian/peritoneal serous carcinoma from diffuse malignant peritoneal mesothelioma." Clin Cancer Res 12(20 Pt 1): 5944-50.
- de Melker, A. A. and A. Sonnenberg (1999). "Integrins: alternative splicing as a mechanism to regulate ligand binding and integrin signaling events." Bioessays 21(6): 499-509.
- DeMali, K. A., C. A. Barlow, et al. (2002). "Recruitment of the Arp2/3 complex to vinculin: coupling membrane protrusion to matrix adhesion." J Cell Biol 159(5): 881-91.
- Demircan, K., E. Gunduz, et al. (2009). "Increased mRNA expression of ADAMTS metalloproteinases in metastatic foci of head and neck cancer." Head Neck 31(6): 793-801.
- Di Guglielmo, G. M., P. C. Baass, et al. (1994). "Compartmentalization of SHC, GRB2 and mSOS, and hyperphosphorylation of Raf-1 by EGF but not insulin in liver parenchyma." EMBO J 13(18): 4269-77.
- Dulhunty, A., P. Gage, et al. (2001). "The glutathione transferase structural family includes a nuclear chloride channel and a ryanodine receptor calcium release channel modulator." J Biol Chem 276(5): 3319-23.
- Echtermeyer, F., J. Bertrand, et al. (2009). "Syndecan-4 regulates ADAMTS-5 activation and cartilage breakdown in osteoarthritis." Nat Med 15(9): 1072-6.
- Edwards, J. C., C. Cohen, et al. (2006). "c-Src control of chloride channel support for osteoclast HCl transport and bone resorption." J Biol Chem 281(38): 28011-22.

- Elkin, M. and I. Vlodavsky (2001). "Tail vein assay of cancer metastasis." Curr Protoc Cell Biol Chapter 19: Unit 19 2.
- Emsley, J., C. G. Knight, et al. (2000). "Structural basis of collagen recognition by integrin alpha2beta1." Cell 101(1): 47-56.
- Escola, J. M., M. J. Kleijmeer, et al. (1998). "Selective enrichment of tetraspan proteins on the internal vesicles of multivesicular endosomes and on exosomes secreted by human B-lymphocytes." J Biol Chem 273(32): 20121-7.
- Even-Ram, S. and K. M. Yamada (2005). "Cell migration in 3D matrix." Curr Opin Cell Biol 17(5): 524-32.
- Fan, Y., X. Y. Xin, et al. (2006). "Knockdown of RAB25 expression by RNAi inhibits growth of human epithelial ovarian cancer cells in vitro and in vivo." Pathology 38(6): 561-7.
- Fassler, R., J. Rohwedel, et al. (1996). "Differentiation and integrity of cardiac muscle cells are impaired in the absence of beta 1 integrin." J Cell Sci 109 (Pt 13): 2989-99.
- Fernandez-Salas, E., K. S. Suh, et al. (2002). "mtCLIC/CLIC4, an organellar chloride channel protein, is increased by DNA damage and participates in the apoptotic response to p53." Mol Cell Biol 22(11): 3610-20.
- Fevrier, B., D. Vilette, et al. (2004). "Cells release prions in association with exosomes." Proc Natl Acad Sci U S A 101(26): 9683-8.
- Fincham, V. J., M. Unlu, et al. (1996). "Translocation of Src kinase to the cell periphery is mediated by the actin cytoskeleton under the control of the Rho family of small G proteins." J Cell Biol 135(6 Pt 1): 1551-64.
- Fornaro, M., G. Tallini, et al. (1996). "Down-regulation of beta 1C integrin, an inhibitor of cell proliferation, in prostate carcinoma." Am J Pathol 149(3): 765-73.
- Frank, D. J., T. Noguchi, et al. (2004). "Myosin VI: a structural role in actin organization important for protein and organelle localization and trafficking." Curr Opin Cell Biol 16(2): 189-94.
- Frasa, M. A., F. C. Maximiano, et al. "Arms is a Rac1 effector that inactivates Rab7 and regulates E-cadherin degradation." Curr Biol 20(3): 198-208.
- Friedl, P. and K. Wolf (2003). "Tumour-cell invasion and migration: diversity and escape mechanisms." Nat Rev Cancer 3(5): 362-74.
- Friedl, P. and K. Wolf (2008). "Tube travel: the role of proteases in individual and collective cancer cell invasion." Cancer Res 68(18): 7247-9.
- Friedlander, M., P. C. Brooks, et al. (1995). "Definition of two angiogenic pathways by distinct alpha v integrins." Science 270(5241): 1500-2.
- Friedli, M., M. Guipponi, et al. (2003). "Identification of a novel member of the CLIC family, CLIC6, mapping to 21q22.12." Gene 320: 31-40.
- Gaggioli, C., S. Hooper, et al. (2007). "Fibroblast-led collective invasion of carcinoma cells with differing roles for RhoGTPases in leading and following cells." Nat Cell Biol 9(12): 1392-400.
- Garcia-Alvarez, B., J. M. de Pereda, et al. (2003). "Structural determinants of integrin recognition by talin." Mol Cell 11(1): 49-58.
- Gillette, J. M., A. Larochelle, et al. (2009). "Intercellular transfer to signalling endosomes regulates an ex vivo bone marrow niche." Nat Cell Biol 11(3): 303-11.
- Goh, L. K., F. Huang, et al. "Multiple mechanisms collectively regulate clathrin-mediated endocytosis of the epidermal growth factor receptor." J Cell Biol 189(5): 871-83.
- Goldenring, J. R., K. R. Shen, et al. (1993). "Identification of a small GTP-binding protein, Rab25, expressed in the gastrointestinal mucosa, kidney, and lung." J Biol Chem 268(25): 18419-22.
- Goodchild, S. C., M. W. Howell, et al. "Metamorphic response of the CLIC1 chloride intracellular ion channel protein upon membrane interaction." Biochemistry 49(25): 5278-89.
- Goodman, S. L., G. Holzemann, et al. (2002). "Nanomolar small molecule inhibitors for alpha v(beta)6, alpha v(beta)5, and alpha v(beta)3 integrins." J Med Chem 45(5): 1045-51.

- Gottschalk, K. E. (2005). "A coiled-coil structure of the α 5 β 3 integrin transmembrane and cytoplasmic domains in its resting state." *Structure* 13(5): 703-12.
- Gould, G. W. and J. Lippincott-Schwartz (2009). "New roles for endosomes: from vesicular carriers to multi-purpose platforms." *Nat Rev Mol Cell Biol* 10(4): 287-92.
- Grimes, M. L., J. Zhou, et al. (1996). "Endocytosis of activated TrkA: evidence that nerve growth factor induces formation of signaling endosomes." *J Neurosci* 16(24): 7950-64.
- Gromov, P., I. Gromova, et al. "Up-regulated proteins in the fluid bathing the tumour cell microenvironment as potential serological markers for early detection of cancer of the breast." *Mol Oncol* 4(1): 65-89.
- Grovdal, L. M., E. Stang, et al. (2004). "Direct interaction of Cbl with pTyr 1045 of the EGF receptor (EGFR) is required to sort the EGFR to lysosomes for degradation." *Exp Cell Res* 300(2): 388-95.
- Guhaniyogi, J. and G. Brewer (2001). "Regulation of mRNA stability in mammalian cells." *Gene* 265(1-2): 11-23.
- Gupta, G. P. and J. Massague (2006). "Cancer metastasis: building a framework." *Cell* 127(4): 679-95.
- Hanahan, D. and R. A. Weinberg (2000). "The hallmarks of cancer." *Cell* 100(1): 57-70.
- Hannigan, G. E., C. Leung-Hagesteijn, et al. (1996). "Regulation of cell adhesion and anchorage-dependent growth by a new β 1-integrin-linked protein kinase." *Nature* 379(6560): 91-6.
- Harrop, S. J., M. Z. DeMaere, et al. (2001). "Crystal structure of a soluble form of the intracellular chloride ion channel CLIC1 (NCC27) at 1.4-Å resolution." *J Biol Chem* 276(48): 44993-5000.
- Haugh, J. M. and T. Meyer (2002). "Active EGF receptors have limited access to PtdIns(4,5)P₂ in endosomes: implications for phospholipase C and PI 3-kinase signaling." *J Cell Sci* 115(Pt 2): 303-10.
- Hayashi, Y., B. Haimovich, et al. (1990). "Expression and function of chicken integrin β 1 subunit and its cytoplasmic domain mutants in mouse NIH 3T3 cells." *J Cell Biol* 110(1): 175-84.
- Heath, J. K., S. J. White, et al. (1997). "The human A33 antigen is a transmembrane glycoprotein and a novel member of the immunoglobulin superfamily." *Proc Natl Acad Sci U S A* 94(2): 469-74.
- Hegmans, J. P., M. P. Bard, et al. (2004). "Proteomic analysis of exosomes secreted by human mesothelioma cells." *Am J Pathol* 164(5): 1807-15.
- Heijnen, H. F., A. E. Schiel, et al. (1999). "Activated platelets release two types of membrane vesicles: microvesicles by surface shedding and exosomes derived from exocytosis of multivesicular bodies and α -granules." *Blood* 94(11): 3791-9.
- Hennigan, R. F., K. L. Hawker, et al. (1994). "Fos-transformation activates genes associated with invasion." *Oncogene* 9(12): 3591-600.
- Henshall, S. (2003). "Tissue microarrays." *J Mammary Gland Biol Neoplasia* 8(3): 347-58.
- Hibbs, M. L., H. Xu, et al. (1991). "Regulation of adhesion of ICAM-1 by the cytoplasmic domain of LFA-1 integrin β subunit." *Science* 251(5001): 1611-3.
- Hidai, C., T. Zupancic, et al. (1998). "Cloning and characterization of developmental endothelial locus-1: an embryonic endothelial cell protein that binds the α 5 β 3 integrin receptor." *Genes Dev* 12(1): 21-33.
- Hingorani, S. R., L. Wang, et al. (2005). "Trp53R172H and KrasG12D cooperate to promote chromosomal instability and widely metastatic pancreatic ductal adenocarcinoma in mice." *Cancer Cell* 7(5): 469-83.
- Hirst, J. and M. S. Robinson (1998). "Clathrin and adaptors." *Biochim Biophys Acta* 1404(1-2): 173-93.
- Hisata, S., T. Sakisaka, et al. (2007). "Rap1-PDZ-GEF1 interacts with a neurotrophin receptor at late endosomes, leading to sustained activation of Rap1 and ERK and neurite outgrowth." *J Cell Biol* 178(5): 843-60.

- Hogg, N., R. Henderson, et al. (2002). "Mechanisms contributing to the activity of integrins on leukocytes." *Immunol Rev* 186: 164-71.
- Holt, O., E. Kanno, et al. (2008). "Slp1 and Slp2-a localize to the plasma membrane of CTL and contribute to secretion from the immunological synapse." *Traffic* 9(4): 446-57.
- Homan, S. M., R. Martinez, et al. (2002). "Regulation of the association of alpha 6 beta 4 with vimentin intermediate filaments in endothelial cells." *Exp Cell Res* 281(1): 107-14.
- Howes, M. T., M. Kirkham, et al. "Clathrin-independent carriers form a high capacity endocytic sorting system at the leading edge of migrating cells." *J Cell Biol* 190(4): 675-91.
- Hruban, R. H., A. Maitra, et al. (2007). "Precursors to pancreatic cancer." *Gastroenterol Clin North Am* 36(4): 831-49, vi.
- Huck, L., S. M. Pontier, et al. "beta1-integrin is dispensable for the induction of ErbB2 mammary tumors but plays a critical role in the metastatic phase of tumor progression." *Proc Natl Acad Sci U S A* 107(35): 15559-64.
- Hughes, P. E., F. Diaz-Gonzalez, et al. (1996). "Breaking the integrin hinge. A defined structural constraint regulates integrin signaling." *J Biol Chem* 271(12): 6571-4.
- Hughes, P. E., T. E. O'Toole, et al. (1995). "The conserved membrane-proximal region of an integrin cytoplasmic domain specifies ligand binding affinity." *J Biol Chem* 270(21): 12411-7.
- Humphries, J. D., P. Wang, et al. (2007). "Vinculin controls focal adhesion formation by direct interactions with talin and actin." *J Cell Biol* 179(5): 1043-57.
- Huveneers, S., H. Truong, et al. (2007). "Integrins: signaling, disease, and therapy." *Int J Radiat Biol* 83(11-12): 743-51.
- Huveneers, S., H. Truong, et al. (2008). "Binding of soluble fibronectin to integrin alpha5 beta1 - link to focal adhesion redistribution and contractile shape." *J Cell Sci* 121(Pt 15): 2452-62.
- Hynes, R. O. (2002). "Integrins: bidirectional, allosteric signaling machines." *Cell* 110(6): 673-87.
- Idone, V., C. Tam, et al. (2008). "Two-way traffic on the road to plasma membrane repair." *Trends Cell Biol* 18(11): 552-9.
- Irizarry, R. A., B. Hobbs, et al. (2003). "Exploration, normalization, and summaries of high density oligonucleotide array probe level data." *Biostatistics* 4(2): 249-64.
- Ivaska, J., K. Vuoriluoto, et al. (2005). "PKCepsilon-mediated phosphorylation of vimentin controls integrin recycling and motility." *EMBO J* 24(22): 3834-45.
- Ivaska, J., R. D. Whelan, et al. (2002). "PKC epsilon controls the traffic of beta1 integrins in motile cells." *EMBO J* 21(14): 3608-19.
- Izaguirre, G., L. Aguirre, et al. (2001). "The cytoskeletal/non-muscle isoform of alpha-actinin is phosphorylated on its actin-binding domain by the focal adhesion kinase." *J Biol Chem* 276(31): 28676-85.
- Izumi, T., H. Gomi, et al. (2003). "The roles of Rab27 and its effectors in the regulated secretory pathways." *Cell Struct Funct* 28(5): 465-74.
- Jalilian, C., E. M. Gallant, et al. (2008). "Redox potential and the response of cardiac ryanodine receptors to CLIC-2, a member of the glutathione S-transferase structural family." *Antioxid Redox Signal* 10(10): 1675-86.
- Jiang, X. and A. Sorkin (2002). "Coordinated traffic of Grb2 and Ras during epidermal growth factor receptor endocytosis visualized in living cells." *Mol Biol Cell* 13(5): 1522-35.
- Kalia, M., S. Kumari, et al. (2006). "Arf6-independent GPI-anchored protein-enriched early endosomal compartments fuse with sorting endosomes via a Rab5/phosphatidylinositol-3'-kinase-dependent machinery." *Mol Biol Cell* 17(8): 3689-704.
- Kamei, M., W. B. Saunders, et al. (2006). "Endothelial tubes assemble from intracellular vacuoles in vivo." *Nature* 442(7101): 453-6.
- Kaplan, R. N., R. D. Riba, et al. (2005). "VEGFR1-positive haematopoietic bone marrow progenitors initiate the pre-metastatic niche." *Nature* 438(7069): 820-7.

- Kashiwagi, M., M. Tortorella, et al. (2001). "TIMP-3 is a potent inhibitor of aggrecanase 1 (ADAM-TS4) and aggrecanase 2 (ADAM-TS5)." J Biol Chem 276(16): 12501-4.
- Kato, A. (1997). "The biologic and clinical spectrum of Glanzmann's thrombasthenia: implications of integrin alpha IIb beta 3 for its pathogenesis." Crit Rev Oncol Hematol 26(1): 1-23.
- Kaur, S., H. A. Kenny, et al. (2009). "{beta}3-integrin expression on tumor cells inhibits tumor progression, reduces metastasis, and is associated with a favorable prognosis in patients with ovarian cancer." Am J Pathol 175(5): 2184-96.
- Kawaguchi, S. and M. E. Hemler (1993). "Role of the alpha subunit cytoplasmic domain in regulation of adhesive activity mediated by the integrin VLA-2." J Biol Chem 268(22): 16279-85.
- Kieffer, J. D., G. Plopper, et al. (1995). "Direct binding of F actin to the cytoplasmic domain of the alpha 2 integrin chain in vitro." Biochem Biophys Res Commun 217(2): 466-74.
- Kim, M., C. V. Carman, et al. (2003). "Bidirectional transmembrane signaling by cytoplasmic domain separation in integrins." Science 301(5640): 1720-5.
- Kim, M., H. R. Jang, et al. (2008). "Epigenetic inactivation of protein kinase D1 in gastric cancer and its role in gastric cancer cell migration and invasion." Carcinogenesis 29(3): 629-37.
- Kim, S., K. Bell, et al. (2000). "Regulation of angiogenesis in vivo by ligation of integrin alpha5beta1 with the central cell-binding domain of fibronectin." Am J Pathol 156(4): 1345-62.
- Kim, Y. B., S. Y. Lee, et al. (2007). "Epigenetic regulation of integrin-linked kinase expression depending on adhesion of gastric carcinoma cells." Am J Physiol Cell Physiol 292(2): C857-66.
- Kirkham, M., A. Fujita, et al. (2005). "Ultrastructural identification of uncoated caveolin-independent early endocytic vehicles." J Cell Biol 168(3): 465-76.
- Klemke, R. L., J. Leng, et al. (1998). "CAS/Crk coupling serves as a "molecular switch" for induction of cell migration." J Cell Biol 140(4): 961-72.
- Kloeker, S., M. B. Major, et al. (2004). "The Kindler syndrome protein is regulated by transforming growth factor-beta and involved in integrin-mediated adhesion." J Biol Chem 279(8): 6824-33.
- Koga, K., K. Matsumoto, et al. (2005). "Purification, characterization and biological significance of tumor-derived exosomes." Anticancer Res 25(6A): 3703-7.
- Kononen, J., L. Bubendorf, et al. (1998). "Tissue microarrays for high-throughput molecular profiling of tumor specimens." Nat Med 4(7): 844-7.
- Koorstra, J. B., G. Feldmann, et al. (2008). "Morphogenesis of pancreatic cancer: role of pancreatic intraepithelial neoplasia (PanINs)." Langenbecks Arch Surg 393(4): 561-70.
- Kozulin, P. and J. M. Provis (2009). "Differential gene expression in the developing human macula: microarray analysis using rare tissue samples." J Ocul Biol Dis Infor 2(4): 176-189.
- Krause, M., E. W. Dent, et al. (2003). "Ena/VASP proteins: regulators of the actin cytoskeleton and cell migration." Annu Rev Cell Dev Biol 19: 541-64.
- Kuroda, T. S., M. Fukuda, et al. (2002). "The Slp homology domain of synaptotagmin-like proteins 1-4 and Slac2 functions as a novel Rab27A binding domain." J Biol Chem 277(11): 9212-8.
- Kwong, K.-S. and E.-H. Wong (2002). "A more powerful step-up procedure for controlling the false discovery rate under independence." Statistics & Probability Letters 56(2): 217-225.
- Lahlou, H., V. Sanguin-Gendreau, et al. (2007). "Mammary epithelial-specific disruption of the focal adhesion kinase blocks mammary tumor progression." Proc Natl Acad Sci U S A 104(51): 20302-7.
- Lamaze, C., A. Dujeancourt, et al. (2001). "Interleukin 2 receptors and detergent-resistant membrane domains define a clathrin-independent endocytic pathway." Mol Cell 7(3): 661-71.

- Landry, D. W., M. H. Akabas, et al. (1989). "Purification and reconstitution of chloride channels from kidney and trachea." *Science* 244(4911): 1469-72.
- Languino, L. R. and E. Ruoslahti (1992). "An alternative form of the integrin beta 1 subunit with a variant cytoplasmic domain." *J Biol Chem* 267(10): 7116-20.
- Lee, J. O., L. A. Bankston, et al. (1995). "Two conformations of the integrin A-domain (I-domain): a pathway for activation?" *Structure* 3(12): 1333-40.
- Lefkowitz, R. J. and S. K. Shenoy (2005). "Transduction of receptor signals by beta-arrestins." *Science* 308(5721): 512-7.
- Legate, K. R., E. Montanez, et al. (2006). "ILK, PINCH and parvin: the tIPP of integrin signalling." *Nat Rev Mol Cell Biol* 7(1): 20-31.
- Legate, K. R., S. A. Wickstrom, et al. (2009). "Genetic and cell biological analysis of integrin outside-in signaling." *Genes Dev* 23(4): 397-418.
- Levental, K. R., H. Yu, et al. (2009). "Matrix crosslinking forces tumor progression by enhancing integrin signaling." *Cell* 139(5): 891-906.
- Li, J., B. A. Ballif, et al. (2005). "Phosphorylation of ACAP1 by Akt regulates the stimulation-dependent recycling of integrin beta1 to control cell migration." *Dev Cell* 9(5): 663-73.
- Li, Z., C. Schem, et al. (2008). "Increased COX2 expression enhances tumor-induced osteoclastic lesions in breast cancer bone metastasis." *Clin Exp Metastasis* 25(4): 389-400.
- Lichtinghagen, R., P. B. Musholt, et al. (2002). "Different mRNA and protein expression of matrix metalloproteinases 2 and 9 and tissue inhibitor of metalloproteinases 1 in benign and malignant prostate tissue." *Eur Urol* 42(4): 398-406.
- Lippincott-Schwartz, J. and D. M. Fambrough (1987). "Cycling of the integral membrane glycoprotein, LEP100, between plasma membrane and lysosomes: kinetic and morphological analysis." *Cell* 49(5): 669-77.
- Lippincott-Schwartz, J. and G. H. Patterson (2009). "Photoactivatable fluorescent proteins for diffraction-limited and super-resolution imaging." *Trends Cell Biol* 19(11): 555-65.
- Littler, D. R., L. J. Brown, et al. "Structure of human CLIC3 at 2 Å resolution." *Proteins* 78(6): 1594-600.
- Littler, D. R., S. J. Harrop, et al. (2004). "The intracellular chloride ion channel protein CLIC1 undergoes a redox-controlled structural transition." *J Biol Chem* 279(10): 9298-305.
- Littler, D. R., S. J. Harrop, et al. "The enigma of the CLIC proteins: Ion channels, redox proteins, enzymes, scaffolding proteins?" *FEBS Lett* 584(10): 2093-101.
- Liu, S. and M. H. Ginsberg (2000). "Paxillin binding to a conserved sequence motif in the alpha 4 integrin cytoplasmic domain." *J Biol Chem* 275(30): 22736-42.
- Liu, S., M. Z. Sun, et al. (2008). "High-performance liquid chromatography/nano-electrospray ionization tandem mass spectrometry, two-dimensional difference in-gel electrophoresis and gene microarray identification of lymphatic metastasis-associated biomarkers." *Rapid Commun Mass Spectrom* 22(20): 3172-8.
- Livak, K. J. and T. D. Schmittgen (2001). "Analysis of relative gene expression data using real-time quantitative PCR and the 2(-Delta Delta C(T)) Method." *Methods* 25(4): 402-8.
- Lobert, V. H., A. Brech, et al. "Ubiquitination of alpha 5 beta 1 integrin controls fibroblast migration through lysosomal degradation of fibronectin-integrin complexes." *Dev Cell* 19(1): 148-59.
- Loh, E., W. Qi, et al. (1996). "Effect of cytoplasmic domain mutations on the agonist-stimulated ligand binding activity of the platelet integrin alphaIIb beta3." *J Biol Chem* 271(47): 30233-41.
- Lu, A., F. Tebar, et al. (2009). "A clathrin-dependent pathway leads to KRas signaling on late endosomes en route to lysosomes." *J Cell Biol* 184(6): 863-79.
- Lu, C., J. Takagi, et al. (2001). "Association of the membrane proximal regions of the alpha and beta subunit cytoplasmic domains constrains an integrin in the inactive state." *J Biol Chem* 276(18): 14642-8.

- Lucci, A., S. Krishnamurthy, et al. (2009). "Cyclooxygenase-2 expression in primary breast cancers predicts dissemination of cancer cells to the bone marrow." Breast Cancer Res Treat 117(1): 61-8.
- Luo, B. H., C. V. Carman, et al. (2007). "Structural basis of integrin regulation and signaling." Annu Rev Immunol 25: 619-47.
- Luo, B. H., T. A. Springer, et al. (2004). "A specific interface between integrin transmembrane helices and affinity for ligand." PLoS Biol 2(6): e153.
- MacIntyre, A. C. and D. J. Cutler (1988). "The potential role of lysosomes in tissue distribution of weak bases." Biopharm Drug Dispos 9(6): 513-26.
- Maeda, K., M. Haraguchi, et al. (2008). "CLIC4 interacts with histamine H3 receptor and enhances the receptor cell surface expression." Biochem Biophys Res Commun 369(2): 603-8.
- Maitra, A. and R. H. Hruban (2008). "Pancreatic cancer." Annu Rev Pathol 3: 157-88.
- Marcantonio, E. E., J. L. Guan, et al. (1990). "Mapping of the functional determinants of the integrin beta 1 cytoplasmic domain by site-directed mutagenesis." Cell Regul 1(8): 597-604.
- Marmor, M. D. and Y. Yarden (2004). "Role of protein ubiquitylation in regulating endocytosis of receptor tyrosine kinases." Oncogene 23(11): 2057-70.
- Martel, V., C. Racaud-Sultan, et al. (2001). "Conformation, localization, and integrin binding of talin depend on its interaction with phosphoinositides." J Biol Chem 276(24): 21217-27.
- Mattila, E., T. Pellinen, et al. (2005). "Negative regulation of EGFR signalling through integrin-alpha1beta1-mediated activation of protein tyrosine phosphatase TCPTP." Nat Cell Biol 7(1): 78-85.
- Mears, R., R. A. Craven, et al. (2004). "Proteomic analysis of melanoma-derived exosomes by two-dimensional polyacrylamide gel electrophoresis and mass spectrometry." Proteomics 4(12): 4019-31.
- Meresse, S., J. P. Gorvel, et al. (1995). "The rab7 GTPase resides on a vesicular compartment connected to lysosomes." J Cell Sci 108 (Pt 11): 3349-58.
- Miaczynska, M., L. Pelkmans, et al. (2004). "Not just a sink: endosomes in control of signal transduction." Curr Opin Cell Biol 16(4): 400-6.
- Miranti, C. K., S. Ohno, et al. (1999). "Protein kinase C regulates integrin-induced activation of the extracellular regulated kinase pathway upstream of Shc." J Biol Chem 274(15): 10571-81.
- Mizejewski, G. J. (1999). "Role of integrins in cancer: survey of expression patterns." Proc Soc Exp Biol Med 222(2): 124-38.
- Mobasher, A., R. Airley, et al. (2004). "Post-genomic applications of tissue microarrays: basic research, prognostic oncology, clinical genomics and drug discovery." Histol Histopathol 19(1): 325-35.
- Moncada-Pazos, A., A. J. Obaya, et al. (2009). "The ADAMTS12 metalloprotease gene is epigenetically silenced in tumor cells and transcriptionally activated in the stroma during progression of colon cancer." J Cell Sci 122(Pt 16): 2906-13.
- Money, T. T., R. G. King, et al. (2007). "Expression and cellular localisation of chloride intracellular channel 3 in human placenta and fetal membranes." Placenta 28(5-6): 429-36.
- Monkley, S. J., C. A. Pritchard, et al. (2001). "Analysis of the mammalian talin2 gene TLN2." Biochem Biophys Res Commun 286(5): 880-5.
- Montanez, E., S. Ussar, et al. (2008). "Kindlin-2 controls bidirectional signaling of integrins." Genes Dev 22(10): 1325-30.
- Moran-Jones, K., J. Grindlay, et al. (2009). "hnRNP A2 regulates alternative mRNA splicing of TP53INP2 to control invasive cell migration." Cancer Res 69(24): 9219-27.
- Morin, P., C. Sagne, et al. (2004). "Functional characterization of wild-type and mutant human sialin." EMBO J 23(23): 4560-70.
- Morton, J. P., N. B. Jamieson, et al. "LKB1 haploinsufficiency cooperates with Kras to promote pancreatic cancer through suppression of p21-dependent growth arrest." Gastroenterology 139(2): 586-97, 597 e1-6.

- Morton, J. P., P. Timpson, et al. "Mutant p53 drives metastasis and overcomes growth arrest/senescence in pancreatic cancer." Proc Natl Acad Sci U S A 107(1): 246-51.
- Moser, M., K. R. Legate, et al. (2009). "The tail of integrins, talin, and kindlins." Science 324(5929): 895-9.
- Muller, P. A., P. T. Caswell, et al. (2009). "Mutant p53 drives invasion by promoting integrin recycling." Cell 139(7): 1327-41.
- Nada, S., A. Hondo, et al. (2009). "The novel lipid raft adaptor p18 controls endosome dynamics by anchoring the MEK-ERK pathway to late endosomes." EMBO J 28(5): 477-89.
- Nam, K. T., H. J. Lee, et al. "Loss of Rab25 promotes the development of intestinal neoplasia in mice and is associated with human colorectal adenocarcinomas." J Clin Invest 120(3): 840-9.
- Naora, H. (2007). "The heterogeneity of epithelial ovarian cancers: reconciling old and new paradigms." Expert Rev Mol Med 9(13): 1-12.
- Narkiewicz, J., D. Klasa-Mazurkiewicz, et al. (2008). "Changes in mRNA and protein levels of human HtrA1, HtrA2 and HtrA3 in ovarian cancer." Clin Biochem 41(7-8): 561-9.
- Neumuller, O., M. Hoffmeister, et al. (2009). "Synaptotagmin-like protein 1 interacts with the GTPase-activating protein Rap1GAP2 and regulates dense granule secretion in platelets." Blood 114(7): 1396-404.
- Nevo, J., A. Mai, et al. "Mammary-derived growth inhibitor (MDGI) interacts with integrin alpha-subunits and suppresses integrin activity and invasion." Oncogene.
- Ng, C. M., S. Bai, et al. (2009). "Mechanism-based receptor-binding model to describe the pharmacokinetic and pharmacodynamic of an anti-alpha(5)beta (1) integrin monoclonal antibody (volociximab) in cancer patients." Cancer Chemother Pharmacol.
- Ng, T., D. Shima, et al. (1999). "PKCalpha regulates beta1 integrin-dependent cell motility through association and control of integrin traffic." EMBO J 18(14): 3909-23.
- Nichols, B. (2003). "Caveosomes and endocytosis of lipid rafts." J Cell Sci 116(Pt 23): 4707-14.
- Nichols, B. J. and J. Lippincott-Schwartz (2001). "Endocytosis without clathrin coats." Trends Cell Biol 11(10): 406-12.
- Niedergethmann, M., F. Alves, et al. (2007). "Gene expression profiling of liver metastases and tumour invasion in pancreatic cancer using an orthotopic SCID mouse model." Br J Cancer 97(10): 1432-40.
- Nishimura, T. and K. Kaibuchi (2007). "Numb controls integrin endocytosis for directional cell migration with aPKC and PAR-3." Dev Cell 13(1): 15-28.
- O'Toole, T. E., Y. Katagiri, et al. (1994). "Integrin cytoplasmic domains mediate inside-out signal transduction." J Cell Biol 124(6): 1047-59.
- O'Toole, T. E., D. Mandelman, et al. (1991). "Modulation of the affinity of integrin alpha IIb beta 3 (GPIIb-IIIa) by the cytoplasmic domain of alpha IIb." Science 254(5033): 845-7.
- Olson, M. F. and E. Sahai (2009). "The actin cytoskeleton in cancer cell motility." Clin Exp Metastasis 26(4): 273-87.
- Olsson, A. K., A. Dimberg, et al. (2006). "VEGF receptor signalling - in control of vascular function." Nat Rev Mol Cell Biol 7(5): 359-71.
- Ostrowski, M., N. B. Carmo, et al. "Rab27a and Rab27b control different steps of the exosome secretion pathway." Nat Cell Biol 12(1): 19-30; sup pp 1-13.
- Oxley, C. L., N. J. Anthis, et al. (2008). "An integrin phosphorylation switch: the effect of beta3 integrin tail phosphorylation on Dok1 and talin binding." J Biol Chem 283(9): 5420-6.
- Pan, Q., O. Shai, et al. (2008). "Deep surveying of alternative splicing complexity in the human transcriptome by high-throughput sequencing." Nat Genet 40(12): 1413-5.
- Pan, S., R. Wang, et al. (2008). "Extracellular Alix regulates integrin-mediated cell adhesions and extracellular matrix assembly." EMBO J 27(15): 2077-90.

- Pankov, R., Y. Endo, et al. (2005). "A Rac switch regulates random versus directionally persistent cell migration." *J Cell Biol* 170(5): 793-802.
- Pankova, K., D. Rosel, et al. "The molecular mechanisms of transition between mesenchymal and amoeboid invasiveness in tumor cells." *Cell Mol Life Sci* 67(1): 63-71.
- Partridge, A. W., S. Liu, et al. (2005). "Transmembrane domain helix packing stabilizes integrin α 5 β 3 in the low affinity state." *J Biol Chem* 280(8): 7294-300.
- Pelkmans, L., T. Burli, et al. (2004). "Caveolin-stabilized membrane domains as multifunctional transport and sorting devices in endocytic membrane traffic." *Cell* 118(6): 767-80.
- Pellinen, T., A. Arjonen, et al. (2006). "Small GTPase Rab21 regulates cell adhesion and controls endosomal traffic of β 1-integrins." *J Cell Biol* 173(5): 767-80.
- Pellinen, T. and J. Ivaska (2006). "Integrin traffic." *J Cell Sci* 119(Pt 18): 3723-31.
- Pellinen, T., S. Tuomi, et al. (2008). "Integrin trafficking regulated by Rab21 is necessary for cytokinesis." *Dev Cell* 15(3): 371-85.
- Petitjean, A., M. I. Achatz, et al. (2007). "TP53 mutations in human cancers: functional selection and impact on cancer prognosis and outcomes." *Oncogene* 26(15): 2157-65.
- Petrova, D. T., A. R. Asif, et al. (2008). "Expression of chloride intracellular channel protein 1 (CLIC1) and tumor protein D52 (TPD52) as potential biomarkers for colorectal cancer." *Clin Biochem* 41(14-15): 1224-36.
- Pfaff, M., S. Liu, et al. (1998). "Integrin beta cytoplasmic domains differentially bind to cytoskeletal proteins." *J Biol Chem* 273(11): 6104-9.
- Pfaffl, M. W. (2001). "A new mathematical model for relative quantification in real-time RT-PCR." *Nucleic Acids Res* 29(9): e45.
- Pierini, L. M., M. A. Lawson, et al. (2000). "Oriented endocytic recycling of α 5 β 1 in motile neutrophils." *Blood* 95(8): 2471-80.
- Pierschbacher, M. D. and E. Ruoslahti (1984). "Cell attachment activity of fibronectin can be duplicated by small synthetic fragments of the molecule." *Nature* 309(5963): 30-3.
- Pollard, T. D. (2007). "Regulation of actin filament assembly by Arp2/3 complex and formins." *Annu Rev Biophys Biomol Struct* 36: 451-77.
- Ponsioen, B., L. van Zeijl, et al. (2009). "Spatiotemporal regulation of chloride intracellular channel protein CLIC4 by RhoA." *Mol Biol Cell* 20(22): 4664-72.
- Powelka, A. M., J. Sun, et al. (2004). "Stimulation-dependent recycling of integrin β 1 regulated by ARF6 and Rab11." *Traffic* 5(1): 20-36.
- Proudfoot, N. J., A. Furger, et al. (2002). "Integrating mRNA processing with transcription." *Cell* 108(4): 501-12.
- Prunier, C. and P. H. Howe (2005). "Disabled-2 (Dab2) is required for transforming growth factor β -induced epithelial to mesenchymal transition (EMT)." *J Biol Chem* 280(17): 17540-8.
- Qian, Z., D. Okuhara, et al. (1999). "Molecular cloning and characterization of a mitogen-activated protein kinase-associated intracellular chloride channel." *J Biol Chem* 274(3): 1621-7.
- Radhakrishna, H. and J. G. Donaldson (1997). "ADP-ribosylation factor 6 regulates a novel plasma membrane recycling pathway." *J Cell Biol* 139(1): 49-61.
- Rajagopalan, M., J. L. Neidigh, et al. (1991). "Amino acid sequences Gly-Pro-Leu-Tyr and Asn-Pro-Glu-Tyr in the submembranous domain of the insulin receptor are required for normal endocytosis." *J Biol Chem* 266(34): 23068-73.
- Ramsay, A. G., M. D. Keppler, et al. (2007). "HS1-associated protein X-1 regulates carcinoma cell migration and invasion via clathrin-mediated endocytosis of integrin α 6 β 1." *Cancer Res* 67(11): 5275-84.
- Rappoport, J. Z. and S. M. Simon (2003). "Real-time analysis of clathrin-mediated endocytosis during cell migration." *J Cell Sci* 116(Pt 5): 847-55.
- Reszka, A. A., Y. Hayashi, et al. (1992). "Identification of amino acid sequences in the integrin β 1 cytoplasmic domain implicated in cytoskeletal association." *J Cell Biol* 117(6): 1321-30.

- Reynolds, A. R., I. R. Hart, et al. (2009). "Stimulation of tumor growth and angiogenesis by low concentrations of RGD-mimetic integrin inhibitors." Nat Med 15(4): 392-400.
- Reynolds, A. R., L. E. Reynolds, et al. (2004). "Elevated Flk1 (vascular endothelial growth factor receptor 2) signaling mediates enhanced angiogenesis in beta3-integrin-deficient mice." Cancer Res 64(23): 8643-50.
- Ricart, A. D., A. W. Tolcher, et al. (2008). "Volociximab, a chimeric monoclonal antibody that specifically binds alpha5beta1 integrin: a phase I, pharmacokinetic, and biological correlative study." Clin Cancer Res 14(23): 7924-9.
- Ridley, A. J. (2006). "Rho GTPases and actin dynamics in membrane protrusions and vesicle trafficking." Trends Cell Biol 16(10): 522-9.
- Rimm, D. L., R. L. Camp, et al. (2001). "Amplification of tissue by construction of tissue microarrays." Exp Mol Pathol 70(3): 255-64.
- Rink, J., E. Ghigo, et al. (2005). "Rab conversion as a mechanism of progression from early to late endosomes." Cell 122(5): 735-49.
- Roberts, M., S. Barry, et al. (2001). "PDGF-regulated rab4-dependent recycling of alphavbeta3 integrin from early endosomes is necessary for cell adhesion and spreading." Curr Biol 11(18): 1392-402.
- Roberts, M. S., A. J. Woods, et al. (2004). "Protein kinase B/Akt acts via glycogen synthase kinase 3 to regulate recycling of alpha v beta 3 and alpha 5 beta 1 integrins." Mol Cell Biol 24(4): 1505-15.
- Rohrer, J., A. Schweizer, et al. (1996). "The targeting of Lamp1 to lysosomes is dependent on the spacing of its cytoplasmic tail tyrosine sorting motif relative to the membrane." J Cell Biol 132(4): 565-76.
- Ronnov-Jessen, L., R. Villadsen, et al. (2002). "Differential expression of a chloride intracellular channel gene, CLIC4, in transforming growth factor-beta1-mediated conversion of fibroblasts to myofibroblasts." Am J Pathol 161(2): 471-80.
- Roskelley, C. D. and M. J. Bissell (1995). "Dynamic reciprocity revisited: a continuous, bidirectional flow of information between cells and the extracellular matrix regulates mammary epithelial cell function." Biochem Cell Biol 73(7-8): 391-7.
- Rossmann, K. L., C. J. Der, et al. (2005). "GEF means go: turning on RHO GTPases with guanine nucleotide-exchange factors." Nat Rev Mol Cell Biol 6(2): 167-80.
- Ruoslahti, E. (1996). "RGD and other recognition sequences for integrins." Annu Rev Cell Dev Biol 12: 697-715.
- Sabharanjak, S., P. Sharma, et al. (2002). "GPI-anchored proteins are delivered to recycling endosomes via a distinct cdc42-regulated, clathrin-independent pinocytotic pathway." Dev Cell 2(4): 411-23.
- Sahai, E. (2005). "Mechanisms of cancer cell invasion." Curr Opin Genet Dev 15(1): 87-96.
- Sahai, E. (2007). "Illuminating the metastatic process." Nat Rev Cancer 7(10): 737-49.
- Sahai, E. and C. J. Marshall (2003). "Differing modes of tumour cell invasion have distinct requirements for Rho/ROCK signalling and extracellular proteolysis." Nat Cell Biol 5(8): 711-9.
- Sakai, T., R. Jove, et al. (2001). "Role of the cytoplasmic tyrosines of beta 1A integrins in transformation by v-src." Proc Natl Acad Sci U S A 98(7): 3808-13.
- Sancak, Y., L. Bar-Peled, et al. "Ragulator-Rag complex targets mTORC1 to the lysosomal surface and is necessary for its activation by amino acids." Cell 141(2): 290-303.
- Sancak, Y., T. R. Peterson, et al. (2008). "The Rag GTPases bind raptor and mediate amino acid signaling to mTORC1." Science 320(5882): 1496-501.
- Sandilands, E., C. Cans, et al. (2004). "RhoB and actin polymerization coordinate Src activation with endosome-mediated delivery to the membrane." Dev Cell 7(6): 855-69.
- Scarpa, A., P. Capelli, et al. (1993). "Pancreatic adenocarcinomas frequently show p53 gene mutations." Am J Pathol 142(5): 1534-43.

- Schaller, M. D., J. D. Hildebrand, et al. (1994). "Autophosphorylation of the focal adhesion kinase, pp125FAK, directs SH2-dependent binding of pp60src." *Mol Cell Biol* 14(3): 1680-8.
- Schefe, J. H., K. E. Lehmann, et al. (2006). "Quantitative real-time RT-PCR data analysis: current concepts and the novel "gene expression's CT difference" formula." *J Mol Med* 84(11): 901-10.
- Schlaepfer, D. D., S. K. Hanks, et al. (1994). "Integrin-mediated signal transduction linked to Ras pathway by GRB2 binding to focal adhesion kinase." *Nature* 372(6508): 786-91.
- Schlaepfer, D. D. and T. Hunter (1996). "Evidence for in vivo phosphorylation of the Grb2 SH2-domain binding site on focal adhesion kinase by Src-family protein-tyrosine kinases." *Mol Cell Biol* 16(10): 5623-33.
- Schlaepfer, D. D., S. K. Mitra, et al. (2004). "Control of motile and invasive cell phenotypes by focal adhesion kinase." *Biochim Biophys Acta* 1692(2-3): 77-102.
- Schutze, S., V. Tchikov, et al. (2008). "Regulation of TNFR1 and CD95 signalling by receptor compartmentalization." *Nat Rev Mol Cell Biol* 9(8): 655-62.
- Schwartz, M. A., M. D. Schaller, et al. (1995). "Integrins: emerging paradigms of signal transduction." *Annu Rev Cell Dev Biol* 11: 549-99.
- Sebzda, E., M. Bracke, et al. (2002). "Rap1A positively regulates T cells via integrin activation rather than inhibiting lymphocyte signaling." *Nat Immunol* 3(3): 251-8.
- Serrels, B., A. Serrels, et al. (2007). "Focal adhesion kinase controls actin assembly via a FERM-mediated interaction with the Arp2/3 complex." *Nat Cell Biol* 9(9): 1046-56.
- Shanks, R. A., M. C. Larocca, et al. (2002). "AKAP350 at the Golgi apparatus. II. Association of AKAP350 with a novel chloride intracellular channel (CLIC) family member." *J Biol Chem* 277(43): 40973-80.
- Shi, F. and J. Sottile (2008). "Caveolin-1-dependent beta1 integrin endocytosis is a critical regulator of fibronectin turnover." *J Cell Sci* 121(Pt 14): 2360-71.
- Shimaoka, M., C. Lu, et al. (2001). "Reversibly locking a protein fold in an active conformation with a disulfide bond: integrin alphaL I domains with high affinity and antagonist activity in vivo." *Proc Natl Acad Sci U S A* 98(11): 6009-14.
- Shukla, A., M. Malik, et al. (2009). "TGF-beta signalling is regulated by Schnurri-2-dependent nuclear translocation of CLIC4 and consequent stabilization of phospho-Smad2 and 3." *Nat Cell Biol* 11(6): 777-84.
- Sigismund, S., E. Argenzio, et al. (2008). "Clathrin-mediated internalization is essential for sustained EGFR signaling but dispensable for degradation." *Dev Cell* 15(2): 209-19.
- Sigismund, S., T. Woelk, et al. (2005). "Clathrin-independent endocytosis of ubiquitinated cargos." *Proc Natl Acad Sci U S A* 102(8): 2760-5.
- Simpson, R. J., S. S. Jensen, et al. (2008). "Proteomic profiling of exosomes: current perspectives." *Proteomics* 8(19): 4083-99.
- Simpson, R. J., J. W. Lim, et al. (2009). "Exosomes: proteomic insights and diagnostic potential." *Expert Rev Proteomics* 6(3): 267-83.
- Singh, A., P. Greninger, et al. (2009). "A gene expression signature associated with "K-Ras addiction" reveals regulators of EMT and tumor cell survival." *Cancer Cell* 15(6): 489-500.
- Singh, H. "Two decades with dimorphic Chloride Intracellular Channels (CLICs)." *FEBS Lett* 584(10): 2112-21.
- Singh, H. and R. H. Ashley (2007). "CLIC4 (p64H1) and its putative transmembrane domain form poorly selective, redox-regulated ion channels." *Mol Membr Biol* 24(1): 41-52.
- Singh, H., M. A. Cousin, et al. (2007). "Functional reconstitution of mammalian 'chloride intracellular channels' CLIC1, CLIC4 and CLIC5 reveals differential regulation by cytoskeletal actin." *FEBS J* 274(24): 6306-16.
- Sinibaldi, D., W. Wharton, et al. (2000). "Induction of p21WAF1/CIP1 and cyclin D1 expression by the Src oncoprotein in mouse fibroblasts: role of activated STAT3 signaling." *Oncogene* 19(48): 5419-27.

- Sottile, J. and J. Chandler (2005). "Fibronectin matrix turnover occurs through a caveolin-1-dependent process." Mol Biol Cell 16(2): 757-68.
- Spiekerkoetter, E., C. Guignabert, et al. (2009). "S100A4 and bone morphogenetic protein-2 codependently induce vascular smooth muscle cell migration via phospho-extracellular signal-regulated kinase and chloride intracellular channel 4." Circ Res 105(7): 639-47, 13 p following 647.
- Springer, T. A. (1997). "Folding of the N-terminal, ligand-binding region of integrin alpha-subunits into a beta-propeller domain." Proc Natl Acad Sci U S A 94(1): 65-72.
- Stoeltzing, O., W. Liu, et al. (2003). "Inhibition of integrin alpha5beta1 function with a small peptide (ATN-161) plus continuous 5-FU infusion reduces colorectal liver metastases and improves survival in mice." Int J Cancer 104(4): 496-503.
- Stupp, R. and C. Rugg (2007). "Integrin inhibitors reaching the clinic." J Clin Oncol 25(13): 1637-8.
- Sudarsanam, S. and D. E. Johnson "Functional consequences of mTOR inhibition." Curr Opin Drug Discov Devel 13(1): 31-40.
- Suginta, W., N. Karoulias, et al. (2001). "Chloride intracellular channel protein CLIC4 (p64H1) binds directly to brain dynamin I in a complex containing actin, tubulin and 14-3-3 isoforms." Biochem J 359(Pt 1): 55-64.
- Suh, K. S., M. Malik, et al. (2007). "CLIC4, skin homeostasis and cutaneous cancer: surprising connections." Mol Carcinog 46(8): 599-604.
- Suh, K. S., M. Mutoh, et al. (2005). "Antisense suppression of the chloride intracellular channel family induces apoptosis, enhances tumor necrosis factor {alpha}-induced apoptosis, and inhibits tumor growth." Cancer Res 65(2): 562-71.
- Suh, K. S., M. Mutoh, et al. (2004). "The organellar chloride channel protein CLIC4/mtCLIC translocates to the nucleus in response to cellular stress and accelerates apoptosis." J Biol Chem 279(6): 4632-41.
- Svensson, L., K. Howarth, et al. (2009). "Leukocyte adhesion deficiency-III is caused by mutations in KINDLIN3 affecting integrin activation." Nat Med 15(3): 306-12.
- Swenson, S., F. Costa, et al. (2005). "Contortrostatin, a snake venom disintegrin with anti-angiogenic and anti-tumor activity." Pathophysiol Haemost Thromb 34(4-5): 169-76.
- Taga, T., A. Suzuki, et al. (2002). "alpha v-Integrin antagonist EMD 121974 induces apoptosis in brain tumor cells growing on vitronectin and tenascin." Int J Cancer 98(5): 690-7.
- Takada, Y., X. Ye, et al. (2007). "The integrins." Genome Biol 8(5): 215.
- Takaori, K. (2007). "Current understanding of precursors to pancreatic cancer." J Hepatobiliary Pancreat Surg 14(3): 217-23.
- Tamura, R. N., C. Rozzo, et al. (1990). "Epithelial integrin alpha 6 beta 4: complete primary structure of alpha 6 and variant forms of beta 4." J Cell Biol 111(4): 1593-604.
- Teckchandani, A., N. Toida, et al. (2009). "Quantitative proteomics identifies a Dab2/integrin module regulating cell migration." J Cell Biol 186(1): 99-111.
- Teis, D., W. Wunderlich, et al. (2002). "Localization of the MP1-MAPK scaffold complex to endosomes is mediated by p14 and required for signal transduction." Dev Cell 3(6): 803-14.
- They, C., M. Boussac, et al. (2001). "Proteomic analysis of dendritic cell-derived exosomes: a secreted subcellular compartment distinct from apoptotic vesicles." J Immunol 166(12): 7309-18.
- Thiery, J. P. (2002). "Epithelial-mesenchymal transitions in tumour progression." Nat Rev Cancer 2(6): 442-54.
- Thomas, G. J., M. L. Nystrom, et al. (2006). "Alphavbeta6 integrin in wound healing and cancer of the oral cavity." J Oral Pathol Med 35(1): 1-10.
- Tohgo, A., E. W. Choy, et al. (2003). "The stability of the G protein-coupled receptor-beta-arrestin interaction determines the mechanism and functional consequence of ERK activation." J Biol Chem 278(8): 6258-67.

- Torka, R., F. Thuma, et al. (2006). "ROCK signaling mediates the adoption of different modes of migration and invasion in human mammary epithelial tumor cells." Exp Cell Res 312(19): 3857-71.
- Touchot, N., P. Chardin, et al. (1987). "Four additional members of the ras gene superfamily isolated by an oligonucleotide strategy: molecular cloning of YPT-related cDNAs from a rat brain library." Proc Natl Acad Sci U S A 84(23): 8210-4.
- Troeberg, L., K. Fushimi, et al. (2009). "The C-terminal domains of ADAMTS-4 and ADAMTS-5 promote association with N-TIMP-3." Matrix Biol 28(8): 463-9.
- Trub, T., W. E. Choi, et al. (1995). "Specificity of the PTB domain of Shc for beta turn-forming pentapeptide motifs amino-terminal to phosphotyrosine." J Biol Chem 270(31): 18205-8.
- Tu, C., C. F. Ortega-Cava, et al. "Endosomal-sorting complexes required for transport (ESCRT) pathway-dependent endosomal traffic regulates the localization of active Src at focal adhesions." Proc Natl Acad Sci U S A.
- Tuckwell, D. (1999). "Evolution of von Willebrand factor A (VWA) domains." Biochem Soc Trans 27(6): 835-40.
- Tulk, B. M., S. Kapadia, et al. (2002). "CLIC1 inserts from the aqueous phase into phospholipid membranes, where it functions as an anion channel." Am J Physiol Cell Physiol 282(5): C1103-12.
- Tuomi, S., A. Mai, et al. (2009). "PKCepsilon regulation of an alpha5 integrin-ZO-1 complex controls lamellae formation in migrating cancer cells." Sci Signal 2(77): ra32.
- Turkson, J., T. Bowman, et al. (1998). "Stat3 activation by Src induces specific gene regulation and is required for cell transformation." Mol Cell Biol 18(5): 2545-52.
- Ulmasov, B., J. Bruno, et al. (2009). "Chloride intracellular channel protein-4 functions in angiogenesis by supporting acidification of vacuoles along the intracellular tubulogenic pathway." Am J Pathol 174(3): 1084-96.
- Ulmer, T. S., B. Yaspan, et al. (2001). "NMR analysis of structure and dynamics of the cytosolic tails of integrin alpha IIb beta 3 in aqueous solution." Biochemistry 40(25): 7498-508.
- Upla, P., V. Marjomaki, et al. (2004). "Clustering induces a lateral redistribution of alpha 2 beta 1 integrin from membrane rafts to caveolae and subsequent protein kinase C-dependent internalization." Mol Biol Cell 15(2): 625-36.
- Valadi, H., K. Ekstrom, et al. (2007). "Exosome-mediated transfer of mRNAs and microRNAs is a novel mechanism of genetic exchange between cells." Nat Cell Biol 9(6): 654-9.
- Valdembri, D., P. T. Caswell, et al. (2009). "Neuropilin-1/GIPC1 signaling regulates alpha5beta1 integrin traffic and function in endothelial cells." PLoS Biol 7(1): e25.
- Vallar, L., C. Melchior, et al. (1999). "Divalent cations differentially regulate integrin alphaIIb cytoplasmic tail binding to beta3 and to calcium- and integrin-binding protein." J Biol Chem 274(24): 17257-66.
- van der Flier, A., I. Kuikman, et al. (1995). "A novel beta 1 integrin isoform produced by alternative splicing: unique expression in cardiac and skeletal muscle." FEBS Lett 369(2-3): 340-4.
- Vang, R., M. Shih le, et al. (2009). "Ovarian low-grade and high-grade serous carcinoma: pathogenesis, clinicopathologic and molecular biologic features, and diagnostic problems." Adv Anat Pathol 16(5): 267-82.
- Verges, M., F. Luton, et al. (2004). "The mammalian retromer regulates transcytosis of the polymeric immunoglobulin receptor." Nat Cell Biol 6(8): 763-9.
- Vial, E., E. Sahai, et al. (2003). "ERK-MAPK signaling coordinately regulates activity of Rac1 and RhoA for tumor cell motility." Cancer Cell 4(1): 67-79.
- Vignoud, L., Y. Usson, et al. (1994). "Internalization of the alpha 5 beta 1 integrin does not depend on "NPXY" signals." Biochem Biophys Res Commun 199(2): 603-11.
- Vinogradova, O., A. Velyvis, et al. (2002). "A structural mechanism of integrin alpha(IIb)beta(3) "inside-out" activation as regulated by its cytoplasmic face." Cell 110(5): 587-97.

- von Zastrow, M. and A. Sorokin (2007). "Signaling on the endocytic pathway." Curr Opin Cell Biol 19(4): 436-45.
- Walker, J. L. and R. K. Assoian (2005). "Integrin-dependent signal transduction regulating cyclin D1 expression and G1 phase cell cycle progression." Cancer Metastasis Rev 24(3): 383-93.
- Wan, W. H., M. B. Fortuna, et al. (1987). "A rapid and efficient method for testing immunohistochemical reactivity of monoclonal antibodies against multiple tissue samples simultaneously." J Immunol Methods 103(1): 121-9.
- Wang, J. W., S. Y. Peng, et al. (2009). "Identification of metastasis-associated proteins involved in gallbladder carcinoma metastasis by proteomic analysis and functional exploration of chloride intracellular channel 1." Cancer Lett 281(1): 71-81.
- Wang, W., S. Goswami, et al. (2004). "Identification and testing of a gene expression signature of invasive carcinoma cells within primary mammary tumors." Cancer Res 64(23): 8585-94.
- Wang, W., J. B. Wyckoff, et al. (2002). "Single cell behavior in metastatic primary mammary tumors correlated with gene expression patterns revealed by molecular profiling." Cancer Res 62(21): 6278-88.
- Wang, Y., S. D. Pennock, et al. (2004). "Platelet-derived growth factor receptor-mediated signal transduction from endosomes." J Biol Chem 279(9): 8038-46.
- Wary, K. K., A. Mariotti, et al. (1998). "A requirement for caveolin-1 and associated kinase Fyn in integrin signaling and anchorage-dependent cell growth." Cell 94(5): 625-34.
- Watanabe, N., L. Bodin, et al. (2008). "Mechanisms and consequences of agonist-induced talin recruitment to platelet integrin α IIb β 3." J Cell Biol 181(7): 1211-22.
- Weaver, V. M., S. Lelievre, et al. (2002). "beta4 integrin-dependent formation of polarized three-dimensional architecture confers resistance to apoptosis in normal and malignant mammary epithelium." Cancer Cell 2(3): 205-16.
- Webb, D. J., H. Zhang, et al. (2007). "alpha5 integrin signaling regulates the formation of spines and synapses in hippocampal neurons." J Biol Chem 282(10): 6929-35.
- Wegener, K. L., A. W. Partridge, et al. (2007). "Structural basis of integrin activation by talin." Cell 128(1): 171-82.
- Weisel, J. W., C. Nagaswami, et al. (1992). "Examination of the platelet membrane glycoprotein IIb-IIIa complex and its interaction with fibrinogen and other ligands by electron microscopy." J Biol Chem 267(23): 16637-43.
- Wennerberg, K., R. Fassler, et al. (1998). "Mutational analysis of the potential phosphorylation sites in the cytoplasmic domain of integrin beta1A. Requirement for threonines 788-789 in receptor activation." J Cell Sci 111 (Pt 8): 1117-26.
- White, D. E., N. A. Kurpios, et al. (2004). "Targeted disruption of beta1-integrin in a transgenic mouse model of human breast cancer reveals an essential role in mammary tumor induction." Cancer Cell 6(2): 159-70.
- Williams, M. J., P. E. Hughes, et al. (1994). "The inner world of cell adhesion: integrin cytoplasmic domains." Trends Cell Biol 4(4): 109-12.
- Wolfers, J., A. Lozier, et al. (2001). "Tumor-derived exosomes are a source of shared tumor rejection antigens for CTL cross-priming." Nat Med 7(3): 297-303.
- Woods, A. J., D. P. White, et al. (2004). "PKD1/PKCmu promotes alpha5beta3 integrin recycling and delivery to nascent focal adhesions." EMBO J 23(13): 2531-43.
- Wubbolts, R., M. Fernandez-Borja, et al. (1996). "Direct vesicular transport of MHC class II molecules from lysosomal structures to the cell surface." J Cell Biol 135(3): 611-22.
- Wubbolts, R., R. S. Leckie, et al. (2003). "Proteomic and biochemical analyses of human B cell-derived exosomes. Potential implications for their function and multivesicular body formation." J Biol Chem 278(13): 10963-72.
- Wunderlich, W., I. Fialka, et al. (2001). "A novel 14-kilodalton protein interacts with the mitogen-activated protein kinase scaffold mp1 on a late endosomal/lysosomal compartment." J Cell Biol 152(4): 765-76.

- Xiong, J. P., R. Li, et al. (2000). "An isoleucine-based allosteric switch controls affinity and shape shifting in integrin CD11b A-domain." J Biol Chem 275(49): 38762-7.
- Xiong, J. P., T. Stehle, et al. (2001). "Crystal structure of the extracellular segment of integrin alpha Vbeta3." Science 294(5541): 339-45.
- Xiong, J. P., T. Stehle, et al. (2003). "New insights into the structural basis of integrin activation." Blood 102(4): 1155-9.
- Yoon, S. O., S. Shin, et al. (2005). "Hypoxia stimulates carcinoma invasion by stabilizing microtubules and promoting the Rab11 trafficking of the alpha6beta4 integrin." Cancer Res 65(7): 2761-9.
- Zaidel-Bar, R., S. Itzkovitz, et al. (2007). "Functional atlas of the integrin adhesome." Nat Cell Biol 9(8): 858-67.
- Zamir, E., B. Z. Katz, et al. (1999). "Molecular diversity of cell-matrix adhesions." J Cell Sci 112 (Pt 11): 1655-69.
- Zerial, M. and H. McBride (2001). "Rab proteins as membrane organizers." Nat Rev Mol Cell Biol 2(2): 107-17.
- Zhang, J., X. Liu, et al. (2009). "RCP is a human breast cancer-promoting gene with Ras-activating function." J Clin Invest 119(8): 2171-83.
- Zhang, T. Y. and M. J. Meaney "Epigenetics and the environmental regulation of the genome and its function." Annu Rev Psychol 61: 439-66, C1-3.
- Zhang, X., G. Jiang, et al. (2008). "Talin depletion reveals independence of initial cell spreading from integrin activation and traction." Nat Cell Biol.
- Zhidkova, N. I., A. M. Belkin, et al. (1995). "Novel isoform of beta 1 integrin expressed in skeletal and cardiac muscle." Biochem Biophys Res Commun 214(1): 279-85.